

Development of Fungal Anti-Attachment Inks for 3D Printed Medical Devices

Thesis presented for degree of Doctor of Philosophy

by

Ling Xin, Yong

Department of Chemical & Environmental Engineering

April 2022

Acknowledgement

This research work was completed with the support of several individuals. First and foremost, I would like to express my gratitude to my supervisors - Professor Derek Irvine, Professor Ricky Wildman and Professor Simon Avery for their guidance and support throughout my PhD journey.

I would also like to extend my appreciation to several researchers that have given me invaluable suggestions and assistance. Yinfeng He for his continuous advice, Zuoxin Zhou for training and helping me out with the liquid handler, Cindy Vallieres for guiding me on the microbiology experiments and Joseph Sefton for his help - in synthesizing and testing many of the polymers used in this work. There are many more colleagues from University of Nottingham - Department of Pharmacy, Life Science, Advanced Manufacturing, Chemistry and Chemical Engineering who have lent a hand in the completion of this work.

I am especially thankful to my family (Mr and Mrs Yong) and friends for their encouragement and support during my PhD studies. Special mention to John Calautit who helped me with proofreading the thesis chapters and my PhD cohort mates for their friendship - Alice Konta, Marica Malenica and Yuyang Wu. Lastly, this work was made possible by funding from EPSRC (Engineering and Physical Sciences Research Council) via research grant EP/N024818/1 titled ‘Formulation for 3D Printing: Creating a Plug and Play Platform for a Disruptive UK Industry’.

Presentations

This research project resulted in several presentations shared during technical conferences:

Poster Title: Development of Flexible Antifungal Copolymer

Conference: UoN Polymer Researcher Symposium 2019

Authors: Ling Xin Yong, Yinfeng He, Cindy Vallieres, Valentina Cuzzucoli Crucitti, Simon Avery, Ricky Wildman, Derek Irvine

Presentation Title: High Throughput Screening for 3D Printable Antimicrobial Polymer

Conference: Polymers for 3D Printing Dusseldorf 2019

Authors: Ling Xin Yong, Zuoxin Zhou, Yinfeng He, Cindy Vallieres, Valentina Cuzzucoli Crucitti, Simon Avery, Ricky Wildman, Derek Irvine

Poster Title: Development of Flexible Antifungal Copolymer

Conference: 3D Medical Printing Conference Maastricht 2020

Authors: Ling Xin Yong, Zuoxin Zhou, Yinfeng He, Cindy Vallieres, Valentina Cuzzucoli Crucitti, Simon Avery, Ricky Wildman, Derek Irvine

Poster Title: High-throughput Screening of Antifungal Polymer for Medical Devices

Conference: 9th MRS-S Conference on Advanced Materials, Singapore 2020 (Virtual)

Authors: Ling Xin Yong, Zuoxin Zhou, Yinfeng He, Cindy Vallieres, Valentina Cuzzucoli Crucitti, Simon Avery, Ricky Wildman, Derek Irvine

Presentation Title: High-throughput Screening Methodology of UV Curable Anti-fungi 3D Printing Ink

Conference: International Virtual Conference on Formulation in Food and Healthcare, ICFFH 2021 (Virtual)

Authors: Ling Xin Yong, Zuoxin Zhou, Yinfeng He, Cindy Vallieres, Simon Avery, Ricky Wildman, Derek Irvine

Presentation Title: High-throughput Screening Methodology of UV Curable Anti-fungi 3D Printing Ink

Conference: ASTM International Conference of Additive Manufacturing, ICAM 2021 (Virtual)

Authors: Ling Xin Yong, Zuoxin Zhou, Yinfeng He, Cindy Vallieres, Simon Avery, Ricky Wildman, Derek Irvine

Abstract

Fungal infections of medical devices caused by *Candida albicans* alone have resulted in up to 50 % mortality. Utilisation of fungal-resistant polymer could reduce mortality rate and reduce complications in patient's health from frequent changes of medical devices. At present, Polydimethylsiloxane (PDMS) is commonly used due to its biocompatibility, excellent temperature and chemical resistance, and its good mechanical and moulding properties. However, in many of its biomedical applications such as voice prostheses and urinary catheters, PDMS can attract yeasts that form biofilms which trigger infections in device users. This is especially so for indwelling voice prostheses as there are currently no commercially available antimicrobial options and the device must be changed every few months.

Fungal biofilm resistant polymers can be incorporated to medical devices simply by dip coating or via additive manufacturing (AM) processes. AM is a manufacturing method that deposits material layer by layer, this method would be especially advantageous for low volume manufacturing and/ or customization. With medical technology advancements progressing towards catering to personalised treatment for individual patients, customization of medical devices with AM technique would be highly desirable. This work evaluates acrylate and methacrylate as ultraviolet (UV) curing polymers in AM processes - stereolithography (SLA) and material jetting. These processes are known to offer a high level of resolution and are also suitable for building smaller parts such as medical devices.

In this work, nine selected polymers with mixed resistance against fungal attachment were used to develop a high throughput screening (HTS) method for discovering fungal anti-attachment polymers. With the developed method, selected polymers were mixed in different ratios and cured under UV, forming copolymers. From the HTS of 30 copolymers, 19 out of 30 copolymers were identified to exhibit reduced *C. albicans* attachment <25 %. These copolymers were predicted with the Flory-Fox equation to have a wide varying range of glass transition temperature (T_g), and this widens the options for fungal-resistant polymers available for use in the medical industry.

Out of the 19 copolymers, Triethylene glycol methyl ether methacrylate (TEGMA) and (R)-α-Acryloyloxy-β,β-dimethyl-γ-butyrolactone (AODMBA) copolymer in the ratio of 40:60 was found to be the most suitable ratio for material jetting. Concurrently, TEGMA:AODMBA$_{40:60}$ was also thermally synthesised into a copolymer for dip coating process. The application of this copolymer was then demonstrated by printing a voice prosthesis flap used by patients who have undergone a laryngectomy.

This inkjet-printed TEGMA:AODMBA$_{40:60}$ copolymer was found to have a T_g of 13.6°C, which is within the targeted T_g range for a flexible medical device. While TEGMA:AODMBA$_{40:60}$ could be inkjet-printed and dip-coated, curability was compromised, and the resolution of the printed part did not capture the finer details. Further modification of the copolymer ink formulation was performed by exploiting acrylate alternatives with similar structures, replacing of monomer with oligomers and inclusion of hyperbranched tripropylene glycol diacrylate (HBP-TPGDA) to

improve the ink’s functionality. Finetuning of the formulation with the above methods was able to improve the printing resolution, a significant improvement was found especially when using similar acrylate alternatives of methacrylate monomers and incorporation of hyperbranched polymers as an additive. However, more work has to be done to study this formulation adjustment in detail and its effect on the end properties.

Contents

Acknowledgement i
Presentations ii
Abstract iii
Contents vi
List of Tables xi
List of Figures xiii
Nomenclature xviii
Abbreviations xix

Chapter 1: Introduction 1
1.1 Medical Device 2
1.2 Device-Associated Infections 4
1.3 Aims & Objectives 7
1.4 Project Methodology 8
1.5 Thesis Structure 9

Chapter 2: Literature Review 11
2.1 Introduction 11
2.2 Fungi 11
2.2.1 The *Candida* genus 12
2.2.2 *Candida albicans* 14
2.3 Medical Devices susceptible to *C. albicans* 15
2.3.1 Voice Prosthesis 17
2.3.2 Catheter 19
2.3.3 Other Devices 21
2.4 Strategies to Prevent Formation of Fungal Biofilm 22
2.5 Dip Coating Process 34
2.6 Polymeric Antimicrobial Coating 36

2.6.1 Non-microbial Adhering Mechanism 38
2.6.2 Antimicrobial Releasing Mechanism 40
2.6.3 Surface Contact Killing Mechanism 41
2.6.4 Summary of Antimicrobial Coatings 42
2.7 Additive Manufacturing Process 42
2.7.1 Different AM Techniques 45
2.7.2 Vat Photopolymerisation 46
2.7.3 Material Jetting 47
2.7.4 Summary of AM Processes 49
2.8 UV Curing Polymerisation 50
2.9 AM in Biomedical Field 52
2.9.1 Microbial-Resistant AM Materials 54
2.10 Gaps, previously, associated work & summary 59

Chapter 3: Experimental Methods & Setup 61
3.1 Introduction 61
3.2 Materials Used 63
3.3 High Throughput Screening (HTS) Method 64
3.3.1 Preparation in 96-Well Plate HTS Array 65
3.3.2 HTS of Viscosity, Surface Tension & Z parameter 68
3.4 Characterization and Evaluation Methods for Resulting Polymers 69
3.4.1 Fourier-Transform Infrared Analysis (FTIR) 69
3.4.2 Differential Scanning Calorimetry (DSC) Analysis 70
3.4.3 Evaluation of Fungal Attachment, Residual & Polymer Toxicity (XTT Assay) 71
3.4.4 Evaluation of Fungal Attachment (Crystal Violet Staining) 73
3.4.5 Raman Spectroscopy 74
3.4.6 Proton Nuclear Magnetic Resonance (^{1}H NMR) 76
3.4.7 Gel Permeation Chromatography (GPC) 77
3.4.8 Time-of-Flight Secondary Ion Mass Spectrometry (ToF-SIMS) 77

3.4.9 Microscopic Imaging 78
3.5 Additive Manufacturing Process 78
3.5.1 Ink Preparation 78
3.5.2 Inkjet Printing 78
3.5.3 Stereolithography 81
3.6 Polymer Synthesis 81
3.6.1 TEGMA Oligomer Synthesis 81
3.6.2 Copolymer Synthesis 82
3.6.3 Hyperbranched Polymer TPGDA Synthesis 83
3.7 Dip Coating Method 84
3.8 Statistic Analysis 85

Chapter 4: Development of High Throughput Screening (HTS) Method 86
4.1 Introduction 86
4.2 UV Curing Apparatus 87
4.3 Evaluation of T_g and FTIR 89
4.4 *C. albicans* Polymer Anti-Attachment and Toxicity 91
4.5 Issues with PEGMA Swelling Influence the Results Observed 95
4.6 Printing Trials 97
4.7 High Throughput Screening (HTS) Method – Viscosity and Surface Tension 101
4.8 Inkjet Printing Results & Regression Analysis of Moulded & Printed Samples ... 103
4.9 Fungal Anti-Attachment of Inkjet-Printed Polymers 109
4.10 SLA Printing Demonstration 111
4.11 Summary 112

Chapter 5: Fungal-Resistant Copolymers 115
5.1 Introduction 115
5.2 Copolymer Matrix Plan 116
5.3 Fungal Anti-Attachment Studies 119
5.4 HTS Viscosity & Surface Tension for Z Parameter 123

5.5 Polymer & Residue Toxicity 126
5.6 Glass Transition Temperature (T_g) of Copolymers 133
5.7 FTIR and Raman Analysis 135
5.8 Time-of-Flight Secondary Ion Mass Spectrometry (ToF-SIMS) 138
5.9 Copolymer Ratio Studies with Proton Nuclear Magnetic Resonance (^{1}H NMR) .. 143
5.10 Summary 148

Chapter 6: Formulations & Applications 150
6.1 Introduction 150
6.2 Inkjet Printing Trial for Selected Copolymers 151
6.3 Evaluating Different TEGMA:AODMBA Ratio 153
6.4 Processing TEGMA:AODMBA$_{40:60}$ with Inkjet Printing and Dip Coating 164
6.5 Fungal Anti-Attachment of Inkjet-Printed & Dip-Coated Samples 165
6.6 Other Evaluations of Printed TEGMA:AODMBA$_{40:60}$ 168
6.7 Ways to Improve Printing Resolution of TEGMA:AODMBA$_{50:50}$ 172
6.7.1 Usage of TEGMA Oligomers 175
6.7.2 Hyperbranched Polymers as Additives 176
6.7.3 Use of Acrylate Monomers 179
6.8 Summary 180

Chapter 7: Conclusion & Future Work 182
7.1 Conclusion 182
7.2 Recommendation for Future Work 185

References 188

Appendix 199
Appendix 1. Differential Scanning Calorimetry (DSC) Thermogram 199
Appendix 2. Fourier-Transform Infrared Spectroscopy (FTIR) Data 201
Appendix 3. Statistical Analysis (ANOVA) 203

Appendix 4. Raman Spectroscopy Data (CLS Images) …….. 207
Appendix 5. Gel Permeation Chromatography (GPC) Peak Analysis Results …….. 209
Appendix 6. Gel Permeation Chromatography (GPC) Chromatogram …….. 214
Appendix 7. Time-of-Flight Secondary Ion Mass Spectrometry (ToF-SIMS) ……. 222
Appendix 8. Nuclear Magnetic Resonance (NMR) …….. 225
Appendix 9. Fungal Attachment Studies for Copolymers …… 228

List of Tables

Table No.	Description	Page
Table 1.1	Examples of medical devices are listed according to their classifications.	3
Table 1.2	Estimated number of procedures and the percentage infection rate in the US each year based on the first-time insertion of a medical device.[18]	5
Table 2.1	Implantable devices are susceptible to the formation of *C. albicans* biofilm and their impact to patients.[42]	16
Table 2.2	Summary table of all the strategies to prevent *C. albicans* biofilm on medical device in section 2.3. (CFU = colony forming unit).	31 - 33
Table 2.3	Providing an overview of the different photocuring AM techniques.[165]	49
Table 2.4	FDA cleared 3D printed biomaterial applications.[2]	53
Table 3.1	GHS classification of monomers and DMPA initiator evaluated from their MSDS document.	64
Table 4.1	Summary of T_g values for the nine polymer samples synthesised using the standalone UV apparatus. Literature values of available polymers were also shared (for polymers where T_g data was not found, N/A signifying “not available” was indicated). DOC measurement of the polymer prepared with UV apparatus was also repeatedly checked for an average of 3 times, n= 3.	91
Table 4.2	Visual observation of printed polymer using 1 % DMPA initiator.	98
Table 4.3	FTIR measurement of moulded polymers with 1 % initiator compared against polymers with 4 % initiator.	99
Table 4.4	Below shows a summary of the significance of improvement from increasing initiator percentage. Therefore, the decision was made to perform the rest of the evaluations and printing test from subsection 4.8 onwards with 4 % DMPA.	101
Table 4.5	The density of monomers as provided by supplier, mean viscosity from an average of 3 measurements, average surface tension with an average of three measurements. Z parameters were tabulated with equation 3.4 found in chapter 3, section 3.3.2.	102
Table 4.6	An overview of the visual observation for the monomers showed that 5/8 monomers could be printed with 4 % DMPA.	103
Table 4.7	Printing parameters and images for TBCHMA and TBCHA.	106
Table 4.8	Summary of fungal and inkjet printing performance.	113
Table 5.1	Low T_g material in the negative range.	117
Table 5.2	Higher T_g material in the positive range.	117
Table 5.3	Summary of copolymers produced with either 1% or 4% initiator that gave *C. albicans* attachment below 25 % in fungal anti-attachment tests. Highlighted in yellow are results that gave more than 25% attachment when 4% DMPA initiator was used. Measurement n=3.	121
Table 5.4	Three repeats of viscosity and three repeats of surface tension for the 19 copolymer candidates (4% initiator) with low fungal attachment.	124

Table 5.5	The density of co-monomers and the tabulated Z parameters for all 19 co-monomer/ polymer candidates.	125
Table 5.6	Summary of estimated T_g.	133 - 134
Table 5.7	Summary of DOC for selected copolymers of TEGMA:AODMBA and TEGMA:TBCHA (both with 4 % DMPA initiator) measured with both FTIR (one measurement) and Raman spectroscopy (average of three measurements).	136
Table 5.8	CLS scores of TEGMA:AODMBA copolymers in three different ratios.	138
Table 5.9	CLS scores of TEGMA:TBCHA copolymers in three different ratios.	138
Table 5.10	The molar ratio of TEGMA:TBCHA in different ratios tabulated from integral from NMR measurement.	144
Table 6.1	Summary of the GPC (results and chromatogram in Appendix 5. and Appendix 6.0) and 1H NMR data AODMBA (spectrum in Appendix 8.) measured for TEGMA:AODMBA with different ratios.	156
Table 6.2	Raw data of fungal attachment with crystal violet was tested by UV spectrophotometry at 600 nm. Values shown are OD600 for dissolved crystal violet. Triplicate data with mean value in the last row (highlighted in bold).	168
Table 6.3	Comparing NMR data of TEGMA:AODMBA ratio prepared by thermally synthesised, inkjet printing and HTS UV apparatus cured.	169
Table 6.4	Comparing Raman data of TEGMA:$AODMBA_{40:60}$ prepared by HTS and inkjet printing.	171

List of Figures

Figure No.	Description	Page
Figure 1.1	Medical device classification according to its regulatory requirements from WHO, 2017.	3
Figure 2.1	Example of fungal nail infection.[46]	12
Figure 2.2	Immunodeficient patients and patients using medical devices are at increased risk of getting infected with candidiasis or in many situations an overlap of both concerns is possible. (Information gathered from Nobile et al.[53] and Ramage et al.[54])	13
Figure 2.3	Biofilm formation stages of *Candida* spp.	15
Figure 2.4	Blom–Singer Classic indwelling voice prosthesis before and after usage for three months.[68]	18
Figure 2.5	Macroscopic biofilm formed on a urinary catheter.[90]	20
Figure 2.6	Type 3 denture stomatitis.[97]	22
Figure 2.7	Several potential problems arising from fungi pathogens and antifungal drugs are gathered from section 2.3.	23
Figure 2.8	CLSM images of *C. albicans* tagged with fluorescence (a) positive control, (b) denture base resin with 1 % Ag NP, (c) denture base resin with 2 % Ag NP, (d) denture base resin with 3 % Ag NP, (d) denture base resin with 5 % Ag NP showing a reduction of filamentous *C. albicans* hyphae with increasing Ag NP content.[102]	25
Figure 2.9	HPLC analysis of the daily release of clotrimazole for 60 days.[83]	28
Figure 2.10	Attachment of *C. albicans* biofilm on AODMBA (3D printed part was placed in a vacuum oven for 7 days, and rinsed in both water and IPA prior to evaluation) when compared to control (PDMS) after 48 hours.[34]	30
Figure 2.11	Key steps of dip coating.[119]	34
Figure 2.12	Formation of wet film at different points.[120]	35
Figure 2.13	Three main key antimicrobial approaches.[117]	37
Figure 2.14	How RepelaCOAT works.[145]	40
Figure 2.15	A typical process of designing a product for AM.[151]	42
Figure 2.16	Several advantages of AM process are summarised in section 2.7.	44
Figure 2.17	Key AM technologies.[157]	45
Figure 2.18	(Left) Schematic of SLA process. (Right) Schematic of DLP process.	47
Figure 2.19	Inkjet printing process.	48
Figure 2.20	Radical polymerisation steps – radical formation, initiation, propagation and termination.[168]	51
Figure 2.21	Vanillin diacrylate-based formula printed with direct laser writing setup.	58
Figure 3.1	Schematic overview of the different stages of work in this thesis and the key experimental setup used.	62
Figure 3.2	The nine monomer candidates were selected to demonstrate the effectiveness of the high throughput (HTS) methodology.	63
Figure 3.3	Ultrasonic cleaner (40kHz frequency, heating power 100W and ultrasonic power 100W) was used to dissolve the initiator into a monomer.	65

Figure 3.4	Microlab STARlet from Hamilton company designed for auto pipetting (Adapted from the company's product catalogue).[192]	66
Figure 3.5	Detail components of the liquid handling apparatus setup.[192]	66
Figure 3.6	Four pipette channel dispensing into well plate, followed by UV curing of the whole 96-well plate to obtain cast polymer.	67
Figure 3.7	FTIR equipment with ATR setup for direct measurement of DOC.	70
Figure 3.8	The sample chamber of DSC where samples were placed in platinum holders above the heating furnace.[193]	71
Figure 3.9	*C. albicans* was inoculated overnight in YPD broth and was later transferred to RPMI medium to be used in well plates for XTT assay. Evaluation of fungal attachment to polymers (coated/ placed in well plates) was carried out for 24 hours. After placement of *C. albicans* for 2 hours, non-attached *C. albicans* were washed away and the attached cells were left to grow for 24 hours. This allows for the evaluation of fungal attachment to polymers.	73
Figure 3.10	HORIBA LabRAM HR Raman microscope evaluates copolymer ratio by providing details of chemical structure.	75
Figure 3.11	Engineering drawing of Dimatix printer and its key component.[195]	79
Figure 3.12	Zoom in detail of the moving printing unit for inkjet cartridge installation.[195]	80
Figure 3.13	(Left) 3 mm disc-shape pattern used for both DOC and studies using 96 well plate, (Middle) 19 mm voice prosthesis flap design, (Right) 2 mm x 2 mm porous design for µSLA.	81
Figure 3.14	Dip coating unit setup with a needle to secure silicone rubber flap prior to dipping into copolymer solution.	85
Figure 4.1	Schematic showing a summary of HTS methodology using a liquid handling apparatus, differential scanning calorimetry (DSC), Fourier-transform infrared spectroscopy (FTIR), and XTT assay for fungal resistance and polymer toxicity evaluation.	87
Figure 4.2	DSC thermogram of AODMBA, half extrapolated from the onset of Cp. AODMBA has Tg at 80.3 °C which was demonstrated by a rigid AODMBA at room temperature.	89
Figure 4.3	DSC thermogram of TEGMA, half extrapolated from the onset of C_p. TEGMA has a very low T_g and is gel-like at room temperature.	89
Figure 4.4	A plot of XTT assay data showing the level of *C. albicans* colonisation on the polymer after 24 hours, PEGDA being included as a known positive control. Mean value based on three measurements, n = 3.	92
Figure 4.5	A plot of the polymer toxicity data defining the quantity of viable cells after 24 hours in contact with the polymer surface.	94
Figure 4.6	PEGMA (Left) After vacuuming and washing process with IPA and SDW. (Right) After completion of XTT assay, the top medium showed a weak presence of *C. albicans* with a strong signal below the swollen polymer.	96
Figure 4.7	Schematic to show the settling of medium and growth of *C. albicans* at the bottom of the well which was not observed at the top of swollen PEGMA polymer.	96

Figure 4.8	TEGMA polymer with 1 % and 4 % DMPA initiator. DOC presented in interval plot, a difference of p-value = 0.002 was found. Average of three measurements for each DMPA %.	100
Figure 4.9	TBCHA polymer with 1 % and 4 % DMPA initiator. DOC presented in interval plot, a difference of p-value = 0.026 was found. Average of three measurements for each DMPA %.	100
Figure 4.10	Comparison of the DOC of polymers printed with both 1 % and 4 % DMPA.	104
Figure 4.11	Comparison of the DOC of polymers moulded with 1 % DMPA, moulded with 4 % DMPA and printed with 4 % DMPA.	107
Figure 4.12	Comparison of the DOC of polymers moulded with 1 % DMPA, moulded with 4 % DMPA and printed with 4 % DMPA.	108
Figure 4.13	XTT assay data to determine the inherent *C. albicans* resistance of the printed disc-shape structures as compared to silicone rubber. Average measurement of three replicates was used.	109
Figure 4.14	Toxicity data for the three printed homopolymers. Average of three replicates were used.	110
Figure 4.15	Schematic design for SLA to determine resolution based on the printing outcome of its pore-like structure	111
Figure 4.16	TBCHMA with 1 % initiator on the leftmost image, rightmost image with initiator increased to 3 % and addition of curcumin. The printed layer showed some improvement in its resolution.	112
Figure 5.1	Schematic of the workflow for chapter 5.	116
Figure 5.2	Copolymer matrix with DEGMA and TEGMA as primary monomers mixed with co-monomers with higher T_g in three different ratios – 75:25, 50:50, 25:75. Total of 30 copolymer types in the matrix were mixed and 120 wells were filled (four repeats were required for fungal attachment assessment).	118
Figure 5.3	Copolymer matrix prepared with 1 % DMPA with DEGMA (Right) and TEGMA (Left) as primary monomers with AODMBA in different ratios. The attachment was greatly reduced when the copolymer has at least 50 % TEGMA or DEGMA.	120
Figure 5.4	Anti-attachment results of TEGMA:TBCHMA with 1 % initiator compared to TEGMA:TBCHMA with 4 % initiator. The ratio of 25:75 fell out of the targeted range with 4 % DMPA.	122
Figure 5.5	(Left) Anti-attachment results of TEGMA:IBMA with 1 % initiator compared to (Right) TEGMA:IBMA with 4 %. Ratio of 25:75 falling out of the targeted range in 4 % DMPA.	123
Figure 5.6	(a-e) TEGMA-based copolymer residue and polymer toxicity results.	127 – 128
Figure 5.7	(a-e) DEGMA-based copolymer residue and polymer toxicity results. residue and polymer toxicity results.	129 - 130
Figure 5.8	Main effects plot of polymer toxicity result considering varying factors – primary polymer type, secondary polymer type, primary polymer ratio and acrylate/ methacrylate type secondary polymer.	131

Figure 5.9	Main effects plot of residue toxicity result considering varying factors – primary polymer type, secondary polymer type, primary polymer ratio and acrylate/ methacrylate type secondary polymer.	132
Figure 5.10	TEGMA is represented by red, AODMBA is represented by blue and TBCHA is represented by green. (top) TEGMA:AODMBA$_{50:50}$, (bottom)TEGMA:TBCHA$_{50:50}$.	137
Figure 5.11	ToF-SIMS spectrum of TEGMA shows mass data in the range of 50 – 100 m/z. A $C_3H_7O^+$ peak is seen at 59.08 m/z and a $C_5H_7^+$ peak at 67.07 m/z.	139
Figure 5.12	ToF-SIMS spectrum of TBCHA shows mass data in the range of 50 – 100 m/z. 77.05 m/z for $C_3H_9O^{2+}$ fragment is more significant in TBCHA than TEGMA.	139
Figure 5.13	ToF-SIMS spectrum of AODMBA shows a prominent peak of $C_4H_9^+$ at 57.08 m/z.	140
Figure 5.14	ToF-SIMS spectrum of three TEGMA:TBCHA copolymers showing spectrum in the range of 70 – 80 m/z. $C_3H_9O^{2+}$ fragment is highlighted in the green box.	140
Figure 5.15	$C_5H_7^+$ TEGMA fragments in different TEGMA:TBCHA ratios.	141
Figure 5.16	$C_3H_9O^{2+}$ TBCHA fragments in the three different TEGMA:TBCHA ratios.	141
Figure 5.17	$C_3H_7O^+$ TEGMA fragments in different TEGMA:AODMBA ratios.	142
Figure 5.18	$C_4H_9^+$ AODMBA fragments in different TEGMA:AODMBA ratios.	143
Figure 5.19	TEGMA:TBCHA$_{25:75}$, where the integral of TEGMA was set as 1 and TBCHA was found to have an integral of 10 in correlation.	145
Figure 5.20	^{1}H NMR of TEGMA:TBCHA$_{50:50}$, where the integral of TEGMA was set as 1 and TBCHA was found to have an integral of 3.43 in correlation.	146
Figure 5.21	^{1}H NMR of TEGMA:TBCHA$_{75:25}$, where the integral of TEGMA was set as 1 and TBCHA was found to have an integral of 1.31 in correlation.	147
Figure 6.1	Overview of work performed for chapter 6.	151
Figure 6.2	Schematic top view design of the printed parts used for this chapter.	152
Figure 6.3	(From Left to Right) Printed TEGMA:AODMBA$_{50:50}$ in disc shapes to be fitted into a 96-well plate, TEGMA:AODMBA$_{50:50}$ in the shape of a voice prosthesis flap, TEGMA:AODMBA$_{50:50}$ creeping after storage for a few days.	154
Figure 6.4	Fungal attachment to TEGMA:AODMBA in various ratios between 30:70 to 50:50. Measurement was taken in triplicates, n =3.	156
Figure 6.5	^{1}H NMR spectrum of thermally synthesised TEGMA:AODMBA$_{40:60}$. AODMBA 1H peak visible at 5.35 ppm and TEGMA 3H peak at 3.39 ppm.	158
Figure 6.6	^{1}H NMR spectrum of HTS UV-cured TEGMA:AODMBA$_{40:60}$. AODMBA 1H peak visible at 5.35 ppm and TEGMA 3H peak at 3.39 ppm.	159
Figure 6.7	DSC of thermally synthesised TEGMA:AODMBA$_{50:50}$.	160
Figure 6.8	DSC of UV-cured TEGMA:AODMBA$_{50:50}$.	160
Figure 6.9	DSC of TEGMA:AODMBA$_{40:60}$ prepared via inkjet printing.	162
Figure 6.10	DSC of TEGMA:AODMBA$_{40:60}$ prepared thermally via radical polymerisation.	162

Figure 6.11	(Left) Silicone rubber voice prosthesis flap, (Right) Dip coated voice prosthesis flap.	163
Figure 6.12	Inkjet-printed TEGMA:AODMBA$_{40:60}$.	164
Figure 6.13	TEGMA:AODMBA$_{40:60}$ copolymer printed voice prosthesis (top sample), AODMBA homopolymer printed voice prosthesis (bottom sample).	164
Figure 6.14	Fungal assessment for inkjet-printed samples.	165
Figure 6.15	From Left to Right – PDMS, dip-coated TEGMA:AODMBA$_{40:60}$, inkjet-printed AODMBA and inkjet-printed TEGMA:AODBMA$_{40:60}$ voice prosthesis flaps (three replicates of each material type were placed in each column).	167
Figure 6.16	^{1}H NMR spectrum of inkjet-printed TEGMA:AODMBA$_{40:60}$. AODMBA 1H peak visible at 5.35 ppm and TEGMA 3H peak at 3.39 ppm.	170
Figure 6.17	Chromatogram and peak analysis from GPC.	172
Figure 6.18	TEGMA:AODMBA$_{50:50}$, (Left) after removing the printed sample from the printer. (Right) after samples were stored for a few days.	173
Figure 6.19	(Left) “22.5” detail on the AODMBA printed voice prosthesis flap, (Right) Vague “22.5” detail on the TEGMA:AODMBA$_{40:60}$ printed voice prosthesis flap.	173
Figure 6.20	Potential ways to improve the reactivity of TEGMA:AODMBA$_{50:50}$.	174
Figure 6.21	(Left) AODMBA with good printing resolution as a comparison. (Right) TEGMA(oligomer):AODMBA$_{50:50}$ showed little improvement, a vertical protruding design was captured unlike TEGMA(monomer):AODMBA$_{50:50}$.	176
Figure 6.22	Schematic of hyperbranched polymer.[209]	177
Figure 6.23	Voice prosthesis flap of TEGMA:AODMBA$_{50:50}$ with 10 % HBP-TPGDA.	178
Figure 6.24	Printing resolution of detail “22.5” in formulation with HPB-TPGDA as additive.	178
Figure 6.25	(Left) DEGEEA chemical structure, (Right) DEGMA chemical structure.	179
Figure 6.26	(Left) AODMBA homopolymer printed, (Middle)TEGMA:AODMBA$_{50:50}$ and (Right) DEGEEA:AODMBA$_{50:50}$ inkjet-printed.	180

Nomenclature

Symbols	Description (units)
T_g	Glass transition temperature (°C)
CO_2	Carbon dioxide
O_2	Oxygen
N_2	Nitrogen
η/μ	Dynamic viscosity (mPa.s)
U_0	Withdrawal speed (mm/s)
ηU_0	Viscous drag
ρ	Density (kg/m^3)
g	Acceleration of gravity (m/s^2)
γ_{LV}	Liquid-Vapour surface tension
γ	Surface tension
r	Nozzle diameter (mm)
Z	Fromm's Z parameter
TiO_2	Titanium dioxide
Q	Volumetric flowrate (m^3/s)
Rt	Radius (mm)
Θ	Contact angle (°)
m	Droplet mass (g)
°C	Degree Celsius (°C)
C_p	Heat Capacity (J/K)
M_n	Number Average Molecular Weight
M_w	Weight Average Molecular Weight
R^2	R squared

Abbreviations

Abbreviations	Description
AM	Additive Manufacturing
3D CAD	Three-Dimensional Computer Aided Design
WHO	World Health Organization
US	United States
USD	United States Dollar
IVD	In vitro Diagnostic Product
HTS	High Throughput Screening
DSC	Differential Scanning Calorimetry
FTIR	Fourier-Transform Infrared Spectroscopy
ToF-SIMS	Time-of-Flight Secondary Ion Mass Spectrometry
^{1}H NMR	Proton Nuclear Magnetic Resonance
XTT	XTT (2,3-Bis-(2-Methoxy-4-Nitro-5-Sulfophenyl)-2H-Tetrazolium-5-Carboxanilide)
UV	Ultraviolet
HIV	Human Immunodeficiency Virus
GI	Gastrointestinal Tract
TL	Total Laryngectomy
TEP	Tracheoesophageal Puncture
PDMS	Polydimethylsiloxane
UTI	Urinary Tract Infection
VP	Ventriculoperitoneal
CLSM	Confocal Laser Scanning Microscopy
Ag NP	Silver Nanoparticles
polyDMAEMAq	Quaternary Dimethylaminoethylmethacrylate
PEIq	Polyethylenimine
AgBr/ NPVP	Silver Bromide Nanocomposite
PMMA	Poly Methyl Methacrylate
TEM	Transmission Electron Microscopy
HPLC	High-Performance Liquid Chromatography
CFU	Colony Forming Unit
PEG	Polyethylene Glycol
QPEG	Quaternary PEG Brush Copolymer
RAFT	Reversible Addition Fragmentation Chain Transfer
SEM	Scanning Electron Microscopy
3D printing	Three-Dimensional Printing
ASTM	American Society for Testing and Material
SLA	Stereolithography
DLP	Digital Light Processing
CLIP	Continuous Liquid Interface Production
LCD	Liquid Crystal Display
MPP	Multiphoton Polymerisation
DMD	Digital Micro Mirror Device

LED	Light Emitting Diode
MJ	Material Jetting
DOD	Drop on Demand
EPOX	3,4 Epoxycyclohexane Methyl 3,4 Epoxycyclohexylcarboxylate
DGEBA	Bisphenol A Diglycidyl Ether
FDA	Food and Drug Administration
PEGT	Percutaneous Endoscopic Gastrostomy Tube
PCL	Polycaprolactone
EHD	Electrohydrodynamic
TCP	Tricalciumphosphate
PLGA	Poly Lactide-co-Glycolic Acid
CAWS	Computer-Aided Wet-Spinning
TTC	Tetrazolium Chloride Assay
AmB	Amphotericin-B
ABS	Acrylonitrile Butadiene Styrene
DOC	Degree of Conversion
HBP	Hyperbranched Polymer
TPGDA	Tripropylene Glycol Diacrylate
TEGMA	Triethylene Glycol Methyl Ether Methacrylate
PEGMA	Poly(ethylene glycol) Methacrylate
DEGMA	Di(ethylene glycol) Methyl Ether Methacrylate
PEGDA	Poly(ethylene glycol) Diacrylate
AODMBA	(R)-α-Acryloyloxy-β,β-Dimethyl-γ-Butyrolactone
EGDPEA	Ethylene Glycol Dicyclopentenyl Ether Acrylate
TBCHA	Tert-Butylcyclohexyl Acrylate
TBCHMA	4-Tert-Butylcyclohexyl Methacrylate
GHS	Globally Harmonized System
MSDS	Material Safety Data Sheet
DMPA	2,2-Dimethoxy-2-Phenylacetophenone
IPA	Isopropanol
SDW	Sterile Distilled Water
RPMI 1640	Roswell Park Memorial Institute 1640
YPD	Yeast Extract-Peptone-Dextrose
PBS	Phosphate-Buffer Saline
CCD	Charge Coupled Device
CLS	Classic Least Squares
GPC	Gel Permeation Chromatography
PDI	Polydispersity Index
PTFE	Polytetrafluoroethylene
PFA	Perfluoroalkoxy
CCTP	Catalytic Chain Transfer Polymerisation
AIBN	2,2’-Azobis(2-methylpropionitrile)
ANOVA	Analysis of Variance

Chapter 1: Introduction

Additive manufacturing (AM) or 3D printing is an advanced manufacturing technique for the direct fabrication of products depositing material layer by layer with a generated three-dimensional Computer Aided Design (3D CAD) file.[1] It is a promising technology with great potential for several industries, one of them being the manufacturing of biomedical devices for the healthcare industry.[2–4] The use of AM process for biomedical device manufacturing provides several advantages as compared to conventional methods. The method allows medical devices to be customisable according to specific patient's therapy requirement, allows the development of new prospective designs with complex geometry that cannot be produced by other manufacturing methods and also improve inventory management of medical devices, so that product will only be manufactured as required.[5]

Every year fungal infections kill more than 1.5 million people,[6] *Candida albicans* (*C. albicans*) is one of the most common fungal species and is frequently found in invasive bloodstream infections which could occur in immunocompromised patients and/ or patients with medical implants.[7,8] On medical devices, these fungi would easily adhere to its surface, quickly developed into biofilm and begin dispersing into the bloodstream triggering infection.[9] The onset of such occurrence would lead to several consequences such as malfunctioning of the implant, a requirement for surgery to remove the implant or in the worst case scenario, death.

While there is a wide range of potential applications for AM biomedical devices, the availability of fungal-resistant materials is extremely limited.[10] In order to address the limitations and challenges, we propose the use of high-throughput screening (HTS) methodology that can quickly and effectively provide a general overview of potential fungal anti-attachment polymers suitable for AM. In this work, we focus specifically on ultraviolet (UV) curing monomers for inkjet printing technique which allows a good printing resolution while using a small quantity of materials within its cartridge. The HTS could also be suitable for the development of any UV curing formulations for other UV AM techniques such as stereolithography (SLA) and multiphoton Polymerisation (MPP).

1.1 Medical Devices

According to World Health Organization (WHO), a medical device is any instrument, apparatus, implement, machine, appliance, implant, reagent for in vitro use, software, material or other similar article, intended by the manufacturer to be used, alone or in combination, for human beings, for one or more specific medical purpose.[11]

Medical devices can range from a device as straightforward as hypodermic needles, tongue depressors, wheelchairs, and stethoscopes to implants such as pacemakers and cochlear implants, in Table 1.1 examples of the medical devices are listed alongside their classifications. The classification terminology depends on the health regulatory board of each country, but they are broken down into four main classes – A, B, C, and D according to their health risk factor. Figure 1.1 depicts the device class according to its regulatory requirement based on the risk factors.

Table 1.1: *Examples of medical devices listed according to their classifications.*[12] [13] [14] [15]

Class	A	B	C	D
Examples				
	Stethoscopes [2]	*Surgical Gloves* [3]	*Neonatal Incubator* [4]	*Cardiac Pacemaker* [5]

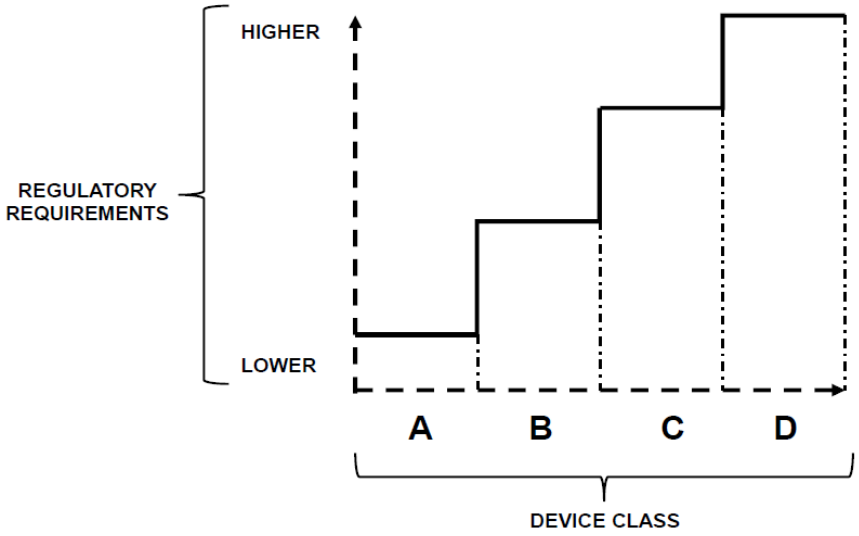


Figure 1.1: *Medical device classification according to its regulatory requirements from WHO, 2017.*

WHO has determined that the classification of all medical devices (excluding in vitro diagnostic product, IVD) depend on the following criteria such as to whether it:

- is life-supporting or sustaining
- is invasive – and for how long
- incorporates medicine
- incorporates human or animal cells

- is an active medical device
- is used with another medical device
- is used by users with technical, scientific and medical expertise.[11]

With the advancement of medical technology to improve quality of life, increase in human lifespan and growth in the ageing population worldwide, [16] increase in usage of medical devices would be expected. Market analysis has forecasted that the compound annual growth rate of medical devices would increase steadily at an average rate of 5.2 % reaching nearly USD 800 million by 2030.[17] Hence continuous improvement in medical devices would be required to meet these healthcare demands while minimising infection risks.

1.2 Device-Associated Infections

Infections are a major concern in medical device application, this is especially concerning for patients requiring the use of indwelling devices which reside within the human host. The large number of indwelling medical devices being used within the United States (US) can be found in Table 1.2; it is worth noting that these numbers only consider first-time insertion of the device as reported in 2001. The number may have since increased with the upsurge in demand as forecasted by market analysis.

As shown in Table 1.2, alongside the estimated number of inserted devices are the infection rate of each device type and its mortality risk, bladder catheters have the highest estimated annual procedure with relatively low mortality risk while cardiovascular devices have an understandably much higher mortality rate. [18] A more recent statistic from a rural hospital in India also shares that 10,621 out of 13,456 patients with medical devices have urinary catheters inserted. 36 of the patients have *Candida*-caused infection.[19] Apart from

the risk of mortality, psychological impairment, morbidity rate and cost impact on the healthcare system are concerns that should not be overlooked. [20–22] In one study which looks into the cost impact of bacteria *Staphylococcus aureus* (*S. aureus*), infection related to prostheses found that the average cost incurred by a hospitalised patient with prosthetic device infection ranges from USD 40,000 – USD 70,000.[23] In a 2004 review article by Kojic and Darouiche, a consolidated table of various sources suggest a cost ranging between USD 15,000 – USD 50,000 on the full treatment of device triggered infection. The same review article also mentioned that 50 % of the healthcare-associated infections, about 1 million cases in the US were caused by indwelling devices,[24] this amounts to a huge financial burden to both patients and healthcare.

Table 1.2: *Estimated number of procedures and the percentage infection rate in the US each year based on the first-time insertion of a medical device.*[18]

Implant	Estimated annual procedures in the US	Percentage infection rate	Attributable mortality[a]
Bladder catheters[b]	>30,000,000	10–30	Low
Central venous catheter[b,c]	5,000,000	3–8	Moderate
Fracture fixation device[b]	2,000,000	5–10	Low
Dental implants[d]	1,000,000	5–10	Low
Joint prostheses[b]	600,000	1–3	Low
Vascular grafts[b]	450,000	1–5	Moderate
Cardiac pacemakers[b,d]	300,000	1–7	Moderate
Mammary implants (pairs)[e]	130,000	1–2	Low
Mechanical heart valves[d]	85,000	1–3	High
Penile implants[b,d]	15,000	1–3	Low
Heart assisted devices[d]	700	25–50	High

Notes
[a] Semiquantitative scale for attributable mortality: low, <5%; moderate, 5–25%; high, >25%.
[b] Numbers estimated by analysis of market reports.
[c] Numbers estimated by review of the medical literature.
[d] Numbers estimated by personal communication with personnel from device-manufacturing companies.
[e] Numbers estimated by review of data provided by medical associations.
Source: Darouiche, 2001.

Microbials such as bacteria and fungi can easily be introduced by the microbial flora within the host inhabiting the human skin, nails, eyes, oropharynx, genitalia, and gastrointestinal tract (GI).[25] Such infections are a result of these microorganisms colonising the device

surface leading to a complex process that eventually produces biofilm. These biofilms can cause device malfunction such as loosening of devices or blockage of valves.[26]

Biofilm is defined as a microorganism community adhered to a surface in a matrix typically described as slime-like due to the formation of extracellular polymeric substances.[27] The first biofilm studied was dental plaque where Dutch scientist Leeuwenhoek scraped white matter between his teeth and observed it under a microscope. He reported “many living animals, which moved very prettily” also known as the bacteria.[28]

Upon implantation of a device, healing requires host cells to colonise the device's surface. However, the microorganisms present will compete with host cells for colonisation.[26] Biofilm formation begins when microorganisms successfully attach themselves to the surface and adhere to one another. Biofilm can also be made up of both single and multi-species microorganisms.

When biofilm reaches the maturation stage, an extracellular matrix consisting of polysaccharides, nucleic acids and proteins is produced as a result. With the protection of such a matrix, biofilms become significantly more resistant to an immune system component and antimicrobial drugs as compared to their planktonic counterparts.[29,30]

Device type, its surface morphology and its surrounding environment could affect the type of biofilm formation and infection development. Surface properties of the device such as its hydrophilicity, roughness, water contact angle measurement, biomaterial stability and porosity have been reported to be important considerations.[26,27] One of the earliest demonstrations of microorganism growth on a foreign object was performed by Elek and Conen. The work shared that the presence of foreign body sutures on human volunteers would significantly increase the number of bacteria, *Streptococcus pyogenes* infection.[31]

While both bacteria and fungi could trigger device-associated infection, fungi have been the least studied microorganism of the two. As discussed in Rodrigues and Nosanchuk's recent viewpoint article, the financial support for fungal disease research is especially low when compared to other infectious diseases.[21] Also, at the point of time when this was written, a search for fungal-resistant polymeric additive manufacturing (AM) material yielded a very limited number of articles [32–34] whereas bacterial-resistant material in a similar context has been studied more extensively as discussed in a review paper by González-Henríquez et. al.[35]

That said, the impact of fungi is proven by the large number of medical devices affected by just one single fungi species, *C. albicans*. The development of antifungal drugs has also been limited as both fungi and humans have eukaryotic cells, which means molecules toxic to fungi can also be toxic to humans.[21,36] Therefore, the discovery of fungal anti-attachment material would be beneficial to further understanding the characteristic of *C. albicans* and would also allow usage of these materials to be considered for medical devices prone to *C. albicans* attachment.

1.3 Aim & Objectives

This research project aims to develop novel bio-functional materials that exhibit *C. albicans* anti-attachment. These materials can potentially be used in AM formulation, or they can also be applied directly as an antifouling coating on biomedical devices using a dip coating process. The following objectives were identified for this work:

- To conduct a comprehensive review on medical devices *prone to C. albicans*, *C. albicans* resistant polymers and their processing methodology

- To establish a high throughput screening (HTS) methodology for preparing and identifying *C. albicans* anti-attachment UV curable homo/ copolymers
- To prepare a library of *C. albicans* anti-attachment copolymers with a wide range of glass transition temperatures (T_g) suitable for various potential applications
- To demonstrate the use of a selected copolymer by manufacturing *C. albicans* anti-attachment flexible voice prosthesis flap with suitable formulation using dip coating and inkjet printing.
- To study and suggest formulation adjustments for improving the inkjet printing process of the selected copolymer.

1.4 Project Methodology

HTS will be developed and used for effective preparation and screening of several UV curing polymers for their *C. albicans* attachment properties, toxicity, viscosity, and surface tension. This allows more efficient output at a much shorter time than before if polymers were to be prepared and tested individually. Using a liquid handling apparatus (liquid handler) several types of curable resin formulation would be deposited on 96 wells microtiter plates (96-well plates). Upon deposition, the monomers would undergo UV curing and form polymers, post-processing steps are required to remove free monomers/ residues that could affect the result. Quantitative analysis by evaluating the metabolic activity of cells with XTT will be used to determine the fungi's response to the material. From the screening process, a handful of methacrylates and acrylates would be further evaluated for their suitability for dip coating and AM process.

1.5 Thesis Structure

The thesis is divided into 7 chapters and an overview of the thesis content is described below:

Chapter 1 Introduction provides a brief explanation of what is a medical device and how it could cause infection in patients. Following that, a step-by-step approach plan to carry out the desired aims and objectives was provided.

Chapter 2: Literature Review focuses on the specific microorganisms – *C. albicans* fungi that were investigated for this research thesis. Comprehensive information on the targeted medical device would be provided, and suitable manufacturing process methods would also be reviewed. Lastly, previous works directly related to the thesis and the gaps to be filled in the present work would be discussed.

Chapter 3 Experimental Methods & Setup presents the various material, methods, processes, equipment, and experimental parameters used for the development of UV curable fungal-resistant inks. Protocols for all testing procedures, polymer synthesis, dip coating process, ink preparation, printing parameters and material characterization will be shown in this chapter.

Chapter 4 Development of High Throughput Screening (HTS) Methods discusses the setup of a HTS method for polymer preparation and fungal assessment. Nine potential starting monomers were selected based on earlier work.[34] Further understanding of the polymers and suitability for AM was studied with Differential Scanning Calorimetry (DSC) and Fourier-Transform Infrared Spectroscopy (FTIR).

Chapter 5 Fungal-Resistant Copolymers continues the work of chapter 4 by mixing selected homopolymers with high and low T_g to obtain a wide variety of copolymers with varying flexibility. The copolymers obtained from the matrix plan were assessed again for their *C. albicans* resistance. The chapter later discusses results obtained from XTT cell viability assay, Nuclear Magnetic Resonance (^{1}H NMR), DSC, FTIR, Time-of-Flight Secondary Ion Mass Spectrometry (ToF-SIMS) and Raman spectroscopy of selected copolymers.

Chapter 6 Formulations & Applications look at how these copolymer inks can be utilised and improved for dip coating and AM processes. The final built coupons (for insertion into 96-well plates) and medical devices would undergo fungal attachment evaluation in order to compare their results against fungal attachment performed of polymers directly coated in 96-well plates (as per chapter 5).

Chapter 7 Conclusion & Future Work draws a conclusion of the thesis based on the data and analysis performed. Recommendations on potential improvement of the research plan with the thesis outcome and future work would also be considered and discussed.

Chapter 2: Literature Review

2.1 Introduction

As the key objective of the work is the develop fungal anti-attachment polymers that can be used in additive manufacturing (AM) and applied in biomedical device applications, this literature review would provide a brief introduction to common fungi species with in-depth details of *C. albicans,* and medical devices affected by these fungi in both sections 2.2 and 2.3. Subsequently, current approaches that have been developed to prevent *C. albicans* biofilm growth are discussed in section 2.4.

Following that, in sections 2.5 and 2.7, the review discusses how these materials can be processed with both dip coating and AM being key application methods. The polymerisation process specific to UV curing AM processes would be mentioned in section 2.8. Section 2.9 will provide further insights on AM, its potential and its significant growth in biomedical applications over the years. Antimicrobial material developmental work similar to the aims of this research especially in dip coating and AM would also be discussed in section 2.6 and subsection 2.9. Lastly, the above review would be summarised, and gaps in the area of work and previously related research work would be wrapped up in section 2.10.

2.2 Fungi

Fungi are eukaryotic organisms that absorb nutrients through their cell walls and are segregated into 5 key divisions (phyla) – Chytridiomycota, Zygomycota, Glomeromycota, Ascomycota and Basidiomycota.[37] They can either be single (e.g. yeasts) or multi-celled

organisms (e.g., moulds). While some fungi species are used in mass manufacturing for foods or drugs, many fungal species have serious negative impacts on crops, food production and human health.[38] Out of an estimated number of 1.5 million fungal species, approximately 300 of them are pathogenic to humans.[39] Many of these species come from the Ascomycota division which houses very diverse species grouped by the common characteristic of producing the ascus reproductive structure. *Candida, Aspergillus* and *Cryptococcus* are three common fungal genera, some species of which can trigger potentially fatal infections in humans.[8,40,41] The following subsection 2.2.1 will briefly introduce *Candida* spp. in general. Section 2.2.2 will provide more information about *C. albicans* as it is one of the most prevalent yeast species found associated with medical devices and is selected as the focus of this research thesis.

2.2.1 The *Candida* genus

Infection with *Candida* (candidiasis) is the leading third or fourth most common cause of hospital-acquired infection.[42–44] In mild cases, candidiasis would infect the superficial layers such as the skin, nails (Figure 2.1) and genitals.[45]



Figure 2.1: *Example of fungal nail infection.*[46]

However, in severe situations, they can emerge as a global healthcare threat, such as the recently-emerged *Candida auris* (*C. auris*) which was found to be multidrug-resistant

and has caused outbreaks in various healthcare facilities.[47–49] In a case study reported by Villanueva-Lozano et al., a *C. auris* outbreak that occurred at their ICU facility recently affected twelve patients. All affected patients had implanted devices and required a prolonged hospital stay of 20 to 70 days.

Candidiasis itself becomes progressively life-threatening when it turns into candidemia where the bloodstream is infected with *Candida*. An average of 400,000 – 700,000 cases of candidemia are reported each year.[21,45] Common pathogenic *Candida* species include *C. albicans*, *C. glabrata*, *C. parapsilosis*, *C. tropicalis* and *C. krusei*.[50–52] Apart from indwelling medical devices, immunodeficient patients are the most susceptible group to acquiring candidiasis.[42] Figure 2.2 show examples of immunodeficient patients that are especially vulnerable to *Candida* infections and example of medical devices prone to *Candida* attachment.[50,53]

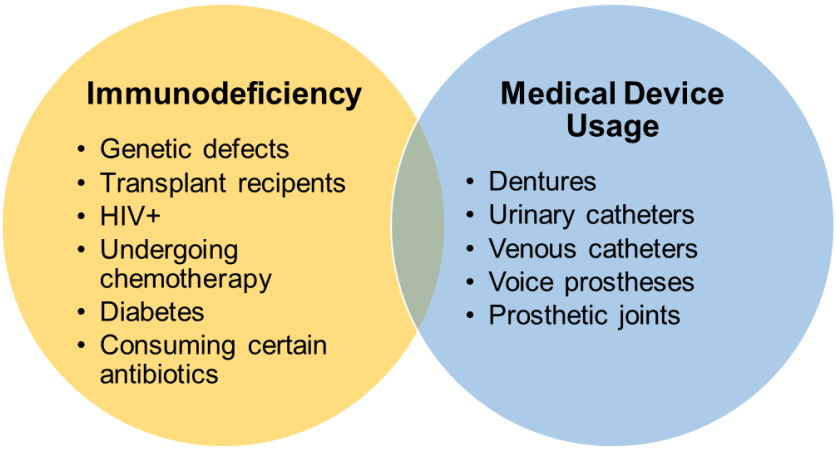


Figure 2.2: *Immunodeficient patients and patients using medical devices are at increased risk of getting infected with candidiasis or in many situations an overlap of both concerns is possible. (Information gathered from Nobile et al.[53] and Ramage et al.[54])*

After planktonic *Candida* cells gather to initiate biofilm formation on a surface, the resulting extracellular matrix, as well as activation of drug efflux pumps, contribute to

increased drug resistance, and biofilm cells can be 30 to 2000 times more resistant than planktonic cells.[8,55] There are several antifungal drugs available namely amphotericin-B (AmB), fluconazole, itraconazole and ketoconazole.[56] Factors that can affect *Candida* biofilm formation include the presence of oxygen, saliva, carbon source and device surface.[42,52] In this work, the focus would be looking specifically at *C. albicans*.

2.2.2 Candida albicans

There are several species of c*andida* yeast but *C. albicans*, an opportunistic pathogenic yeast is the most prevalent and infectious of all yeast species.[53] Recent studies in the US, Europe and China confirm that *C. albicans* remain the leading cause of invasive candidiasis.[44,57,58] While, *C. albicans* can typically be found in part of healthy commensal flora and colonises the GI, reproductive tract, oral cavity and skin of humans,[53,59] this fungus can easily transit from commensal to pathogen due to its range of virulence factors.[59,60]

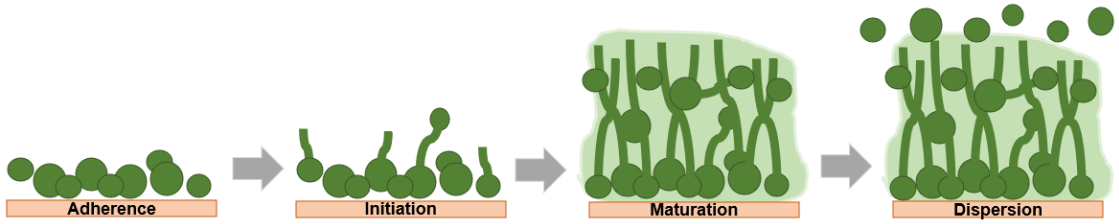


Figure 2.3: *Biofilm formation stages of Candida spp.*

As shown in Figure 2.3, biofilm formation by *C. albicans* has three developmental phases, the yeast cells first adhere to a surface, grow as a budding yeast in a *pseudo* hyphal state and undergo a further morphological transition to become filamentous form via the extension of hyphae.[43,61] Mature *Candida* biofilms contain a dense network of yeasts, hyphae, and pseudohyphae within an extracellular matrix (comprising carbohydrates,

proteins and other compounds).[9] Yeast cells can be shed from biofilms (e.g. formation on implanted medical devices) leading to further dispersion of fungal cells into organs and human tissues and potentially triggering invasive systemic infections.[59,62] Depending on the medical device and its location within the host, a device-associated infection can also cause permanent disfigurement and psychological trauma from device malfunctioning and surgery is often required to remove and/ or replace devices.[7]

The importance of fungal infection research should not be neglected.[20–22] The range of available antifungal drugs is much more limited than antibacterial, and drug-resistant fungi are becoming an increasing burden to society.[63] Several antifungal drugs are also associated with side effects in patients.[36] Furthermore, fungi are commonly found in multispecies polymicrobial biofilms through interactions with bacteria, which further complicates treatment strategies.[64,65] For example, in more than 20 % of *C. albicans* infections, *S. aureus* isolates were also detected and it was reported that both *S. aureus* and *C. albicans* become more resistant to antibacterial/ antifungal drugs when found alongside one another.[66] Therefore, preventing fungal infection would be one key to subduing wider complications.

2.3 Medical Devices susceptible to *C. albicans*

A high mortality rate is associated with serious *C. albicans* infections, ranging from 30 - 50 %,[9,59,67] and much of this can stem from device-associated candidiasis. The use of such devices in humans increases with age and in immunocompromised patients. *C. albicans* biofilms formation can arise on devices including vascular catheters, voice prostheses, dentures, cardiac devices, prosthetic joints and breast implants.[7,9,53,68–71] Table 1.1 (with reference to a review by Ramage et al.[54]) provides an overview of the risk

of infection for each device and their respective key *Candida* species. In the following sub-sections, the key medical devices susceptible *C. albicans* biofilm formation will be discussed.

Table 2.1: *Implantable devices susceptible to the formation of C. albicans biofilm and their impact on patients.*[42]

Devices	Usage per year in the US	Infection risk (%)	Main *Candida* Species
Central and peripheral venous catheters	5 million	3 to 8	*albicans, glabrata, parapsilosis*
Hemodialysis and peritoneal dialysis catheters	240,000	1 to 20	*albicans, parapsilosis*
Prosthetic joints	600,000	1 to 3	
Neurosurgical shunts	40,000	6 to 15	*albicans*
Urinary catheters	Tens of millions	10 to 30	
Breast implants	130 000	1 to 2	
Endotracheal tubes	Millions	10 to 25	*albicans, grabata*
Intracardiac prosthetic devices	400,000	1 to 3	
Dentures	>1 million	5 to 10	
Voice prostheses	Thousands	50 to 100	*albicans, tropicalis*

2.3.1 Voice Prosthesis

Voice prostheses have the highest infection risk due to the location of the device which exposes it to continuous high humidity, and flow of saliva, food and drinks causing it to be exceptionally vulnerable to microbial growth followed by the onset of fungal biofilm.[72,73] In a recent study by Pentland et al., the authors found that an increase in carbon dioxide (CO_2) from exhaled breath stimulates the yeast to hyphal switch, promoting mature biofilm

formation. This is especially critical for voice prostheses since these devices are placed in the throat environment with high CO_2 levels during exhalation.[74]

Voice prostheses are devices used to restore voice in patients with advanced laryngeal cancer. Often total laryngectomy (TL) may be a necessary measure to remove the tumours.[75] and TL would involve removal of the entire larynx consisting of the vocal fold, hyoid bone, epiglottis, thyroid, cricoid cartilage and some tracheal cartilage rings. Quality of life would be greatly impacted after TL as patients have to breathe through stoma with loss of their speech ability.

There are three voice restoration methods after TL: oesophageal speech which is a learned skill; electromechanical speech which uses an external electronic voice box; tracheoesophageal (shunt) speech which involves the use of a voice prosthesis. To date, tracheoesophageal (shunt) speech has become the most effective and preferred method for voice restoration. Tracheoesophageal (shunt) speech would require performing a tracheoesophageal puncture (TEP) between the trachea and oesophagus followed by insertion of the voice prosthesis.

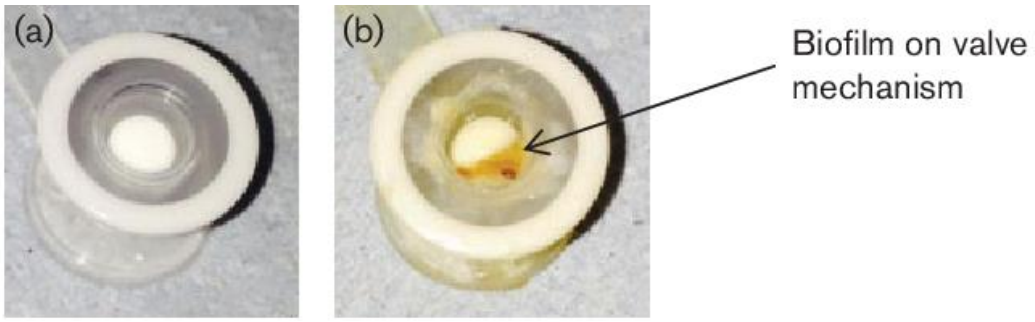


Figure 2.4: *Blom–Singer Classic indwelling voice prosthesis before and after usage for three months.*[68]

Voice prostheses used with TEP are typically made with polydimethylsiloxane (PDMS) was then developed in the 1980s by Singer and Blom. However, PDMS material itself is highly susceptible to *C. albicans*, especially when placed in a non-sterile environment.[54] Figure 2.4 obtained from a work by Talpaert et al. shows the biofilm growing on the valve of the voice prosthesis after usage for only three months. Buijssen et al. reported that 77 % of microorganisms found on 66 biofilms of used voice prosthesis are *C. albicans*. [70] *C. albicans* and *C. tropicalis* were found to be more prevalent when bacteria such as *Rothia dentocariosa* and *S. aureus* were also present. This suggests that the presence of bacteria could be influential in the growth of fungi and evidence supporting this was published by Swidergall et al. [66]

Fungi growth on voice prosthesis also increases with radiation treatment after TL, in the review with 26 patients by Miyazaki et al., radiation treatment after TL found an 81 % increase in the presence of *Candida* cells.[76] This is likely due to suppressed immunity of patients with such a radiation treatment. A recent work published in 2020 found that *Candida* spp. dominated the microorganisms found in 129 voice prostheses, with 46.5 % of them containing *C. albicans*.[77]

The growth of biofilm will eventually lead to dysfunctional voice prosthesis causing aspiration pneumonia. A detailed compilation of several case studies performed with Provox® voice prostheses showed that the lifetime of their voice prostheses can range from an average of 4 – 8 months.[78]

With the highest infection risks to fungi compared to other medical devices, various works continuously look at other ways of reducing biofilm growth associated with voice

prostheses. This may potentially be addressed either by antifungal treatment such as usage of oral wash [79] and precision antifungal treatment,[80] development of voice prosthesis maintenance methodology [81] and strategies to inhibit biofilm growth on voice prosthesis.[82–86] In this subsection, the various case studies from different sources confirm that preventing *C. albicans* growth on voice prostheses is critical to improving the wellbeing and reducing health risks for this group of patients.

2.3.2 Catheters

Several types of catheters (as mentioned in Table 2.1) are at risk of *C. albicans* colonisation. Key catheters of concern would be urinary and venous catheters. Urinary catheters have the most annual usage with tens of millions being installed within the US alone, it also has a relatively high infection risk of up to 30 %.[54] An example of biofilm growing on the urinary catheter can be found in Figure 2.5. Urinary catheters are used in patients who have urinary continence or urinary retention. Research data gathered for urinary catheter-associated urinary tract infection (UTI) evaluated 100 samples of which 26 samples presented with UTI. Among the 26 samples, *C. albicans spp*. were found in 38.47 %.[87] Another study of *Candida* bloodstream infection collected data from senior citizens in intensive care units in China. The authors found that 29 out of 294 patients were infected with candidemia and about 28.6 % were as a result of *C. albicans*.[88] Risk factors for the presence of *C. albicans* in urine often also depend on the patient's age, gender, hospitalization time and recent use of antibiotics. For critically vulnerable patients, *C. albicans* in the kidney is the main site of candidemia and may be hard to detect when asymptomatic. A careful treatment strategy has to be planned to minimise mortality rate.[89]



Figure 2.5: *Macroscopic biofilm formed on urinary catheter.*[90]

Second to urinary catheters, the second most common catheter type that is prone to *C. albicans* is the venous catheter, which has an average usage of 5 million each year.[54] Venous catheters are typically inserted into collarbones for chemotherapy, blood transfusion and to provide intravenous fluids. Here they are directly in contact with blood, which increases the risk of candidemia in patients. Several studies observed yeast cells on such catheters, Fesharaki et al. gathered information on patients from a cardiovascular hospital in Iran.[91] They reported 15 out of 223 had fungal growth, out of which 5 were *C. albicans*. A type of central venous catheter known as peripherally inserted central catheter (PICC) is frequently used in pre-mature infants that require fluids or medications. Another study in China by Zhang et al. studied 124 premature infants (21 of them had to be excluded from the study for various reasons such as death or change in catheter etc.).[92] They found that 24 premature infants out of the remaining 103 had fungal cells growing on their PICC tips. Fungal isolates were identified as *C. albicans* and *C. glabrata*. The study demonstrates a real-life mitigable risk of fungal infection in these premature infants.

In the healthcare setting, catheters play an especially important role to aid varying groups of patients, be it for urine drainage or for providing fluid and medication. Case studies have proven the frequent growth of *C. albicans* and other microorganisms which can put patients at risk of severe infection.

2.3.3 Other Devices

Several other medical devices such as dentures, prosthetic joints and neurosurgical shunts can also develop fungal biofilms. Aside from dentures, many are less frequently studied as they have lower infection risk and/ or usage. Nevertheless, it poses a different set of problems as there are no clear guidelines on treatment strategies since such infections are rarer to come by.[93] Some of these devices also require complex surgery procedures should the device require removal or replacement. Baradkar et al. studied six cases of candidiasis caused by ventriculoperitoneal (VP) shunts out of 24 infected infants, where VP shunts were used to treat hydrocephalus (build-up of fluid in the cavities within the brain). The most common isolate found was *C. albicans,* accounting for 66.6 % of isolates.[94]

Another example looking at prosthetic joints, in a rare case study of a 75-year-old woman who was twice infected due to her hip prosthesis. First with *Staphylococcus capitis* and then a secondary infection with *C. albicans*.[95] In another work by Rubino et al., they found eleven cases of *Candida* infection in prosthetic joints between 2007 – 2014 in their hospital. The record suggests these patients often have co-morbidity such as diabetes and heart disease, in one case, the patient had to have a leg amputated in order to control the spread of infection.[96]



Figure 2.6: *Type 3 denture stomatitis.*[97]

The base of a denture is in contact with gum and often has a build-up of biofilm, in many studies they were also detected to be *C. albicans*.[98,99] While dentures are removable and such occurrences can be prevented with proper oral hygiene and cleaning of dentures, biofilm formation can still occur when patients have co-morbidity such as diabetes [100] or are unable to adhere to an oral cleaning routine.[101] This eventually leads to localized infection in the mouth known as stomatitis as seen in Figure 2.6. Apart from voice prostheses and catheters, *C. albicans* are often found in other medical devices and considerations should be taken to prevent the propagation of such fungal infections.

2.4 Strategies to Prevent Formation of Fungal Biofilms

In section 2.3 the various medical devices that could be affected by *C. albicans* were discussed. It was observed that the impact of such a fungal infection can affect people from all age groups from new-born infants to the ageing population. With the mentioned concerns of biofilm formation (as summarised below in Figure 2.7), it is critical to prevent morbidity and mortality by applying antifungal strategies to these medical devices.



Figure 2.7: *Several potential problems arising from fungal pathogens and antifungal drugs are gathered from section 2.3.*

Approaches such as maintaining the cleanliness of removable medical devices are subject to non-compliance, depending on users. For indwelling devices, detection of fungal attachment can be challenging, and removal/ replacement surgery of infected devices is physiologically and financially stressful for patients. Therapy with antifungal drugs can help to treat such infections but many issues still exist – e.g., side effects, lack of treatment guidelines for certain device infections, limited antifungal drugs available in the market, increasing fungal resistance to drugs and risk of mortality still stands once an infection has taken place. In this section, the research performed on preventing such fungal attachment issues with a focus on *C. albicans* will be discussed. The advantages

and disadvantages of these strategies will also be considered, discussed, and summarised at the end of the section in Table 2.2.

With the severity of the problem, several approaches to mitigate fungal growth on medical devices have already been investigated. Metal coatings were considered, as metals such as gold can disrupt cell walls. D. Arweiler-Harbeck et al. studied gold and titanium coatings on the surface of silicone voice prostheses using anodic vacuum arc plasma deposition. However, there were challenges in producing a homogeneous coating with gold; titanium on the other hand can produce a smooth and homogeneous coating. More studies will be required to evaluate its potential and its performance over a long time usage.[84]

Another type of metal, silver, is known for its excellent antimicrobial properties. However, results have not been proven consistent and the metal's toxicity on ingestion could be a concern if the device is within or near the mouth or throat. A work performed by Li et al. studied the antifungal effect by adding silver nanoparticles to denture base acrylic resin. Reduction in *C. albicans* was found with increasing silver nanoparticles (Ag NP), as per the confocal laser scanning microscopy (CLSM) images in Figure 2.8 below.[102] In another study, silver collagen-coated vascular prosthesis significantly reduces *C. albicans* biofilm in serum-free medium but was ineffective in the presence of 50% serum. The work concluded that silver-coated vascular graft was unsuitable for the prevention of *C. albicans* growth, as serum protein affects the concentration of silver cations delivery.[103]

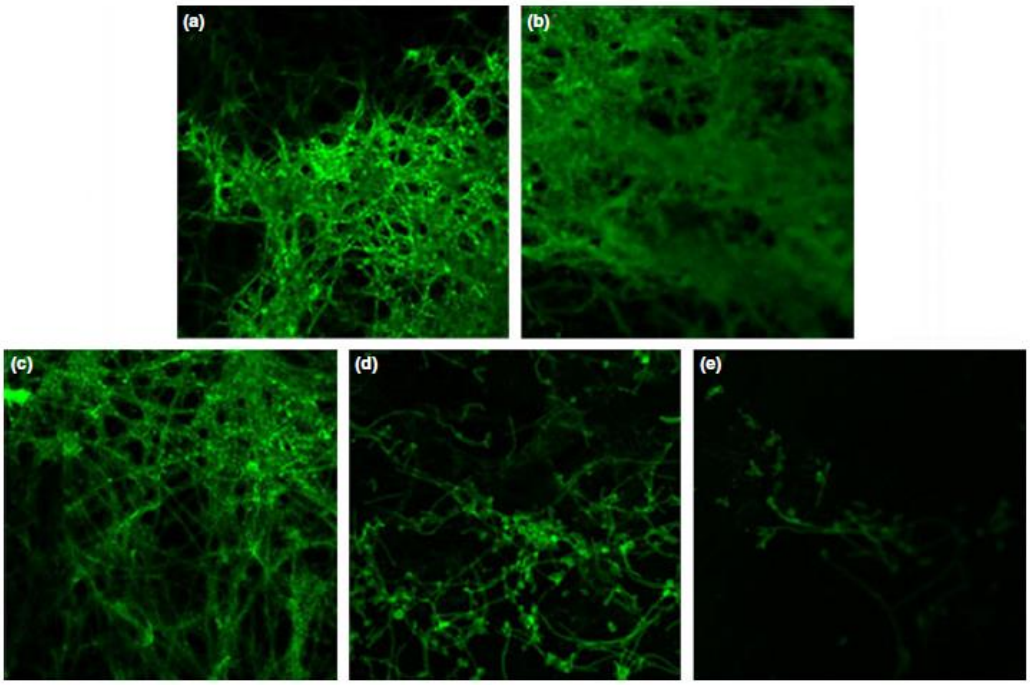


Figure 2.8: *CLSM images of C. albicans tagged with fluorescence (a) positive control, (b) denture base resin with 1 % Ag NP, (c) denture base resin with 2 % Ag NP, (d) denture base resin with 3 % Ag NP, (d) denture base resin with 5 % Ag NP showing a reduction of filamentous C. albicans hyphae with inceasing Ag NP content.*[102]

In another study, the authors compared Gendine-coated (novel antiseptic dye) urinary catheters, silver hydrogel-coated urinary catheters and uncoated catheters. The catheters were all tested in vitro and in vivo (a rabbit model), showing anti-adherence of *Candida* species only in Gendine-coated urinary catheters.[104] Silver works as an antimicrobial by disrupting cell membranes when nucleophilic sulfhydryl, hydroxyl and amino groups in proteins form bonds with the silver cation. Silver cations could also replace other positively charged ions which are important for regulating cellular functions. In the previously-mentioned work that yielded negative results with silver, the failure could be due to silver's inability to release silver cation which is vital for silver to work as an antimicrobial.[71] Clinical failure of silver nitrate hydrogel-coated catheters has also

been reported. In the report written by Selek et al., two cases of macroscopic *C. albicans* biofilm were found on these catheters (as shown above in subsection 2.2.2, Figure 2.5) when antibacterial treatment yielded no improvement.

Apart from silver itself, silver compounds have also been evaluated for inhibiting *C. albicans*. 7% of silver oxide when incorporated into silicone rubber for the flap valve of voice prostheses was proven to increase the mean lifetime of voice prostheses from 36 to 110 days. None of the 33 patients tested had any allergy or side effects due to the silver oxide. [85]

Incorporation of metal ions aside, polymers have also been frequently investigated for mitigation of *C. albicans*. Polymers with charge (i.e., cation) have also been studied for preventing *C. albicans biofilm*. Kristof De Prijck et al. described their quaternary dimethylaminoethylmethacrylate (polyDMAEMAq) and polyethylenimine (PEIq) covalently bonded to the surface of silicone rubber voice prosthesis. For polyDMAEMAq, quaternization with bromooctane worked the best; anything with longer chains such as bromohexadecane and bromooctadecane did not have any impact on resisting biofilm growth. polyDMAEMAq with quaternization agent bromooctane was able to reduce up to 92% of biofilm growth. PEIq was able to reduce *C. albicans* adhesion by 35.4 % to 74.3 % depending on the quaternization agent.[86] Another work presented by Mahmoud et al. shared two newly synthesized polymers of triphenyl phosphonium salt, a modified poly (methylmethacrylate-co-vinylbenzoylchloride) and a modified linear poly (chloroethylvinylether-co-vinylbenzoylchloride) and evaluated their capabilities in antimicrobial attachment with *C. albicans* and *C. tropicalis*. Both polymers evaluated exhibited broad antimicrobial behaviour against *the Candida spp*.[105] These polymers have

positively charged quaternary ammonium groups or phosphonium groups that were able to destroy fungi cell walls.

A paper attempted the use of both strategies with quaternary ammonium grafted silver bromide nanocomposite (AgBr/ NPVP) in poly methyl methacrylate (PMMA) denture resin. The AgBr/ NPVP was blended into PMMA powder and transmission electron microscopy (TEM) was used to show AgBr embedded within cationic NPVP. A very comprehensive set of evaluations were performed, showing that the end product was non-toxic and antifungal activity was present throughout the four weeks evaluation.[106]

The effect of plasma treatment on its own has also been assessed for its effect on suppressing *C. albicans* attachment. Argon was used as a heavy gas particle in an evaluation to understand its effect in vitro and in vivo on microbial adhesion on voice prostheses. While in vitro experiments showed a reduction in biofilm formation on the plasma-treated hydrophilized silicone rubber, in vivo tests on patients found slightly less biofilm on the original hydrophobic side of the silicone rubber than on the plasma-treated portion.[107]

Another way of preventing microbial attachment exploits the use of antifungal drugs by modifying the surface of the medical device. Several works by Coad's group looked at the usage of antifungal coatings with a focus on contact-killing mechanisms.[108–110] For example, Naderi et al. explored the covalent bonding of anidulafungin and micafungin onto glass slips and silicon wafers with plasma polymer coating. Not only was it effective in preventing *C. albicans*, it was also tested to be reusable up to at least 5 times.[109] Another work within the group from Michl et al. used a method of bioconjugating

casponfungin onto surfaces via epoxide plasma polymer. Casponfungin helps to inhibit 1,3-b-(D) glucan synthase proteins that are involved in cell wall synthesis. The surface with casponfungin could reduce *C. albicans* growth by log 6.[108] Another work looking at attaching antifungal agents to the surface used an interesting but more tedious approach. The first step was to graft glycidyl methacrylate and then immobilise ergosterol for binding with antifungal agents (natamycin, nystatin and miconazole). Miconazole did not bind with ergosterol and only the polyene types had interactions. The most favourable result was the surfaces bound with nystatin.[111]

While the incorporation of antifungal drugs has been demonstrated to be a possible route for effective fungal control on medical devices, it is also important to evaluate the release of antifungal drugs over time to prevent overdose and toxicity concerns in the host. Methodologies using antifungal drugs may be of concern at a later point when antifungal drug depletes, and fungal attachment occurs again thereafter. Sionov et al. have also recently performed an in vitro study of ethyl cellulose coating embedded with clotrimazole on voice prostheses. They reported that the presence of clotrimazole could resist switching to hyphae which are key to preventing mature-biofilm formation.[83] Sustained release of clotrimazole was evaluated for 60 days, and high-performance liquid chromatography (HPLC) analysis of the daily release can be found in Figure 2.9.

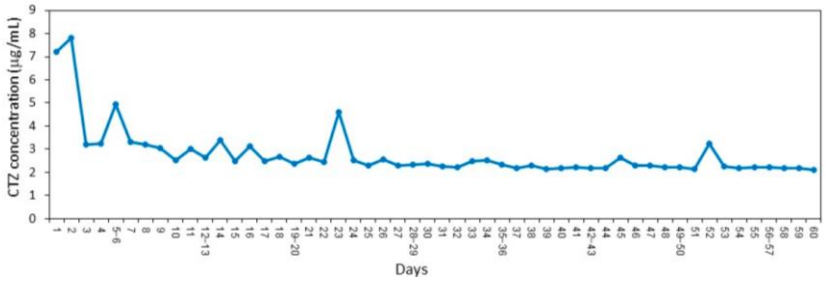


Figure 2.9: *HPLC analysis of the daily release of clotrimazole for 60 days.*[83]

Other ways have also been evaluated to prevent *C. albicans* biofilm, such as the use of newly discovered molecules. In one such case, Filastatin, a *C. albicans* resistant molecule named and discovered by Fazly et al., through a high throughput screening.[112] Following that, Vargas-Blanco attempted in his work the inhibition *C. albicans* cells attachment in vitro on common biomaterials - bioactive glass, silicone and dental resin. It was reported that the introduction of filastatin inhibits the attachment of *C. albicans* by 99.06%, 77.27% and 60.43% on the mentioned material surfaces, respectively.[113]

Natural ingredients have also been studied for antifungal effects. Camphor from the camphor tree is a terpenoid compound reported to resist fungi diseases in plants. Santos et al. incorporated camphor in flexible diamond-like carbon films and coated them on polyurethane (common material used for catheters). The reduction of *C. albicans* biofilm formation was found to be at least 90 % and the benefit of these films is their ability to be used for flexible medical devices.[114] This is one of the few works that does consider suitability for flexible medical devices. However, it is worth noting that camphor can be toxic to humans and should be used with care.

Another methodology for preventing *C. albicans* maximises the use of surface smoothness to prevent attachment. Távora evaluated the use of ethyl-cyanoacrylate coating (an adhesive) to inhibit *C. albicans* biofilm in dentures. It works when used as a coating but did not work when incorporated into the bulk material. The hypothesis for this phenomenon is due to the modification of denture surface when using such a coating, reducing roughness and hydrophilicity.[115] More recently, polymers with inherent anti-attachment properties to *C. albicans* cells have been discovered through a high throughput screening method. One of the polymers, (r)-α-acryloyloxy-β,β-dimethyl-γ-

butyrolactone (AODMBA) was demonstrated to be successfully produced by both dip coating and AM process. Printed product retained its capacity to reduce *C. albicans* attachment by an average of 84 % as per the graph in Figure 2.10.[34]

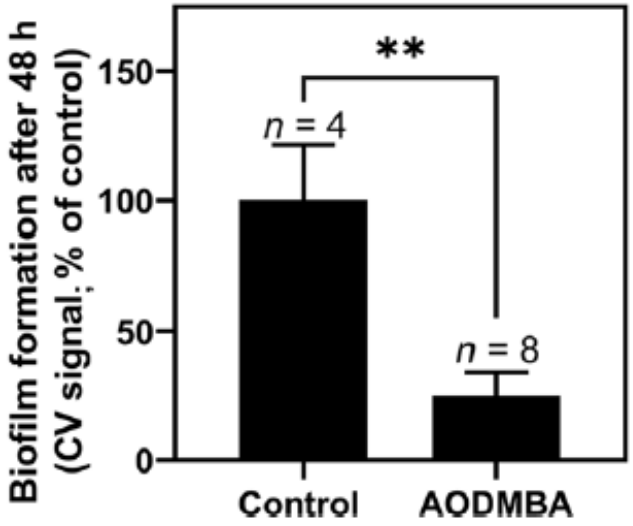


Figure 2.10: *Attachment of C. albicans biofilm on AODMBA (3D printed part was placed in a vacuum oven for 7 days, and rinsed in both water and IPA prior to evaluation) when compared to control (PDMS) after 48 hours.*[34]

In this section 2.4, the various methods developed to mitigate *C. albicans* growth on material surfaces were reviewed. Many of these works focus on voice prostheses, catheters and dentures as these are the areas that are commonly vulnerable to *C. albicans* adhesion as discussed in section 2.2. Common strategies include using metal ions, the discovery of anti-attachment materials, the introduction of antifungal drugs and the use of quaternary polymers. Unfortunately, one of the popular strategies using silver has not always been successful in mitigating *C. albicans* growth.[90,104] Its inability to release its ion in certain environmental conditions may be the key reason for its failure.

A summary of all the strategies described in this section, their advantages, processing methods, effectiveness and limitations are shared in Table 2.2 below, most of the solutions provided here require the inclusion of some antimicrobial additive or drugs to work. Many of these works did not consider flexibility as a key requirement for silicone rubber/ polyurethane-based medical devices. These considerations will be included in this research thesis. Several of the strategies reviewed in this section also leverage the use of the coating process as it is a straightforward method, therefore in the following section, dip coating process will be explained in detail.

Table 2.2: *Summary table of all the strategies to prevent C. albicans biofilm on medical devices in section 2.3. (CFU = colony forming unit).*

Ref	Description	Method/ Process	Device/ Material	Effectiveness	Advantages	Limitations
84	Gold and Titanium Coating <100 nm	Anodic vacuum arc plasma deposition	Voice prosthesis / Silicone rubber	Infiltration of yeast in silicone rubber not witnessed in coated voice prosthesis	Titanium produces a homogeneous coating	Inconsistent coating for gold
85	Silver oxide	Silver oxide blended into silicone rubber	Voice prosthesis / silicone rubber	Increase device median lifetime by 36 days	No allergy observed in 33 patients case study	Risk of toxicity with silver ingestion
86	Quaternized dimethylaminoethylmethacrylate (polyDMAEMAq)	Grafting	Voice prosthesis / silicone rubber	Up to 92 % reduction, depending on the quaternization agent	Relatively quick curing process	Unknown toxicity
	Quaternized polyethylenimine (PEIq)	Grafting	Voice prosthesis / silicone rubber	Up to 74 % reduction, depending on the quaternization agent	No additional initiator is required for the curing process	Long mixing time of > 24 hours
107	Surface treatment – Argon plasma	Plasma treatment	Voice prosthesis / silicone rubber	In vitro studies found reduced microbial adhesion	Does not require additional compounds, additives or chemicals	Requires a long preparation time/ did not work in vivo, hydrophilised surface had

						more fungal attachment/
83	Clotrimazole, ethyl cellulose, Klucel EF & ethanol solution	Coating	Voice prosthesis / silicone rubber	Resist hyphae formation which helps to mitigate biofilm	Sustained release for 60 days	Continuous exposure to drugs can lead to drug-resistant fungi
34	(r)-α-acryloyloxy-β,β-dimethyl-γ-butyrolactone	Coating/ AM	Voice prosthesis / Silicone Rubber	Reduction of fungi presence by an average of 84 %	Inherent anti-attachment ability without the addition of antimicrobials	Printed material too rigid
104	Gendine-coated (gentian violet & chlorhexidine), silver hydrogel coated and uncoated catheter in rabbit model	Coating	Urinary catheter/ Silicone rubber	0 CFU per cm^2 for gendine-coated	Broad spectrum effect against bacteria and Candida	More studies required to understand the long-term stability and suitability of gendine coating
114	Diamond-like carbon film & camphor in flexible diamond-like carbon films	Coating	Venous catheter/ Polyurethane	Film only: 91 % reduction Film & camphor: 99 % reduction	Suitable for flexible application	Camphor is toxic to humans
102	Silver nanoparticles	Milling of resin and nanosilver	Denture/ Acrylic resin	5 % silver concentration yields the lowest biofilm thickness, lowest live fungi	Reduces fungi attachment	Risk of toxicity with silver ingestion
106	Silver Bromide/ Quaternary ammonium grafted nanocomposite (AgBr/ NPVP)	Blended into material	Dentures/ PMMA	Antifungal activity increases with increasing AgBr/ NPVP	Non-cytotoxic	Risk of toxicity with silver ingestion, reduced curing in PMMA when increasing AgBr/ NPVP
115	Ethyl-cyanoacrylate	Coating/ Bulk material	Denture	Lower biovolume of 19 x 10^3 μm^3 as compared to control 517 x 10^3 μm^3	Works as a coating by providing a smooth surface	Does not work when mixed with the base resin

103	Collagen-coated knitted polyester vascular graft with silver acetate	Coating	Vascular prosthesis	Effect without serum only	Works well in a serum-free environment	Silver ion release is inhibited with the introduction of serum
111	Antifungal nystatin	Grafting	Silicone rubber	Reduction from ~ Log 7 CFU per cm^2 to Log ~ Log 5.3 CFU per cm^2	Slow release of the drug, < 10 % released on day 14	2 steps requiring a long preparation time
108	Bioconjugation of the antifungal agent onto surfaces	Epoxide plasma	Silicon wafer	Log 6 decrease in *C. albicans* attachment	Single step bioconjugation	Requires overnight incubation
109	Covalent bonding of anidulafungin & micafungin	Plasma polymer coating	Glass slip & Silicon wafer	Reduce fungi by >6 log	Reused for 5x for 10 days without reduction in antifungal effect	Requires a few steps preparation process
113	Filastatin (Small molecule inhibitor)	Blended into material	Bioactive glass, Silicone rubber & Dental resin	99.06% (bioactive glass)/ 77.27% (silicone rubber) & 60.43% (dental resin)	Reduce fungi growth significantly, works easily with several materials	Unknown stability and safety of long-term usage
105	Triphenyl phosphonium salt of poly (methylmethacrylate-co-vinylbenzoylchloride) (Polymer 1) & poly (chloroethylvinylether-co-vinylbenzoylchloride) (Polymer 2)	Tested as a polymer	N/A	Inhibition zone of Polymer 1: 0.9cm +/-0.06, Polymer 2: 0.7+/-0.06	Also, work for other *Candida spp.*	Long synthetic process

2.5 Dip Coating Process

Section 2.5 will look at the fundamental of dip coating and look at the benefit of this process technique. While there are other coating techniques available, dip coating is a straightforward and low-cost liquid deposition process used to produce a homogeneously

coated medical device. The process is waste-free, offers good thickness control, and is simple to build within research laboratories yet easily scalable to industrial volume.[116,117] Another key advantage of dip coating is its ability to evenly coat complex objects.[118] As described in Figure 2.11, the process consists of three simple steps – dipping, withdrawal, and drying.

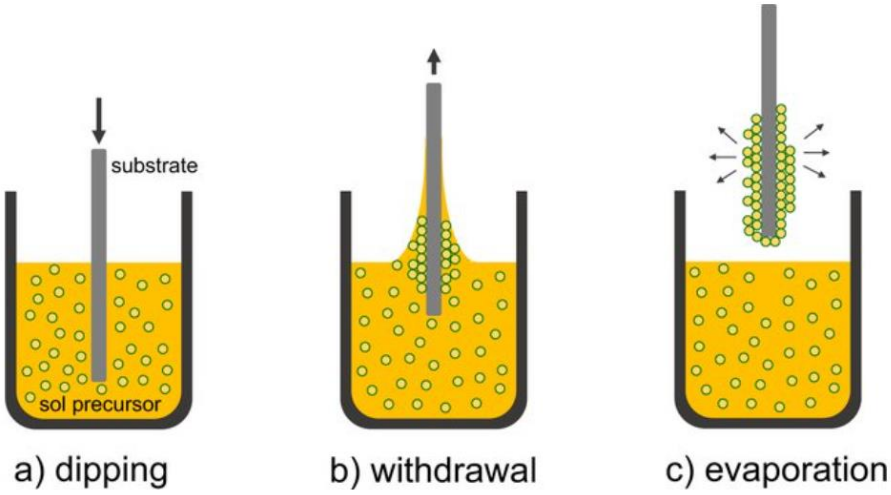


Figure 2.11: *Key steps of dip coating.*[119]

During withdrawal, the interaction can be categorised into 2 forces, draining and entraining forces, where draining forces draw solution away from the dipped object and entraining forces retain solution onto the object's surface. The formation of a wet film can be broken down into four different regions - static meniscus, dynamic meniscus, constant thickness zone and wetting zone as seen in Figure 2.12 below.

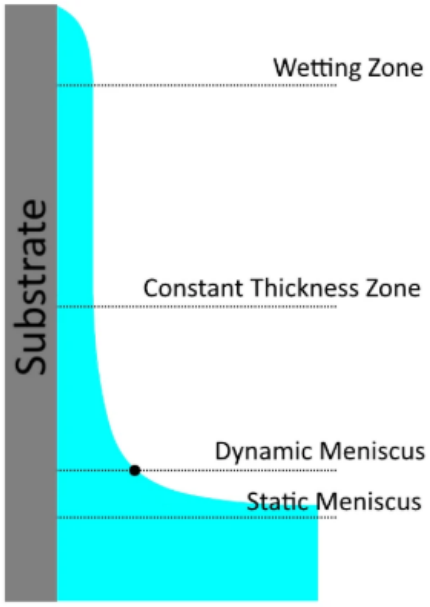


***Figure 2.12**: Formation of wet film at different points.*[120]

The dynamic meniscus and solution will determine the wet film thickness and the dynamic of the dip coating can be estimated with the following equations. Dynamic meniscus which is the stagnation point between entraining and draining forces would be used to determine the wet film thickness as per Equation 2.1.[120] In Equation 2.1, liquid viscosity and withdrawal speed must be high enough and deposited film thickness is the balance between viscous drag and gravity force.

$$h_0 = c_1\left(\frac{\eta U_0}{\rho g}\right)^{1/2} \quad \textbf{Equation 2.1}$$

Where liquid viscosity = η, withdrawal speed = U_0, the viscous drag = ηU_0, gravity force (ρg) where ρ is = liquid density, g = acceleration of gravity and the constant c_1 = 0.8 for Newtonian liquids.

When the substrate withdrawal speed ranges from ~1–10 mm/s and liquid viscosity are low, the deposited thickness is determined by the ratio of viscous drag to liquid-vapour surface tension according to Landau and Levich (Equation 2.2).

$$h_0 = \frac{(\eta U_0)^{2/3}}{\gamma_{LV}^{1/6}(\rho g)^{1/2}} \qquad \textbf{Equation 2.2}$$

Where liquid viscosity = η, withdrawal speed = U_0, the viscous drag = ηU_0, gravity force (ρg) where ρ is = liquid density, g = acceleration of gravity, liquid-vapour surface tension = γLV.

The withdrawal and drying steps are critical stages in determining the deposited film thickness. End results are also dependent on three main variables – surface tension of dipped object, rheological properties, and yield stress of the coating solution. [121] The simplicity of this process allows it to be commonly used with ease. In the following section 2.6, some antimicrobial coating studies that work with the dip coating process will be discussed.

2.6 Polymeric Antimicrobial Coatings

Medical coatings are often added to further enhance and improve the functionality of medical devices. In the medical field, coatings are mainly used for improving physical properties, modulating host-biomaterial interactions, preventing attachment of microbial and releasing drugs. One of the earliest applications for device coating is to lubricate the surface to minimise host cell trauma.[117] Biomedical device coating is also a much more developed field as compared to AM process, convenience, speed and ease of application are some of its key advantages.

Due to its versatility, polymeric materials have found themselves in various device coating applications, from ophthalmic coating [122] to polymer coating binding drugs to the surface of a coronary stent.[123] Polymers have gathered great interest in the field of antimicrobial coating as it is easily functionalised, can be cost-efficient and is also biocompatible.[117,124] Antimicrobial coating market is projected to reach USD 4.19 billion in 2021 and medical devices will be the largest application out of all industries. Some of the key players within the antimicrobial coatings industry are companies such as BASF SE (BASF), Microban Products Company (Microban) and Specialty Coating Systems (SCS).[125]

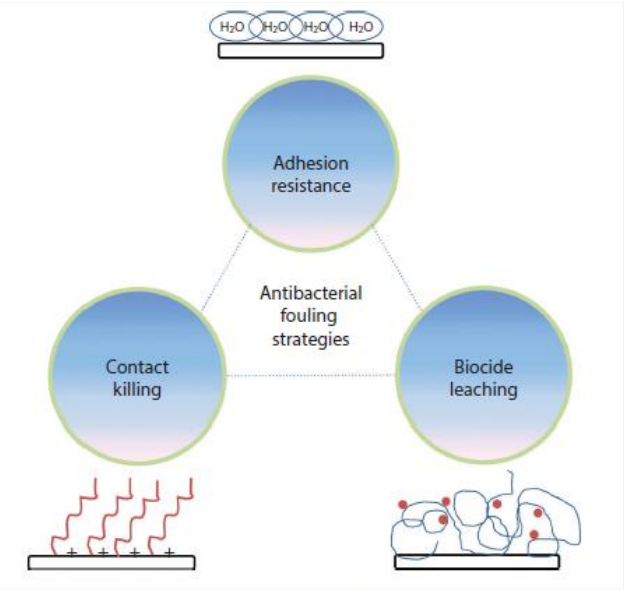


Figure 2.13: *Three main key antimicrobial approaches.*[117]

The three key mechanisms when relating to antimicrobial coating are non-microbial adhering, antimicrobial agent, releasing and surface contact killing approach, as depicted in Figure 2.13. In the following subsections, some common polymeric antimicrobial coating approaches both commercially available and newly developed antimicrobial

coating will be discussed. Such similar coating approaches were also highlighted in the earlier section looking at strategies to prevent *C. albicans* biofilm.[86,105,126]

2.6.1 Non-microbial Adhering Mechanism

Non-microbial adhering layer repels microbial attachment and prevents the build-up of biofilm instead of killing it. Their mechanisms are based on surface characteristics or chemical modifications to achieve hydrophilic, charged, or superhydrophobic low-energy surface polymers.[127,128] Polymers such as polyethylene glycol (PEG) and oxazolines are commonly evaluated as hydrophilic polymers,[129] whereas polybetaines and polyampholytes as zwitterionic polymers.[117,124,130]

Polymer brush structures have been widely reported to prevent protein adsorption. [131,132] In principle, when protein molecules or bacteria encounter a hydrophilic polymer brush, the decrease in the conformational entropy and increase in osmotic pressure within the brush would repel them both.[133] In a recent work comparing quaternary PEG brush copolymer (QPEG) against quaternary copolymer (control) found that QPEG punctures a modelled lipid membrane of *Escherichia Coli (E. Coli)*, suggesting PEG brush materials can cause bacteria membrane disruption.[134] PEG brush hydrogen bonds with water to form a layer acting as steric repulsion and 7 – 17 nm thickness of PEG coating in vitro has shown resistance to protein and bacteria.[135]

Zwitterionic polymers are polymers consisting of equally positive and negative charges, this allows the formation of a hydration layer separating bacteria and its substrate via electrostatic interactions.[128] While there appears to be increasing work with regards to the antifouling use of zwitterionic polymers, the synthesis process of such polymers is often

tedious and challenging as zwitterionic compounds are typically hygroscopic. Other difficulties could also arise from sensitive or incompatible chemical reactions.[136]

In recent work, Peng et al. performed a comprehensive evaluation of reversible addition fragmentation chain transfer (RAFT) polymerised zwitterionic sulfobetaine/ N-hydroxysuccinimide methacrylate block copolymer coating on PDMS catheter. Copolymer with a higher density of zwitterionic component on the surface was found to repel *S. aureus* in vitro when tested and evaluated with scanning electron microscopy (SEM) for 21 days.[137] For a better understanding of the structure and its effect on microbial resistance, simulation works have also been carried out with results positively correlating hydration ability with grafting efficiencies [138] and also a positive relationship between hydration and antifouling capabilities.[139]

Zhou et al. developed parylene N coating on PDMS and PMMA to increase wettability and significantly repel *C. albicans* attachment. [140] Parylene are linear polycrystalline thermoplastics with distinctive physiochemical properties and are also biocompatible.[141] Using the material on a titanium microcatheter, parylene coating was also compared against polyurethane coating and titanium itself. Average bacterial colonies were significantly reduced for both *S. aureus* and *Pseudomonas aeruginosa (P. aeruginosa)*.[142] Commercially available antimicrobial parylene coatings incorporated with contact-killing antimicrobial agents will also be discussed later in subsection 2.6.3.

2.6.2 Antimicrobial Releasing Mechanism

Antimicrobial release coating releases antimicrobial agents to its surrounding. Antimicrobial agents can be antibiotics, antimicrobial peptides, quaternary small

molecules, silver, or other metal-based materials. Ideally, the controlled release of agents would minimise the risk of host toxification and allow the device to be well protected from microorganisms for a longer time. When using antibiotics, an increase of antibiotic-resistant bacterial strains is typically a cause for concern as these bacteria are harder to treat than non-resistant bacteria.[143] A handful of the strategies to prevent *C. albicans* were already discussed in section 2.4 such as the controlled release of clotrimazole drug coating [54] and silver ion release coating [103] also fall into the antimicrobial releasing coating. Another example of such a work would be one by Gottenbos et al. and their studies on covalently coupled 3-(trimethoxysilyl) propyldimethylocta-decylammonium chloride which was effective against *S. aureus*, *E. coli* and *P. aeruginosa*.[144]

Antimicrobial coating using releasing mechanism is readily available in the market. AST Products Inc. offers an antimicrobial coating known as RepelaCOAT™. Its mechanism is as per Figure 2.14 where salt ions and/ or antibiotics bonded onto polymer surface is gradually released in the presence of sodium or calcium ion within the bodily fluid.[145]

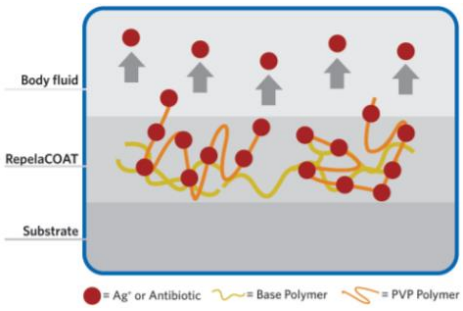


Figure 2.14: *How RepelaCOAT works.*[145]

BASF has also published a patent which describes a combination of two antimicrobial components, alkylaminoamino methacrylate/ acrylate polymer with antimicrobial metal such as silver ion into a coating polymer formulation. The two components when

incorporated into coating can achieve 6 log reduction in a timeframe of 2 hours. It is said to work against various microorganisms including *S. aureus*, *E. Coli* and *C. albicans.*[146]

2.6.3 Surface Contact Killing Mechanism

The surface contact killing mechanism works by the interference of cell function such as cell respiration, cell division or formation of cell walls.[130] In terms of polymer-based surface contact killing coatings, dual mechanisms of anti-adhering polymers and contact killing antimicrobial agent has also been explored by some organisations. Hydromer Inc. (Hydromer) presents a heat curable polymeric formulation which lowers protein adsorption reducing microbial attachment.[147] A news article from 2012 suggested that Hydromer works with N8 Medical Inc. on the incorporation of an antimicrobial compound, Ceragenin in their polymeric antimicrobial coating.[148,149] Another organisation, Biointeraction produces AvertPlus™ an antimicrobial coating that would reduce biofilm formation. Biointeraction's patent describes the use of polymer functionalised with antimicrobial pendant groups comprising of guanidine group or quaternary ammonium salt.[150]

2.6.4 Summary of Reviewed Antimicrobial Coatings Studies

Section 2.6 provides an overview of the antimicrobial market, the key mechanisms and discussed various examples of work done on antimicrobial coating. There are several patented commercial products already available for antimicrobial coating which suggest the importance of such coatings and the maturity of using coating technology for medical devices. Moving forth, in the next section AM processes will be introduced, AM in the biomedical field and developmental work on antimicrobial AM materials will be discussed in section 2.9.

2.7 Additive Manufacturing Process

AM or 3D printing is an advanced manufacturing technique for the direct fabrication of products and components depositing material layer by layer. This is done by using a generated 3D CAD file for the building of 3D objects. The detailed process of developing a product with AM can be found in Figure 2.15 below. There are generally seven steps to developing a product manufactured with AM – conceptual development, 3D CAD application, generation of .stl file and G code, manufacturing, cleaning and often a post-processing step will be required.[151]

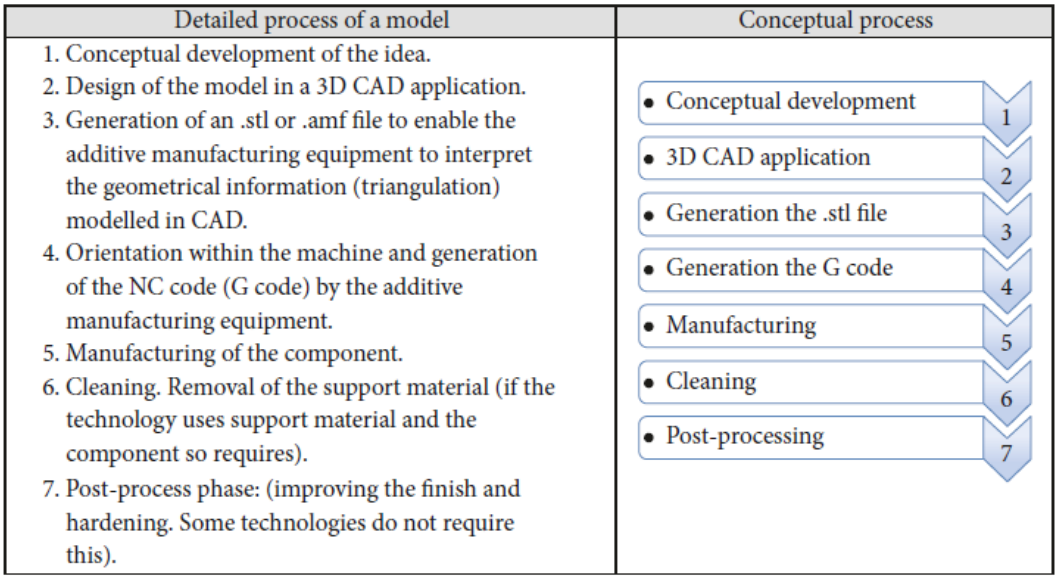


Figure 2.15: *Typical process of designing a product for AM.*[151]

AM first emerged in the 1980s with stereolithography technology (vat polymerisation process) innovated by 3D Systems. In the 1990s, 2 new AM technologies were also introduced – material extrusion and sheet lamination.[152] Since then, there have been progressively several new AM processes being designed. The technology was initially used for rapid prototyping purposes but in recent years has been increasingly used for consumer product manufacturing.

As mentioned before, there are several attractive benefits as compared to conventional subtractive manufacturing. AM process largely differs from subtractive manufacturing whereby materials are removed in a controlled manner and typically require some form of tooling such as an iron cast injection mould. Such tooling requires time and may incur a high cost for low-volume production. AM technology allows a variety of different designs to be manufactured all within a single piece of equipment.[1]

Depending on the size and structure of parts, reports have suggested that AM would typically benefit from small volume manufacturing of fewer than 5000 pieces.[153,154] AM process also allows for on-demand manufacturing instead of forecast-based manufacturing, reducing cost and wastage from unsold products.[1] Other benefits of AM include reduction of waste material, manufacturing with multi-materials within a single AM process,[155] allowing customisation of product and ability to produce product with challenging geometry. Figure 2.16 below provides an overview of many AM benefits.

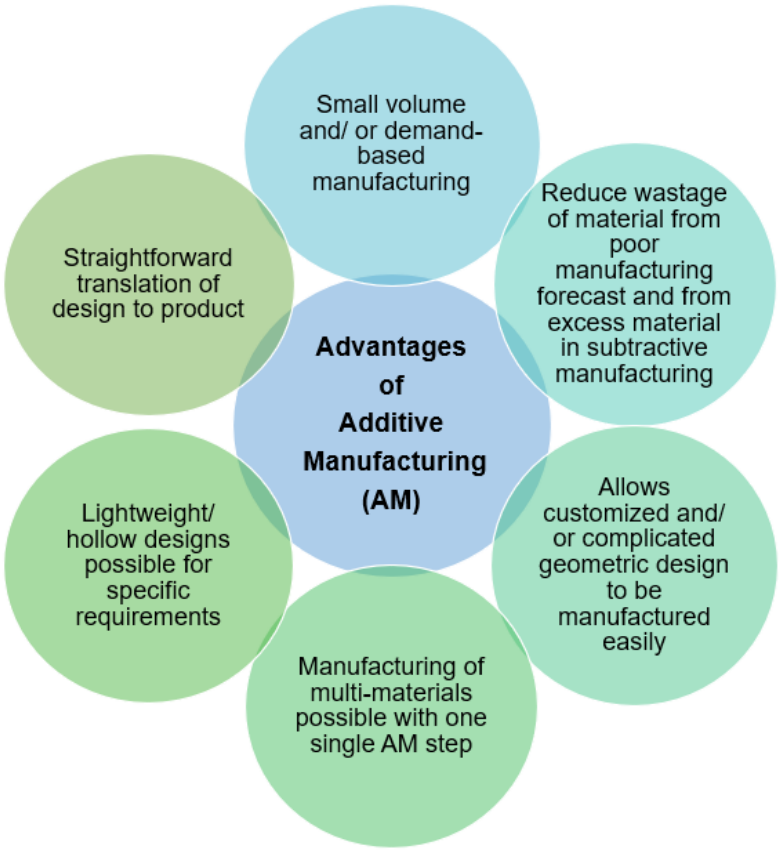


Figure 2.16: *Several advantages of AM process are summarised in section 2.7.*

2.9.1 Microbial-Resistant AM Materials

While there is a wide range of potential biomedical applications for AM processes, availability of microbial-resistant AM material is scarce and a handful of these developments were covered in the only review on "Antimicrobial Polymers for Additive Manufacturing" published in 2019.[35] Some approaches reviewed were akin to works presented in section 2.4 and section 2.6 discussing strategies to prevent *C. albicans* biofilm and antimicrobial coating. Such as leveraging the potential of quaternary ammonium salt, the inclusion of metal compounds and the incorporation of antimicrobial drugs. Example of works reviewed includes SLA printable quaternary ammonium infused synthetic copolymer with contact killing abilities[180] and antibiotics releasing

polycaprolactone (PCL) fabricated with electrohydrodynamic (EHD) printing.[181] Since AM for biomedical devices is a new and exciting field that is only gaining increasing interest in the last 10 years,[4] many of these AM processable antimicrobial materials were developed in the last 5 - 6 years.

One of the earlier works that consider the evaluation of microbial growth on 3D structure polymer was written by Al-Ahmad et al.[182] In 2007, the work studies the adhesion of six oral types of bacterial and *C. albicans* on 3D-bioplotted scaffolds to be considered for bone replacement in oral surgery. Bone scaffolds were made with 3 different materials – tricalcium phosphate (TCP), calcium/ sodium alginate and poly lactide-co-glycolic acid (PLGA), highest amount of *C. albicans* adherence was found in PLGA, followed by TCP then alginate whereby only some amount of *C. albicans* were found. ~~*C. albicans*~~ were observed via SEM and CLSM. While the work does not explore in depth the reason why *C.albicans* are more susceptible to growing on PLGA and TCP, it considers the importance of antimicrobial material while discussing future strategies to reduce such microbial attachment.

Puppi et al. proposed in their paper the use of a tissue engineering scaffold to release Levofloxacin, an antibiotic.[183] Using computer-aided wet-spinning (CAWS) technique, a critical-sized bone segment of a rabbit's model was built. A total of 3 scaffold samples were built based on star PCL scaffold – PCL, PCL with low and high dosages of Levofloxacin. The advantage of this work is the use of one step manufacturing process where Levofloxacin could be added to the polymeric solution directly and no post-processing was required. In vitro evaluation showed fast release of about 50 % of Levofloxacin in the first 4 days and stable release after 30 days. The work cleverly uses

the porosity morphology of wet-spun fibre to encapsulate antibiotics. Improving the system for better control in the first four days which resulted in fast release would minimise the chance of intoxication in the host from antibiotics overdose.

In another work considered for dental application, Totu et al. explored the use of Titanium dioxide (TiO_2) nanoparticles within commercially available PMMA for SLA against bacterial and *Candida scotti* (*C. scotti*).[32] Five samples with different weight % of TiO_2 were prepared – 0.2 %, 0.4 %, 0.6 %, 1.0 % and 2.5 %. Antimicrobial results performed with Tetrazolium chloride assay (TTC) found that the minimum amount of TiO_2 nanoparticles required for antimicrobial efficiency against *C. scotti* was 0.4 %. PMMA dispersed with 0.4 % TiO_2 nanoparticle was also chosen to further build the SLA prototype denture sample with much success. The evaluation showed the good potential of TiO_2 nanoparticles as an antimicrobial composite, additional mechanical and biocompatibility evaluation would further confirm its suitability in the clinical environment. It is also important to ensure that the TiO_2 nanoparticles would not leech from the PMMA resin.

Also, for dental application, in 2018 a work by Nagrath et al. was published on PMMA functionalised with AmB contained within PCL microsphere.[33] This work was done specifically targeting *C. albicans* colonisation as this was found to affect over 65 % of denture users.[184] 0.2 % w/v AmB loaded microsphere were mixed with PMMA in the ratio of 2:1. Drug release was characterised with FTIR using 344 – 355 nm region where AmB drug would appear and presence of *C. albicans* was evaluated using dry cell weight method. Printed samples with one, five and ten layers all showed a significant reduction in *C. albicans* biomass. Drug release for one layer sample also demonstrated consistent drug release with FTIR and spectrophotometry tested on 3D printed samples in release

media. For five- and ten-layers samples there were some abnormalities on the FTIR reading as the AmB spectrum with 344 – 355 nm was not observed during the drug release evaluation. The work showed the potential of PCL as a controlled drug release polymer for an antimicrobial agent, AmB. At the same time, there are also more works required to better understand the impact of printing layers and their drug release ability over a longer period.

Since the publication of the review paper in 2019 by González-Henríquez et al., [10] several new findings on antimicrobial AM polymers were shared. Most of these works focused on assessing their work for bacterial strains and incorporate the use of nano metal particles or metal compounds in the AM polymeric material. [185–187] An interesting series of works published by Navaruckiene et al. looked at developing vanillin acrylate-based resin (printed structures as shown in Figure 2.21 below) as an antimicrobial UV curable polymer. Vanillin is a vanilla-tasting organic compound that has been proven to be antibacterial and the focus of their work look at optical 3D printing applications.[188–190] The developed formulations were tested on *E. Coli*, *S. aureus*, *Aspergillus niger* and *Aspergillus terreus*. Both vanillin acrylate and methacrylate showed significant antibacterial activities. Antifungal activities were present but less significant than that of the antibacterial. The work also considered rigid and flexible end products based on finetuning of formulation with solvent, initiator and monomer ratio and/ or types.

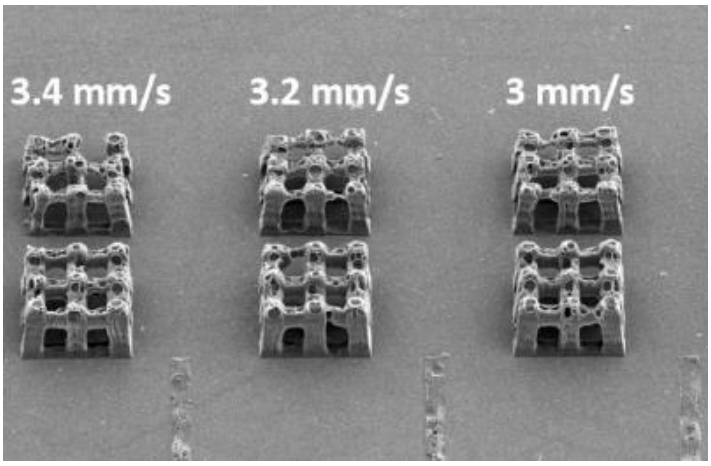


Figure 2.21: *Vanillin diacrylate-based formula printed with direct laser writing setup.*

Another new development by Li et al. studied the inclusion of quaternary ammonium salt-based antibacterial agents into thiol–ene–acrylate ternary systems for DLP AM process. The formulations were tested against *E. Coli* and *S. aureus*, both were found to be effective. However, the mechanical and thermal properties of the printed product reduce with increasing antibacterial agent.[187] Lastly, recent work that considers *C. albicans* anti-attachment AM processable polymer was mentioned in section 2.4 where AODMBA was successfully inkjet-printed.[34]

In section 2.9.1, the works on antimicrobial strategies for AM process were reviewed. Most reports that focused on AM-ready materials were tested against bacterial strains with less than a handful of work evaluating fungi. Therefore, this is an important gap that needs to be closed to widen the application of AM for biomedical devices, while reducing the risk of fungal infection for patients. In the following section, we will discuss in depth the gaps and work associated with this research study.

2.7.1 Different AM Techniques

While there are several different commercial names of AM systems, as per the American Society for Testing and Material (ASTM) International, ASTM F2792-12a “Standard Terminology for Additive Manufacturing Technologies”, there are seven categories of AM processes – vat photopolymerisation, material jetting, binder jetting, material extrusion, powder bed extrusion, sheet lamination and direct energy deposition.[156] Figure 2.17 depicts these seven common AM processes showing a schematic of the technology.

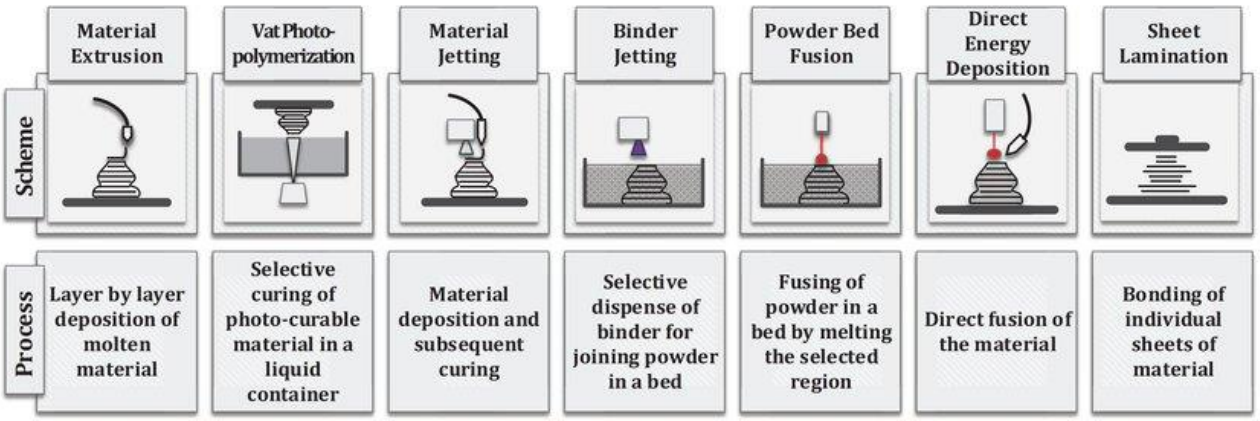


***Figure 2.17**: Key AM technologies.*[157]

The choice of AM technology would depend greatly on the required materials, design, resolution and size of the printed parts. It is possible to use AM on a wide range of materials including metals, ceramics, and polymers. Apart from direct energy deposition, all other AM processes are suitable for printing polymeric material.

For this research work, UV curing AM techniques were selected for processing the materials as they allow fine resolution printing and multi-material printing which is advantageous for medical devices. Hence, in the following subsections, a more thorough

background on UV type AM process - material jetting and vat photopolymerisation will be discussed in detail as these are the key UV curing AM systems.

2.7.2 Vat photopolymerisation

Vat photopolymerisation is a process utilising a tank of liquid photopolymer resin which is selectively cured by exposure to radiation energy. Radiation can come from gamma rays, X-rays, electron beams, UV, and visible light with UV being the most used light source. Upon curing of resin with radiation exposure, the platform moves the part downwards and additional layers on top are cured subsequently. The fabricated product is removed and rinsed away from residual resin.

Vat photopolymerisation generally produces parts that have a relatively good level of accuracy and finishing. Acrylate type monomers would undergo free-radical polymerisation while epoxy type undergoes cationic polymerisation. Vat resin formulation typically includes a photo-initiator, liquid monomers, reactive diluent and other additives.[158] In such UV-cured products, a post-curing process would be beneficial in improving the degree of conversion (DOC) and consequently the mechanical properties of the end product.[159]

Stereolithography (SLA), digital light processing (DLP), continuous liquid interface production (CLIP), liquid crystal display (LCD) and multiphoton polymerisation (MPP) all fall under vat photopolymerisation. SLA is one of the earliest AM processes developed and is a more commonly known vat AM process with commercially available AM printers by Formlab and Stratasys.

The key difference between SLA and DLP lies in the method used to expose parts to radiation. As seen in Figure 2.18 below, SLA (Left image) uses a point-wise vector scan

approach where two motors known as galvanometers swiftly target laser beam across the print area while DLP (Right image) uses a layer-wise mask projection approach where a digital micromirror device (DMD) would be used to flash a single layer of the entire platform. The fabricated parts from DLP would result in small rectangular bricks known as a voxel. A less common process known as LCD is similar to DLP but uses UV light coming from an array of light emitting diodes (LED) shining through.

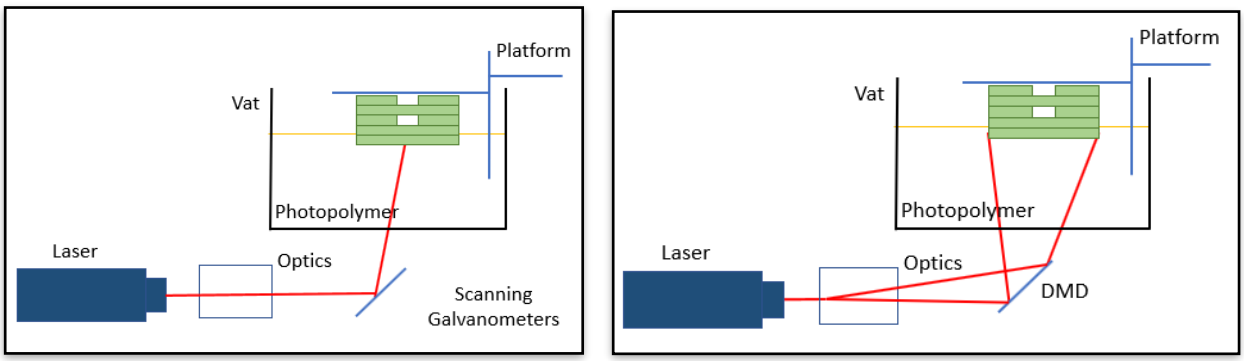


Figure 2.18: *(Left) Schematic of SLA process. (Right) Schematic of DLP process.*

Continuous liquid interface production (CLIP) has a similar setup as the DLP, but CLIP uses an additional oxygen penetrable film to prevent polymerisation at the surface near the UV source. With the film in place, the step for recoating after printing each layer is removed allowing CLIP to be noticeably faster than DLP.[160] MPP is a point-to-point approach which uses femtosecond laser radiation allowing print resolution as fine as 100 nm. This approach is used for the realisation of microstructure. Unlike other approaches, MPP is not a layer-by-layer method, the laser used in MPP can move in any direction within the resin.[161]

2.7.3 Material Jetting

The concept of material jetting (MJ) is akin to that of a 2-dimensional inkjet printer, droplets of ink are ejected from a print head and deposited layer by layer to create a part

as shown in Figure 2.19. Printed ink can be molten materials, monomers or oligomers and are either solidified upon cooling (direct printing) or cured via UV polymerisation (reactive printing) with the presence of an initiator and catalyst.[156] Reactive printing is more common in material jetting as monomers and/ or oligomer inks prepared are inclined towards a lower viscosity. For the UV curing of inks to undergo UV polymerisation, a UV light is introduced after droplets were deposited each time.

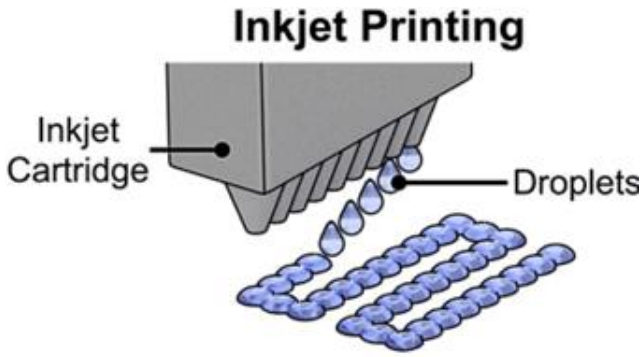


Figure 2.19: *Inkjet printing process.*[162]

The advantages of this method are primarily its dispensing uniform droplets with fine resolution and its capability to build parts with multiple materials and/ or colours which are not as readily available in many other AM processes. The printing solution is also stored within a cartridge minimising the use of a larger amount of material as compared to vat photopolymerisation. That said, due to the mechanism of inkjet printing, the ink viscosity, surface tension, density and process variable are extremely critical to the quality of the product.[163]

There are two main approaches as to how the material can be jetted - either by continuous or drop-on-demand (DOD) mode. In DOD mode, ink is pumped into the printhead from a fluid reservoir causing a continuous flow of ink to be ejected from the nozzle. Upon

ejection from the nozzle, flow breaks into droplets due to Rayleigh instability. Additional procedures such as vibrating, modulating and perturbing can be included to provide more consistent droplets. As the droplets are produced at a consistent interval, their deposition upon ejection from nozzles is controlled by an electrostatic charge where a charging field would be introduced to the droplets. The charged droplets will undergo a deflection field and be directed to their desired endpoint. Continuous mode printhead is from the older inkjet technology which has comparatively higher droplet ejections.

As mentioned earlier the properties of ink and parameter setting are critical for a successful print. Viscosity and surface tension are the key ink parameters to consider for inkjet printability. Fromm's Z parameter, which predicts printability, can be calculated when dynamic viscosity and surface tension values of ink are both used in equation 2.3.[164]

$$z = \frac{\sqrt{\rho r \gamma}}{\mu} \qquad \textbf{Equation 2.3}$$

Where μ is dynamic viscosity, γ is surface tension, ρ is the density of the ink, r is nozzle diameter

2.7.4 Summary of AM Processes

In summary, section 2.7 gives an overview of AM processes currently available with a focus on vat polymerisation MJ that uses a UV curing approach in polymerisation. An overview of all the UV-curing AM processes is summarised and compared in Table 2.3 below.

Table 2.3: *Providing an overview of the different photocuring AM techniques.*[165]

Technique	Lamp source	Printing size	Photocuring mechanism	Precision
SLA	355 nm Laser beam	No limit	Hybrid photocuring	Fair
DLP	385–405 nm LED lamp	Limited	Radical photocuring	Very good
LCD	405 nm LED lamp	Limited	Radical photocuring	good
MJP	No limit	No limit	Radical, cationic, or hybrid	Outstanding
CLIP	385–405 nm LED lamp	Limited	Radical photopolymerization and thermal polymerization	Very good

UV curing polymers have certain advantages over thermal curing. For example, UV-cured materials are more thermally stable in higher temperature environments, the process is more consistent and does not depend on solvent, and UV-cured polymers will have lesser shrinkages. In the following section 2.8, the polymerisation mechanism behind these UV processes and the influencing factors would be elaborated on and compared.

2.8 UV Curing Polymerisation

As UV curing AM processes are the focus of this thesis, it is important to understand the mechanism of UV curing mechanism. Therefore, this section will provide insights into the chemistry behind UV curing polymerisation.

There are two key UV curing polymerisation mechanisms. Free radical polymerisation and cationic polymerisation. Cationic polymerisation transfers a charge from monomer to monomer during chain growth and is often used to cure epoxy resin. Onium salt is utilised as a photoinitiator for the production of strong acid under UV light, the rest of the chain growth reaction will not be affected by UV light but is driven by thermal energy.[166] Cationic polymerisation is sensitive to moisture which may reduce the effect of its catalyst. Cationic polymerisation is typically used in the coating industry but has also been studied for AM

processes. Commercially available epoxy monomers for AM include 3,4 epoxycyclohexane methyl 3,4 epoxycyclohexylcarboxylate (EPOX) and bisphenol A diglycidyl ether (DGEBA).[167]

Another UV curing polymerisation which is a key mechanism investigated for this work look at the use of free radical polymerisation. Free radical polymerisation consists of three key steps initiation, propagation, and termination. Figure 2.20 shows these key steps and the UV energy igniting radicals which kick starts the initiation process.

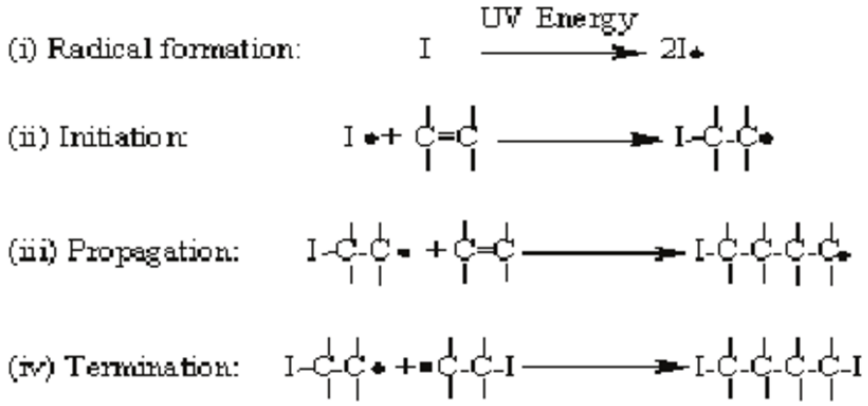


Figure 2.20: *Radical polymerisation steps – radical formation, initiation, propagation and termination.*[168]

During the initiation stage, the initiator will be activated by taking in energy from UV sources generating free radicals. These free radicals will begin chain propagation by breaking the C=C bond to C-C, extending the polymer chain. As the radical polymerisation proceeds, the free radical concentration keeps increasing and terminates when two free radicals combine. Radical polymerisation is especially sensitive to the presence of oxygen and will react with one another to generate inactive chain ends.

A typical formulation of UV curing inks would include monomer/ oligomers, photoinitiators, diluents and other additives. Photoinitiators can be classified as Norrish Type I or Norrish

Type II based on their radical producing mechanism. Type I photoinitiators typically contain benzoyl groups such as hydroxyacetophenones and phosphine oxides. The carbonyl group of the initiator absorbs a photon and is transformed into a radical. Type II photoinitiators include benzophenone and its derivatives, the curing process also requires an accelerator. In Type II, the initiator absorbs UV light to form excited molecules which abstract an electron from the accelerator, the accelerator then reacts with a monomer to initiate polymerisation. In UV-curing AM processes, both radical and cationic polymerisation can be used. In some cases, a hybrid curing process has also been explored.[165]

Section 2.8 has covered the polymerisation mechanism for UV curing processes and provided us insights on what is the requirement of the formulations and environment for UV curing inks. Moving forth, we will discuss the works performed on using AM in the biomedical field and antimicrobial materials that have been developed for AM.

2.9 AM in Biomedical Field

The use of AM process for manufacturing biomedical devices provides several advantages when compared to conventional production methods. One of the most recognised benefits is the potential for customisation of the device according to the patient's needs and therapeutic requirements. The use of AM also allows for the creation of designs with very complex geometries, which are not easily producible by other manufacturing methods, therefore widening the range of potential applications that can be treated by the use of biomedical devices.[169,170] Finally, it also increases the ease of incorporating drugs or antibiotics into the layers during AM processing, which allows a controlled drug release profile to be achieved.[171]

As much as it is attractive, AM has yet to reach its full potential in terms of application commercialisation due to the stringent requirements of the Food and Drug Administration (FDA). Also, FDA does not approve of specific materials used in the manufacturing of the device and only approves of the finished device itself.[172] Table 2.4 presents a handful of FDA-cleared devices using AM processes and many of these materials are alloys for metallic implants or orthodontic applications. In terms of polymeric materials, only a handful of them has found their footing as dental medical devices as FDA-cleared biomaterials. One of the most commercially known dental medical devices would be Invisalign, which is a leading brand of teeth aligners that are more aesthetically pleasing than traditional braces.

Table 2.4: *FDA cleared 3D printed biomaterial applications.*[2]

Applications	Material
Screw & Abutment	CP-Ti
Artificial valve, Stent, Bone fixation	Ti-6A1-4V
Crowns, Knee joint, Hip joint	Ti-5Al-2.5Fe
Spinal implant	Ti-15 Zr-4Nb-2Ta-0.2Pd
Crown, Bridges, Dentures, Implants	Ti-29Nb-13Ta-4.6Zr
Crown, Bridges, Dentures, Implants	83%-87%Ti-13%-17%Zr (Roxolid)
Crown, Bridges, Dentures	316L
Knee joint, Hip joint, Surgical tools, Screw	Co-Cr-Mo, Co-Ni-Cr-Mo
Artificial valve, Plates, Bolts, Crowns, Knee joints, Hip joints, Catheters, Stents	NiTi
Dental bridges, Articular cartilage, Hip joint femoral surface, Knee joint bearing surface, Scaffolds	PMMA, PE, PEEK
Bones, Dental implants, Orthopedic implants	$SiO_2/CaO/Na_2O/P_2O_5$
Porous implants, Dental implants	Zirconia
Dental implants	Al_2O_3
Implant coating material	$Ca_5(PO_4)_3(OH)$

One of the recent reviews by Kumar et al. highlighted publications involving AM in the biomedical field have been increasing annually. From 18 publications in 2011 to 222 publications in 2019 (only from the top ten journals as per Web of Science).[4] Work has been explored for a wide range of healthcare applications, including customised prostheses,[173,174] pharmaceutical drug delivery biomedical implants and devices,[175,176] medical models and surgery guides.[177]

In this section, the benefits of AM for biomedical devices and the increasing number of healthcare-related research using AM processes will be reviewed. In the following subsection 2.7.1, microbial-resistant AM materials that were developed will be discussed. An interesting recent case study reported resolving a complicated bedside clinical problem with AM. The team used an AM-built valve to clamp a leak in a percutaneous endoscopic gastrostomy tube (PEGT) tube when all other options were exhausted.[178] The work followed up with an update, where the evaluation of microbiology found sparse microbial growth of *C. albicans*, *C. krusei* and *Staphylococcus epidermidis*, similar to the PEGT which was safely inserted into the patient without triggering infection. [179] While this is a case study based on a single patient, a real-life demonstration within a hospital proves the potential and benefit of AM for medical devices. The risk of microbial infection here can also be greatly reduced if an antimicrobial polymer was used. This case study provides us insight into how AM and antimicrobial materials can help patients and support the work of our frontline healthcare workers.

2.10 Gaps, previously associated work & summary

This chapter has given an overview of the growing concern of pathogenic fungal problems in healthcare facilities, highlighting the neglect of fungal research as compared to other

microorganisms such as bacteria. The literature review also discussed the various methods to prevent fungal (*C. albicans*) growth on medical devices and processing methods to prepare antimicrobial and/ or antifungal materials were introduced. However, there exist some research gaps that can be further explored.

AM has several advantages when it comes to biomedical applications. For example, it allows the personalisation of medical devices according to patients' needs and can also support the logistic needs of medical devices in hospitals by allowing the manufacturing of medical devices on the spot instead of going through typical logistics which may require longer shipping time. However, there are very limited AM processable materials that have considered its effect and/ or ability on resisting *C. albicans,* with even lesser work considering their suitability for flexible medical devices. With the increasing interest and consideration of AM process for biomedical devices, the availability of such materials would be very beneficial to both patients and healthcare workers. A study performed by one of the largest manufacturers of AM printers and production systems, Stratasys, also emphasises the importance of antimicrobial for AM medical devices, especially when printed parts are made of materials such as acrylonitrile butadiene styrene (ABS) are unable to undergo heat sterilisation with an autoclave.[191]

This study aims to minimise the research gap by looking at AM processable polymers with inherent *C. albicans* anti-attachment properties, which is important for extending the material options available for AM of biomedical devices. This work is an extension of research performed by Vallieres et al.,[34] that has found *C. albicans* anti-attachment with inkjet printable AODMBA. However, the report has shared that the T_g of the material is too high for usage in flexible medical device applications. Therefore, this work would look

at mitigating the existing research gap while widening the UV curable material options for AM process and biomedical applications.

Chapter 3: Experimental Methods & Setup

3.1 Introduction

This chapter will share the step-by-step experimental methods and experimental setup information used in the evaluations throughout the following chapters 4, 5 and 6. The HTS developed for this work (described in chapter 4) consists of several rapid testing methods that would be used to evaluate the monomers/ polymers and provide analytical data on the degree of conversion (DOC), fungal anti-attachment, polymer toxicity, viscosity, and surface tension. The HTS methodology would be used to prepare and study a larger library of mixed co-monomers and copolymers in chapter 5.

In the copolymer matrix, additional studies of Time-of-Flight Secondary Ion Mass Spectrometry (ToF-SIMS), Proton Nuclear Magnetic Resonance Spectroscopy (^{1}H NMR), Raman spectroscopy and assessment of residue toxicity towards fungi for selected co-monomers/ copolymers provide more insights on the properties of the inks. ToF-SIMS, NMR spectroscopy would allow a better understanding of copolymer ratio and distribution of components within the copolymer, while residue toxicity allows us to specifically evaluate the impact of monomeric and/ or oligomers residue (after UV curing) which may have a toxic effect on *C. albicans* cells.

Lastly, chapter 6, looks at the application of the copolymer selected from HTS process. The selected copolymer would be synthesised and prepared as a dip coating solution. The selected co-monomers would also be inkjet-printed into copolymer and improvement of inkjet printing formulation was prepared via the addition of additives, usage of

oligomers and adjusting of copolymer ratio. The polymerisation of all materials used in chapter 6 will also be described in this chapter. The three stages and the required experimental setup/ method for each stage are depicted in the flow chart in Figure 3.1 below. The figure shows the experimental setup and method used in its respective chapter and shares the flow of the work packages from HTS method development to utilisation of this HTS method and then to application test in the last stage.



Figure 3.1: *Schematic overview of the different stages of work in this thesis and the key experimental methods used.*

3.2 Materials Used

Nine monomers were selected to form a combinatorial library for this HTS printability development. The monomers were selected based on their varying fungal anti-attachment performance, T_g, and curability and were also ensured to be non-toxic. The nine resultant polymeric materials utilised were based on triethylene glycol methyl ether methacrylate (TEGMA, 729841, Sigma Aldrich), poly(ethylene glycol) methacrylate (PEGMA, 409537, Sigma Aldrich) average Mn 360, di(ethylene glycol) methyl ether methacrylate (DEGMA, 447927, Sigma Aldrich), poly(ethylene glycol) diacrylate (PEGDA, 437441, Sigma Aldrich) average Mn 575, (r)-α-acryloyloxy-β,β-dimethyl-γ-butyrolactone (AODMBA, 376361-5, Sigma Aldrich), ethylene glycol dicyclopentenyl ether acrylate (EGDPEA, 407968, Sigma Aldrich), isobornyl methacrylate (IBMA, 392111, Aldrich), 4-tert-butylcyclohexyl acrylate (TBCHA, 467545, Sigma Aldrich) and 4-tert-butylcyclohexyl methacrylate (TBCHMA, Nourcryl MC 110, Akzo Nobel). The selected monomers (the chemical structure are found in Figure 3.2) had been demonstrated to exhibit varying levels of *C. albicans* resistance in the earlier work.[34]

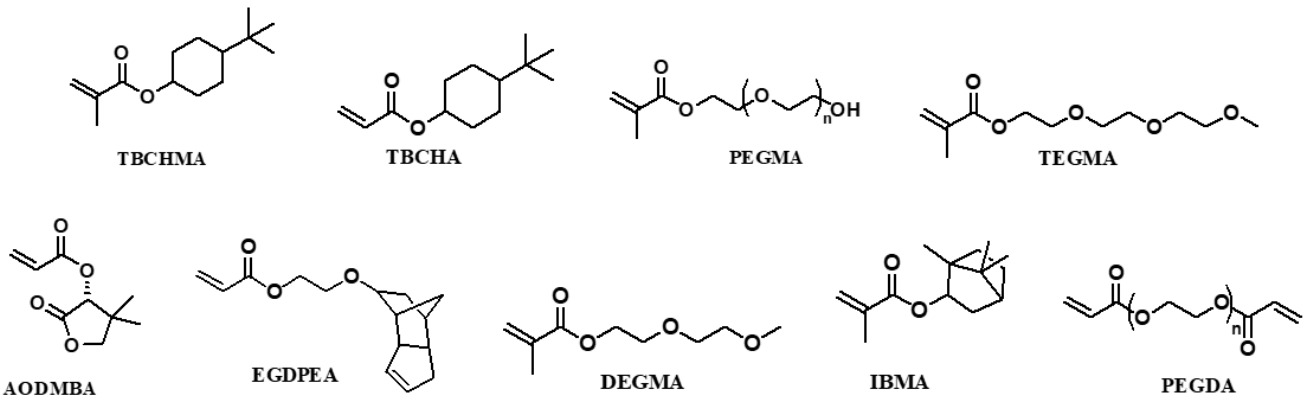


Figure 3.2: *The nine monomer candidates selected to demonstrate the effectiveness of the high throughput (HTS) methodology.*

The selection process also considers different factors such as curability/ reactivity (of both methacrylate and acrylate types), their varying T_g and level of toxicity to humans based on the Globally Harmonised System (GHS) of Classification and Labelling of Chemicals classification stated in material safety datasheet (MSDS, GHS classification of monomers summarised in Table 3.1). Highly toxic monomers with high toxicity risk and carcinogenic classification would not be considered during the selection process.

Table 3.1: *GHS classification of monomers and DMPA initiator evaluated from their MSDS document.*

Abbreviation	Full Name	GHS Classification
TBCHMA	4-Tert-Butylcyclohexyl Methacrylate	Skin corrosion/ irritation (Cat. 2) Eye irritation (Cat. 2) Specific target organ toxicity, repeated exposure
TBCHA	4-Tert-Butylcyclohexyl Acrylate	Skin corrosion/irritation (Cat. 2) Serious eye damage/eye irritation (Cat. 2a) Specific target organ toxicity, single exposure
PEGMA	Poly (Ethylene Glycol) Methacrylate	Skin corrosion/irritation (Cat. 2)
TEGMA	Triethylene Glycol Methyl Ether Methacrylate	Not a hazardous substance or mixture.
AODMBA	(r)-α-Acryloyloxy-β,β-Dimethyl-γ-Butyrolactone	Skin corrosion/irritation (Cat. 2)
EGDPEA	Ethylene Glycol Dicyclopentenyl Ether Acrylate	Skin corrosion/irritation (Cat. 2)
DEGMA	Di (Ethylene Glycol) Methyl Ether Methacrylate	Not a hazardous substance or mixture.
IBMA	Isobornyl Methacrylate	Not a hazardous substance or mixture.
PEGDA	Poly (Ethylene Glycol) Diacrylate	Skin corrosion/irritation (Cat. 2), Serious eye damage/ eye irritation (Cat. 1) Skin sensitisation (Cat. 1)
DMPA	2,2-Dimethoxy-2-phenylacetophenone	Acute toxicity, Oral (Cat. 4) Specific target organ toxicity, repeated exposure (Cat. 2)

3.3 High Throughput Screening (HTS) Methods

In section 3.3, the various key methods used in the fungal anti-attachment HTS polymers would be shared and discussed.

3.3.1 Preparation in 96-Well Plate HTS Array

The level of 2,2-dimethoxy-2-phenylacetophenone, DMPA (either 1 or 4 w/v %, 196118, Sigma Aldrich) required for polymerisation was dissolved into the respective monomer using an ultrasonic cleaner (Figure 3.3) for up to 15 minutes. 5 ml glass bottles containing monomers and initiator were wrapped with aluminium foil to minimise exposure to UV and was purged with N_2 for 5 minutes after it was dissolved. The solution was then transferred into 1.5 ml polypropylene microcentrifuge tubes held within the holder of the liquid handling apparatus (Microlab STARlet, Hamilton Robotics, Inc.) as per the equipment shown in Figure 3.4 below. A four-channel pipette liquid (highlighted in Figure 3.6) handling head equipped with 50 µl pipettes (CO-RE non-filter tips, Hamilton Robotics, Inc.) was then utilised to perform high-throughput dispensing of monomers into the wells of 96-well plates. For the preparation of copolymers, the individual amount of monomers was dispensed into a well and automatically pipette mixed with a five-cycle aspiration process.



Figure 3.3: *Ultrasonic cleaner (40kHz frequency, heating power 100W and ultrasonic power 100W) was used to dissolve the initiator into a monomer.*



Figure 3.4: *Microlab STARlet from Hamilton company designed for auto pipetting (Adapted from company's product catalogue).*[192]

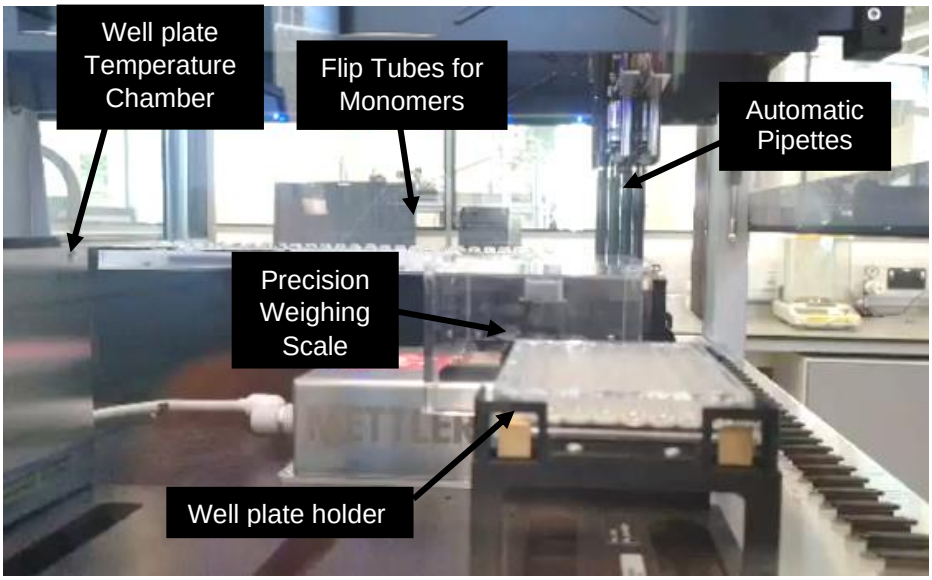


Figure 3.5: *Detail components of the liquid handling apparatus setup.*[192]

The mechanism operates using air displacement, and all four channels were equipped with pressure sensors to monitor pressure change during pipetting. The 96-well plate filled with monomers was then exposed to a Phoseon ™ Technology 365 nm wavelength UV

source at a distance of approximately 10 cm away for 5 minutes. This constant 5 minutes of exposure resulted in a UV energy input within the range of 3000 – 3500 mJ/cm^2 according to measurement with a UV light meter from OAL Instrument. UV energy measurement is straightforward and involves the use of a UV light meter, turning on the switch and leaving it under desired UV light exposure and time to collect UV energy information.

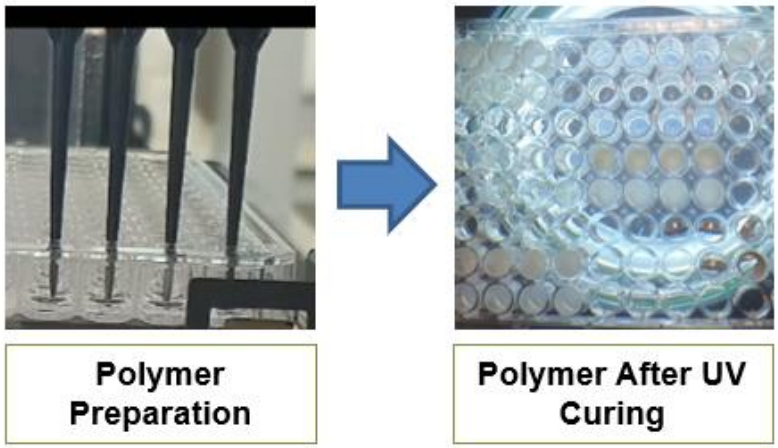


Figure 3.6: *Four pipette channel dispensing into well plate, followed by UV curing of whole 96-well plates to obtain a moulded polymer.*

The well plate was then placed in a Heraeus vacuum oven under vacuum conditions at room temperature for seven days to remove residual monomers before it was rinsed with isopropanol (IPA) and sterile distilled water (SDW). Each well was rinsed with 100 µl of IPA then 100µl of SDW and later soaked in 100 µl of SDW within the incubator at 37 °C for 48 hours. SDW was removed from all wells and the well plate was then placed under UV light in a biosafety cabinet for 20 minutes to eliminate potential microbial contamination prior to evaluation of fungal attachment.

3.3.2 HTS of Viscosity, Surface Tension & Z Parameter

This analysis was conducted following a high throughput method developed for inkjet printing inks by Zhou et al.[164] The same four-channel pipette liquid handling apparatus (Microlab STARlet, Hamilton Robotics) was used to determine the workability of inkjet candidates. For viscosity measurement, 300 µl of monomer was added into 96 well polypropylene plate (260252, Thermo Scientific), and the pipette automatically extracts each monomer from their respective wells before proceeding to dispense out its content. The 96-well plates were also placed in a temperature chamber as per Figure 3.5 to ensure viscosity was measured at a constant room temperature of 25 °C. Pressure during dispensing was recorded by a pressure sensor equipped in the pipettes, and thus the viscosity could be calculated using Equation 3.2 by generating a pressure versus time curve with continuous dispensing of monomers.

For surface tension, it was measured with the assistance of a high-precision balance (WX205SDUV/15, Mettler Toledo) that was installed into the liquid handling apparatus (shown in Figure 3.5). About 100 µl of monomer was aspirated into a pipette and displaced at a rate of 5 µl/s on the weighing scale. Calculation of surface tension could be determined by equation 3.3. Fromm's Z parameter, which predicts printability, can be calculated when dynamic viscosity and surface tension values of ink are both used in equation 3.4. Mean values of three measurements for both viscosity and surface tension were used to ensure repeatability and minimise experiment error.

$$P_{gas} = \int_0^H \frac{8\mu Q}{\pi\left(\frac{Rt+R(t-0.01)}{2}\right)^4} dH - \rho g(0.02 - H_t) - \frac{2\gamma \cos\theta}{R_t} \quad \textbf{(Equation 3.2)}$$

Where µ is dynamic viscosity, *Q is volumetric flow rate*, *Rt is the radius*, *ρ is density*, *g is gravity*, and *Θ is the contact angle*

$$\gamma_{sample} = m_{sample} \frac{\gamma_{water}}{m_{water}} \quad \textbf{(Equation 3.3)}$$

Where γ is surface tension, *m is droplet mass*

$$z = \frac{\sqrt{\rho r \gamma}}{\mu} \quad \textbf{(Equation 3.4)}$$

Where μ is dynamic viscosity, γ is surface tension, ρ is the density of the ink, r is nozzle diameter

3.4 Characterisation and Evaluation Methods for the Resulting Polymers

3.4.1 Fourier-Transform Infrared Analysis (FTIR)

FTIR evaluation was conducted using a Spectrum Two Spectrophotometer (Perkin Elmer) equipped with Universal Attenuated Total Reflection (UATR Diamond/ ZnSe) as shown in Figure 3.7. This technique was used to characterise the degree of conversion (DOC) from monomers to polymer, i.e., the level of cure. The wavelength of the measurement was set to a range of 700 to 4000 cm^{-1}, and an accumulation of three scans was collected. The data was baseline corrected and normalised to the principal peak in the 1720 – 1740 cm^{-1} region which represents the C=O group of the acrylate functionality. C=O group would remain the same in both monomer and polymer as it does not take part in the polymerisation process. The DOC was then determined by calculation as per Equation 3.5, comparing the area of the peaks in around 1618 - 1637 cm^{-1} region which were defined as the C=C. Decreasing the C=C bond correlates to increasing DOC as the C=C bond converts to C-C bond during the polymerisation process. FTIR scans were repeated thrice to check their repeatability and to minimise experiment error. Tabulated mean values were used in the comparison of DOC.

$$\mathrm{DOC} = \left(1 - \frac{\mathrm{A_{C=C}/A_{C=O}}}{\mathrm{A'_{C=C}/A'_{C=O}}}\right) x\ 100\ \% \qquad \textbf{Equation 3.5}$$

where $A_{C=C}/A_{C=O}$ is the peak area in polymerised resin and $A'_{C=C}/A'_{C=O}$ is the peak area of non-polymerised resin.

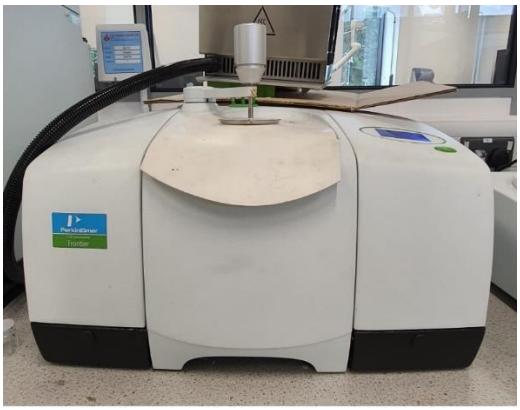


Figure 3.7: *FTIR equipment with ATR setup for direct measurement of DOC.*

3.4.2 Differential Scanning Calorimetry (DSC) Analysis

DSC was conducted on a Perkin Elmer DSC8000, it was used to characterise the T_g of the polymers and copolymers synthesised. A standard DSC measuring pan from Perkin Elmer was used for the measurement, 5 to10 mg of samples were placed into the pan and the lid was secured with a standard sample pan crimper press. A reference sample was prepared with an empty sample pan and placed in the right platinum holder as shown in Figure 3.8, the sample pan with the actual sample was then placed in the left platinum holder. Both holders were also covered with a platinum lid. The DSC profile was programmed to heat from -70 °C to 200 °C, the materials were heated and cooled twice at a rate of 5 °C/min, and the 2nd heat curve was utilised to analyse T_g temperature by extrapolation method.

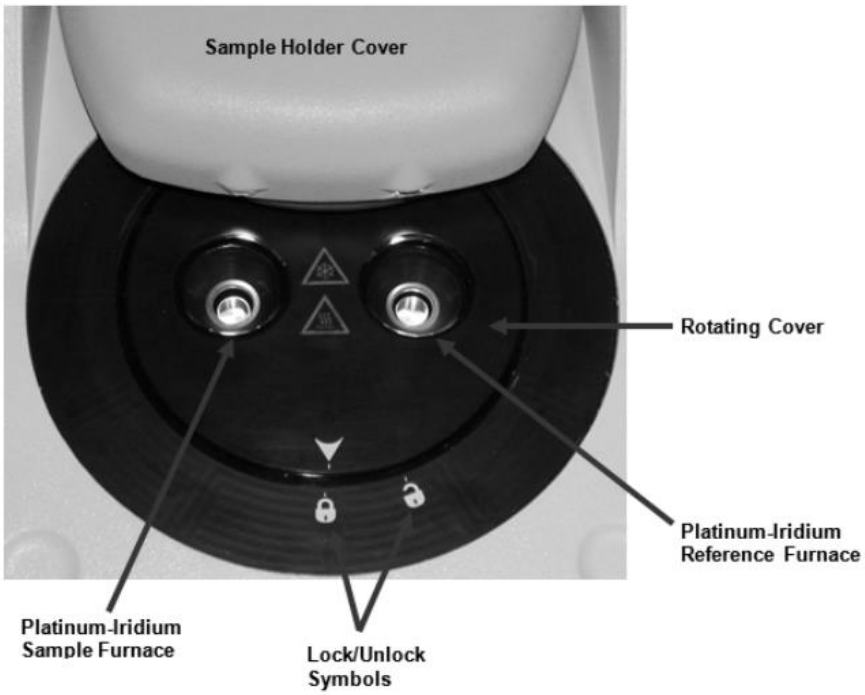


Figure 3.8: *The sample chamber of DSC where samples were placed in platinum holders above the heating furnace.* [193]

3.4.3 Evaluation of Fungal Attachment, Residual & Polymer Toxicity (XTT Assay)

The XTT tetrazolium salt (2,3-Bis-(2-Methoxy-4-Nitro-5-Sulfophenyl)-2H-Tetrazolium-5-Carboxanilide) assay (XTT assay) followed the method reported by Vallieres et al.[34] For every XTT assessment, a well with Roswell Park Memorial Institute (RPMI) 1640 medium, a known positive control (PEGDA), a known negative (AODMBA), blank (of polystyrene well plate surface) and three data measurements were used in tabulation and comparison of fungal metabolic activity.

C. albicans carrying a CAF2-yCherry construct was grown overnight in 50 ml conical flasks (inoculated from colonies) containing Yeast Extract-Peptone-Dextrose (YPD) broth at 37 °C with orbital shaking at 150 rpm. The overnight cultures were washed twice in RPMI 1640 medium and then diluted to 125,000 cells/ml in RPMI medium. Aliquots of

100 µl were transferred to wells of the 96-well plate with moulded polymer cured in the plates, before static incubation for two hours at 37 °C. Non-adherent cells were removed by three washes with phosphate-buffer saline (PBS). 100 µl RPMI 1640 was added to the remaining attached cells of each well, and the 96-well plate was incubated statically at 37 °C for 24 hours. A schematic overview of the process is depicted in Figure 3.9.

To measure biofilm metabolic activity after 24 h with XTT, the wells were rinsed again thrice with PBS to remove non-adherent cells, and the reaction was initiated by combining XTT and menadione at final concentrations of 210 $\mu g.ml^{-1}$ and 4.0 µM, respectively (42 µl of the XTT and menadione mix was added to 158 µl of fresh RPMI in each well). After two hours of static incubation, 100 µl of the reaction solutions were transferred to a new 96-well plate, and formazan absorbance at 490 nm was analysed using a BioTek EL800 microplate spectrophotometer.

Tests of both polymer toxicity and residual toxicity followed a similar procedure as the fungal attachment assay with XTT described above. In polymer toxicity, the PBS rinse steps to remove non-adherent cells after 2 hours and at 24 hours were omitted. Well plate with polymer, RPMI medium and cells were left in the incubator for 24 hours straight. After 24 hours, measurement of metabolic activity was measured directly with 42 µl of the XTT and menadione mix (with the same concentration as attachment assays) and 70 µl fresh RPMI was added to the remaining RPMI in each well. After 2 hours, 100 µl of reaction solutions were transferred into a new well plate and evaluated with BioTek EL800 microplate spectrophotometer.

In residue toxicity evaluation, polymers prepared in the 96-well plates were first soaked in 100 µ**l** of RPMI medium for 24 hours in the incubator. The process assumes low

molecular weight residues will leech out from the polymer into the medium. 125,000 cells/ml were then prepared and added to this 100 µl medium and incubated for 24 hours straight. After 24 hours, the measurement of metabolic activity repeats as per the steps carried out in polymer toxicity evaluation.

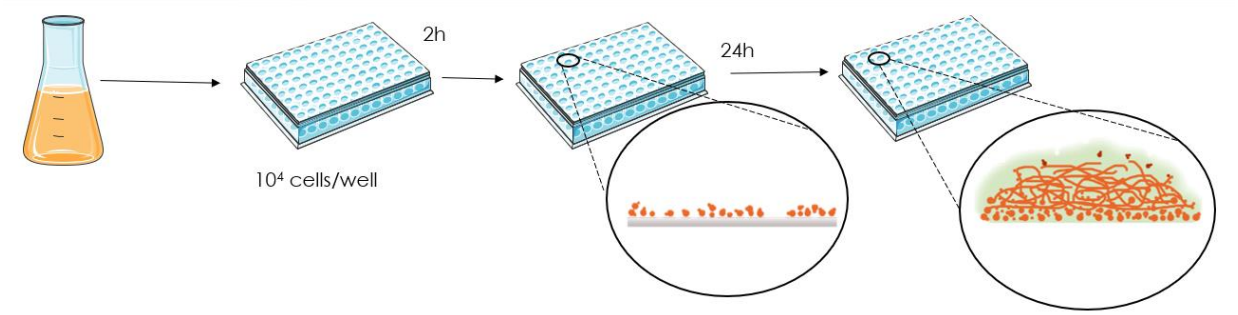


Figure 3.9: *C. albicans was inoculated overnight in YPD broth and was later transferred to RPMI medium to be used in well plates for XTT assay. Evaluation of fungal attachment to polymers (coated/ placed in well plates) was carried out for 24 hours. After placement of C. albicans for 2 hours, non-attached C. albicans were washed away and the attached cells were left to grow for 24 hours.*

3.4.4 Evaluation of Fungal Attachment (Crystal Violet Staining)

This method was reported as part of the protocol by He et al. and was considered for a voice prosthesis flap device as a scale-up alternative to XTT assay.[194] The voice prosthesis flap samples were fitted into a 12-well plate. While both XTT assay and crystal violet staining can be used to evaluate the presence of fungi, crystal violet works differently by binding to negatively charged surface molecules and polysaccharides in the extracellular matrix of fungi cells. The key advantage of crystal violet when compared to XTT is the lower cost and the ability to visually observe where the fungi are attached to the polymer. However, it was also reported that crystal violet may not be compatible with all materials.

The preparation of *C. albicans* in broth is similar to the steps described in 3.4.3. *C. albicans* carrying a CAF2-yCherry construct were grown overnight in YPD broth at 37 °C with orbital shaking at 150 rpm. The overnight cultures were washed twice in RPMI 1640 medium and then diluted to cell suspension at a final concentration of 1×10^6 ml^{-1} cells in RPMI 1640. Aliquots of 1 ml were then transferred to each well of the 12-well plate, before static incubation for two hours at 37 °C. Voice prosthesis flap samples were then transferred to a new plate and non-adherent cells were removed by three washes with 2ml of PBS, 1 ml fresh RPMI 1640 was added to the remaining attached cells in each well, and the 12-well plate was incubated statically at 37 °C for 48 hours. After 48 hours, the RPMI medium was carefully removed using a pipette and samples were transferred to another new plate. Attached *C. albicans* were stained with 2ml of 0.5 % w/v crystal violet solution for a minute at room temperature, washed thrice with 2ml PBS. For quantification with BioTek EL800 microtiter plate reader at 600 nm, dissolve the remaining crystal violet (which is adhering to the sample) with 1ml ethanol and transfer 100 µl into a 96-well plate.

*3.4.5 Raman Spectroscopy***

Raman spectroscopy was performed using a HORIBA LabRAM HR Raman microscope (Figure 3.10). Spectra were acquired using a 785 nm laser (at ~20 mW power), a 100x objective and a 200 µm confocal pinhole. For simultaneously scanning for a range of Raman shifts, 300 lines mm^{-1} rotatable diffraction gratings along a path length of 800 mm were employed. Spectra were detected using a Synapse CCD detector (1024 pixels) thermoelectrically cooled to −60 °C. Before spectra collection, the instrument was

**Raman Spectroscopy: Experiment and data analysis were supported by Graham Rance from Nanoscale and Microscale Research Centre (nmRc), University of Nottingham. Raman Spectroscopy was also funded by nmRc nanoprime funding.

calibrated using the zero-order line and a standard Si (100) reference band at 520.7 cm^{1}. In this configuration, the spectral resolution obtained is better than 1.7 cm^{-1}.



Figure 3.10: *HORIBA LabRAM HR Raman microscope evaluates copolymer ratio by providing details of chemical structure.*

Similar to tabulation in FTIR, Equation 3.5, the DOC from monomer to polymer was determined by measuring the change in the ratio of peak areas associated with the C=C (~1640 cm^{-1}) and C=O (~1730 cm^{-1}) bonds before and after polymerisation.

(Point Spectral Measurement) For each monomer, one single point spectrum was acquired over the range 490-1870 cm^{-1} (one spectral window) with 20-60 s integration time and 2-4 accumulations to automatically remove the spikes from cosmic rays and improve the signal-to-noise ratio. For each polymer, three single-point spectra from random locations were acquired under similar conditions. The spectra were then averaged to give a mean value.

(Multispectral Array Measurement) For each polymer, multispectral images were created by collecting spectra (2 s integration time, 1 accumulation, range 490-1870 cm^{-1}, 1 spectral window) in 2 µm steps from within a 50x50 µm area (676 spectra in total). Spectra were manually de-spiked, extracted within the range 500-1400 cm^{-1} and fitted with the component polymer spectra using Classic Least Squares (CLS) regression analysis within Labspec 6.5 software. Images were generated by plotting the scores from CLS analysis. CLS scores were normalised to a total of 100%.

*3.4.6 Proton Nuclear Magnetic Resonance (^{1}H NMR)***

^{1}H NMR was used to evaluate the copolymer ratio and polymerisation reaction of copolymers and hyperbranched polymer tripropylene glycol diacrylate (HBP-TPGDA). ^{1}H NMR evaluation was performed on a Bruker AV400 spectrometer (400 MHz) at 25 ºC. Samples were prepared as 5-10 mg/ml solutions in deuterated chloroform ($CDCl_3$) and pipetted into an NMR sample tube. Spectra were recorded at 400 MHz on a Bruker AV400 instrument and referenced to the residual solvent peak (7.26 ppm for $CDCl_3$). Analysis of spectra was then carried out using Mestrelab Mnova 10.0 software.

(Determination of molar ratio in copolymers with ^{1}H NMR) The residual solvent $CHCl_3$ peak (7.26 ppm) was used as an internal reference. Assessment of the ratio was tabulated with reference to methoxy group of TEGMA (singlet at 3.39 ppm), three methoxy groups of TBCHA (singlet at 1.88 ppm) and dimethyl group in AODMBA (doublet at 5.35 ppm).

(Determination of polymerisation progress in HBP-TPGDA) The residual solvent $CHCl_3$ peak (7.26 ppm) was used as an internal reference. The polymerisation progress

can be witnessed by a reduction in acrylate peaks which are the three multiplets between 5.5-6.5 ppm. In addition, a broad peak growing at ~2.6 ppm is typical of the polymerisation process.

*3.4.7 Gel Permeation Chromatography (GPC)***

GPC test provides information on polydispersity index (PDI) and molecular weight of oligomers, polymers and copolymers. Samples were dissolved in HPLC-grade tetrahydrofuran at a concentration of 2 mg ml^{-1} and allowed to equilibrate for 2 hours. Equilibrated samples were filtered through a 0.22 µm PTFE syringe filter. The filtered solutions were analysed by GPC using an LC 1120 HPLC pump eluting in tetrahydrofuran at a temperature of 35 °C at a flow rate of 1 ml min^{-1} through an Agilent PLgel Mixed-C column and a differential refractive index detector. Calibration was performed using narrow PDI polystyrene standards at a flow rate of 1 ml min^{-1}. Analysis was performed offline using ASTRA software (Wyatt Technology Corp.).

** NMR & GPC: Experimental and data analysis were supported by Joseph Sefton and Amy Stimpson from Centre for Additive Manufacturing (CfAM), University of Nottingham.

*3.4.8: Time-of-Flight Secondary Ion Mass Spectrometry (ToF-SIMS)***

Polymer samples were prepared with HTS UV Curing as per 3.3.1. ToF-SIMS is a measurement technique used to analyse the surface and is used as a complimentary technique to evaluate the copolymer ratio on the surface. Mass spectrum was obtained on a ToF IV instrument IONTOF GmbH (Münster, Germany) equipped with a 25 keV bismuth ion beam. A pulsed low-energy electron flood gun was applied for charge compensation. Scanning was performed in a sawtooth mode with one ion pulse per pixel and one frame per patch. The following settings were used, raster size 500 × 500 $µm^2$

with a raster resolution of 256 x 256 pixel, beam current primary ion current of ~1.0 pA for Bi^{3+}, at a cycle time of 100 µs. 20 scans were acquired for each mass spectrum. Positive polarity SIMS data were analysed using SURFACE LAB 7.0 software from IONTOF GmbH (Münster, Germany).

**ToF-SIMS: Experiment and data analysis were supported by Nichola Starr and Stefanie Kern from Nanoscale and Microscale Research Centre (nmRc), University of Nottingham. ToF-SIMS test was also funded by nmRc nanoprime funding

3.4.9: Microscopic Imaging

Microscopic samples looking at inkjet printing resolution were imaged and measured using five and/ or ten times resolution with Nikon Eclipse LV100ND Optical Microscope.

3.5 Additive Manufacturing Process

3.5.1 Ink Preparation

AM inks with good dispersion and minimal contamination are essential for stable printing performance, hence the preparation steps include further N_2 purging and filtering process. For the main studies with HTS and inkjet printing, inks were prepared with either 1 w/v % or 4 w/v % loading of DMPA initiator. Monomers were pipetted into a 5 ml glass vial (wrapped with aluminium foil) with a magnetic stirrer, and a suitable amount of DMPA was added. The mixture was stirred at 1000 rpm at room temperature for 15 to 20 minutes to dissolve the DMPA initiator. Once dissolved, the inks were purged with N_2 gas for five minutes before being filtered through a 5 µm PTFE syringe filter that removes particles/ contaminants.

Inks prepared for SLA printing process followed the same preparation steps except that the initiator used was Iragure 819 from BASF (1 – 4 w/v %) instead and includes 1 w/v % of curcumin on top of monomers and initiators. Curcumin added in SLA printing

formulation acts as a wavelength absorber to enhance the curing process under atmospheric conditions.

3.5.2 Inkjet Printing

Dimatix materials printer (DMP-2830, Fujifilm) is a piezo-based jetting system whereby the Z parameter (tabulated with viscosity and surface tension as per Equation 3.4 in subsection 4.3.2) is critical in the droplet formation process. The protocol of ink evaluation is similar to the method written by He et al. [194] Figure 3.11 shows the engineering drawing and the different components in the printer. The printer was also enclosed in a nitrogen purging chamber with oxygen levels kept between 0.25 ± 0.05 % during the printing process. This minimises the polymerisation inhibiting effect of O_2 during the free radical photo-polymerisation curing.

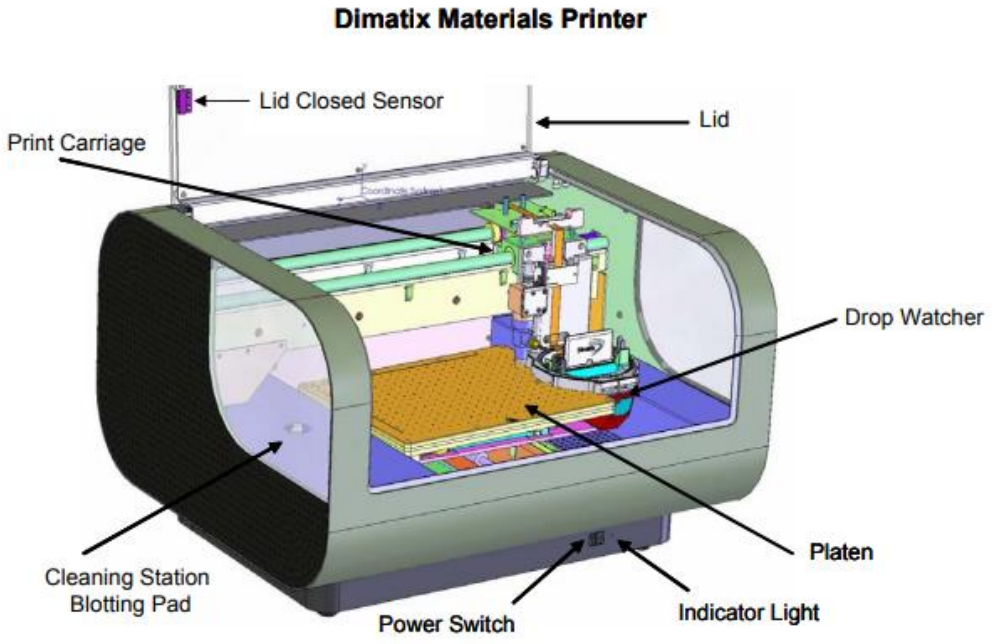


Figure 3.11: *Engineering drawing of Dimatix printer and its key component.*[195]

Inks were filled into 10 pl disposable printheads, Dimatix Materials Cartridge (DMC-11610, Fujifilm) with 16 jet nozzles, as per Figure 3.12. Before the start of printing, it is important to ensure that a new blotting pad is placed in the printer and to assess the droplet formation under the fiducial camera. Parameters including cartridge temperature (up to 70 °C) can be adjusted to obtain stable droplet formation. The in-line UV source came from a 365 nm UV LED unit (800 mW/cm^2, Printed Electronics Limited, Tamworth, UK) and was applied around the cartridge height of 0.5 mm after every single row of ink jetting onto a thin, flexible transparent sheet. Cartridge temperature settings range from 40 to 55 °C depending on monomer viscosity, 1 to 10 kHz frequency depending on the curability of the monomer. In order to better compare the different inks and to minimise varying parameters, all inks were printed with 20 µm drop space and the printing voltage was kept constant at 25 V.

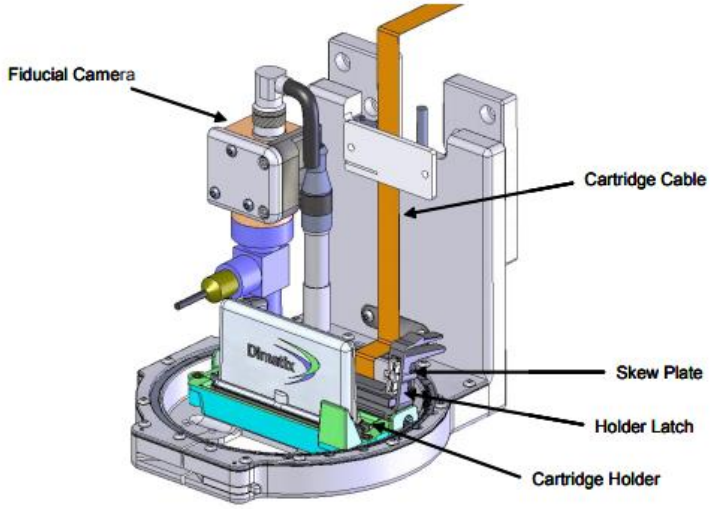


Figure 3.12: *Zoom in detail of the moving printing unit for inkjet cartridge installation.*[195]

(Inkjet Printing of 2-layers Disc-shape) For comparison studies of DOC between HTS UV-moulded polymers and inkjet-printed samples, 2 layers of a 3 mm disc-shape as per left image in schematic Figure 3.13.

(Inkjet Printing of 100-layers Disc-shape) Similar 3 mm disc-shape as above, in 100 layers for fungal anti-attachment studies and toxicity evaluations performed in a 96-well plate.

(Inkjet Printing of 110-layers Voice Prosthesis Flap) Printing files designed referring to an actual voice prosthesis flap provided by Atos Medical. The full length of the voice prosthesis flap is 1.9 cm.

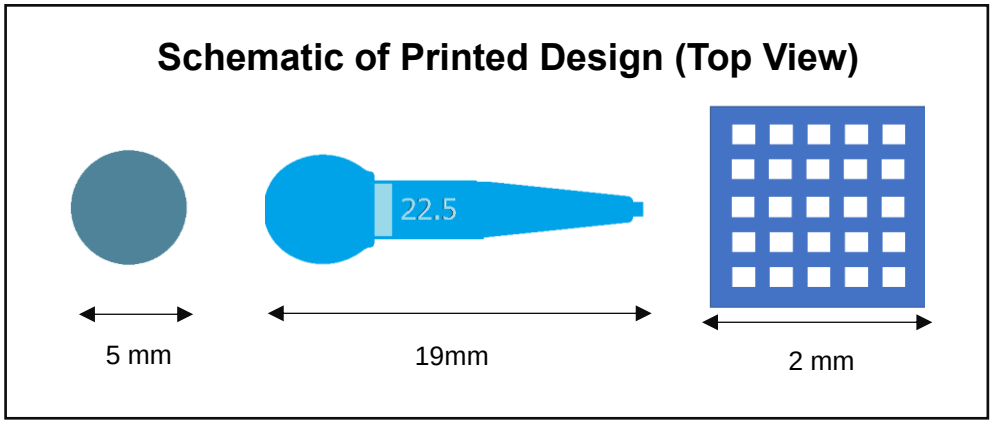


Figure 3.13: *(Left) 3 mm disc-shape pattern used for both DOC and studies using 96-well plate, (Middle) 19 mm voice prosthesis flap design, (Right) 2 mm x 2 mm porous design for µSLA.*

*3.5.3 Stereolithography (SLA)***

The ink was printed using a Boston Micro Fabrication (BMF) nanoArch S130 Projection µSLA system with a 2µm printing resolution. The system is equipped with a 405 nm wavelength UV source, a DMD as a digital dynamic mask, a projection lens and a perfluoroalkoxy (PFA) membrane for layer control. 5ml of inks were filled into a customised vat for printing trial with a maximum sample size of 2mm x 2mm x 2mm (Design as per rightmost image in Figure 3.13 above). The 3D structure was achieved at

**SLA: SLA printing was supported by Yinfeng He from Centre for Additive Manufacturing (CfAM), University of Nottingham.

UV intensity of 141 with 20 seconds of exposure time for the first layer followed by 6 seconds of exposure time for the following layers. Each layer thickness was set to 5µm.

3.6 Polymer Synthesis

*3.6.1 TEGMA Oligomer Synthesis***

The oligomer was synthesised with a catalytic chain transfer agent (CCTP) incorporated into radical polymerisation for the production of a low molecular weight product. 2,2'-azobis(2-methylpropionitrile) (AIBN) (2.21 × 10-4 mol , 1 mol% of total monomer content), cobalt(II) bromide hexahydrate (6.86×10^{-6} mol) and dimethyl glyoxime (1.37×10^{-5} mol) were added to a 50 ml round bottom glass vessel equipped with a magnetic stirrer. TEGMA (5 ml, 2.21 × 10-4 mol) was added and the solution was stirred to dissolve the solids. The vessel was sealed with a rubber septum and purged with inert argon gas for one hour at room temperature. After one hour, the glass vessel would be flooded with argon and hence be able to maintain an inert atmosphere. The vessel was then heated to 80 °C for three hours in an oil bath with continuous magnetic stirring. After which, the vessel was quench cooled to 0 °C in an ice water bath to terminate the polymerisation reaction, yielding a viscous yellow solution. The reaction mixture was analysed by ^{1}H NMR and GPC to determine conversion and molecular weight distribution.

*3.6.2 Copolymer Synthesis***

Selected copolymer ratios were synthesised for the dip coating process, the below process describes the synthesis of TEGMA:AODMBA$_{40:60}$. AIBN (2.21×10^{-4} mol, 1 mol % of total monomer content) were added to a 50 ml round bottom glass vessel equipped with a magnetic stirrer. Cyclohexanone (12.5 mL) was added with a syringe and the resulting solution was stirred at room temperature to dissolve the AIBN. TEGMA (2.00

mL, 8.84 × 10^{-3} mol) and AODMBA (2.17 mL, 1.33 × 10^{-2} mol) were added to the solution in sequence with a syringe. The vessel was sealed with a rubber septum, and the solution was purged with argon gas for an hour at room temperature. After one hour, the glass vessel would be flooded with argon and hence be able to maintain an inert atmosphere. The vessel was heated to 70 °C in an oil bath for 24 hours with continuous magnetic stirring. After 24 hours the vessel was removed from the oil bath and allowed to cool to room temperature yielding a viscous, pale-yellow solution. The crude product consisted of 20 ml volume with cyclohexanone and precipitated dropwise into a 200 ml of 0 °C IPA. The supernatant was decanted, and the precipitate was washed with a further 50 ml of 0 °C IPA. The precipitate was allowed to dry at room temperature for an hour, then dissolved in 20 ml cyclohexanone and precipitated again into 200 ml of 0°C IPA. The precipitate was then collected, and the excess solvent was allowed to evaporate overnight before drying in a 25 °C vacuum oven for 72 hours to remove residual solvent. The resulting solid was analysed by both ^{1}H NMR and GPC to determine the copolymer ratio and molecular weight distribution. Different ratios of copolymer (i.e., TEGMA:AODMBA$_{50:50}$) prepared would have their molar ratio tabulated accordingly.

*3.6.3 Hyperbranched Polymer TPGDA Synthesis***

HBP-TPGDA was prepared with TPGDA monomer (1ml, 3.0 x 10^{-3} mol), 3-Mercaptopropionic acid (0.2 ml, 2.0 x10^{-3} mol), AIBN (5 mg, 1 mol % of total monomer content) and cyclohexanone (2 ml) were added to a glass vessel equipped with a magnetic stirrer. The vessel was sealed with a rubber septum, and the solution was purged with argon gas for an hour at room temperature. After which the reaction was submerged in an oil bath at 65 ºC for the required reaction time. The gelation point is

**Polymer Synthesis: TEGMA Oligomer and copolymer synthesis were performed by Joseph Sefton and HBP-TPGDA was synthesized by Amy Stimpson from Centre for Additive Manufacturing (CfAM), University of Nottingham.

defined as the point in which the reaction solution stops stirring due to hyperbranch-hyperbranch coupling, or crosslinking, and is confirmed by attempting to dissolve the mixture in a solvent. The synthesis reaction was carried out for five minutes lesser than the predetermined gel point to produce solvent soluble HBP-TPGDA. The crude product was added dropwise to cold hexane (in a volume ratio of a 20:1 excess of the polymerisation solvent used). The yielded polymer was an opaque viscous liquid collected through vacuum filtration. The resulting solid was analysed by both ^{1}H NMR and GPC to determine the copolymer ratio and molecular weight.

3.7 Dip Coating Method

Apart from the demonstration of AM with the selected copolymers, dip coating of the polymers was another method of utilising these copolymers in medical devices. For the dip coating process, a dip coating unit, model HO-TH-01 from Holmarc Opto-Mechatronics Ltd was used. A copolymer solution in dichloromethane solvent was prepared at a concentration of 200 mg /ml. A needle was used to securely pierce through the silicone rubber voice prosthesis flap and the other end of the needle was fastened tightly to the dip coating equipment (as shown in Figure 3.14). The dip coating unit was set to move the needle into a vial with coating solution at a rate of 9 mm/s and retract at a speed of 2 mm/s. The voice prosthesis flap was first dipped into a silicone rubber primer and allowed to dry for five minutes before being dipped another three times into copolymer solution, each coating process had a drying time of at least five minutes. Finally, the sample was left to dry at room temperature for an hour before it was placed in a vacuum oven for 24 hours to remove the remaining solvent.



Figure 3.14: *Dip coating unit setup with a needle to secure silicone rubber flap prior to dipping into copolymer solution.*

3.8 Statistical Analysis

The key statistical analysis used in this work were performed with Minitab 18 software. Statistical analysis includes analysis of variance (ANOVA) to assess if the data between groups are statistically different. ANOVA was performed when comparing improvement in DOC of HTS UV-cured polymer between 1 % and 4 % DMPA initiator, assessing residue and polymer toxicity data and studying the impact of TEGMA:AODMBA ratios (30:70, 35:65, 40:60, 50;50) on its fungal attachment results. In order to determine the predictability of DOC between HTS UV-cured polymer to inkjet-printed polymer, a non-linear regression model was selected to fit the obtained values, a non-linear polynomial model was able to best fit the obtained DOC values. Lastly, standard deviation and mean value in collected data were either tabulated with Microsoft Excel 2019 or achieved during graph plotting with the software Graphpad Prism 8.

Chapter 4: Development of High Throughput Screening (HTS) Methods

4.1 Introduction

This chapter describes the design and validation of a process to achieve the HTS of materials to evaluate if they exhibit the following combination of properties: (a) suitability for AM processing, (b) demonstrate fungal anti-attachment properties and (c) exhibit target mechanical properties from the cured final polymer. Nine candidate monomers were selected by data-mining the results of a previous study that used a HTS microarray method to screen 281 methacrylate and acrylate polymers for their fungal anti-attachment.[34] However, the previous screening focused on evaluating a large number of methacrylate and acrylate that could prevent fungal attachment and did not consider inkjet printability or their mechanical properties. The screening method developed in this study will build on this initial screening programme by scaling up the polymer preparation and considering the AM processability and the properties of the end product. This HTS methodology was subsequently used in chapter 5 to prepare and evaluate a larger library of copolymers to obtain materials with varying glass transition temperatures (T_g). In chapter 4, one homopolymer candidate was also used to demonstrate its suitability in SLA processing, this exhibited the potential of this HTS methodology and also exhibited the potential of inks to be used on other UV-based polymerisation AM techniques.

4.2 UV Curing Apparatus

As the polymers are to be UV-cured, a standalone UV light (365 nm) curing apparatus (as shown in Figure 4.1 was built and evaluated). This apparatus was used as an alternative curing strategy over printing every single sample with the inkjet printer, which was found to be a processing bottleneck in determining the AM suitability of the formulated inks.

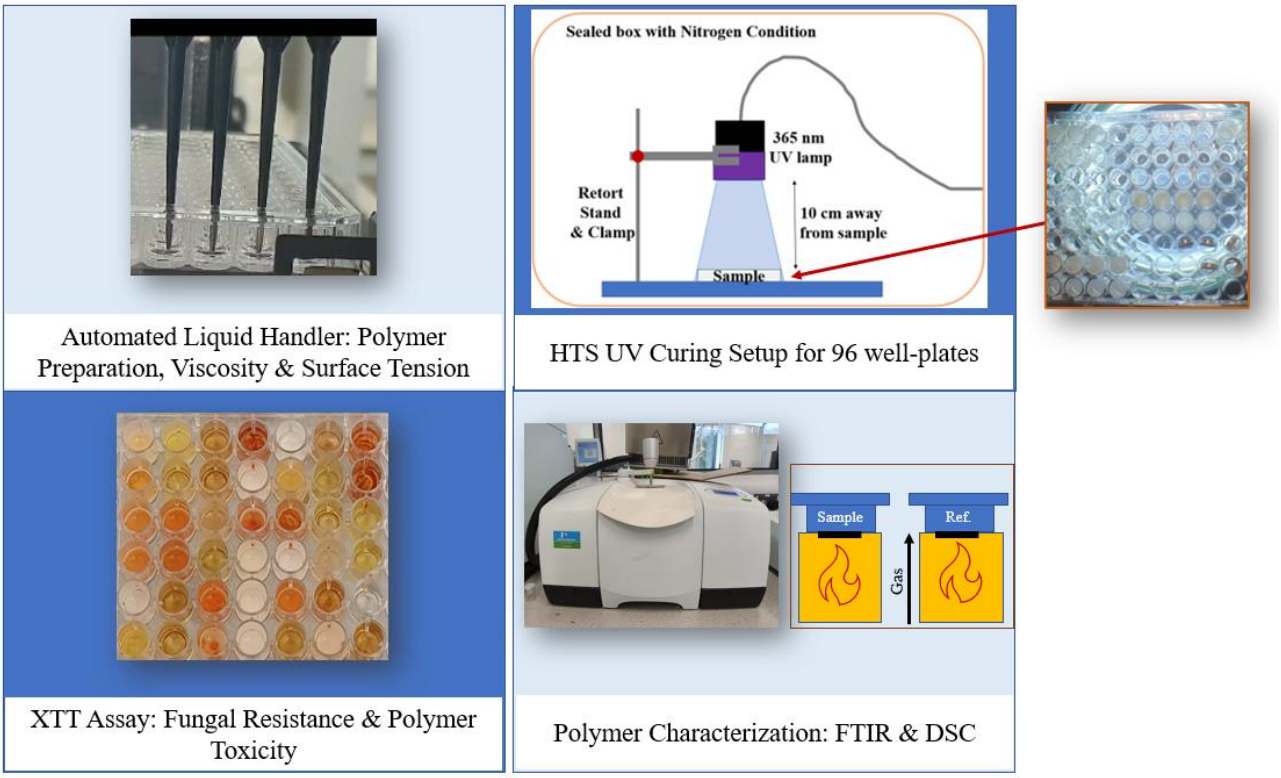


Figure 4.1: *Schematic showing a summary of HTS methodology using a liquid handling apparatus, differential scanning calorimetry (DSC), Fourier-transform infrared spectroscopy (FTIR), and XTT assay for fungal resistance and polymer toxicity evaluation.*

The aim was to remove from the evaluation process the time needed to individually print a disc shape sample of 3 mm in diameter via layer-by-layer deposition that could then be introduced into a 96-well plate for conducting of fungal attachment assay. It can take an estimated time of about 5 hours or more to print 100 layers, depending on the ink's curability and reactivity. Therefore, this proposed method, which would mould the various monomers directly into a 96-well plate, would allow a more efficient and high throughput preparation method. Furthermore, the automated multi-pipette liquid handler was adopted to rapidly deposit monomers into the well plate, which were then cured simultaneously with the standalone UV curing apparatus. The performance of these well plate moulded samples in the 96-well plate was then compared with that of the 2-layer inkjet-printed samples to ensure that trustworthy results were produced. 2-layer printed samples were selected for this comparison because that would ensure sufficient material thickness for direct evaluation with FTIR ATR.

As it was known from the trial that 2-layer printing would take about five minutes, it was estimated that the standalone UV system also needed to deliver a constant UV exposure time of five minutes which is the same time required for 2-layer printing. Also, a longer constant exposure time under a strong UV lamp source may generate much higher UV energy levels which could lead to UV photodegradation in the polymers. Thus, the evaluation commenced with direct five minutes exposure time with the standalone UV light source. UV strength of the standalone UV apparatus was measured for five minutes and was found to be roughly 3,000 mJ/cm^2 (method described in chapter 3, under subsection 3.3.1). Later in section 4.4, the DOC of the inkjet-printed layers (for 2-layers) and DOC of UV apparatus cured samples would be evaluated and analysed to provide a

correlation of both methods. However, it is important to note that the standalone UV curing apparatus will not be identical to the UV source in the Dimatix printer, as the UV light in the printer continuously moves in a sweeping motion along the printing axis with every droplet deposition. The standalone UV apparatus was also placed further to the well plate when compared to the UV source attached to the inkjet printer. UV standalone apparatus was placed 10 cm away from the well plate so that every well can be sufficiently exposed.

4.3 Evaluation of T_g and FTIR

Monomers were mixed with 1 % DMPA initiator and polymerised using the UV apparatus curing parameters described in section 4.2. The polymer preparation began with 1 % initiator so as minimise the risk of excess unreacted initiator that may be toxic to humans. The cured polymers were then subjected to DSC analysis, providing T_g data that would aid in the definition of the rigidity/ flexibility of the polymers prepared from the above nine monomers. Figure 4.2 & 4.3 show examples of the DSC spectra obtained for AODMBA and TEGMA (DSC spectra for other polymers can be found in Appendix 1.)

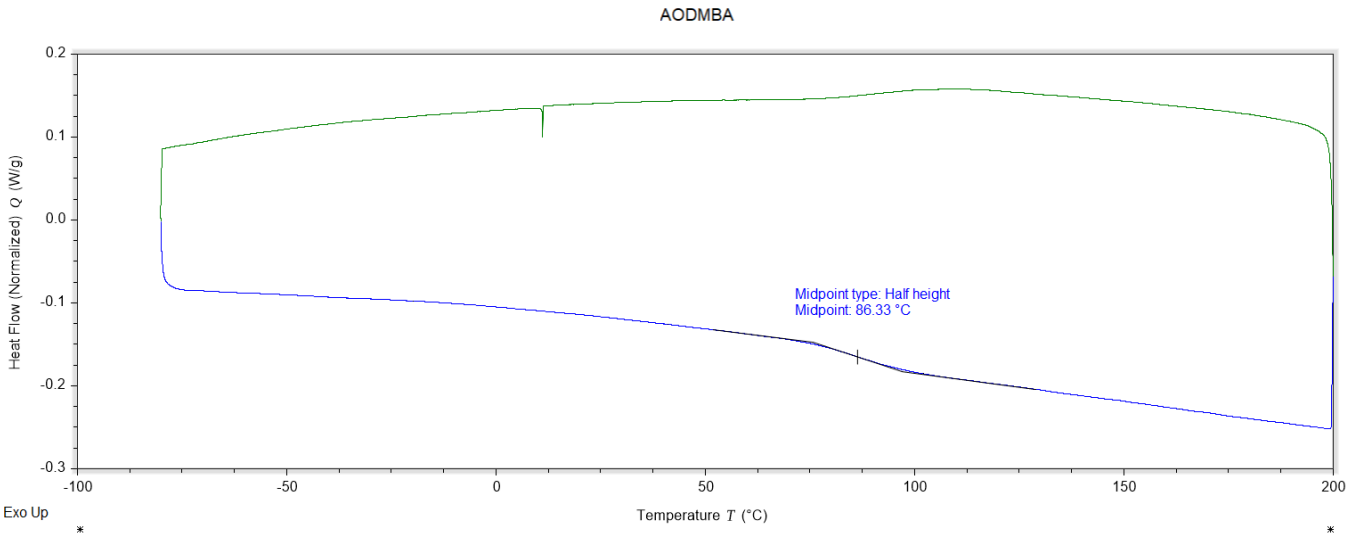


Figure 4.2: *DSC thermogram of AODMBA, half extrapolated from the onset of C_p.*

AODMBA has T_g at 80.3 °C which was demonstrated by a rigid AODMBA at room temperature.

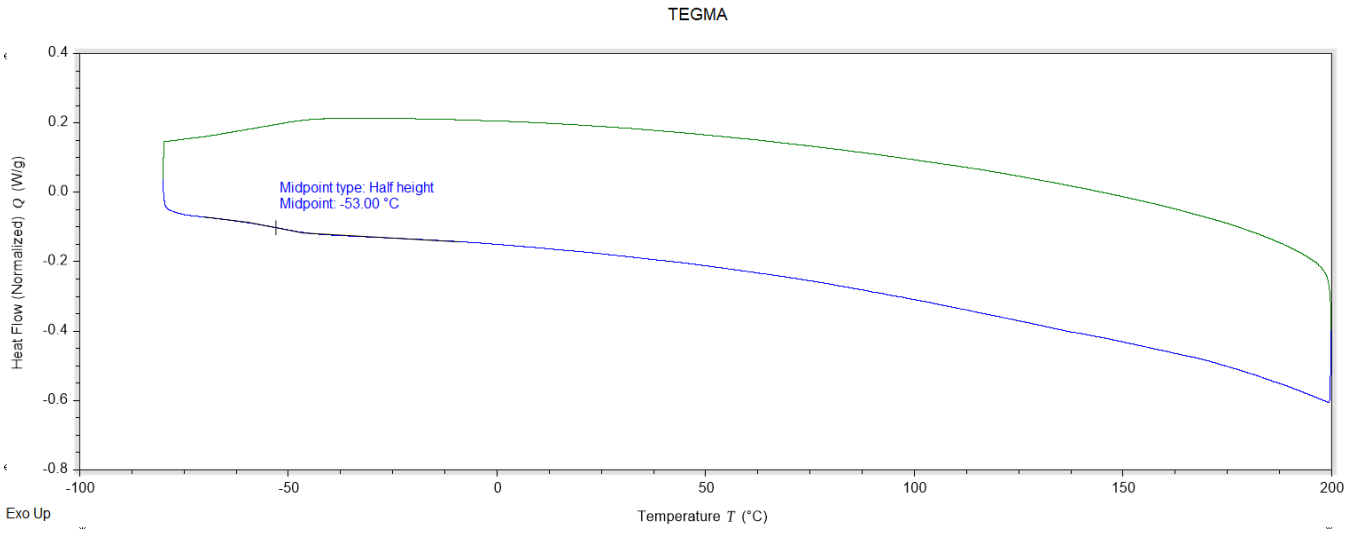


Figure 4.3: *DSC thermogram of TEGMA, half extrapolated from the onset of C_p. TEGMA has a very low T_g and is gel-like at room temperature.*

The DSC run profile was set to heat and cool twice with a heating-cooling profile from -70 to 200 °C and T_g data was determined from half extrapolation of heat capacity (C_p) from the onset. The ethylene oxide-containing polymers within the test set (I.e., DEGMA, TEGMA and PEGDA were all noted to exhibit low T_g in the negative Celsius range. As a result, TEGMA and DEGMA were visibly soft and gel-like at room temperature due to their low T_g. Meanwhile, PEGDA, which also has a low T_g, was observed to be more structured and solid. This was attributed to the presence of two reactive centres in the diacrylate, which allows it to undergo better curing and to be able to form a three-dimensional network upon exposure to UV. In PEGMA sample, no T_g was detected even as the samples were repeated in DSC evaluation, PEGMA was continuously tested and the lack of T_g will be discussed in section 4.4. The remaining polymers have higher T_g values falling within the range of 23 – 159 °C. A summary of the T_g and DOC exhibited by the test samples can be found in Table 4.1.

Table 4.1: *Summary of T_g values for the nine polymer samples synthesised using the standalone UV apparatus. Literature value of available polymers was also shared (for polymers where T_g data was not found, N/A signifying not available was indicated). DOC measurement of the polymers prepared with UV apparatus was also repeatedly checked for an average of 3 times, n= 3.*

POLYMER	DEGMA	PEGMA	TEGMA	PEGDA	AODMBA	TBCHMA	TBCHA	IBMA	EGDPEA
Literature value of T_g (°C)	-35.2[196]		N/A	N/A	N/A	130 - 178[197]	N/A	N/A	N/A
T_g (°C)	-36.0	*Not Detected*	-53	-24	86	159	121	88	23
DOC 1	53.9		66.5	48.1	61.4	68.7	80.5	47.5	71.4
DOC 2	62.4		60.1	61.6	75.4	79.8	83.9	57.0	81.7
DOC 3	63.6		59.7	71.7	60.3	82.4	84.4	55.4	75.5
Ave. DOC	64.0		60.0	62.0	63.0	78.0	83.0	68.0	84.0

The DOC was measured with FTIR by observing the conversion of carbon double bond to evaluate the level of cure of each polymer that had been obtained in the standalone UV treatment. This was done as per equation 3.1 and as described in chapter 3, subsection 3.4.1. DOC was measured thrice, and an average value was obtained. An in-depth discussion of the DOC analysis can be found in later section 4.6.

4.4 *C. albicans* Polymer Anti-Attachment and Toxicity

XTT assay is limited when it comes to providing information on the formation of *C. albicans* biofilm however it is high throughput and can detect the metabolic activity of living *C. albicans* cells. Hence, in this study, XTT assay was selected for in vitro quantification of both cell proliferation and polymer toxicity assessment. Figure 4.4 below shows a summary of the *C. albicans* attachment for all nine polymers based on the mean data of three measurements (n=3).

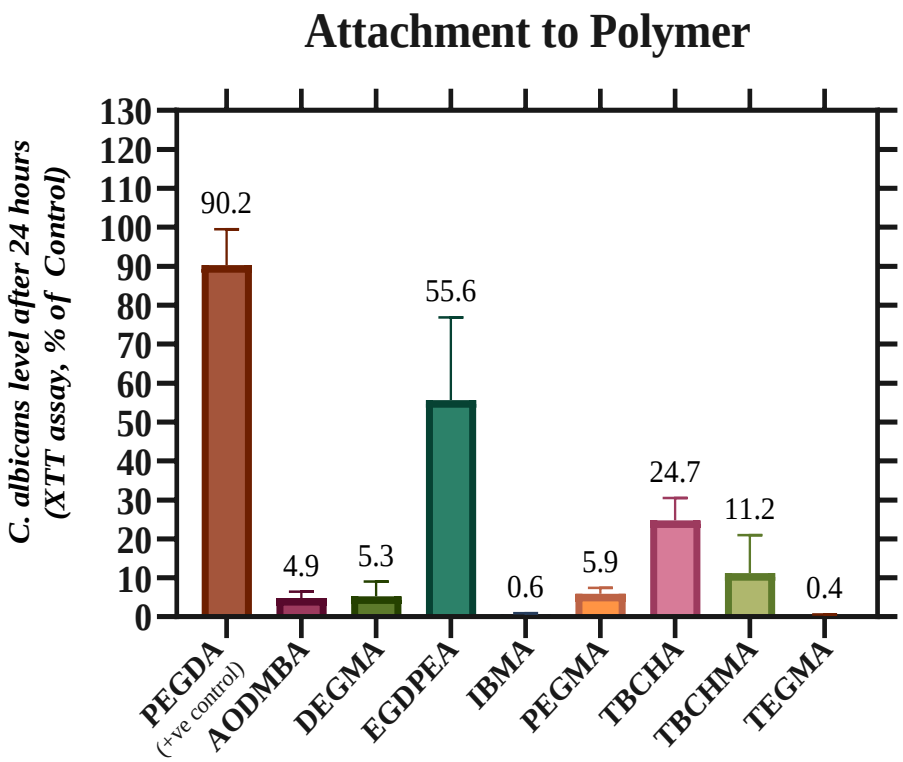


Figure 4.4: *Plot of XTT assay data showing the level of C. albicans colonisation on the polymer after 24 hours, PEGDA being included as a known positive control. Mean value based on three measurements, n = 3. (TBCHA data was based on a total of 2 measurements only, n = 2 as the 3rd sample was likely to be contaminated)*

The data from the attachment assay showed that all the test materials except for EGDPEA (and the PEGDA positive control) were able to resist *C. albicans* colonisation. They all exhibited <15 % of *C. albicans* attachment after 24 hours when compared to the polystyrene well-plate surface which was the value used to normalise the data. Among these, ethylene oxide-containing materials, PEGMA, DEGMA and TEGMA, were all found to swell during the assay.

This led these samples to expand from the 96-well plate in the presence of moisture from the medium and disintegrate. Later T_g and FTIR confirmed that there was no conversion of PEGMA monomer to polymer under the selected curing condition, thus no T_g could be detected. For DEGMA and TEGMA, the visual observation of swelling was similar to that of PEGMA, and this was attributed to a combination of their; (a) low T_g (-36 °C and -53 °C respectively), (b) affinity to become solvated by water as they are hydrophilic materials and/ or (c) a lower level of cure because they are methacrylate which is known to cure slower than acrylate.[41]

However, both TEGMA and DEGMA were not omitted from the remaining studies because the DOC and T_g data (as summarised in Table 4.1) were obtainable from these polymers. This confirmed that they had undergone the polymerisation process under the selected UV conditions. While the XTT assay shows that PEGMA has good initial resistance to *C. albicans*, the polymer was removed from further evaluation as no DOC was detected in the FTIR measurement. The problem with PEGMA swelling will be further elaborated on in later section 4.5.

Fungi cell toxicity was studied with XTT assay for quantification of *C. albicans* metabolic activity, the key difference between these two evaluations is the inclusion of polymer washing steps for fungal attachment evaluation (as detailed in chapter 3, subsection 3.4.3). A summary of the polymer toxicity data with *C. albicans* can be found in Figure 4.5.

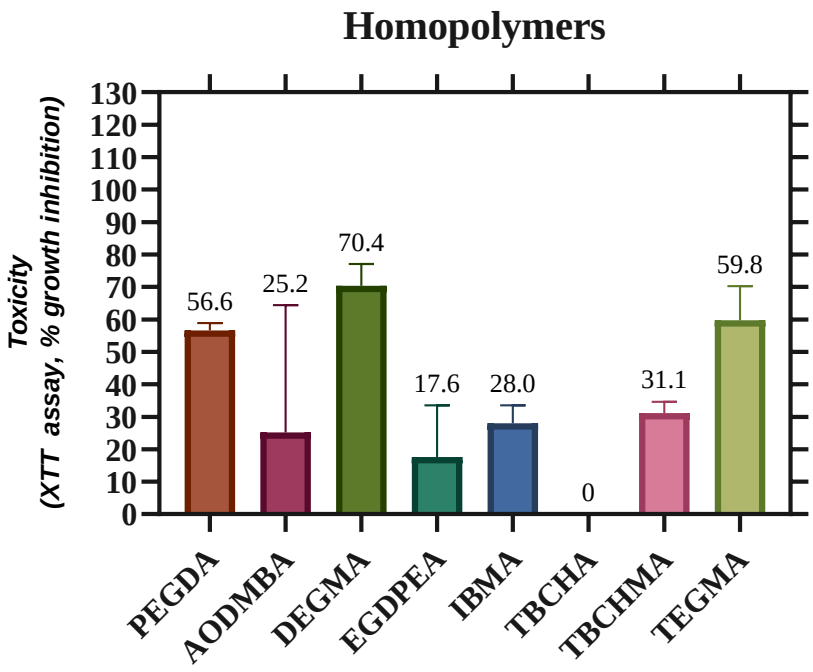


Figure 4.5: *Plot of the homopolymer toxicity data after 24 hours in contact with the polymer surface.*

The toxicity evaluation showed that all the non-ethylene oxide-containing materials (AODMBA, EGDPEA, IBMA, TBCHA and TBCHMA) had polymer toxicity results < 35 %, but there was still a high amount of *C. albicans* metabolic activity after interaction with the polymers for 24 hours. These values were compared to the metabolic activity on the polystyrene well-plate surface. This corroborated that the low *C. albican*s attachment level was not due to incidental toxicity effects related to the test materials. Meanwhile, the ethylene oxide-containing materials, especially DEGMA and TEGMA exhibited higher toxicity levels. This was likely to be attributed to either its material properties, i.e., the gel-like structure due to their low T_g values (I.e., -36 °C and -53 °C respectively) and their affinity for water as they are hydrophilic materials. Its physical form was thought to result

in cell toxic oligomer/ monomers residues being present, which could not be thoroughly removed by the post-polymerisation washing/ cleaning process adopted for this study.

PEGMA, DEGMA and TEGMA typically exhibit a lower level of cure compared to acrylates. This is due to the large steric hindrance of methyl group in methacrylate.[198] Thus, such low T_g material would be challenging to handle and be used in any product or part. In chapter 5 these properties will be discussed further when these methacrylates are combined with more rigid polymers to obtain copolymer properties for better suitability in a biomedical device. Such modification will also be demonstrated to benefit AM processing.

While PEGDA also contains ethylene oxide groups, it is much harder in structure and the above phenomenon observed in PEGMA, DEGMA and TEGMA was not an issue for PEGDA. This could be explained by several possibilities. Firstly, PEGDA has two functional acrylates which would be faster to react than methacrylate, PEGDA raw material itself already has a molecular weight of 575 and would be likely to form a longer polymeric chain after UV curing.

4.5 Issues with PEGMA Swelling Influence the Results Observed

As mentioned earlier in subsections 4.4 and 4.5, several problems arose when working with PEGMA and this monomer/ polymer was hence excluded from further evaluations throughout the thesis. In this subsection, the problem will be further discussed. The PEGMA polymer swells and turns porous when in contact with water in the assay media and also during washing stages conducted just before the fungal attachment assessment.

While performing the XTT assay, PEGMA also appeared to emit a strong formazan signal from the bottom of the well-plate (as per Figure 4.6).



Figure 4.6: *PEGMA (Left) After vacuuming and washing process with IPA and SDW. (Right) After completion of the XTT assay, the top medium showed a weak presence of C. albicans with a strong signal below the swollen polymer.*

On a closer inspection, this observed behaviour was due to swelling PEGMA, which led the medium with *C. albicans* cells to flow downwards around the peripheral of the polymer samples until it reached the bottom polystyrene well plate. Since the well plate material was susceptible to *C. albicans* attachment, it led to the phenomenon as explained in the schematic of Figure 4.7, where low cell attachment was observed from the top medium, but strong formazan was seen at the bottom.

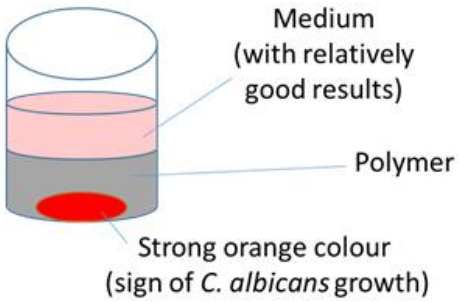


Figure 4.7: *Schematic to show the settling of medium and growth of C. albicans at the bottom of the well which was not observed at the top of swollen PEGMA polymer.*

When measured, the medium on top of PEGMA showed a very low *C. albicans* attachment of 5.9 %. When assessing the properties of all UV moulded samples, all other polymers showed DOC and T_g after UV curing but not PEGMA. As PEGMA has a hydrophilic nature, interaction and swelling with moisture in the medium is a possible phenomenon especially if it is also insufficiently cured. It was hypothesised that the behaviour observed in Figure 4.7 was mainly because PEGMA has a low level of cure under the conditions of UV curing selected for this evaluation. A second trial was conducted where the DMPA initiator concentration was increased to 8 % w/v (originally 1 % DMPA) to confirm this hypothesis. This was then cured with the standalone UV apparatus with an extended hour of UV exposure instead of the standard five minutes utilised for the data generated in section 4.5. The PEGMA prepared with the above condition yielded a polymer with 46.6 % DOC. Our hypothesis was confirmed by the results and issues met with PEGMA in all the evaluations. Hence, the decision was to remove the polymer from the test matrix as it may not be sufficiently reactive for the inkjet printing process.

4.6 Printing Trials

The monomers were then included in a printing assessment which was designed to compare the DOC achieved when using an inkjet printer. This is to confirm that the standalone method can validate DOC achieved in an inkjet printer and is capable to be used as a predictive method.

The nine monomers with dissolved initiators were introduced into the inkjet printing cartridge to conduct a printing trial with the Dimatix inkjet printer, full ink preparation and printing process can be found in chapter 3, subsection 3.5.1. This trial aimed to evaluate

if printing layers could result in highly cured test pieces, that also exhibited good shape and structure. Dimatix inkjet printer was stored within a glove box to ensure the environment has oxygen content ranging from 0.2 – 0.3 % during the printing process. This was done to improve the curability of the monomers, as it minimises the potential of reaction of radicals with oxygen leading to an unwanted reaction that inhibits the polymerisation.

Table 4.2: *Visual observation of printed polymer using 1 % DMPA initiator.*

Polymers	1 % w/v DMPA
AODMBA	Solid
PEGDA	Solid
TBCHA	Liquid
TBCHMA	Liquid
IBMA	Liquid
EGDPEA	Liquid
TEGMA	Liquid
DEGMA	Liquid

Table 4.2 above shows the results from the printed layers based on visual observation. Apart from PEGDA and AODMBA (highlighted in green), all other monomers (highlighted in red) did not form structured layers and remained in liquid form. Thus, to improve the curability of the monomer set with the inkjet printer, the initiator level was increased to 4 %, a level chosen by referencing a work by He et al.[176] Theoretically, increasing curability would also help in the reduction of fungal cytotoxicity from the polymers and improve their material properties by reducing the level of residual monomers in the test pieces. The FTIR analysis of the 1 % and 4 % initiator experiments are compared side by side in Table 4.3 below.

Table 4.3: *FTIR measurement of moulded polymers with 1 % initiator compared against polymers with 4 % initiator.*

Polymers	Moulded Polymer - 1% Initiator					Moulded Polymer - 4% Initiator				
	DOC (%) 1	DOC (%) 2	DOC (%) 3	Mean DOC (%)	Std. Dev.	DOC (%) 1	DOC (%) 2	DOC (%) 3	Mean DOC (%)	Std. Dev.
TEGMA	66.5	60.1	59.7	62.1	3.8	82.1	80.5	77.2	79.9	2.5
DEGMA	53.9	52.4	63.6	56.6	6.1	89.3	85.5	96.1	90.3	5.3
AODMBA	61.4	75.4	60.3	65.7	8.4	83.4	81.9	78.9	81.4	2.3
TBCHA	80.5	83.9	84.4	83.0	2.1	88.5	88.7	86.4	87.9	1.3
TBCHMA	68.7	79.8	82.4	76.9	7.3	95.7	92.9	96.9	95.2	2.1
IBMA	47.5	57.0	55.4	53.3	5.1	74.2	77.1	62.3	71.2	7.8
EGDPEA	71.4	81.7	75.5	76.2	5.2	87.5	89.4	93.3	90.1	3.0
PEGDA	48.1	61.6	71.7	60.5	11.8	82.0	64.9	81.2	76.0	9.7

As per table 4.4, an increase of DMPA initiator from 1 % to 4 % resulted in a significant improvement in the average DOC for seven out of eight polymers to at least 70 %. The only exception was PEGDA where the p-value significance was found to be >0.05. This may be due to the wider range of data obtained for the three measurements in both 1 % and 4% initiator leading to a higher standard deviation. Also, the structure of the 3D network will become convoluted and not all vinyl groups within the structure will not be able to react due to the complicated network. The other polymers demonstrated a significant increase in DOC. For example, in Figure 4.8 TEGMA polymer showed a difference with a significance of 0.002 (p-value). TBCHA polymer (in Figure 4.9) showed the least increase in average DOC only increasing from 83.0 % to 87.9 % between 1 % and 4 % initiator. However, the p-value was still significant at 0.026.

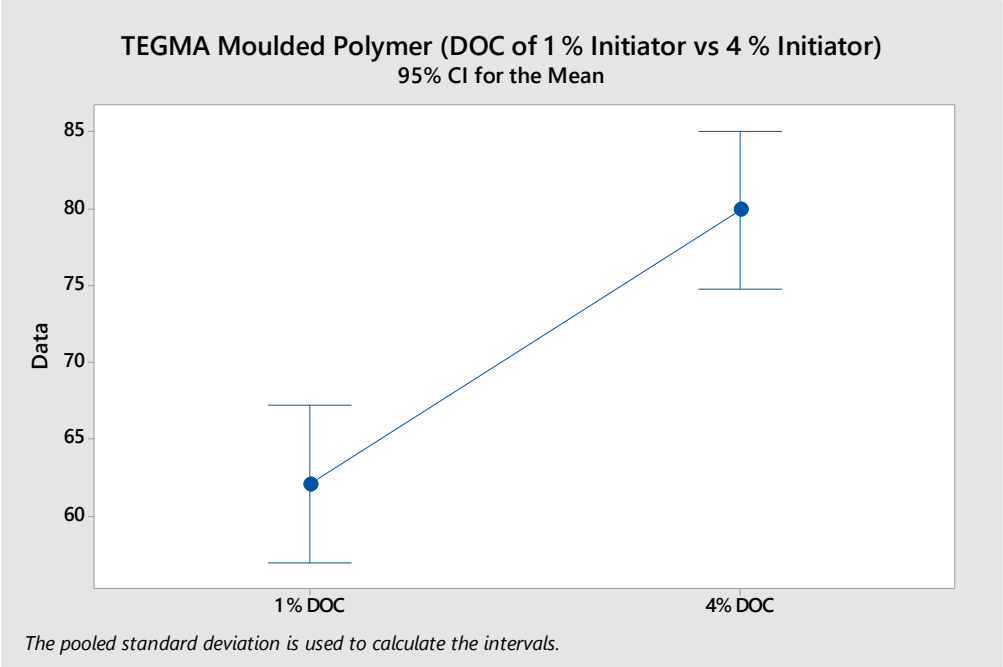


Figure 4.8: *TEGMA polymer with 1 % and 4 % DMPA initiator. DOC presented in interval plot, a difference of p-value = 0.002 was found. Average of three measurements tested for each DMPA %.*

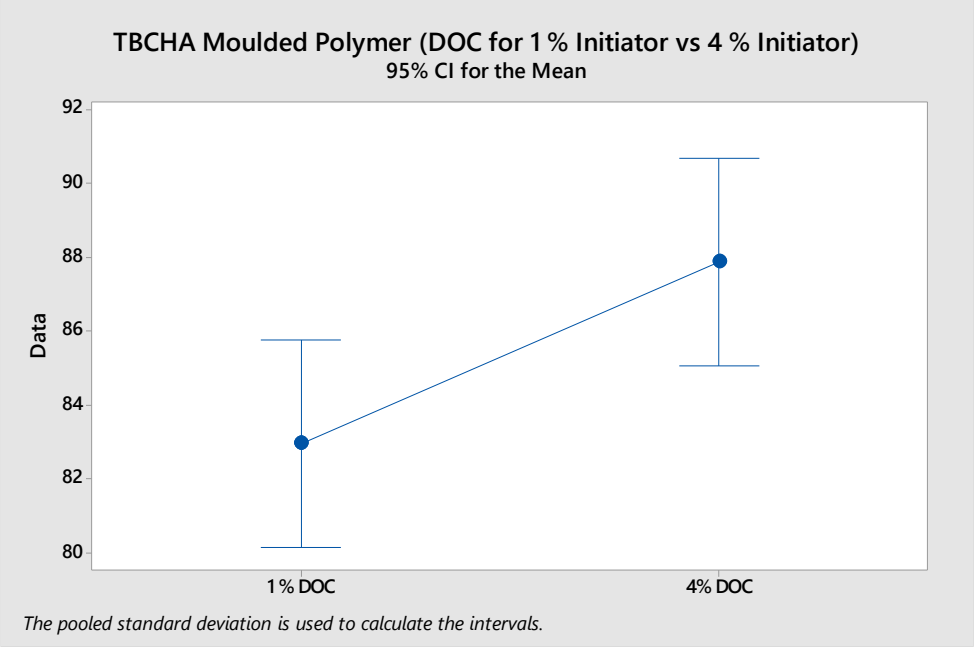


Figure 4.9: *TBCHA polymer with 1 % and 4 % DMPA initiator. DOC presented in interval plot, a difference of p-value = 0.026 was found. Average of three measurements tested for each DMPA %.*

Table 4.4: *Below shows a summary of the significance of improvement from increasing initiator percentage. Therefore, the decision was made to perform the rest of the evaluations and printing test from section 4.8 onwards with 4 % DMPA.*

Polymers	p-value of 1 % vs 4 % DMPA
AODMBA	0.036
PEGDA	0.152
TBCHA	0.026
TBCHMA	0.014
IBMA	0.030
EGDPEA	0.016
TEGMA	0.002
DEGMA	0.002

4.7 High Throughput Screening (HTS) Method – Viscosity and Surface Tension

Prior to printing the monomers, it was necessary to understand how the droplet will form during the inkjet printing process. This helps to ensure the production of a consistent layer with stable droplets throughout the printing. Fromm's parameter Z is commonly used to assess the printability of the ink, and it is based on knowledge of the ink's dynamic viscosity, surface tension, density, and the printer's nozzle diameter (21.5 μm for the Dimatix 2800 series). The accepted theory defines that, to obtain stable droplet printing, a system Z value should be >1 but <10. Anything <1 would result in a viscous droplet, and anything > 10 would cause the formation of unwanted satellite droplets.[199] Using the HTS method developed for the evaluation of viscosity and surface tension allows rapid testing as compared to using conventional equipment.[164] Table 4.5 below provides a summary of the density, viscosity, surface tension and Z parameter.

Table 4.5: *Density of monomers as provided by supplier, mean viscosity from an average of 3 measurements, average surface tension with an average of three measurements. Z parameters were tabulated with equation 3.4 found in chapter 3, section 3.3.2.*

Polymers	Z Parameter	Density (ρ)	Mean Viscosity @ RT (Pa.s)	Std. Dev. Viscosity (±)	Mean Surface Tension (mM/m)	Std. Dev. Surface Tension (±)
TEGMA	4.96	1.027	5.51	0.57	33.80	0.56
DEGMA	11.73	1.02	2.30	0.17	33.11	0.02
AODMBA	0.69	1.125	42.93	6.42	36.62	0.34
TBCHA	3.66	1.108	7.83	1.34	34.56	0.48
TBCHMA	3.16	0.95	8.34	0.19	34.14	0.12
IBMA	3.42	0.983	7.95	0.12	35.04	0.09
EGDPEA	1.30	1.085	23.25	1.66	38.90	0.13
PEGDA	0.45	1.12	69.75	2.20	41.19	0.02

All measurements of viscosity were conducted at room temperature. The data in Table 4.5 demonstrated that five out of the remaining eight monomers had Z parameters within the preferred inkjet printing range. DEGMA had a lower dynamic viscosity than the other monomers, and so its Z parameter was calculated to be 11.72, which meant that it was more likely to cause unwanted satellite droplets. AODMBA and PEGDA had Z parameters lower than 1 which would potentially be too viscous for jetting in a typical cartridge temperature setting and without the addition of solvent to the ink formulation. This data set also allows for the estimation of alternative printing parameters that would improve monomers with Z parameters lower than 1. E.g., such monomers can have their cartridge temperature increased to improve their jetting performance. Consequently, as per the next section which discusses the printing results in more detail, the evaluation of AODMBA and PEGDA ink demonstrated dispersion of stable and consistent droplets when cartridge temperature was increased to 55 °C.

4.8 Inkjet Printing Results & Regression Analysis of Moulded & Printed Samples

In this section, all monomer inks with 4 % initiator underwent detailed printing analysis with information gathered from sections 4.6 and 4.7. Table 4.6 below shows an overview of the curability and printability of the monomers. Five out of the eight monomers formed good printing layers when compared to the evaluation with 1 % initiator when only two out of eight were curable.

Table 4.6: *An overview of the visual observation for the monomers showed that 5/8 monomers could be printed with 4 % DMPA.*

Polymers	4 % w/v DMPA
AODMBA	Solid
PEGDA	Solid
TBCHA	Solid
TBCHMA	Solid
IBMA	Gel-Like
EGDPEA	Solid
TEGMA	Gel-Like
DEGMA	Gel-Like

Meanwhile, Figure 4.10 shows FTIR data comparison of AODMBA monomer, a printed double layer with 1 % DMPA and a printed double layer with 4 % DMPA. A decrease in peak size for carbon double bonds was observed from the FTIR spectrum when comparing AODMBA polymer with 1 and 4 % DMPA, demonstrating that DOC improvement could also be witnessed in the printed polymer.

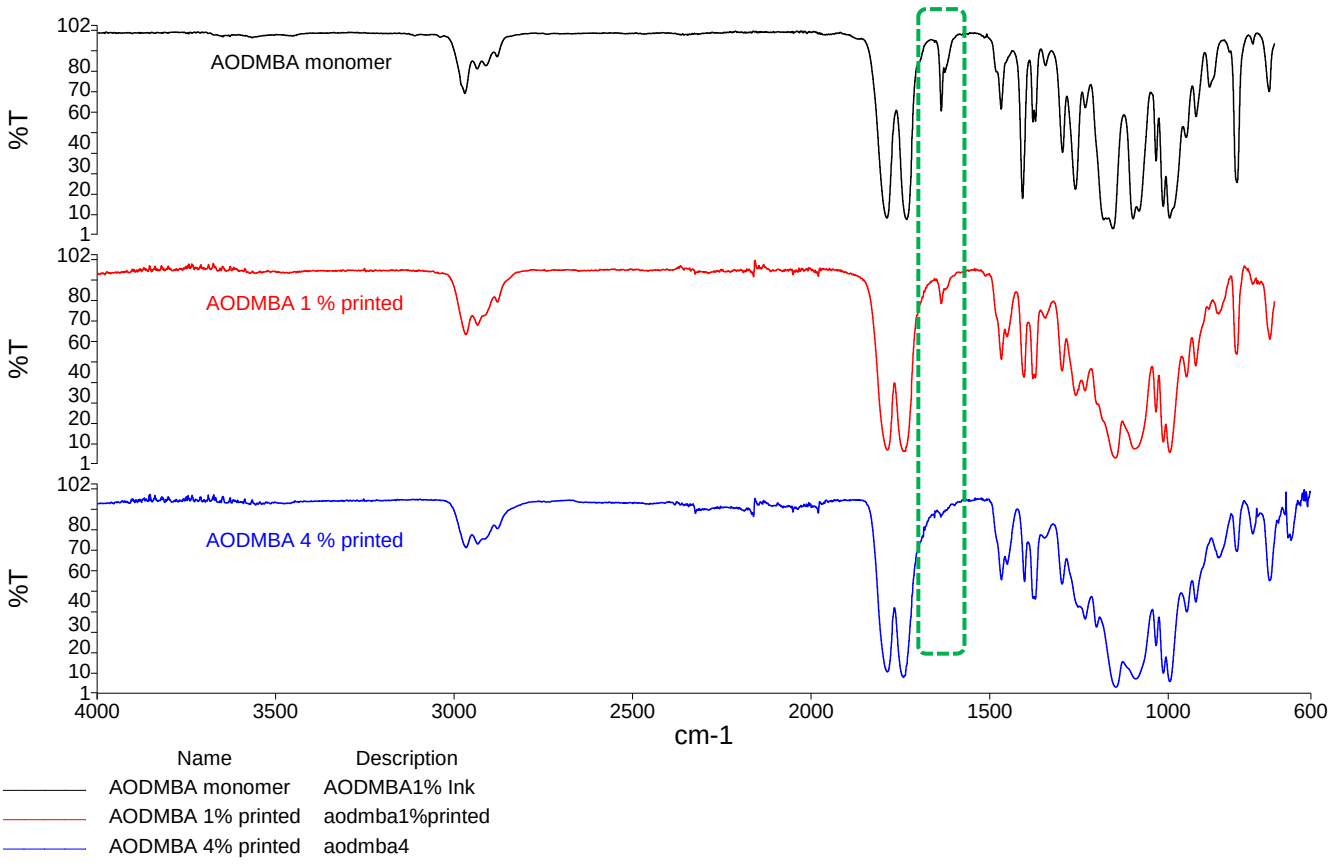


Figure 4.10: *Comparing C=C bond peak area at 1640 cm^{-1} on polymers printed with both 1 % and 4 % DMPA.*

While the increase in initiator delivered an improvement in the level of cure achieved with TEGMA, DEGMA and IBMA, the printed materials appeared soft and gel-like after printing. For TEGMA and DEGMA, this was attributed to their very low T_g values, experimentally defined to be -53 °C and -36 °C respectively. For IBMA, which exhibits a relatively high T_g value of 88 °C, this observation was likely due to insufficient cure as the HTS assessment predicted IBMA (at 4 % initiator loading) to have an average DOC of only 63.3 %, which was the lowest of all the nine polymers tested.

The information on the Z parameters allowed the printing conditions to be chosen such that all the monomers showed good jetting behaviour with steady droplets. A controlled cartridge temperature of 40 °C was used for all monomers with Z parameters between 1 – 10. While the viscosity measurement was taken at room temperature of 25 °C, 40 °C was chosen as it provides a stable temperature when printing under colder ambient conditions. For AODMBA and PEGDA, a cartridge temperature of 55 °C was applied in order to improve jetting behaviour of the monomers. Lastly, for DEGMA which had the highest Z parameter because of its low viscosity, the viscosity could be increased with the addition of fillers. However, no formulation change was performed in this chapter as it requires a consistent comparison of all monomers and polymers.

Of the polymers evaluated in this work, AODMBA, TBCHA and TBCHMA were the three main candidates where HTS methodology has proven to have good fungal anti-attachment characteristics and was directly printable via inkjet printing. The successful printing of AODMBA has been reported previously, [194] whereas for TBCHA and TBCHMA high throughput assays from this work have highlighted these candidates' suitability for inkjet printing. Therefore, printing parameters and results for TBCHA and TBCHMA were compared in Table 4.7 below.

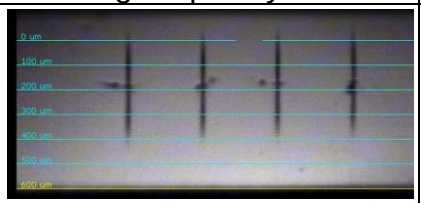
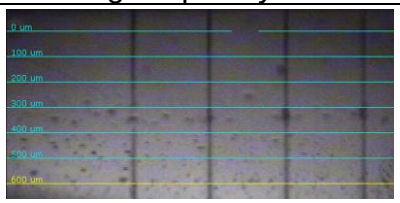
Both the monomers were printed into 3 mm circular disc shape sample with a total of 100 layers. While both TBCHMA and TBCHA were inkjet printable. As an acrylate, TBCHA has faster curing kinetics when compared to TBCHMA, which was proven both in literature reports and in actual printing tests.[198] With TBCHA, stable layers could be easily formed using a printing parameter of 5 kHz, where UV light exposure sweeps past the deposited droplet at a faster rate when compared to 1 kHz used for TBCHMA. Printed

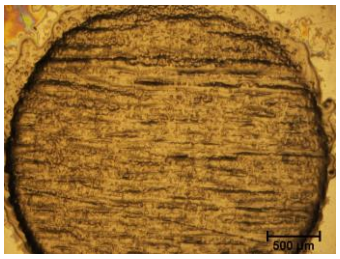
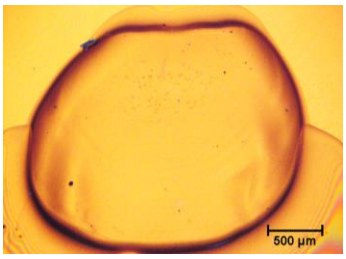
layers of TBCHA were noted to have a defined structure, and clear resolution of printing lines was observed under five to ten times magnification with a microscopic lens.

In the case of TBCHMA, the jetting frequency was decreased to 1 kHz which helps to lengthen the exposure time to UV light by reducing cartridge movement speed. The longer UV exposure time helps the layer formation, but the resolution was still much lower than TBCHA. A microscopic image of a single printed layer of TBCHMA exhibited low-resolution printing and the intended round disc shape was also slightly distorted due to its slow curing.

The results of printing 100 layers for both TBCHMA and TBCHA are found in the middle row of Table 4.7 which demonstrates that the printing resolution (with curing speed) also influences the overall AM built. TBCHA has a much more defined cylindrical structure while TBCHMA has a dome-like top structure in comparison due to its poorer curability leading to a slump effect on the top layers of TBCHMA.

Table 4.7: *Printing parameters and images for TBCHMA and TBCHA.*

Printability/ Results	**TBCHA with 4 % w/v DMPA initiator**	**TBCHMA with 4 % w/v DMPA initiator**
Dimatix DMP- 2830 Printing Parameters	Oxygen <2000 ppm, Drop space 20 µm, Jetting frequency 5 kHz	Oxygen <2000 ppm, Drop space 20 µm, Jetting frequency 1 kHz
Ink during jetting process		
Inkjet-printed polymer with 100 layers		

Microscopic image of 1 printed layer of material in 5x resolution		

Lastly, the FTIR data of both the moulded polymers and printed polymers were compared in a regression model. This was conducted to define if solely using the HTS methodology standalone curing could be used to determine the polymer's DOC in Dimatrix inkjet printing. Figure 4.11 shows the average DOC reading of all polymers evaluated in the following conditions; moulded polymers with 1 % DMPA, moulded polymers with 4 % DMPA and 2-layers of inkjet-printed polymers with 4 % DMPA.

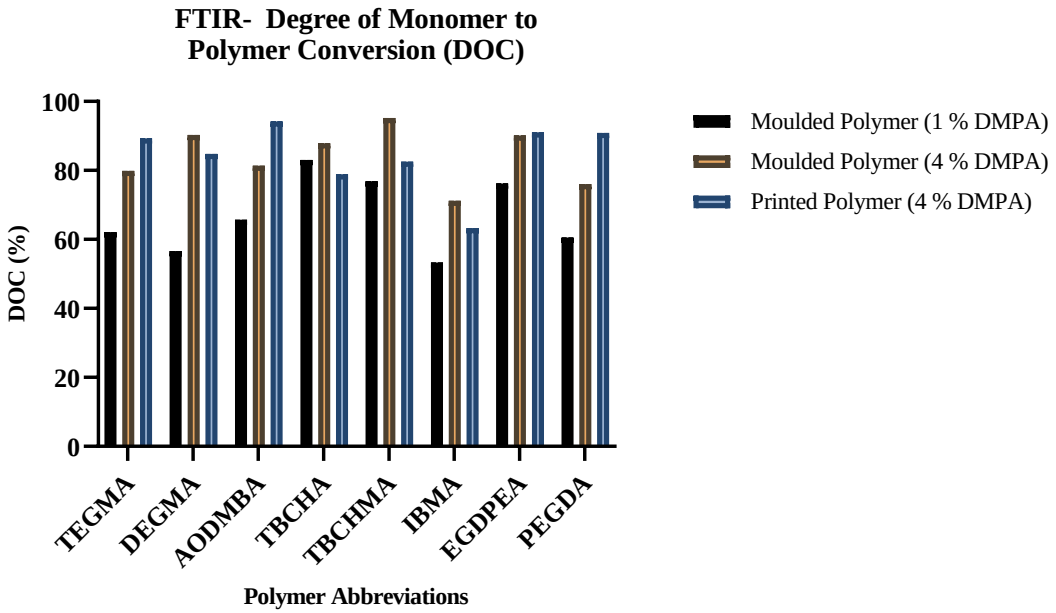


Figure 4.11: *Comparison of the DOC of polymers moulded with 1 % DMPA, moulded with 4 % DMPA and printed with 4 % DMPA.*

Both moulded polymers and printed polymers with 4 % DMPA were observed to have relatively close DOC values for several of the polymers especially EGDPEA, TBCHA and DEGMA. Thus, a regression analysis (see Figure 4.12) was performed to compare the 4% moulded polymers with the equivalent printed polymer.

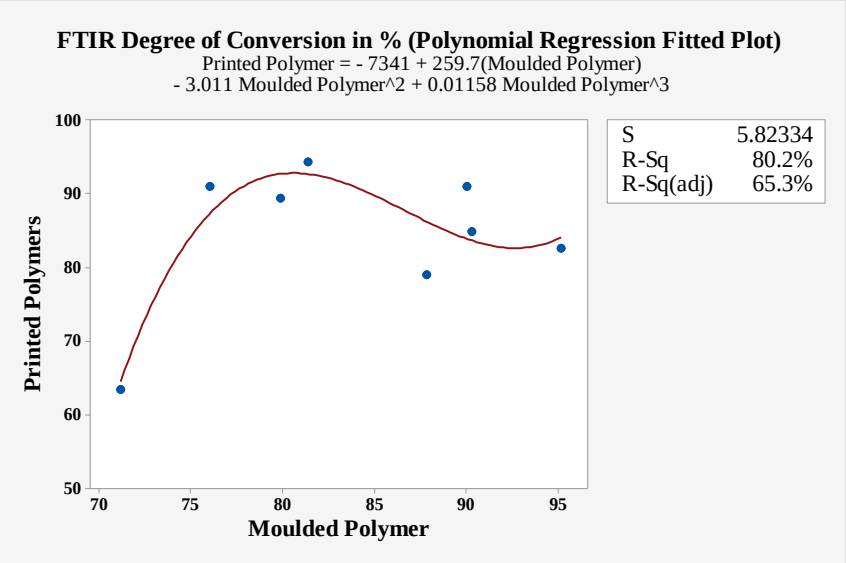


Figure 4.12: *Comparison of the DOC of polymers moulded with 1 % DMPA, moulded with 4 % DMPA and printed with 4 % DMPA.*

The analysis found that the best fit was possible using a polynomial regression fitted plot. An R^2 value of 80.2% was tabulated from the analysis, this R^2 value is considered a sufficiently strong correlation to support the use of the moulded polymer method to rapidly predict the DOC level of inkjet-printed samples for all new monomers. However more collected data in future would be required to strengthen this correlation and this is only a preliminary predictive attempt. It was also noted that, while TBCHMA was printable and has a relatively high DOC in both the moulded and printed sample of 95.2 % and 82.5 % respectively, the presence of methacrylate had reduced its curing speed and therefore its

printed structure was less defined. Low T_g materials are softer at room temperature would also influence the printing layer. Hence, the inclusion of T_g and functional groups in future prediction analysis would improve the predictability of monomer performance in inkjet printing.

4.9 Fungal Anti-Attachment of Inkjet-Printed Polymers

The final test conducted with these AM polymers was to confirm if the printed TBCHA, TBCHMA and AODMBA materials were still resistant to fungal attachments after printing. The earlier work evaluated only moulded polymers. PDMS, which was commonly used in medical devices, was also included in this XTT colorimetric assay for comparison purposes with the newly printed homopolymers and this data is shown in Figure 4.13.

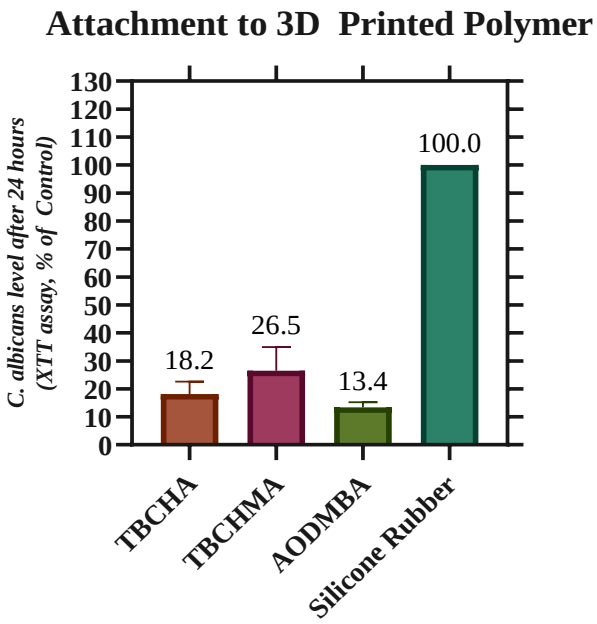


***Figure 4.13**: XTT assay data to determine the inherent C. albicans resistance of the printed disc-shape structures as compared to silicone rubber. Average measurements of three replicates were used.*

Printed TBCHA, TBCHMA or AODMBA resulted in only 13.4 - 26.5% *C. albicans* attachment when compared to silicone rubber. This attachment to printed samples was slightly higher than the fungal anti-attachment evaluation of the moulded samples (Section 4.4, Figure 4.6). However, the data was still below or close to the previously defined cut-off value for good anti-attachment of <25%.[34] The printed samples were also examined for toxicity as shown in Figure 4.14 and all three polymers were close to the results of moulded samples.

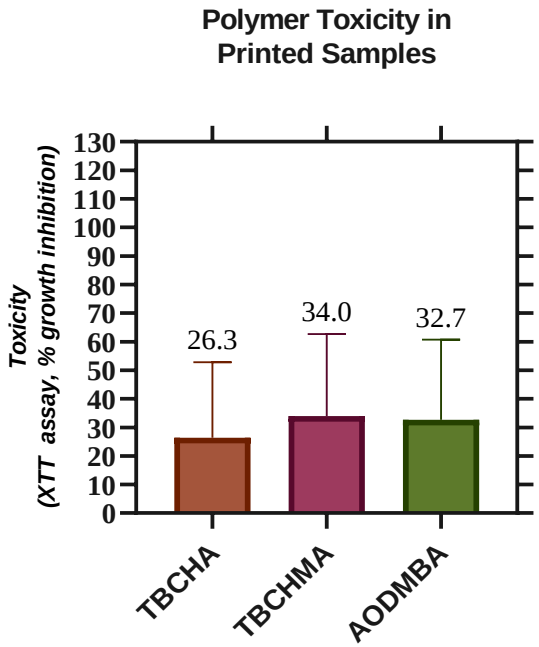


Figure 4.14: *Toxicity data for the three printed homopolymers. Average of three replicates were used.*

The mean toxicity data of AM processed samples was slightly higher than the samples moulded into the well plate from section 4.4, figure 4.5. This minor difference may be a result of the tweezing and moving of printed samples each time during the in-between

PBS washing stage. In general, we can conclude that the printing process did not introduce additional toxic effects on the *C. albicans* cells.

4.10 SLA Printing Demonstration

While the key AM process in this work was on material jetting, a quick trial with SLA was performed to evaluate the potential of such UV curing polymer to be used for SLA. Hence, for the last assessment in this chapter, a single monomer was selected for evaluation in stereolithography (SLA) processing. As UV curing monomers can also be used in other AM processes, TBCHMA was selected for printing test with SLA printer, BMF nanoArch S130 Projection µSLA system. TBCHMA was selected for evaluation as it was the least reactive of the printable monomers (which was also fungal-resistant) and requires more parameter evaluation. Hence, if TBCHMA could be printed in SLA, then it will be unlikely to be a concern for TBCHA which bears a faster reactivity acrylate group to be printed. The printing trial started with the use of 1 % initiator and 1 % curcumin used as a photo absorber.

One significant difference between the SLA and the earlier inkjet process was the lack of a controlled environment as SLA was performed in a typical atmospheric condition without oxygen inhibition. The presence of oxygen in the atmosphere around the printing resin could lead to the free radicals may react with oxygen to inhibit polymerisation. For this SLA demonstration, a square shape of 2 mm x 2mm with uniform pores design was used for the printing, as per the schematic in Figure 4.15.

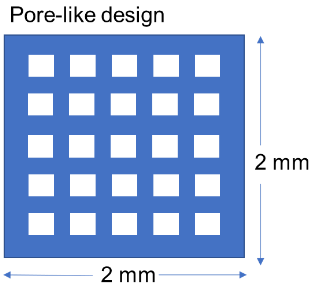


Figure 4.15: *Schematic design for SLA to determine resolution based on the printed outcome of its pore-like structure.*

The gradual finetuning of the TBCHMA formulation by incrementally increasing the loading of initiator to 3 % resulted in an improvement in the resolution of the pores as seen in the rightmost image of Figure 4.16. Even so, much more work and formulation adjustment would be required for TBCHMA to work well for SLA printing. Due to the different curing methods and conditions, the formulating process for SLA and inkjet printing differs and should be evaluated as a separate project. This section only evaluates its potential and SLA processing will be part of future work studies.

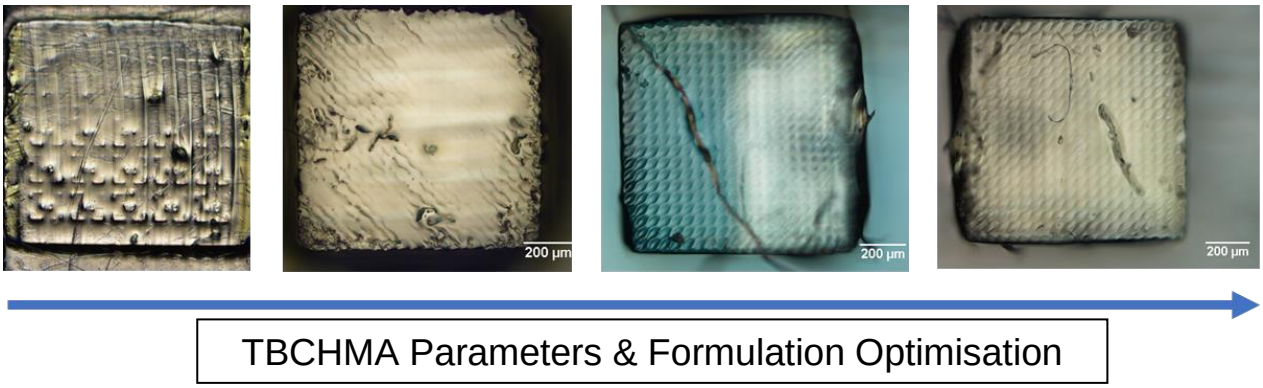


Figure 4.16: *TBCHMA with 1 % initiator on the leftmost image, rightmost image with initiator increased to 3 % and addition of curcumin. The printed layer showed some improvement in its resolution.*

4.11 Summary

In chapter 4, curability, printability and fungal anti-attachment behaviour of the selected nine polymers were demonstrated with this newly developed HTS methodology. seven out of the nine polymers evaluated were able to resist *C. albicans* and five out of the remaining eight polymers (after PEGMA was removed from further evaluation) were printable formulations. Individual polymer performance was summarised as per Table 4.8 below.

Table 4.8: *Summary of fungal and inkjet printing performance.*

Polymers	Fungal Anti-Attachment	Dimatix Inkjet Printable
TBCHMA	Yes	Yes
TBCHA	Yes	Yes
PEGMA	Yes	N/A
TEGMA	Yes	No
AODMBA	Yes	Yes
EGDPEA	No	Yes
DEGMA	Yes	No
IBMA	Yes	No
PEGDA	No	Yes

The liquid handling apparatus used in this HTS methodology automatically dispense and evaluate the workability of the polymers in inkjet printing by providing the surface tension and viscosity. This helps to improve evaluation speed greatly when compared to testing the monomer samples individually and manually with a tensiometer and rheometer.

The standalone UV curing apparatus mimics inkjet printing curing sufficiently allowing a quick evaluation of the polymer and its curing potential by performing FTIR of the moulded polymer to determine its DOC. The collected DOC data of moulded polymers were

compared with the DOC of printed polymers. The results fitted well into a polynomial regression plot with an R^2 value of 80.2 %. From the printing trial in this chapter, it can also be concluded that higher DOC and higher T_g in a monomer have a greater chance of being directly printable. This can be taken into consideration before attempts to print ink formulations in future.

In the process of demonstrating the HTS methodology, TBCHA and TBCHMA are both new printable candidates found to have fungal anti-attachment and good printing properties for the inkjet process. Both the inkjet-printed and moulded samples consistently demonstrated strong fungal anti-attachment and similar cytotoxicity results. A quick trial for SLA was performed but the trial confirms that a lot more formulation tuning would be required in this process for future work. The work continues in chapters 5 and 6 focussing on inkjet as AM process and as materials used in this method development were either too soft or too brittle for actual use, with a newfound understanding of their properties, the next two chapters will look at preparing customised copolymers with functional T_g that allows for an actual application.

Chapter 5: Fungal-Resistant Copolymers

5.1 Introduction

Copolymerisation is a common approach to customise the T_g of methacrylate and acrylate-type polymers. This chapter describes the application of the HTS methodology that was developed in chapter 4 to prepare co-monomers and evaluate copolymers for their AM processability, fungal anti-attachment and mechanical properties. The 8 monomeric candidates used for developing the HTS methodology were mixed in different ratios to obtain a large library of copolymeric materials. The goal of this chapter is to demonstrate the effectiveness of HTS in preparing and evaluating a large library of co-monomers/ copolymers, by mixing low T_g and high T_g materials achieving a wide range of copolymers with varying T_g that can be used in different applications due to the differing material/ mechanical properties that they will deliver. The selected copolymers were also investigated via molecular spectroscopy to define their achieved DOC level and copolymer ratio. Figure 5.1 below shows the schematic of the workflow for the copolymer study. First and foremost, the co-monomer mixtures that would be used to synthesise the copolymers would be prepared and mixed automatically with the liquid handler before they underwent the HTS evaluation process to assess their fungal attachment, inkjet processability, toxicity, DOC value and copolymer ratio.

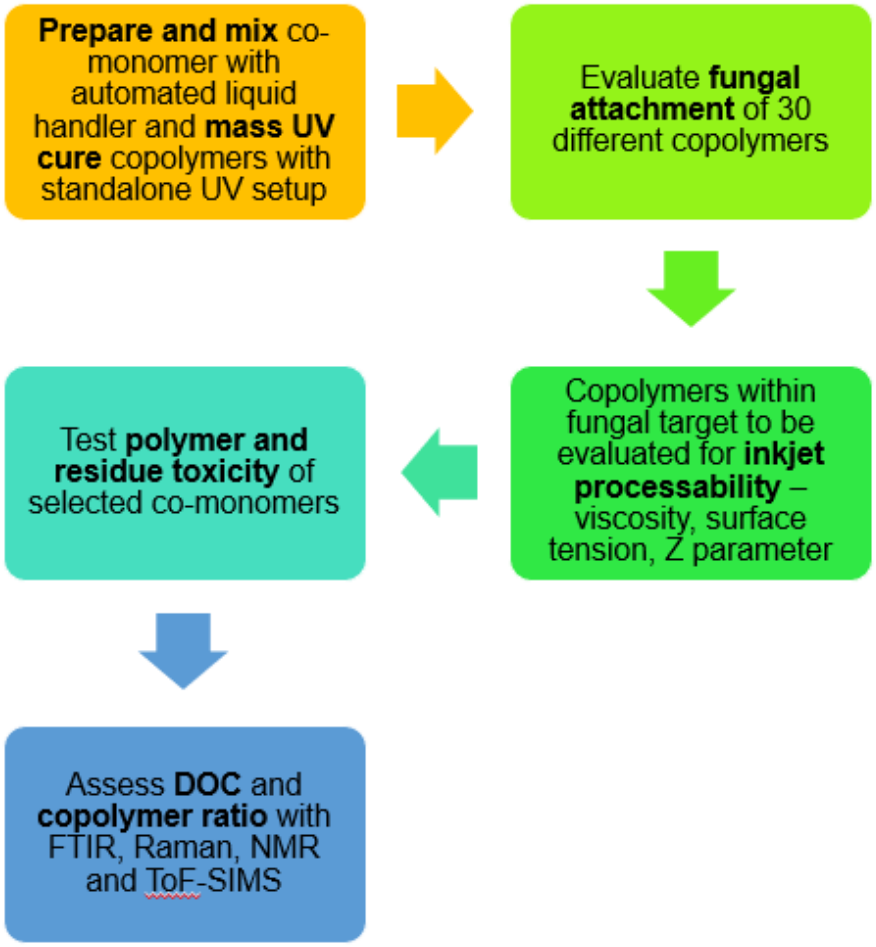


Figure 5.1: *Schematic of the workflow for chapter 5.*

5.2 Copolymer Matrix Plan

The eight polymers that were evaluated with DSC in chapter 4 could be classified into a category of "low T_g" where polymers exhibited T_g values in the negative range. (See Table 5.1) the rest of the polymers are classified as "high T_g" (Table 5.2). Actual experimental T_g would also be influenced by its molecular weight and DOC as well.

Table 5.1: *Low T_g material in the negative range.*

Polymer	T_g (°C)	Fungal Attachment (%)	DOC (%)
DEGMA (Gel-like)	-36	5.3	64.0
TEGMA (Gel-like)	-53	0.4	60.0
PEGDA	-24	90.2	62.0

Table 5.2: *Higher T_g material in the positive range.*

Polymer	Tg (°C)	Fungal Attachment (%)	DOC (%)
AODMBA	86	4.9	63.0
TBCHMA	159	11.2	78.0
TBCHA	121	24.7	83.0
IBMA	88	0.6	68.0
EGDPEA	23	55.6	84.0

As DEGMA and TEGMA also have good *C. albicans* anti-attachment properties, they were set as primary monomers in the copolymer matrix. In chapter 4, all polymers apart from DEGMA and TEGMA were found to be hard structured polymers after UV curing. Therefore, the higher T_g materials were selected to be secondary monomers to reduce the gel-like phenomenon in DEGMA and TEGMA by potentially increasing the T_g and/ or improving curing behaviour with its acrylate groups.

Although PEGDA could form a hard structure, it was omitted from the studies as it was only selected as a positive control (fungal attachment of 90.2 % as shown in Table 5.1). EGDPEA was also found to have no fungal anti-attachment properties towards *C. albicans* (fungal attachment of 55.6 % as stated in Table 5.2), however, it was included in the copolymer matrix as it has potential in aligned bacterial anti-attachment studies.[200] Therefore, including the combination of both IBMA (with a fungal attachment of 0.6 %) and EGDPEA in this matrix with both TEGMA/ DEGMA and IBMA/ EGDPEA in a copolymer could contribute to the prevention of both fungi and bacteria attachment (such as *P. aeruginosa*, *S. aureus* and *E. coli*). Such an antimicrobial copolymer can be further developed in future work.[201] The co-monomers were prepared in three different co-monomer ratios of 75:25, 50:50 and 25:75 between the primary and secondary monomers in order to achieve a range of T_g values (as shown in Figure 5.2).

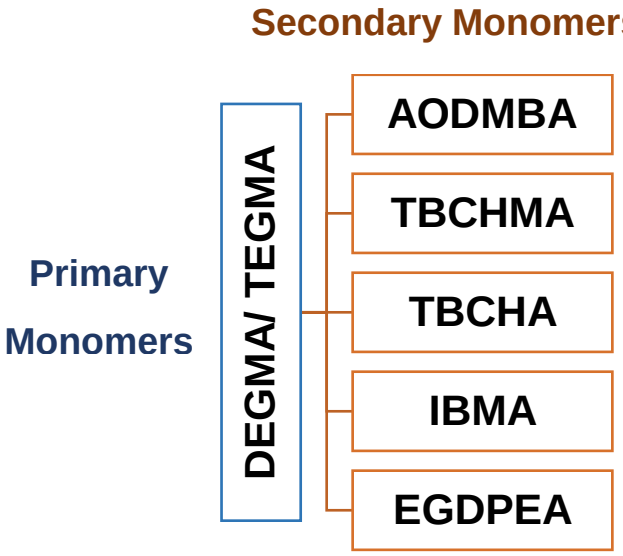


Figure 5.2: *Copolymer matrix with DEGMA and TEGMA as primary monomers mixed with co-monomers with higher T_g in three different ratios – 75:25, 50:50, 25:75. Total of 30 copolymer types in the matrix were mixed and 120 wells were filled (four repeats were required for fungal attachment assessment).*

The copolymer matrix will result in a total of 30 co-monomer mixtures when considering the different ratios and different types of co-monomers combinations that were planned. Four wells of samples are prepared for each type of copolymer therefore the liquid handler was utilised to automatically mixed all 120 (four repeats of 30 co-monomers) into a 96 well plate before HTS curing was performed with the standalone UV curing apparatus and subjected to curing at parameters described in chapter 3, section 3.3.1.

5.3 Fungal Anti-Attachment Studies

30 copolymers created with 1 % initiator using the HTS method were put through XTT assay to assess their abilities to reduce *C. albicans* attachment. The relative level of attached *C. albicans* was determined by XTT reduction activity. 23 out of the 30 evaluated materials gave *C. albicans* attachment below 25 % when compared to the control, which is the surface of polystyrene well-plate used for the assessment (25% is an arbitrary threshold set to sift out potential candidates as per earlier fungal anti-attachment work [34]). The resultant 23 copolymers are presented in Table 5.3 below, with 12 belonging to TEGMA-based copolymers and 11 from DEGMA-based copolymers.

In TEGMA- or DEGMA-type copolymers, it was apparent that although many of the homopolymers tested (i.e., AODMBA, TBCHMA and TBCHA) in chapter 4 showed low fungal attachment of 0.0 – 11.2 %), adding them into copolymer does not guarantee that fungal attachment remains low. This could be attributed to several possibilities, such as a change in surface roughness, surface energy or possibly disruption of the chemical structure that repels *C. albicans* due to copolymerisation.[202–205] It was also observed that typically the copolymers that exhibited consistent lower fungal attachment contained at

least a molar ratio of 50 % TEGMA or DEGMA in the co-monomer mix, such as TEGMA/ DEGMA copolymerised with AODMBA (Figure 5.3). A quick test to confirm this was performed by preparing TEGMA:AODMBA and DEGMA:AODMBA in the ratio of 10:90 to study its “trend”. As per Figure 5.3 below, the ratio of 10:90 for both copolymers yielded a higher attachment of fungi as well.

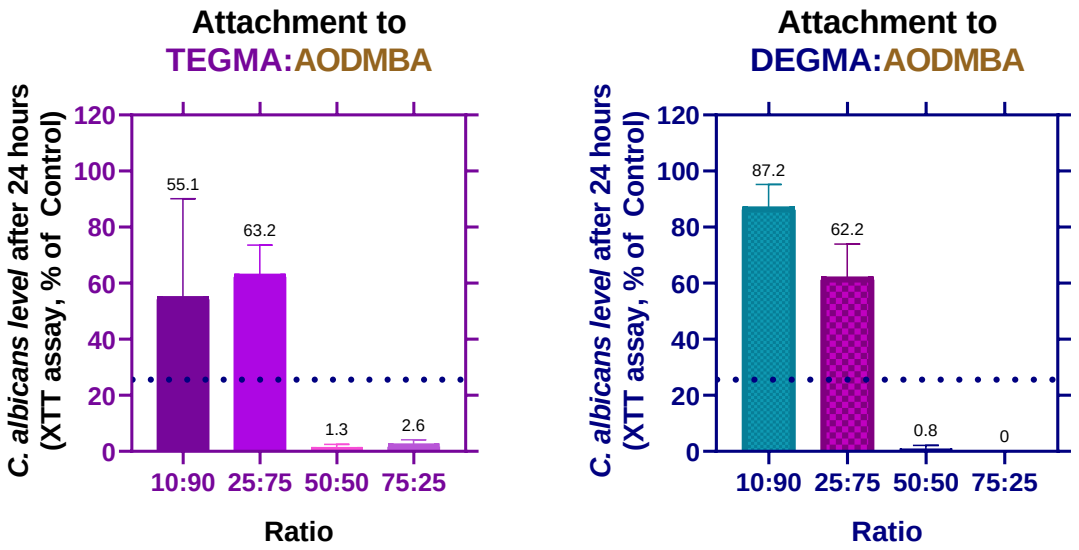


Figure 5.3: *Copolymer matrix prepared with 1 % DMPA with DEGMA (Right) and TEGMA (Left) as primary monomers with AODMBA in different ratios. The attachment was greatly reduced when the copolymer has at least 50 % TEGMA or DEGMA.*

The first *C. albicans* anti-attachment assay had copolymers prepared with 1 % initiator, mimicking the initial initiator percentage used for attachment assays performed in chapter 4, section 4.4. As the later printing trials in chapter 4 confirm that performances in homopolymers with 4 % DMPA initiator had comparatively much better curing during inkjet printing, the second series of *C. albicans* anti-attachment was performed for copolymers produced with 4 % DMPA initiator. This copolymer matrix with 4 % DMPA initiator only considered the *C. albicans* attachment for the 23 copolymer candidates

which already had given < 25 % attachment with 1 % DMPA initiator, a summary of results can be found in Table 5.3.

Table 5.3: *Summary of copolymers produced with either 1% or 4% initiator that gave C. albicans attachment below 25 % in fungal anti-attachment tests. Highlighted in yellow are results that gave more than 25% attachment when 4% DMPA initiator was used. Average of three measurements, n=3.*

Copolymer	Primary Polymer Ratio	Secondary Polymer Ratio	*C. Albicans* Attachment (%)	
			1st Evaluation using 1 % DMPA	2nd Evaluation using 4 % DMPA
TEGMA:AODMBA	0.75	0.25	2.61	0.88
	0.50	0.50	1.33	1.72
TEGMA:TBCHMA	0.75	0.25	5.59	0.76
	0.50	0.50	6.22	2.37
	0.25	0.75	15.07	58.7
TEGMA:TBCHA	0.75	0.25	5.44	7.56
	0.50	0.50	2.47	6.18
TEGMA:IBMA	0.75	0.25	6.25	1.53
	0.50	0.50	17.80	15.98
	0.25	0.75	8.49	70.31
TEGMA:EGDPEA	0.75	0.25	0.99	2.02
	0.50	0.50	2.75	3.55
DEGMA:AODMBA	0.75	0.25	0.00	1.76
	0.50	0.50	0.79	17.9
DEGMA:TBCHMA	0.75	0.25	5.72	0.00
	0.50	0.50	21.25	49.43
DEGMA:TBCHA	0.75	0.25	1.59	1.07
	0.50	0.50	4.85	12.25
DEGMA:IBMA	0.75	0.25	24.32	2.40
	0.50	0.50	7.77	29.62
	0.10	0.90	10.44	16.64
DEGMA:EGDPEA	0.75	0.25	3.93	2.40
	0.50	0.50	10.01	0.88

Anti-attachment results of copolymers with 4 % initiator showed similar trends as compared to the earlier evaluation of copolymers with 1 % initiator (Table 5.3). General phenomenon showed that copolymers with a lower proportion of either TEGMA or DEGMA typically fell outside of the targeted fungal anti-attachment when 4 % initiator was

used; a total of four copolymers fell out of the targeted range. For example, in TEGMA:TBCHMA$_{25:75}$, with 1 % initiator the *C. albicans* attachment was < 20 % and when the initiator was increased to 4 %, attachment of *C. albicans* increases to > 50 %. One possible explanation for this is that a lower initiator percentage may lead to lesser monomer-to-polymer conversion. Hence, the low attachment may be partly resultant of free monomers/ oligomers residues that were toxic to the fungal cells.

The four copolymers that exhibited increased *C. albicans* attachment is especially evident in copolymers where the secondary monomer was IBMA and TBCHMA (as shown in Figure 5.4 and 5.5). Taking these out of the list for future evaluation, the library of fungal resistance copolymers was further reduced to 19 candidates.

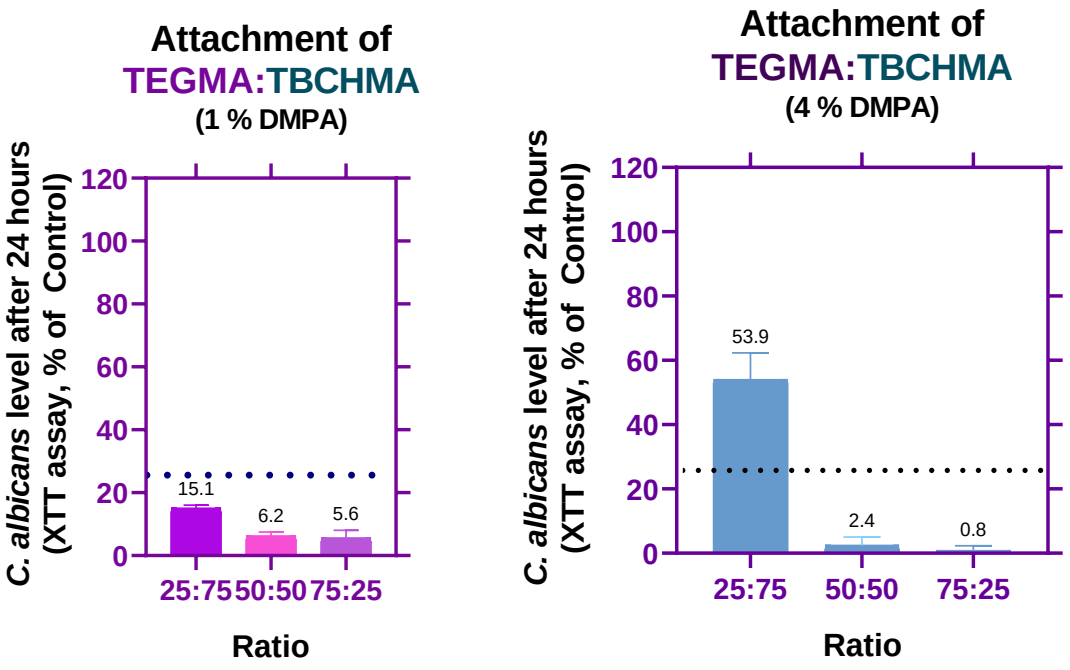


Figure 5.4: *Anti-attachment results of TEGMA:TBCHMA with 1 % initiator compared to TEGMA:TBCHMA with 4 % initiator. The ratio of 25:75 fell out of the targeted range with 4 % DMPA.*

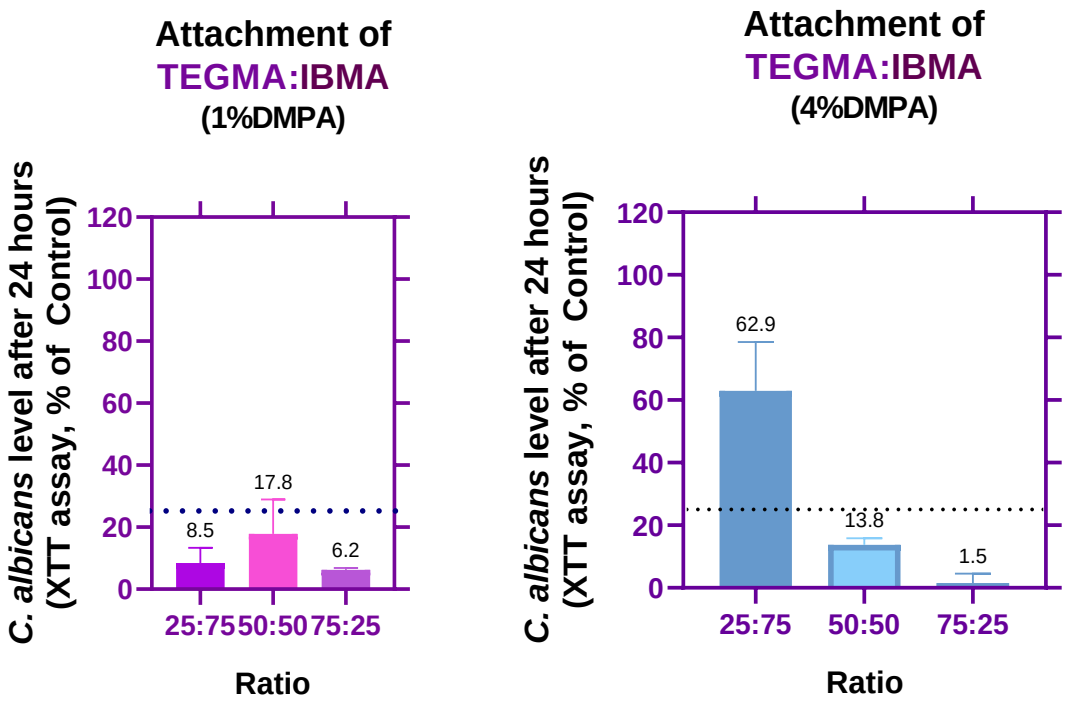


Figure 5.5: *(Left) Anti-attachment results of TEGMA:IBMA with 1 % initiator compared to (Right) TEGMA:IBMA with 4 %. Ratio of 25:75 falling out of targeted range in 4 % DMPA.*

5.4 HTS Viscosity and Surface Tension for Z parameter

HTS method developed by Zhou et. al [164] for automated evaluation of viscosity and surface tension using the liquid handler was discussed in chapter 4. The incorporation of this approach into the fungal anti-attachment evaluation allowed for the rapid and automated assessment of viscosity and surface tension immediately after the co-monomer mixtures are prepared in the liquid handler. A summary of both the viscosity (evaluated at room temperature) and surface tension for the 19 candidates was repeated thrice and summarised as per Table 5.4 below.

Table 5.4: *Three repeats of viscosity and three repeats of surface tension for the 19 copolymer candidates (4% initiators) with low fungal attachment.*

Co-monomers	Mean Viscosity @ RT (Pa.s)	Std. Dev. Viscosity (±)	Mean Surface Tension (mN/m)	Std. Dev. Surface Tension (±)
TEGMA:AODMBA$_{75:25}$	6.53	0.20	33.46	0.60
TEGMA:AODMBA$_{50:50}$	9.15	0.27	33.70	0.86
TEGMA:TBCHMA$_{75:25}$	5.56	0.13	32.61	0.94
TEGMA:TBCHMA$_{50:50}$	5.68	0.12	33.50	1.39
TEGMA:TBCHA$_{75:25}$	5.57	0.58	33.23	0.93
TEGMA:TBCHA$_{50:50}$	4.81	0.20	33.13	1.71
TEGMA:IBMA$_{75:25}$	5.59	0.54	33.63	0.33
TEGMA:IBMA$_{50:50}$	5.59	0.18	35.43	0.76
TEGMA:EGDPEA$_{75:25}$	7.26	0.27	33.69	0.09
TEGMA:EGDPEA$_{50:50}$	9.37	0.24	34.79	0.26
DEGMA:AODMBA$_{75:25}$	4.23	0.13	31.74	0.53
DEGMA:AODMBA$_{50:50}$	6.58	0.31	32.89	0.21
DEGMA:TBCHMA$_{75:25}$	2.81	0.28	33.95	0.04
DEGMA:TBCHA$_{75:25}$	2.83	0.10	34.07	0.38
DEGMA:TBCHA$_{50:50}$	2.88	0.30	33.22	0.69
DEGMA:IBMA$_{75:25}$	3.26	0.26	34.23	0.15
DEGMA:IBMA$_{10:90}$	7.04	0.21	34.26	0.20
DEGMA:EGDPEA$_{75:25}$	5.24	0.69	33.31	0.51
DEGMA:EGDPEA$_{50:50}$	7.03	0.37	34.76	0.56

The viscosity measurements were demonstrated to be both repeatable and repeat values were in close agreement with standard deviations ranging between 0.12 – 0.69. The highest mean viscosity from the 19 co-monomers was 9.37 mPa.s for TEGMA:EGDPEA$_{50:50}$ and the lowest was 2.81 mPa.s for DEGMA:TBCHMA$_{75:25}$. The co-monomers were noted to exhibit a narrower range of viscosities compared to the measurement in chapter 4 where the mean measurement of AODMBA monomer was 42.93 mPa.s and EGDPEA monomer was 23.24 mPa.s (chapter 4, section 4.7, Table 4.5). It was then hypothesised that this observation was contributed by the mixing of two

co-monomers. The mixing has helped to reduce intermolecular interactions between the polymer chains and hence lowered the viscosity. For example, in TEGMA:EGDPEA$_{50:50}$, the measured viscosity is much lower than EGDPEA, and has only a mean value of 9.37 mPa.s. Surface tension measurements were also repeatable for all co-monomers with all co-monomer values being within the range of 31 – 35. The density of the co-monomers is tabulated in Table 5.5 and calculated based on the monomeric ratio by referring to the density of the individual monomers provided in the technical datasheet (chapter 4, section 4.7, Table 4.5).

Table 5.5: *Density of co-monomers and the tabulated Z parameters for all 19 co-monomer/ polymer candidates.*

Co-monomers	Density (ρ)	Z Parameter
TEGMA:AODMBA$_{75:25}$	1.052	4.21
TEGMA:AODMBA$_{50:50}$	1.076	3.05
TEGMA:TBCHMA$_{75:25}$	1.008	4.78
TEGMA:TBCHMA$_{50:50}$	0.989	4.70
TEGMA:TBCHA$_{75:25}$	1.047	4.91
TEGMA:TBCHA$_{50:50}$	1.068	5.73
TEGMA:IBMA$_{75:25}$	1.016	4.85
TEGMA:IBMA$_{50:50}$	1.005	4.95
TEGMA:EGDPEA$_{75:25}$	1.042	3.78
TEGMA:EGDPEA$_{50:50}$	1.056	3.00
DEGMA:AODMBA$_{75:25}$	1.046	6.32
DEGMA:AODMBA$_{50:50}$	1.073	4.19
DEGMA:TBCHMA$_{75:25}$	1.003	9.64
DEGMA:TBCHA$_{75:25}$	1.042	9.76
DEGMA:TBCHA$_{50:50}$	1.064	9.58
DEGMA:IBMA$_{75:25}$	1.011	8.38
DEGMA:IBMA$_{10:90}$	0.987	3.83
DEGMA:EGDPEA$_{75:25}$	1.036	5.20
DEGMA:EGDPEA$_{50:50}$	1.053	3.99

Fromm's parameter Z (listed in Table 5.5) was then tabulated with the nozzle diameter, co-monomer density, surface tension and dynamic viscosity data obtained from the HTS method using Equation 5.1.

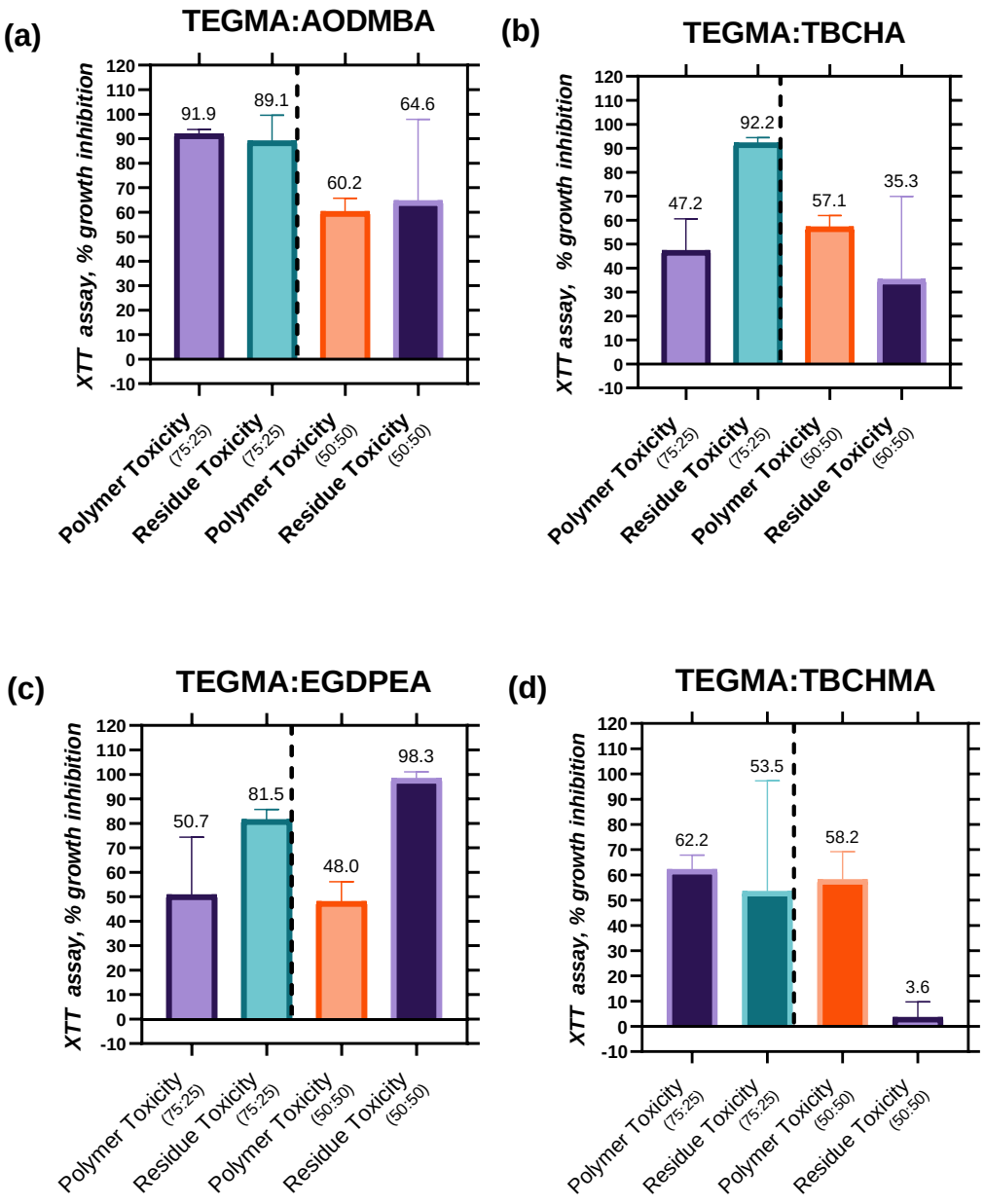
$$Z = \frac{\sqrt{\rho r \gamma}}{\mu} \quad \textbf{Equation 5.1}$$

The Z parameters for all the co-monomers were found to fall within the ideal range of 1-10 signifying that droplet formation with inkjet printing will unlikely be a bottleneck during the inkjet printing process. Again, comparing the co-monomer Z values to those of the monomers measured in chapter 4, DEGMA had a tabulated Z parameter of 11.73 and AODMBA had a Z parameter of 0.69, which both fall out of the ideal range for inkjet printing. Thus, mixing the monomers also have a positive effect in obtaining a Z parameter within the ideal range to minimise potential printing challenges.

5.5 Polymer & Residue Toxicity Studies

After investigating fungal anti-attachment and Z parameters with HTS methodology, it is also vital to understand the potential toxicity effect of the copolymers on *C. albicans*. All copolymers used from this evaluation onwards focused on copolymer mixtures with 4 % DMPA initiator loading. This was also the formulation used in the inkjet printing trials, as it had been demonstrated to deliver higher DOC values. This evaluation helps to better understand if copolymers worked primarily by anti-attachment properties and to identify if copolymer variations had an impact on toxicity when compared to their homopolymer counterparts. In addition to studying the toxicity of copolymers (polymer toxicity), an evaluation to determine the toxicity of the potential residues, such as monomer and

oligomer that may leach from the copolymers (residue toxicity) was also included (method described in detail in chapter 3, subsection 3.4.3). Figure 5.6 below shows the toxicity information for both polymer and residue of TEGMA-based copolymers.



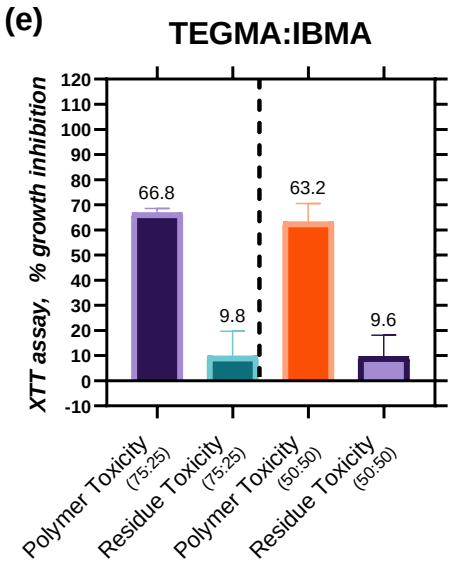
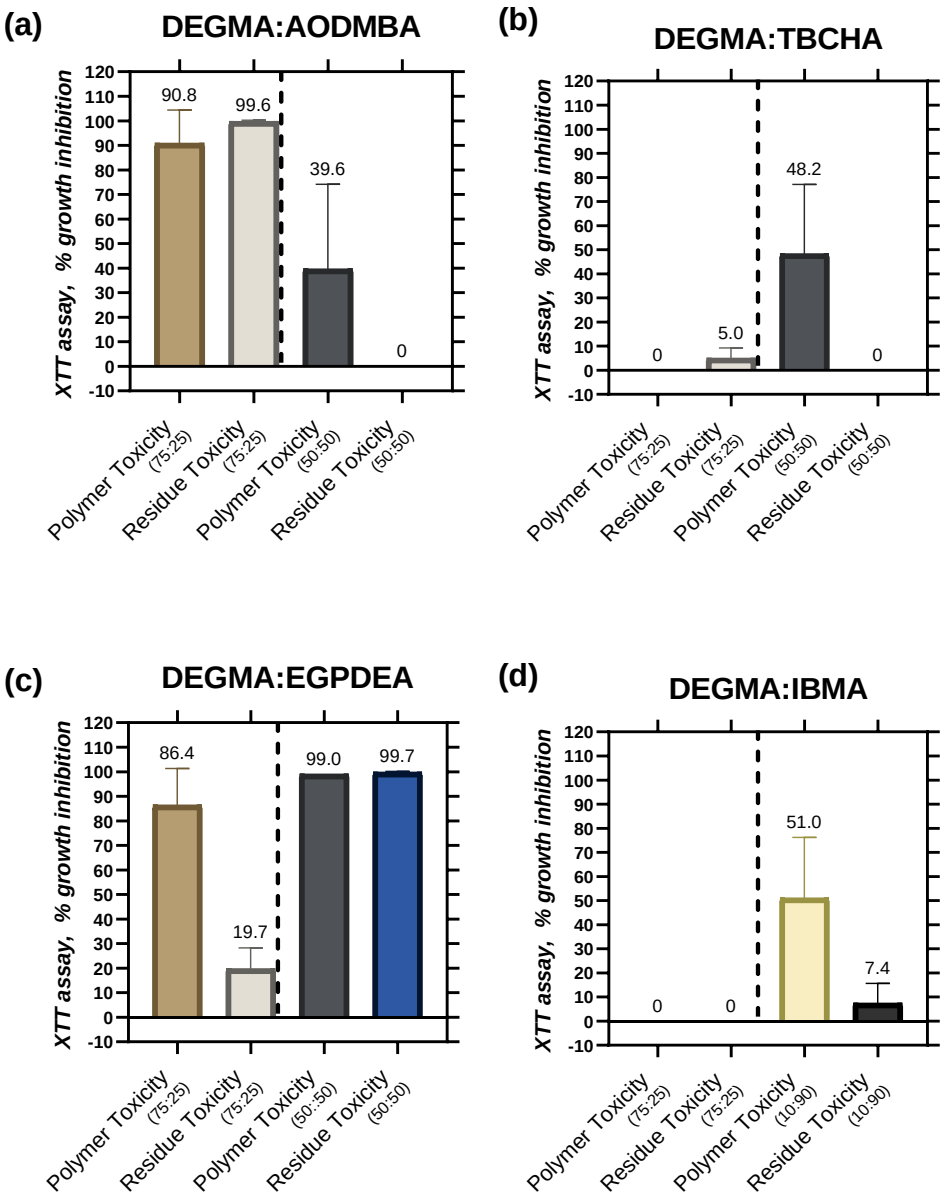


Figure 5.6: *(a-e) TEGMA-based copolymer residue and polymer toxicity results.*

Some levels of toxicity toward *C. albicans* cells were observed in several TEGMA-based copolymers. For example, when evaluating polymer toxicity, TEGMA:AODMBA$_{75:25}$ (Figure 5.6a) has the highest toxicity at 91.9 % out of all the TEGMA-based copolymers. Reduction of TEGMA ratio in TEGMA:AODMBA$_{50:50}$ resulted in lower toxicity towards the fungi. In TEGMA:AODMBA copolymers, residue toxicity towards the fungi were of equally high value as the polymer toxicity and is likely to be the main cause of toxicity in the polymers as oligomers and monomers may still be trapped within the copolymer. Similar to TEGMA:AODMBA, the phenomenon of high residue toxicity can also be seen in other TEGMA-based copolymers, such as TEGMA:EGDPEA and TEGMA:TBCHA (Figure 5.6c and 5.6b). Nonetheless, even though some toxicity effects from the residues persisted, the fungi anti-attachment effect was still notably present in copolymer ratios of TEGMA:AODMBA$_{50:50}$, TEGMA:EGDPEA$_{50:50}$ and TEGMA:TBCHA$_{50:50}$ as confirm by the fungal anti-attachment XTT results. Interestingly TEGMA:TBCHMA (Figure 5.6d) and

TEGMA:IBMA (Figure 5.6e) copolymers had much lower residue toxicity of 3.6 – 9.8 % comparatively but were tested to have higher polymeric toxicity. One possible explanation for this could be because of the difficulty in removing entrapped oligomers and/ or monomers during residue toxicity evaluation.



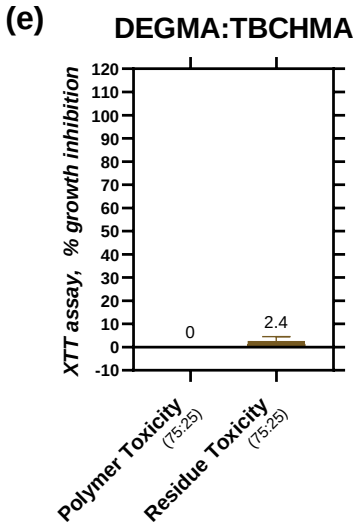


Figure 5.7: *(a-e) DEGMA-based copolymer residue and polymer toxicity results. residue and polymer toxicity results.*

For DEGMA-based materials, toxicity was also evident in a few of the copolymer variants especially DEGMA:EGDPEA$_{75:25}$ (Figure 5.7c), DEGMA:EGDPEA$_{50:50}$ (Figure 5.7c) and DEGMA:AODMBA$_{75:25}$ (Figure 5.7a). A few of the copolymers have an exceptionally low level of toxicity between 0 – 5.0 % in both polymer and residue toxicity data, for example in DEGMA:TBCHMA$_{75:25}$ (Figure 5.7e), DEGMA:IBMA$_{75:25}$ (Figure 5.7d) and DEGMA:TBCHA$_{75:25}$. While DEGMA and TEGMA have a very similar structure and are both hydrophilic, the toxicity results did not have many similarities for a majority of the copolymer types and its ratio.

As minimal trends were observed in the toxicity studies, ANOVA analysis was used to study the impact of the primary polymer type, secondary polymer type and copolymer ratios on the toxicity results. Secondary polymer type was found to have a significant effect on both the polymer toxicity and residue toxicity with p-values being 0.008 and

0.000 respectively. Another factor that has influenced only residue toxicity was the type of primary polymer (TEGMA or DEGMA) used, the p-value of analysis was 0.012. As the secondary polymer type appears to have a significant influence in both sets of toxicity data, further analysis was made to evaluate whether an acrylate or a methacrylate secondary polymer would be significant. AODMBA, TBCHA and EGDPEA were classified as acrylate with TBCHMA and IBMA representing methacrylate. P values of 0.000 and 0.047 were found for both polymer toxicity and residue toxicity data.

Finally, main effect plots (Figures 5.8 and 5.9 below) were prepared to evaluate the trends of the factors studied. The key significant factor that affects both toxicity data was secondary polymer type, with a significant dependence on whether it belongs to an acrylate or a methacrylate. Primary polymer type DEGMA/ TEGMA have a significant influence on the residue toxicity with DEGMA-based copolymers demonstrating lesser toxicity in comparison to TEGMA-based copolymers.

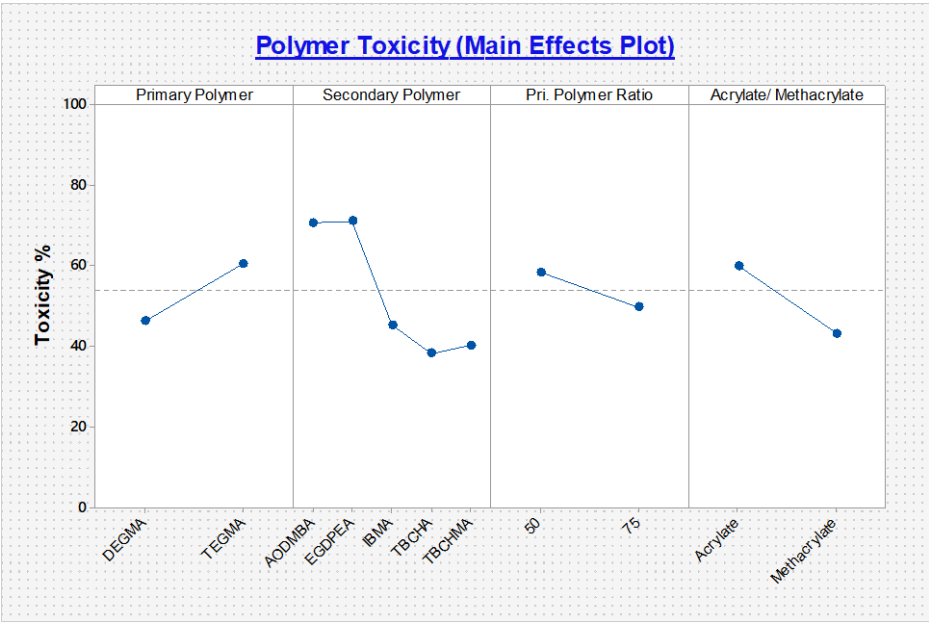


Figure 5.8: *Main effects plot of polymer toxicity result considering varying factors – primary polymer type, secondary polymer type, primary polymer ratio and acrylate/ methacrylate type secondary polymer.*

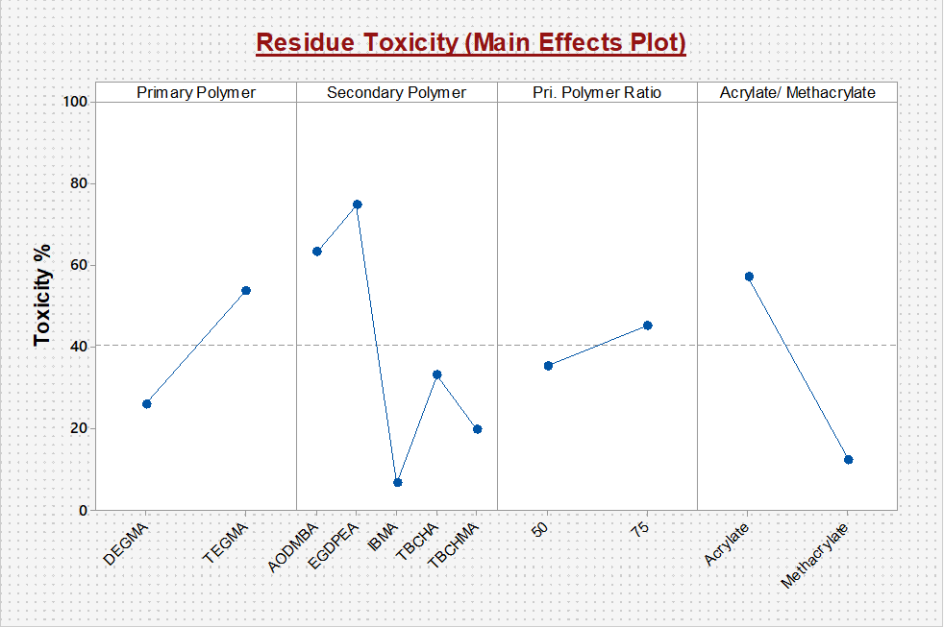


Figure 5.9: *Main effects plot of residue toxicity result considering varying factors – primary polymer type, secondary polymer type, primary polymer ratio and acrylate/ methacrylate type secondary polymer.*

A possible hypothesis relating to the impact of DEGMA/ TEGMA type on residue toxicity results could be due to its hydrophilicity and T_g differences. TEGMA has lower T_g than DEGMA, hence, the biological species might embed into the softer and gel-like residues. An interesting finding was that secondary polymers appeared to result in lower toxicity in both data sets when it is a methacrylate type polymer.

However, this study only considered two types of methacrylates – IBMA and TBCHMA therefore more work should be done to further assess the impact of such factors on the toxicity towards fungi. Also, available studies have found that acrylate is more toxic to mammal cells only but no study of acrylate toxicity effect on *C. albicans* has been

studied.[206] This study also does not consider interaction factors and the physical impact of surface roughness [202] and/ or surface energy [205] that could potentially influence the results. The brief statistical outlook allows some understanding of possible causes of toxicity effects on fungi. Also, a future improved protocol that can better remove oligomer/ monomer residues would be beneficial in an improved assessment and can also further lower such fungi toxicity effects.

5.6 Glass Transition Temperature (T_g) of Copolymers

As the T_g of the homopolymers were earlier assessed with DSC in chapter 4, a method to obtain an estimate of the copolymers' T_g was to utilise the Flory-Fox equation (as per Equation 5.2). This allows quick tabulation of copolymer T_g by considering the weight fraction of the homopolymers and its measured homopolymer T_g. [207] The theoretical value of all the 19 copolymer candidates that had exhibited the targeted fungal anti-attachment are listed in Table 5.6 below.

$$\frac{1}{T_g} = \frac{w_1}{T_g} + \frac{w_2}{T_g} \qquad \textbf{Equation 5.2}$$

Table 5.6: *Summary of estimated T_g.*

Copolymer	Primary Polymer Ratio	Secondary Polymer Ratio	Estimated Tg
TEGMA:AODMBA	0.75	0.25	-29.3
	0.50	0.50	0.1
TEGMA:TBCHMA	0.75	0.25	-22.2
	0.50	0.50	18.6
TEGMA:TBCHA	0.75	0.25	-24.8
	0.50	0.50	11.6
TEGMA:IBMA	0.75	0.25	-29.2
	0.50	0.50	0.4
TEGMA:EGDPEA	0.75	0.25	-37.9
	0.50	0.50	-20.6

DEGMA:AODMBA	0.75	0.25	-13.9
	0.50	0.50	12.8
DEGMA:TBCHMA	0.75	0.25	-5.9
DEGMA:TBCHA	0.75	0.25	-8.8
	0.50	0.50	25.4
DEGMA:IBMA	0.75	0.25	-13.7
	0.10	0.90	70.1
DEGMA:EGDPEA	0.75	0.25	-31.2
	0.50	0.50	-9.8

For example, for a flexible medical device application, targeted T_g would be ideal between -10 – 15 °C.[201] The library of materials will potentially be useful in varying medical devices which require different T_g. However, it is worthwhile noting that the estimated T_g with Flory-Fox Equation does not take into consideration interaction, the reactivity of the monomers (i.e., presence of free monomer) and the eventual molecular weight of the final copolymer which are factors that could affect its T_g.[208] Later in chapter 6, section 6.6, T_g of the selected copolymer candidates for printing a flexible medical device part would be evaluated for its experimental T_g.

Out of all the 19 copolymers with fungal anti-attachment ability, TEGMA:AODMBA$_{50:50}$. TEGMA:TBCHA$_{50:50}$, TEGMA:IBMA$_{50:50}$, DEGMA:TBCHMA$_{75:25}$, DEGMA:TBCHA$_{75:25}$, DEGMA: EGDPEA$_{50:50}$ met the targeted T_g needed to manufacture a flexible medical device. Data presented in chapter 4 showed that a high amount of TEGMA/ DEGMA could lead to low curing/ gel-like material and methacrylate often have slower curing behaviour during the inkjet printing process. With these considerations in mind, copolymers with higher TEGMA/DEGMA were omitted from further studies and only TEGMA:AODMBA$_{50:50}$ and TEGMA:TBCHA$_{50:50}$ was selected for the inkjet printing assessment that would be discussed in chapter 6, section 6.2.

5.7 FTIR and Raman Analysis

Before evaluating TEGMA:AODMBA$_{50:50}$ and TEGMA:TBCHA$_{50:50}$ co-monomer directly for inkjet printing assessment. Further analyses were carried out to better assess the UV copolymerisation and DOC of the three ratios, 75:25, 50:50 and 25:75 for both TEGMA:AODMBA and TEGMA:TBCHA. The studies were performed to better understand how the different ratios could affect both the materials and fungal anti-attachment properties. The three different ratios of moulded TEGMA:AODMBA and TEGMA:TBCHA were evaluated using FTIR as in chapter 4 and the DOC results were validated with Raman spectroscopy. Raman spectroscopy is a complementary technique to FTIR which can also provide multispectral data that is useful for the investigation of phase separation. Furthermore, the co-monomers molar ratio may not represent the final copolymer ratio if the reactivity of monomers is vastly different, therefore Raman spectroscopy alongside ^{1}H NMR in section 5.9 was carried out to assess the copolymer ratio. In Raman spectroscopy, multispectral images were used to interpret copolymer ratio with classic least square (CLS) regression analysis.

Both FTIR and Raman data sets had DOC calculated using Equation 3.1 found in chapter 3, subsection 3.4.1. The tabulated data can be found in below Table 5.7. Results for TEGMA:TBCHA showed that DOC reduces with a higher ratio of TEGMA due to the slower curing nature of methacrylate for TEGMA:TBCHA copolymers. This result was not replicated in TEGMA:AODMBA copolymer, DOC measurement of TEGMA:AODMBA$_{75:25}$ was 100 % and FTIR measurement was 97.1%. This suggests the possibility that TEGMA:AODMBA can achieve better monomer to polymer conversion with UV curing and may lead to better structure formation during the inkjet printing process. Better

conversion to polymer for TEGMA:AODMBA was attributed to the similar reactivity ratios between monomers due to the steric size of the pendant group in AODMBA. Thus, minimising skewed stoichiometry during the polymerisation process.

Table 5.7: *Summary of DOC for selected copolymers of TEGMA:AODMBA and TEGMA:TBCHA (both with 4 % DMPA initiator) measured with both FTIR (one measurement) and Raman spectroscopy (average of three measurements).*

Polymer	DOC (FTIR) (N = 1)	DOC (Raman) (N = 3)
TEGMA	68.5	71.3±0.5
TBCHA	100.0	99.5±0.0
AODMBA	80.2	89.0±0.1
$TEGMA:AODMBA_{75:25}$	97.1	100.0±0.0
$TEGMA:AODMBA_{50:50}$	98.0	100.0±0.0
$TEGMA:AODMBA_{25:75}$	100.0	100.0±0.0
$TEGMA:TBCHA_{75:25}$	85.8	66.5±0.1
$TEGMA:TBCHA_{50:50}$	100.0	98.2±0.2
$TEGMA:TBCHA_{25:75}$	100.0	100.0±0.0

Raman mapping, which is based on collecting multispectral images, was then conducted to provide additional information on the distribution of the repeating units within the material. This is important when reacting two co-monomers because there is also the possibility of phase separation between the primary and secondary monomer as the polymerisation occurs. This is crucial when considering TEGMA, which is more hydrophilic as compared to the secondary monomers. The mapping images for all six copolymer variants showed homogeneously spread intensity for both TEGMA:AODMBA and TEGMA:TBCHA copolymers (selected mapping images as shown in Figure 5.10, the

remaining images can be found in Appendix 4.), indicating little evidence of phase separation in these copolymers. The consolidated CLS score of the copolymers can be found in below Tables 5.8 and 5.9 for TEGMA:AODMBA and TEGMA:TBCHA respectively.

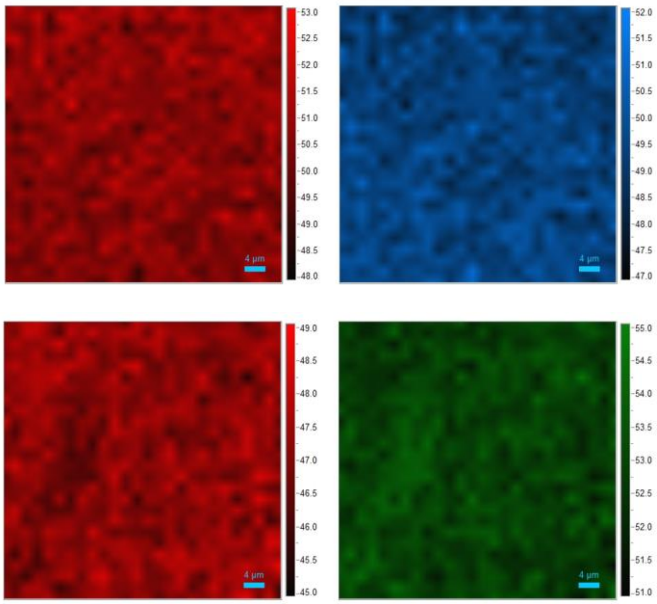


Figure 5.10: *TEGMA is represented by red, AODMBA represented by blue and TBCHA represented by green. (top) TEGMA:AODMBA$_{50:50}$, (bottom)TEGMA:TBCHA$_{50:50}$.*

Table 5.8: *CLS scores of TEGMA:AODMBA copolymers in three different ratios.*

Polymer	TEGMA CLS score / %	AODMBA CLS score / %
TEGMA:AODMBA$_{25:75}$	24.9 ± 0.6	75.1 ±0.6
TEGMA:AODMBA$_{50:50}$	50.6 ± 0.6	49.4 ±0.6
TEGMA:AODMBA$_{75:25}$	73.1 ± 0.6	26.9 ± 0.6

Table 5.9: *CLS scores of TEGMA:TBCHA copolymers in three ratios.*

Polymer	TEGMA CLS score / %	TBCHA CLS score / %
TEGMA:TBCHA$_{25:75}$	20.9 ± 0.8	79.1 ± 0.8
TEGMA:TBCHA$_{50:50}$	47.1 ± 0.5	52.9 ± 0.5
TEGMA:TBCHA$_{75:25}$	77.0 ± 0.5	23.0 ± 0.5

The CLS scores of the copolymers were found to match closely to the feed molar ratio of the co-monomers with a very slight deviation. This confirms that the copolymer ratios of the six copolymers evaluated were very close to the intended ratios. All in all, the Raman spectroscopy data confirms that the UV copolymerisation was successful with high DOC and also was of close value to the intended copolymer ratios.

5.8 Time-of-Flight Secondary Ion Mass Spectrometry (ToF-SIMS)

Moulded samples of both TEGMA:TBCHA (Figure 5.14) and TEGMA:AODMBA in the three selected ratios of 75:25, 50:50 and 25:75 were all assessed with ToF-SIMS analysis. ToF-SIMS analyses the surface of these samples by bombarding it with ions, fragment ions will then provide information on the compositions and the distribution of polymer within the samples. Mass spectrum data of the positive fragment ions were used for the analysis. TEGMA:TBCHA, $C_5H_7^+$ has an ion mass 67.07 m/z was selected as a fragment of TEGMA and $C_3H_9O^{2+}$ with an ion mass of 77.05 m/z was chosen as the representative of TBCHA fragment (Refer to Figure 5.11 and Figure 5.12 below).

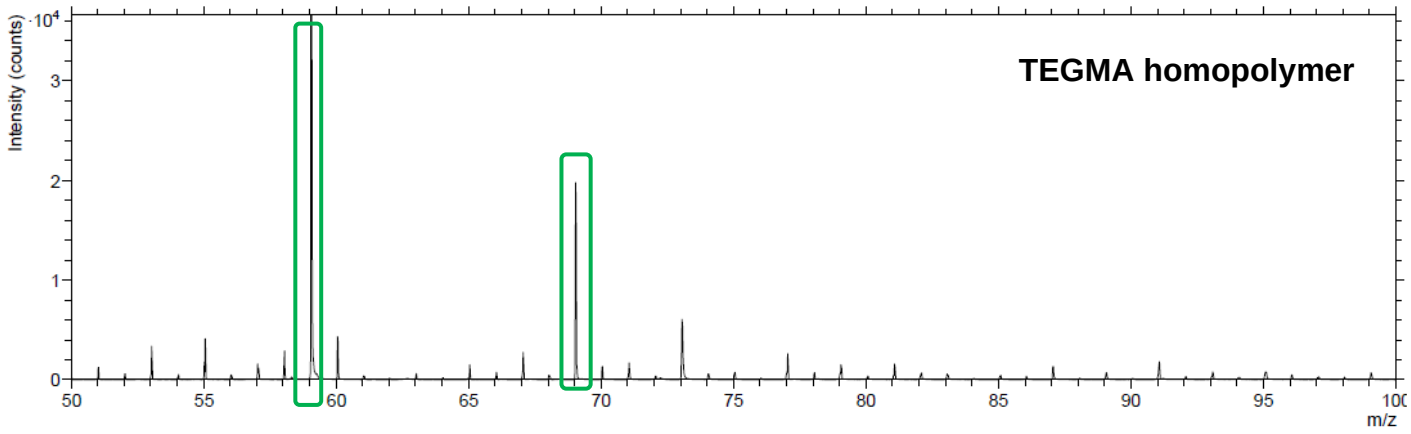


Figure 5.11: *ToF-SIMS spectrum of TEGMA showing mass data in the range of 50 – 100 m/z. A $C_3H_7O^+$ peak is seen at 59.08 m/z and a $C_5H_7^+$ peak at 67.07 m/z.*

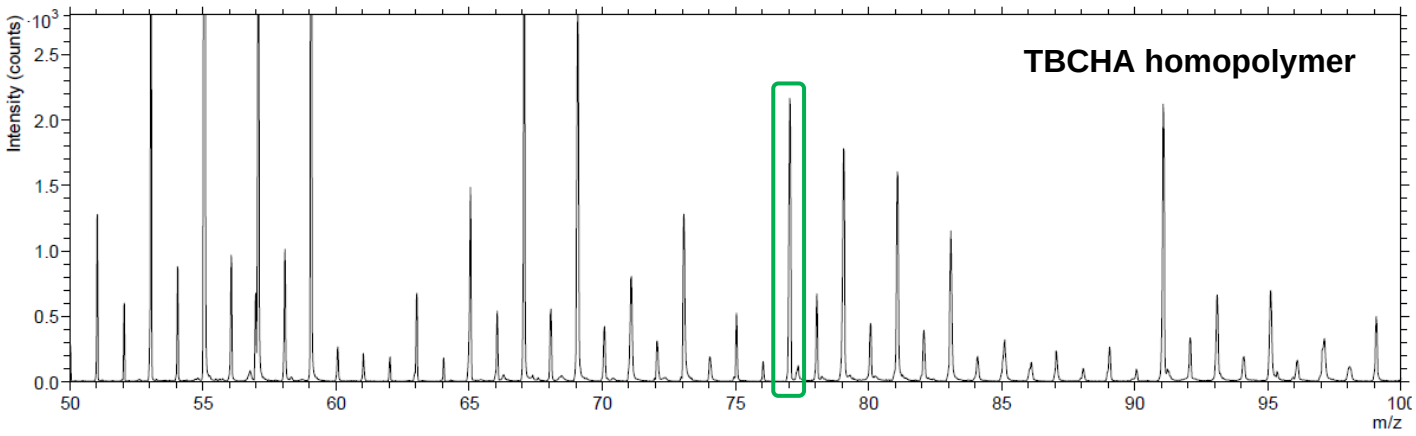


Figure 5.12: *ToF-SIMS spectrum of TBCHA showing mass data in the range of 50 – 100 m/z. 77.05 m/z for $C_3H_9O^{2+}$ fragment is more significant in TBCHA than TEGMA.*

For TEGMA:AODMBA copolymer, $C_3H_7O^+$ with an ion mass of 57.08 m/z (refer to Figure 5.13 of TEGMA homopolymer spectrum) was selected as it was a prominent TEGMA fragment, while AODMBA was presented with C_4H_9+ AODMBA fragments showing ion mass at 57.08 m/z (as per Figure 5.13).

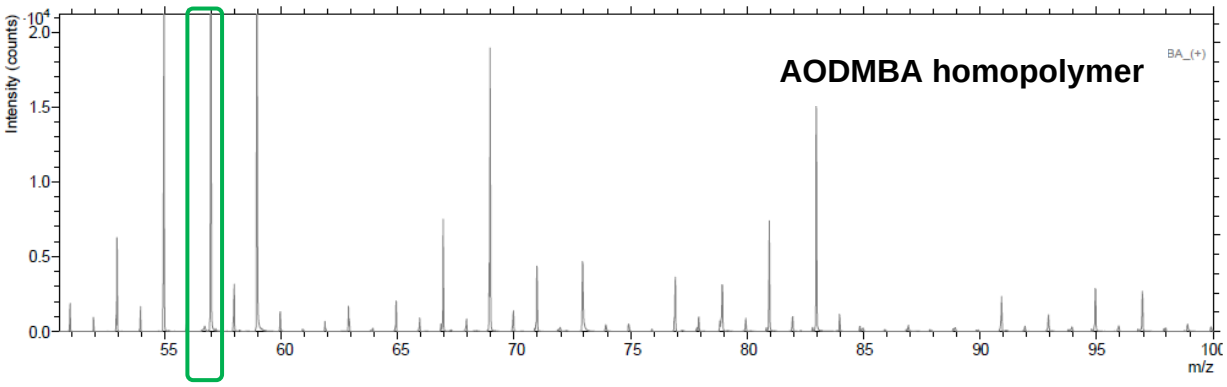


Figure 5.13: *ToF-SIMS spectrum of AODMBA showing a prominent peak of* $C_4H_9^+$ at 57.08 m/z.

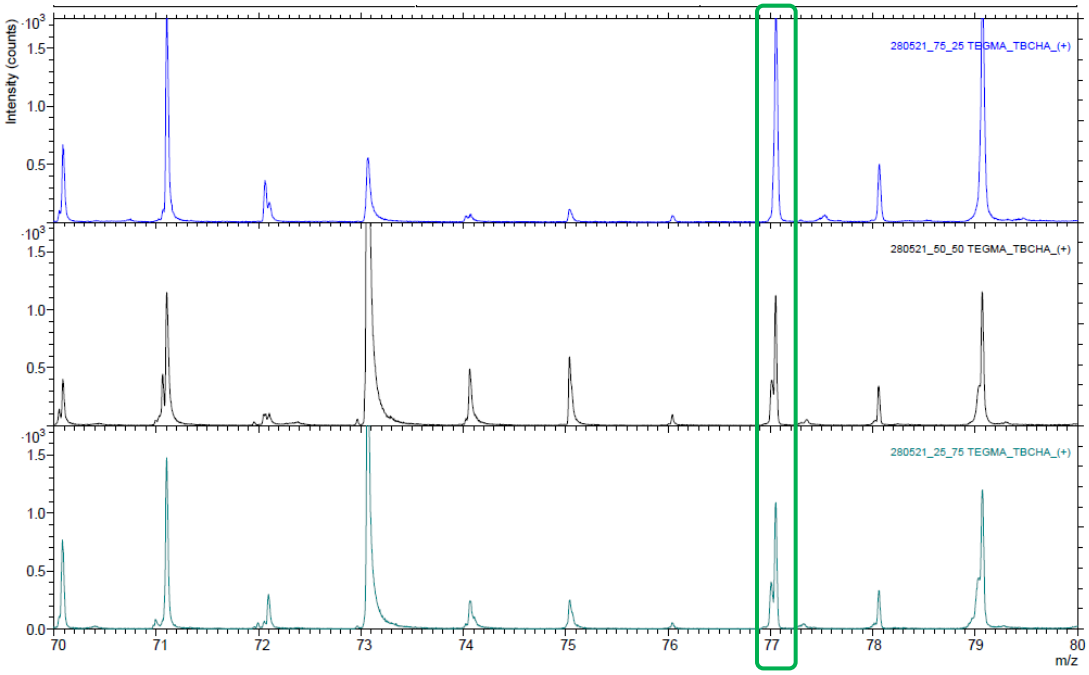


Figure 5.14: *ToF-SIMS spectrum of three TEGMA:TBCHA copolymers showing spectrum in the range of 70 – 80 m/z.* $C_3H_9O^{2+}$ *fragment is highlighted in the green box.*

An overview of both the TEGMA and TBCHA fragments found in the three different copolymer ratios is summarised in the graph below in Figure 5.15 and Figure 5.16. In

both Figure 5.15 and Figure 5.16, ratios appear to correlate well with the incorporated ratio of TEGMA as per feed ratio.

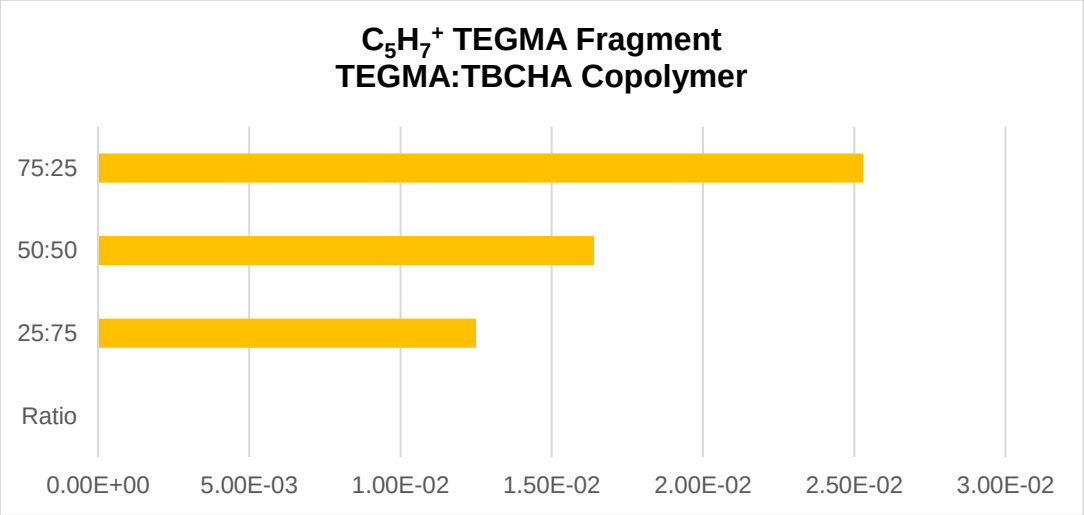


Figure 5.15: *$C_5H_7^+$ TEGMA fragments in different TEGMA:TBCHA ratios.*

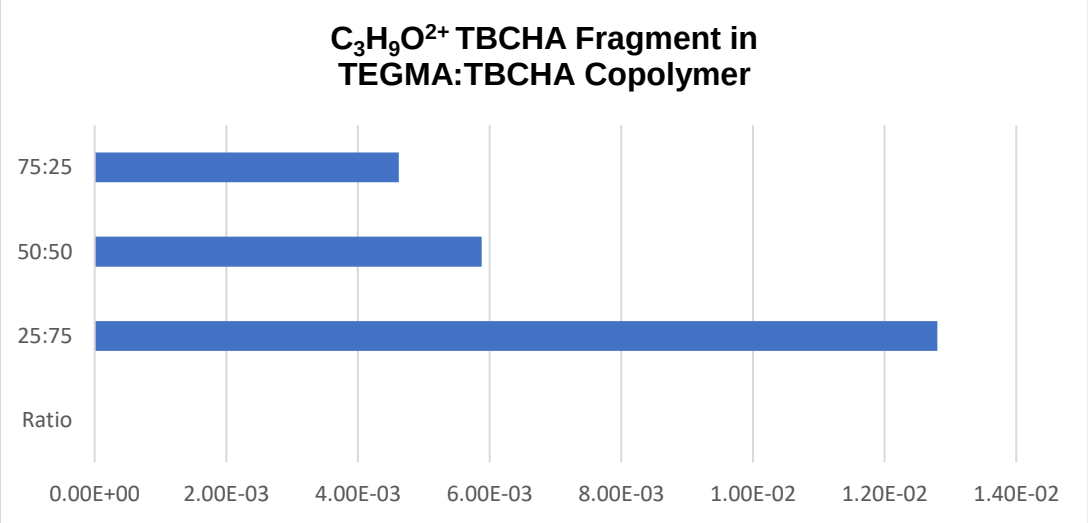


Figure 5.16: *$C_3H_9O^{2+}$TBCHA fragments in the three different TEGMA:TBCHA ratios.*

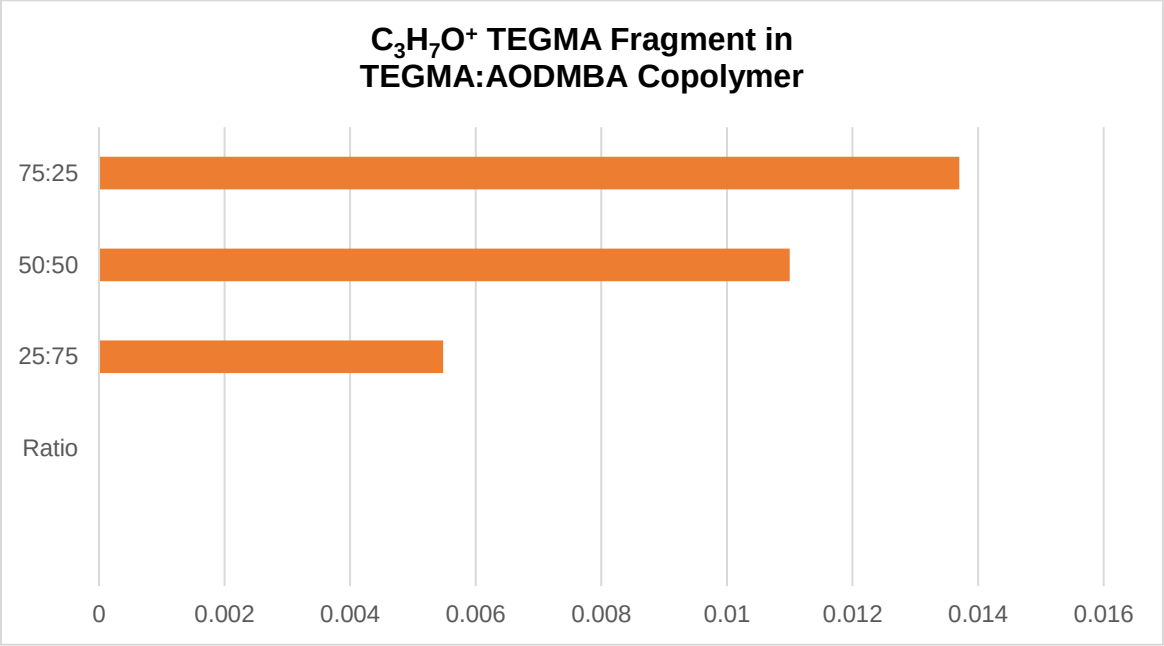


Figure 5.17: *$C_3H_7O^+$ TEGMA fragments in different TEGMA:AODMBA ratios.*

The resultant fragment ions intensity corresponded well to the feed ratio when in comparison between the three different ratios. In TEGMA:AODMBA copolymer, the graph in Figure 5.17 also depicts a similar trend for $C_3H_7O^+$ TEGMA fragment chosen for assessing this copolymer ratio. TEGMA fragment increases with the increase in TEGMA ratio within TEGMA:AODMBA copolymer. However, when analysing AODMBA fragment $C_4H_9^+$ (Figure 5.18), the ion intensity unexpectedly did not relate to the AODMBA feed ratio of copolymer feed ratio.

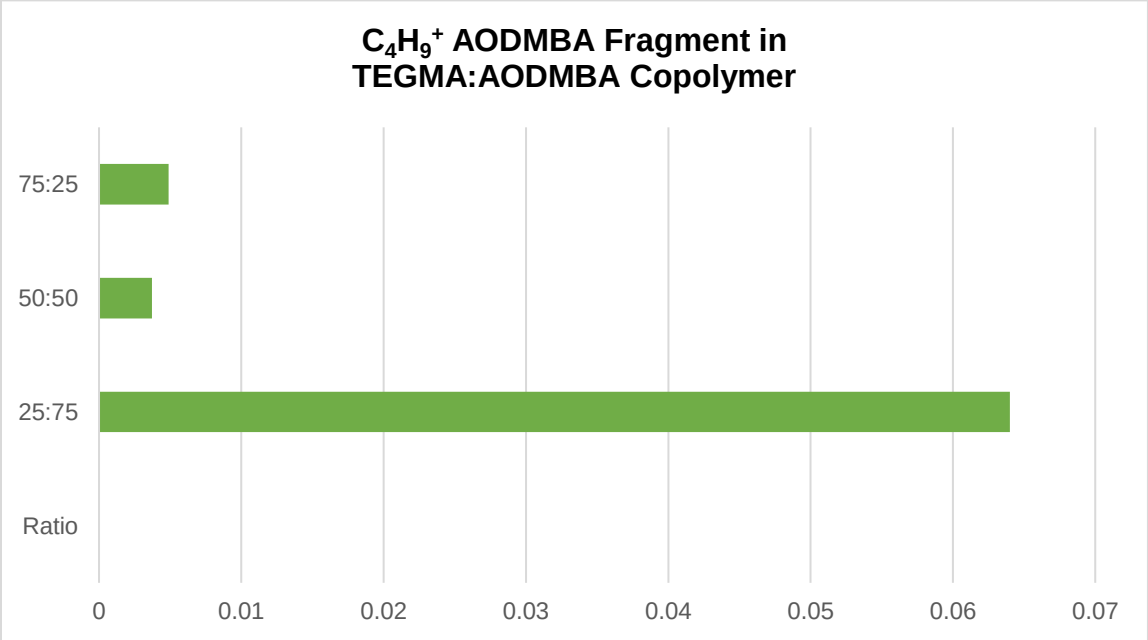


Figure 5.18: *$C_4H_9^+$ AODMBA fragments in different TEGMA:AODMBA ratios.*

TEGMA:AODMBA$_{50:50}$ had 0.00373 ion intensity of AODMBA fragment ion, $C_4H_9^+$. While TEGMA:AODMBA$_{75:25}$ had ion intensity of 0.00489 for the same AODMBA fragment ion. As the intensity of the $C_4H_9^+$, in general, was lower than other evaluated fragments, a slight deviation of data may be the cause. The samples were only evaluated once, therefore future work should repeat these ToF-SIMS measurements for at least three measurements will improve the study.

5.9 Copolymer Ratio Studies with ^{1}H NMR

^{1}H NMR was another technique that was adopted to verify the actual copolymer ratio in the final cured product, if unique resonances can be found in the spectra, it can be used to identify the number of repeating units via comparison of the integrals for these signals. In this way, giving the potential to define the copolymer ratio. In this section, ^{1}H NMR was

performed only on the moulded TEGMA:TBCHA in different ratios (75:25,50:50 and 25:75) to validate the copolymer ratio data from Raman spectroscopy and ToF-SIMS.

^{1}H NMR analysis of TEGMA:AODMBA can be found in later chapter 6, section 6.3 where thermally synthesised TEGMA:AODMBA copolymers prepared in a formal chemical reaction in different ratios are compared to the materials resulting from moulding the TEGMA:AODMBA. Molar ratio of the copolymer can be determined by comparing the integral of the significant peak from each component.

In TEGMA, the three hydrogen protons from the methoxy group can be found at 3.40 ppm while TBCHA has nine hydrogen protons from its three methyl groups showing at 0.89 ppm. The integral when tabulated will result in Table 5.10 showing the actual molar ratio of both components within the copolymer.

Table 5.10: *Molar ratio of TEGMA:TBCHA in different ratios tabulated from integral from ^{1}H NMR measurement.*

Co-monomer TEGMA:TBCHA (Molar Ratio)	TEGMA Integral	TBCHA Integral	TEGMA Integral per proton	TBCHA Integral per proton	100 / (Σintegrals)	Actual % TEGMA	Actual % TBCHA
25:75	1	10.00	0.33	1.11	69.20	23.07	76.93
50:50	1	3.43	0.33	0.38	139.97	46.66	53.34
75:25	1	1.31	0.33	0.15	208.61	69.54	30.46

The end molar ratio of the copolymers was found to closely match the feedstock molar ratio addition of TEGMA and TBCHA monomers. However, evaluation with ^{1}H NMR found that in all three ratios of TEGMA:TBCHA$_{25:75}$ (Figure 5.19), TEGMA:TBCHA$_{50:50}$ (Figure 5.20) and TEGMA:TBCHA$_{75:25}$ (Figure 5.21) has a slightly lower molar ratio of the TEGMA units when compared to the molar ratio of TEGMA added in the co-monomer. This again suggests that TEGMA may have lower reactivity due to its methacrylate group as compared to TBCHA which has an acrylate functional group.

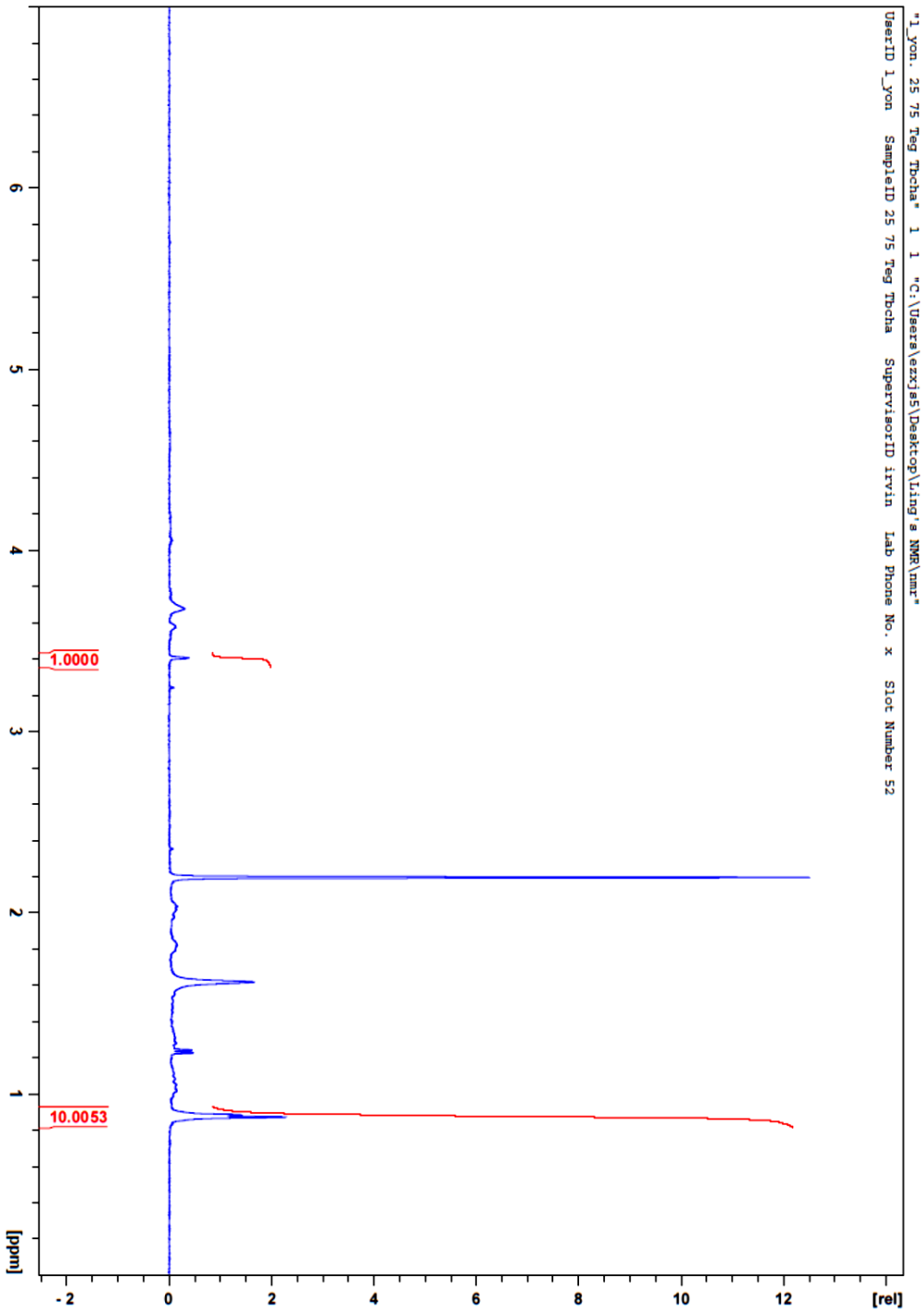


Figure 5.19: *TEGMA:TBCHA$_{25:75}$, where the integral of TEGMA was set as 1 and TBCHA, was found to have an integral of 10 in correlation.*

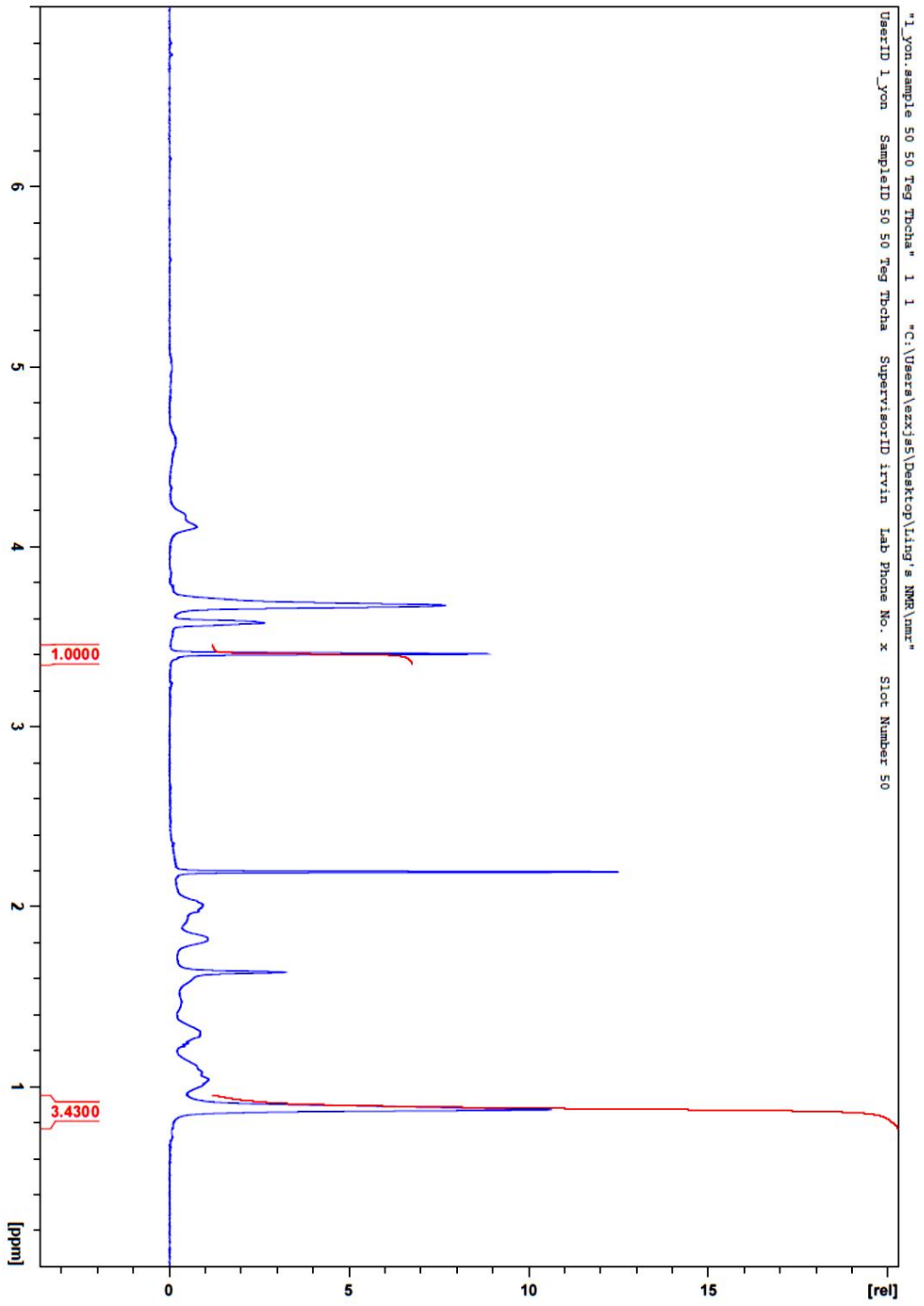


Figure 5.20: *^{1}H NMR of TEGMA:TBCHA$_{50:50}$, where the integral of TEGMA was set at 1 and TBCHA was found to have an integral of 3.43 in correlation.*

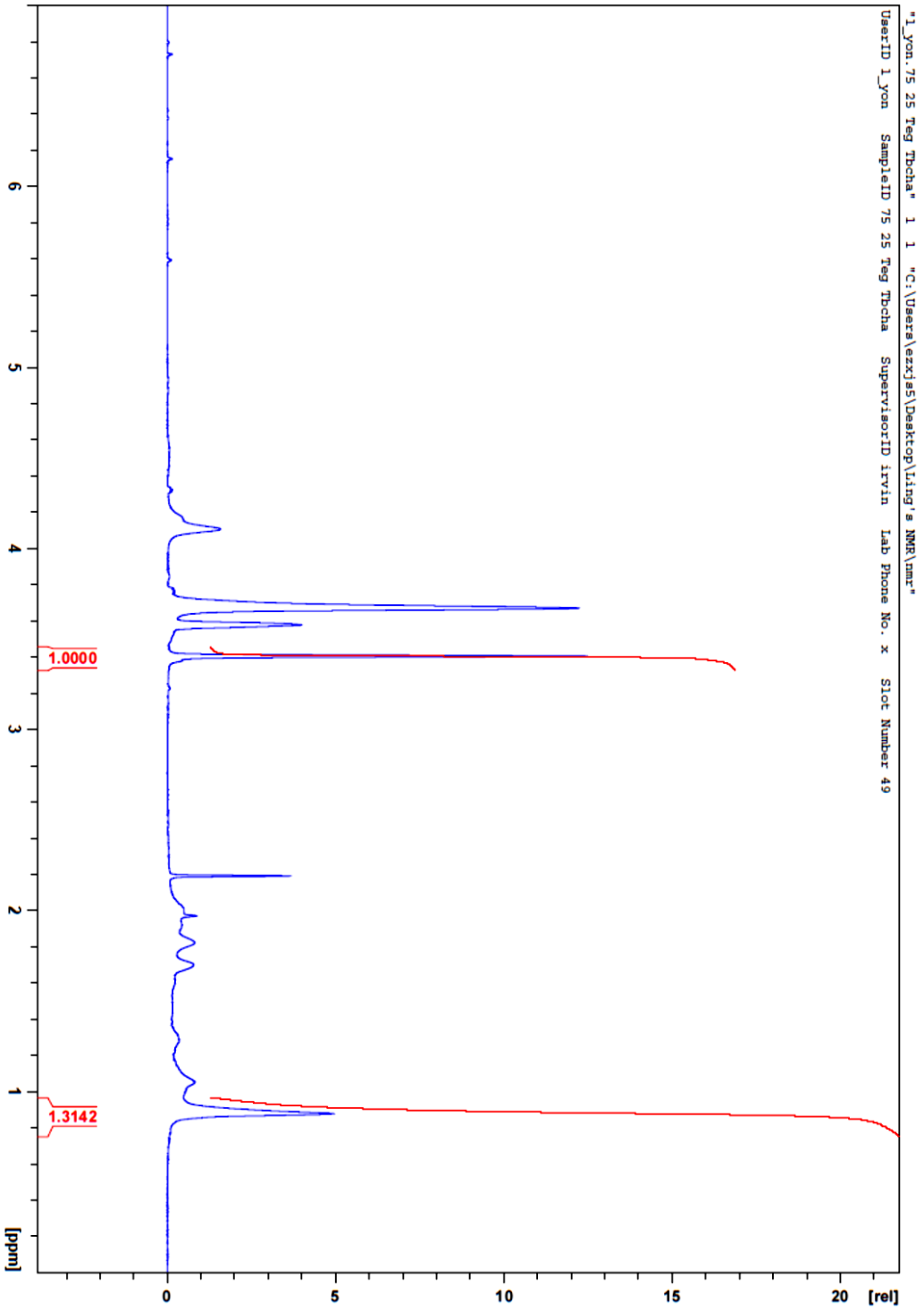


Figure 5.21: *^{1}H NMR of TEGMA:TBCHA$_{75:25}$, where the integral of TEGMA was set as 1 and TBCHA, was found to have an integral of 1.31 in correlation.*

5.10 Summary

In chapter 5, the copolymer matrix was developed from the eight monomers/ polymers that were evaluated when developing the HTS method in the earlier chapter. The HTS methodology developed was successfully utilised to prepare 120 wells moulded copolymers consisting of 30 different copolymer variations. 19 out of the 30 copolymers had *C. albicans* attachment of < 25 % and have the potential to be used in medical device applications which require fungal resistance. Fungal anti-attachment results of copolymers were not as per predicted. Many of the homopolymers selected met the targeted fungal resistance when evaluated in chapter 4, however when adding the monomers of these fungal resistance homopolymers into copolymers, the same fungal resistance ability was not observed.

DOC and copolymer ratio studies did not find any potential suspects for the change in fungal adhesion behaviour. In toxicity studies of copolymers, the type of secondary polymer appears to have a significant effect on both residue and polymer toxicity. Type of primary polymer – using either DEGMA or TEGMA was also found to have a significant effect on residue toxicity. This suggests that there may be some level of toxicity effect on the fungi and a more thorough post-polymerisation cleaning may be required to reduce this situation. For example, TEGMA which has been linked to very soft, with low T_g and hydrophilic behaviour may also be likely to trap residues that are not easily removed by the chosen post-polymerisation washing process leading to toxicity phenomenon. In this chapter, the T_g of all the copolymers was also estimated with Flory-Fox Equation.

For the work in chapter 6 soft and flexible voice prosthesis flap was chosen as the end application. Earlier studies attempting to print AODMBA homopolymer resulted in a very

rigid material which breaks easily and was therefore unsuitable for voice prosthesis flap.[34] Targeted T_g of -10 to 15 °C was required for such application and 6 of the 19 fungal anti-attachment copolymers had T_g within the desired range. With considerations of UV curing reactivity, toxicity and the material's affinity to water, TEGMA:AODMBA$_{50:50}$ and TEGMA:TBCHA$_{50:50}$ copolymers were selected for application studies and inkjet printing studies in chapter 6.

Prior to that, it was important to also validate the DOC and the copolymer ratios of the moulded copolymers to confirm the suitability of HTS methodology for copolymer studies. DOC from FTIR and Raman spectroscopy has agreeing data. Actual copolymer ratios were studied via three methods, Raman, ToF-SIMS and ^{1}H NMR. The majority of the data confirms that copolymer ratios were similar to the intended copolymer molar feed ratios, and Raman mapping found a good distribution of the repeating units. This signifies that the developed HTS in chapter 4 was able to successfully prepare numerous copolymers for formulation development.

Chapter 6: Formulations & Applications

6.1 Introduction

The earlier chapters 4 and 5 discussed the development and utilisation of HTS methodology to evaluate a large number of fungal-resistant polymers and copolymers. In chapter 5, TEGMA:AODMA$_{50:50}$ and TEGMA:TBCHA$_{50:50}$ were both identified as the final candidate "hit" copolymers selected for evaluation out of the 19 fungal-resistant copolymers screened. These two copolymers were considered as they exhibited T_g values within the required specification to function well in flexible medical device applications.

Therefore, in this chapter, these two co-monomers were evaluated further to determine their curability and printability properties, and to define if they would be suitable for usage in inkjet printing processes. The final formulation that was demonstrated from this experimental study to meet the printing requirements, would be analysed and printed into the targeted medical device segment, a flexible flap of a voice box prothesis. The printed part would have its material properties evaluated, including fungal anti-attachment, T_g, final copolymer ratio and molecular weight with gel permeation chromatography (GPC). Hence, the material formulations were printed without an additional crosslinker to allow these evaluations to be conducted. The data from these initial printing trials would then be used to further improve the ink formulation by attempting formulation adjustment studies i.e., by fine-tuning the ratio of the co-monomers, addition of additives etc.

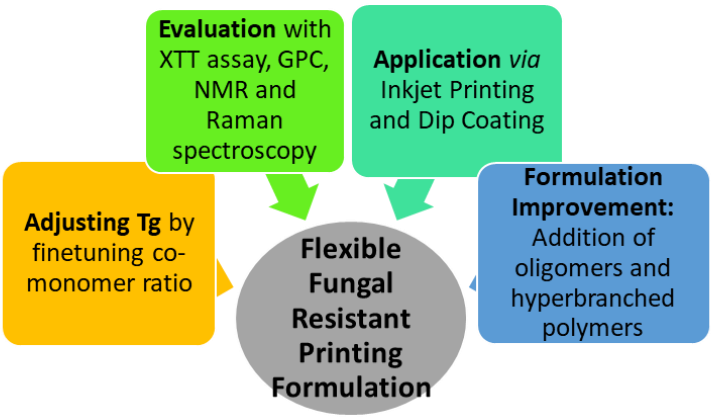


Figure 6.1: *Overview of work performed for chapter 6.*

Should inkjet printing prove to be impossible with the chosen anti-attachment formulation, then dip coating could also be considered as a processing method to coat medical-grade silicone rubber voice prosthesis flap with the fungal-resistant copolymer. In order to obtain a copolymer solution for dip coating, copolymers would have to be synthesised via a radical chain polymerisation where the monomers are dissolved into a suitable solvent for the process. The dip-coated part was also tested for its fungal resistance alongside with inkjet-printed samples to evaluate if there may be any potential differences.

6.2 Inkjet Printing Trial for Selected Copolymers

A printing trial was conducted to evaluate the printing performance of the two selected fungal anti-attachment copolymers – TEGMA:AODMBA$_{50:50}$ and TEGMA:TBCHA$_{50:50}$ identified from the HTS evaluation of copolymers in chapter 5. The trial involved printing layers of the materials to ensure that the co-monomer mixtures can be properly cured and printed with good fidelity of shape and structure. In this trial, two printing patterns were selected (Figure 6.2), a 100 layers of 3 mm disc shape and a 110 layers structure designed to mimic a silicone rubber voice prosthesis flap provided by Atos Medical.

Again, to minimise oxygen content within the mixture, 4 % initiator was dissolved into the prepared co-monomers formulations and these inks were then purged with nitrogen for 5 minutes. Furthermore, the Dimatix inkjet printer was also situated within a glove box purged with nitrogen (Oxygen level controlled to 0.1 – 0.3 %). This trial was conducted by attempting to print the structures shown in Figure 6.2.

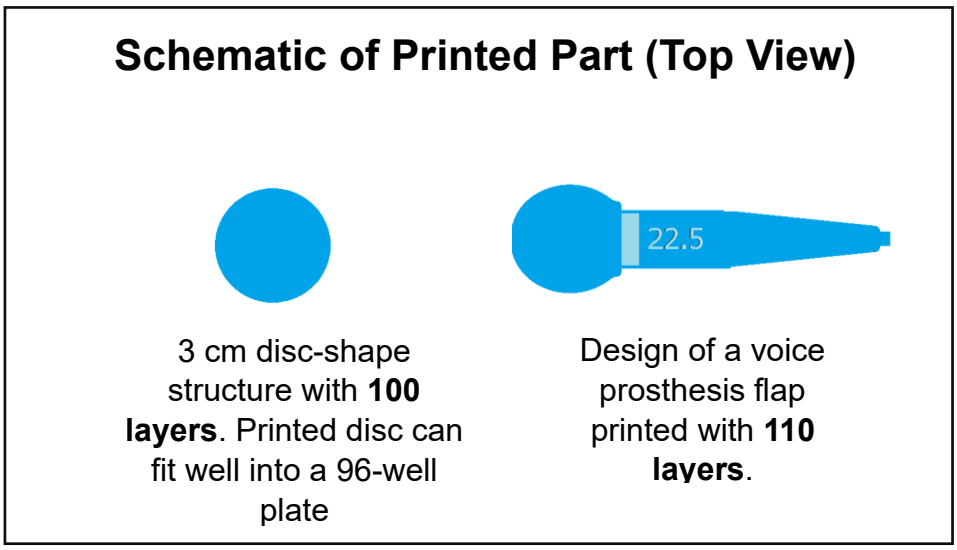


Figure 6.2: *Schematic top view design of the printed parts used for this chapter.*

It was demonstrated that TEGMA:AODMBA$_{50:50}$ could achieve printing (see Figure 6.2) using printing parameters of frequency 1 Hz, drop spacing of 20 µm and cartridge temperature at 40 °C. However, the TEGMA:TBCHA$_{50:50}$ copolymer system was not printable regardless of the inkjet printing parameters applied and was therefore omitted from further studies. When tested in chapter 4, the curability of AODMBA monomer was shown to be better than that of TBCHA. AODMBA could form good printing layers with only 1 % initiator, while TBCHA requires 4 % initiator in the work reported in earlier chapter 4.

One possible reason for this phenomenon is the presence of two carbonyl groups in AODMBA while TBCHA only has only one carbonyl group. Thus, the double bond in AODMBA may have additional electron-density and will be more inclined to free radical attack. Including TEGMA in copolymers was also concluded to significantly reduce the printability of co-monomer inks in both the inks tested. This was because the printing trial of homopolymers in chapter 4, showed that both TBCHA and AODMBA on their own were able to print successfully with a good printing resolution of about 50 μm when the ink formula uses a 4 % initiator. However, when mixed as a co-monomer, TEGMA:AODMBA$_{50:50}$ was printable but has very poor printing resolution with the same level of initiator. Furthermore, the printed parts were also found to be extremely soft and would creep over time as shown in Figure 6.3, while TEGMA:TBCHA$_{50:50}$ was unable to form any structured layer at all.

These co-monomers would likely benefit from additional post-curing process and/ or formulation adjustments, for example, the addition of a crosslinker. In later section 6.7, the focus will look at different ways to further improve curing behaviour by adjusting formulations of TEGMA:AODMBA$_{50:50}$. The following section first looks at improving curing by first adjusting TEGMA:AODMBA ratios, crosslinker was not included here as this allow the studies to be conducted on TEGMA:AODMBA copolymer only.

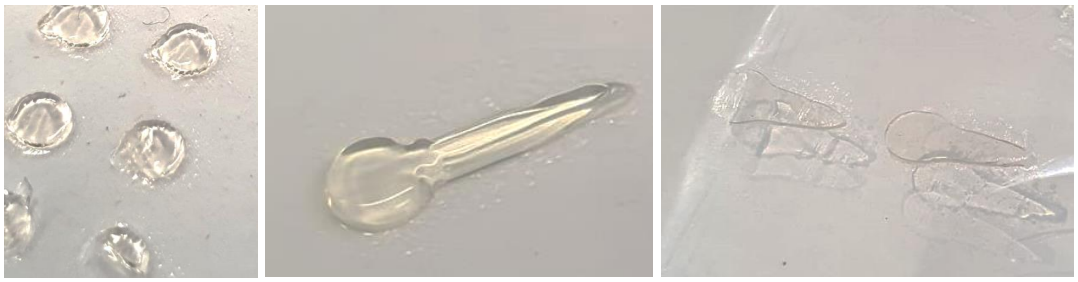


Figure 6.3: *(From Left to Right) Printed TEGMA:AODMBA$_{50:50}$ in circular disc shapes designed to be fitted into a 96-well plate, TEGMA:AODMBA$_{50:50}$ in the shape of a voice prosthesis flap, TEGMA:AODMBA$_{50:50}$ creeping after storage for few days.*

6.3 Evaluating Different TEGMA:AODMBA Ratios

The study from this point aimed to investigate only TEGMA:AODMBA copolymers as TEGMA:TBCHA$_{50:50}$ ink could not achieve a stable structured device print. The first step toward formulation modification for printing was to reconsider the TEGMA:AODMBA ratio. As the earlier HTS evaluation had only considered three co-monomer ratios of 75:25, 50:50 and 25:75. This section looked specifically at fungal anti-attachment properties and mechanical properties of different TEGMA:AODMBA ratios between 75:25 and 50:50, investigating the ratios of 30:70, 35:65, 45:55 and 40:60. These were prepared via the HTS UV curing apparatus following the HTS methodology described in chapter 4. The investigation target to define if these ratios could exhibit improved curing or increased T_g due to the greater inclusion into the co-monomer ratio of (a) the monomer known to homopolymerise well and (b) the higher T_g AODMBA. Fungal attachment assays were performed for all these copolymer ratios, and the results are shown in Figure 6.4.

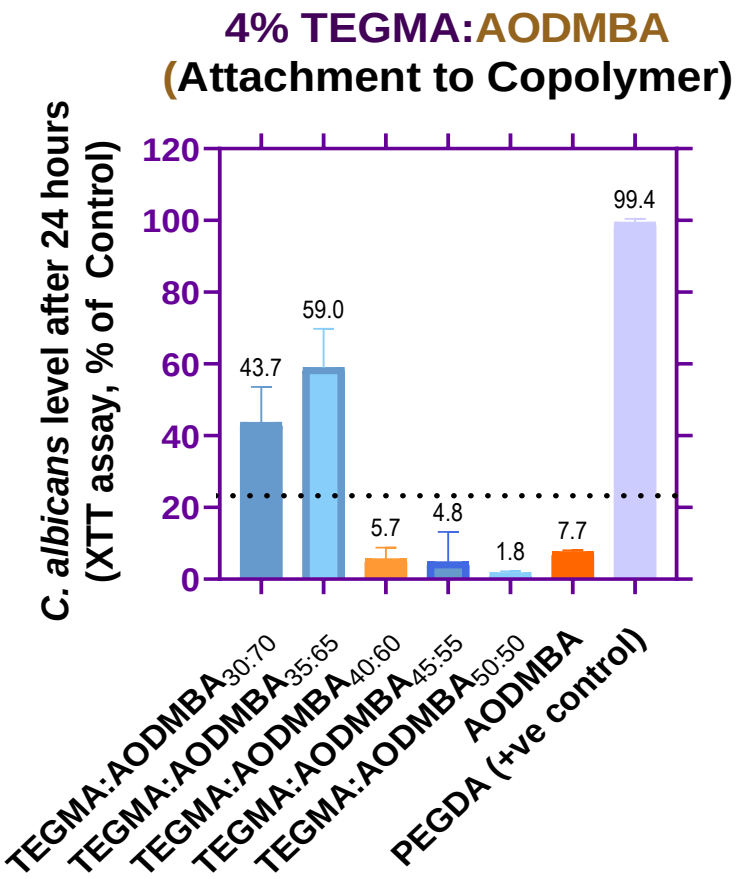


Figure 6.4: *Fungal attachment to TEGMA:AODMBA in various ratios between 30:70 to 50:50. Measurement was taken in triplicates, n =3.*

The change of ratio to 30:70 and 35:65 from 50:50 resulted in s a significant increase (p-value = 0.00) in the fungal attachment, the mean (n=3) fungal attachment at 50:50 was 1.8 % and 59.0% at the ratio of 35:65. Meanwhile, both 40:60 and 45:55 ratios were both shown to be able to retain low fungal attachment with average *C. albicans* attachment of in the range of 4.8 – 5.7 %. For comparison of inkjet printing and dip coating processing, TEGMA:AODMBA copolymers were also thermally synthesised in the ratio of 35:65, 40:60 and 50:50.

The synthesised copolymers and UV-cured copolymers were subjected to NMR and GPC analysis to evaluate the actual ratio and molecular weight of the polymers synthesised. Summary of feed ratio versus the achieved experimental copolymer ratio, polydispersity index (PDI), number average (M_n) molecular weight and weight average (M_w) molecular weight obtained from GPC analysis can be found in Table 6.1.

Table 6.1: *Summary of the GPC (results and chromatogram in Appendix 5. and Appendix 6.) and ^1H NMR data AODMBA (spectrum in Appendix 8.) measured for TEGMA:AODMBA with different ratios.*

TEGMA:AODMBA	Feed ratio	Ratio by NMR	M_n (g mol^{-1})	M_w (g mol^{-1})	PDI
Prepared via radical heat polymerisation					
35:65	35 : 65	33.6 : 66.4	41450	113900	2.75
40:60	40 : 60	38.1 : 61.9	44000	121600	2.76
50:50	50 : 50	50.2: 49.8	49930	148400	2.97
Prepared via HTS UV curing					
35:65	35 : 65	38.1 :61.9	58010	196700	3.39
40:60	40 : 60	41.5 : 58.5	58930	183400	3.11
50:50	50 : 50	51.2 : 48.8	50540	195600	3.81

The molecular weight of polymers is an important consideration as it would have an impact on the final mechanical properties. On average, GPC data shows that copolymers prepared via standalone UV curing apparatus from HTS methodology produce copolymers with higher M_n and M_w than those prepared in the laboratory via thermally driven, radical polymerisation solvent-based reaction. The HTS UV apparatus cured

TEGMA:AODMBA was found to have several smaller peaks and wider PDI results which could be due to the presence of oligomers. This is attributed to diffusion issues as the viscosity during polymerisation is higher without the presence of a solvent.

In terms of copolymer ratios, thermally synthesised copolymers had lower incorporation of TEGMA in the ratio of 35:65 and 40:60 when assessed with the ^{1}H NMR spectrum. Whereas in HTS UV-cured copolymers, TEGMA incorporation for all three tested ratios was higher than the feed ratio. While differences were observed between thermally synthesised and UV-cured copolymers, copolymer ratios obtained did not deviate too far from the feed ratio introduced. Example of the ^{1}H NMR spectrum for UV-cured and thermally synthesised TEGMA:AODMBA$_{40:60}$ can be found below in Figure 6.5 and Figure 6.6.

In chapter 5, section 5.6, the estimated T_g with TEGMA:AODMBA$_{50:50}$ was 0.1 °C. The new ratio TEGMA:AODMBA$_{40:60}$, was intended to help reduce the problem of creeping observed in the TEGMA:AODMBA$_{50:50}$. When calculated using the Flory-Fox equation this copolymer was predicted to have a higher T_g of 14.0 °C. Both the UV-cured and thermally synthesised copolymers of TEGMA:AODDMBA$_{50:50}$ and TEGMA:AODMBA$_{40:60}$ had their T_g assessed with DSC. Figure 6.7 shows the measured T_g of thermally prepared TEGMA:AODMBA$_{50:50}$ to be 3.27 °C, while Figure 6.8 below shows T_g of UV-cured TEGMA:AODMBA$_{50:50}$ to be -3.25 °C, which were of relatively close values towards the calculated prediction.

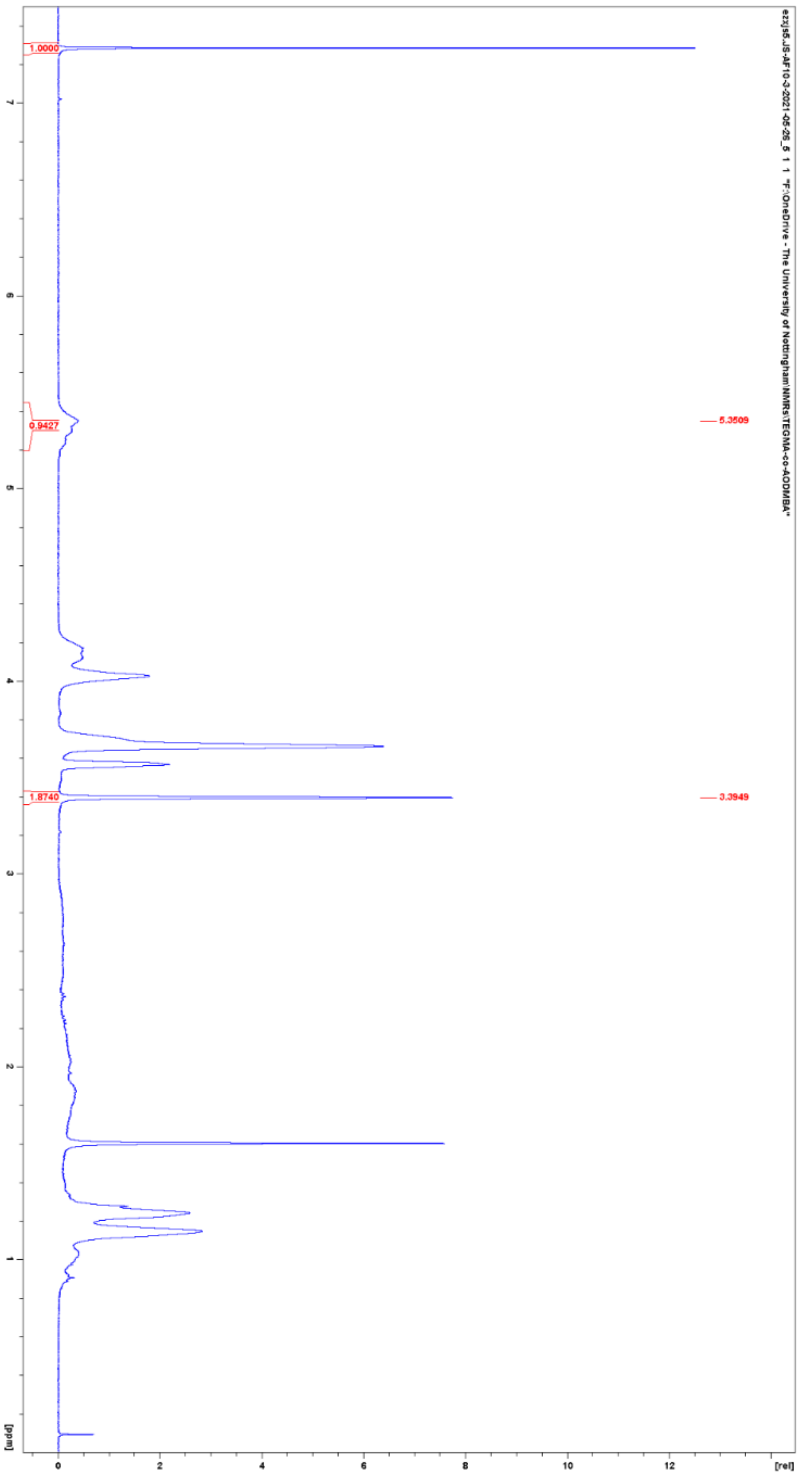


Figure 6.5: *^{1}H NMR spectrum of thermally synthesised TEGMA:AODMBA$_{40:60.}$ AODMBA 1H peak visible at 5.35 ppm and TEGMA 3H peak at 3.39 ppm.*

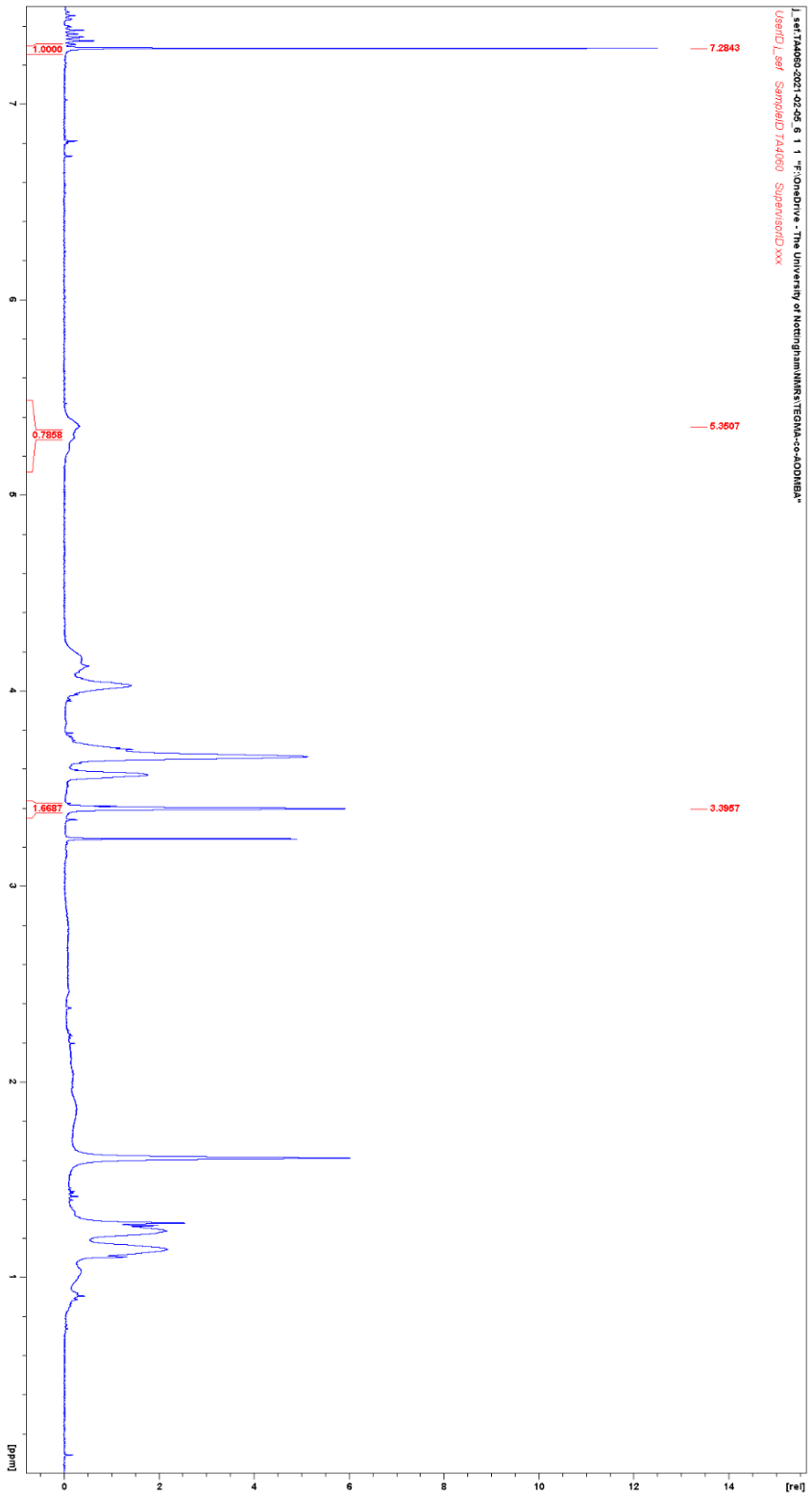


Figure 6.6: ^{1}H *NMR spectrum of HTS UV-cured TEGMA:AODMBA$_{40:60}$. AODMBA 1H peak visible at 5.35 ppm and TEGMA 3H peak at 3.39 ppm.*

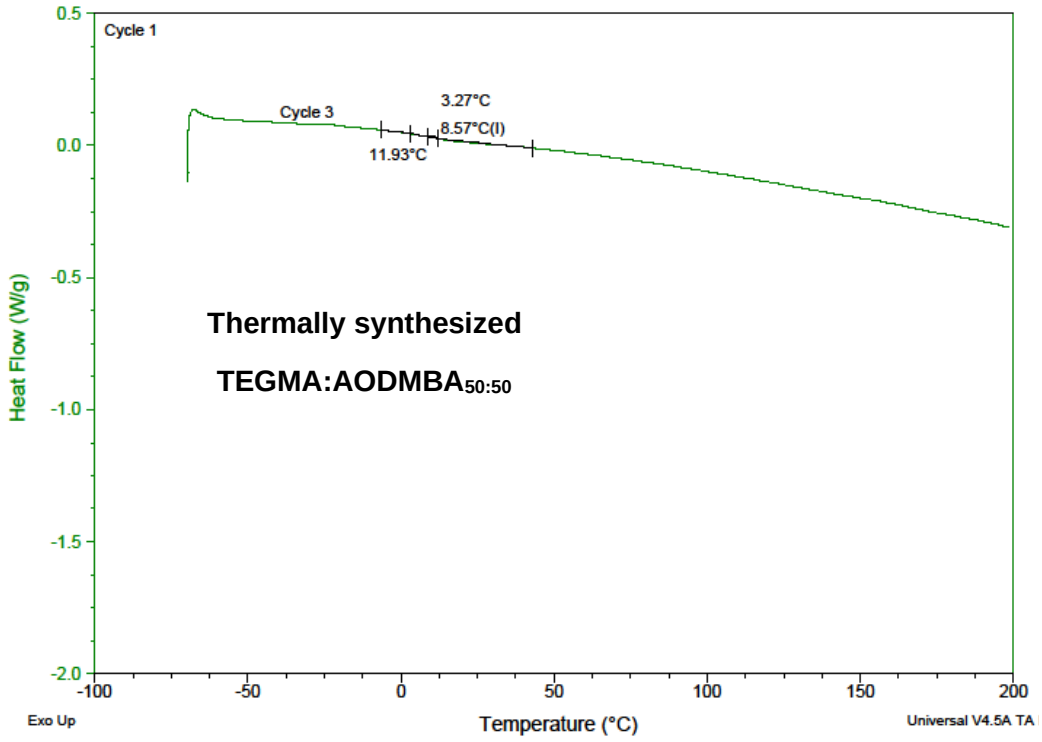


Figure 6.7: DSC of thermally synthesised TEGMA:AODMBA$_{50:50}$.

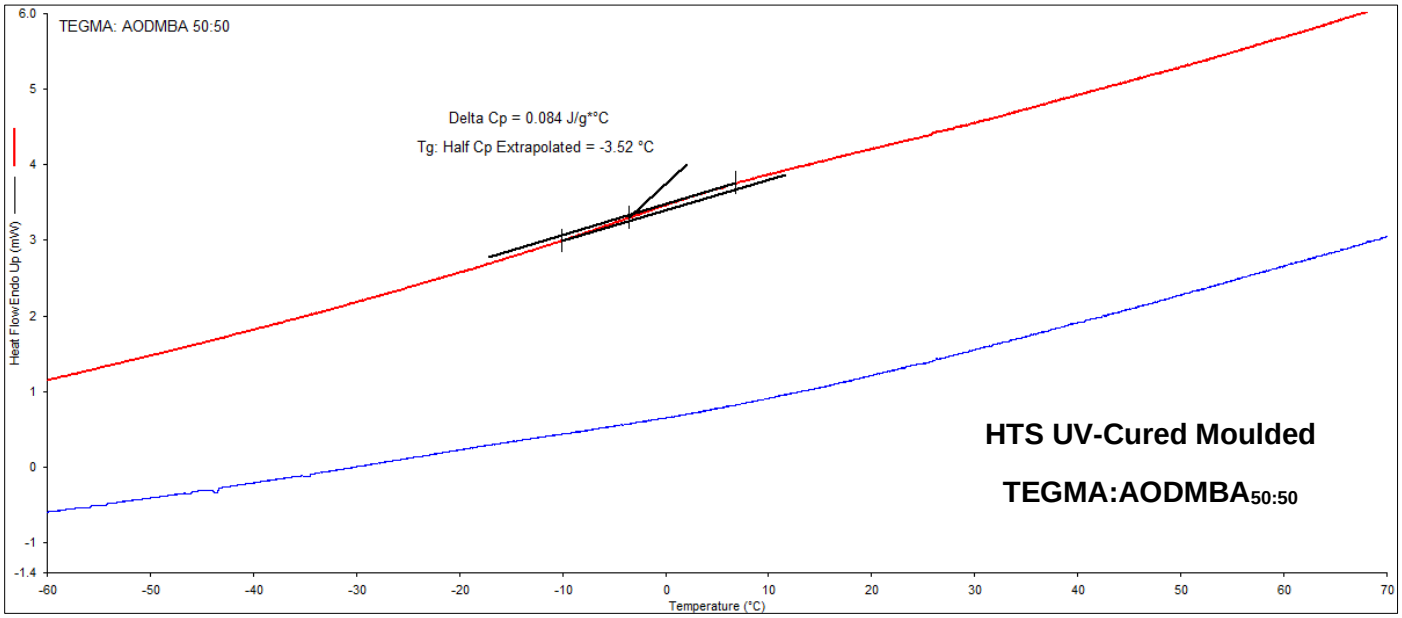


Figure 6.8: DSC of UV-cured TEGMA:AODMBA$_{50:50}$.

As for TEGMA:AODMBA$_{40:60}$, the inkjet-printed copolymer (prepared from section 6.4) had a tested T_g value of 13.6 °C (Figure 6.9) and the thermally synthesised copolymer showed a T_g of 28.4 °C (Figure 6.10). The T_g value of the inkjet-printed sample was very similar to the estimated T_g by Flory-Fox Equation. However, the thermally synthesised copolymer did not exhibit a T_g that was close to both the inkjet-printed sample and the T_g estimated by Flory-Fox Equation. The difference is likely to be a cause of the deviation in the copolymer ratio.

This was observed in the NMR measurement (data in Table 6.1) where radical polymerised copolymers often have a lower TEGMA ratio as compared to the HTS UV moulded copolymer samples. In TEGMA:AODMBA$_{40:60}$, the tested copolymer ratio was 38.1: 61.9. Since TEGMA is the co-monomer which contributes most significantly to lowering the T_g of the end copolymer and the value of thermally synthesised TEGMA:AODMBA$_{40:60}$ has a T_g closer to the T_g value of copolymer in the ratio of 35:65 instead. Calculation with Flory-Fox Equation estimates that TEGMA:AODMBA$_{35:65}$ has a T_g value of 21.4 °C. Generally, the Flory-Fox equation was shown to provide a good estimate for tested copolymers and can be used along with the HTS methodology minimising the need to test T_g for all copolymers individually in the matrix.

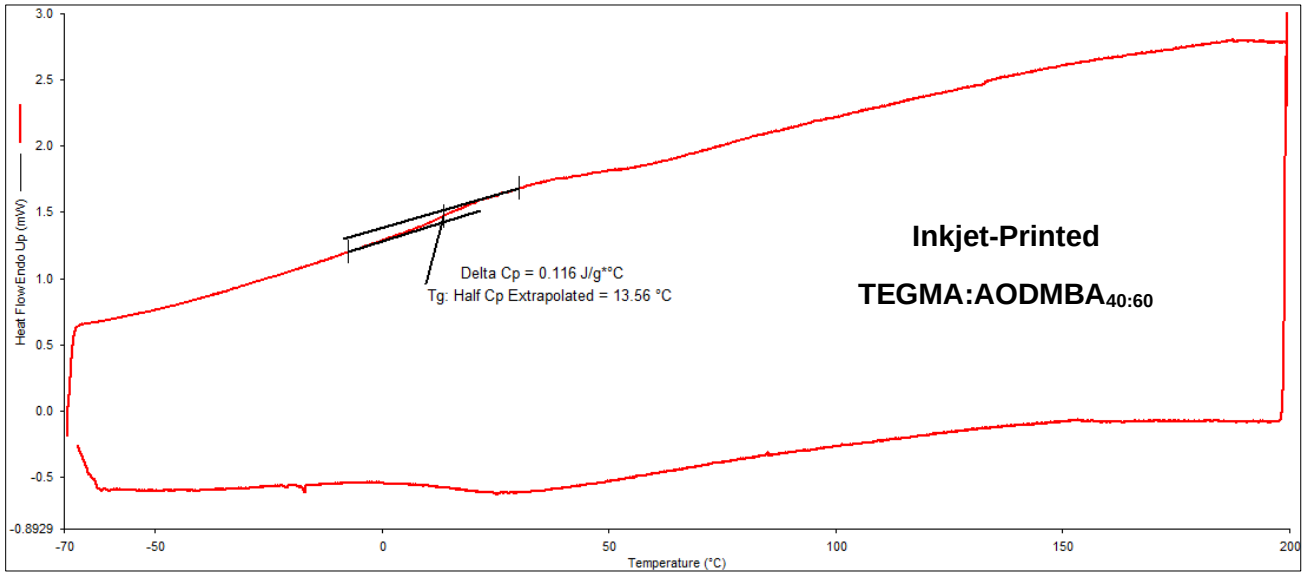


Figure 6.9: *DSC of TEGMA:AODMBA$_{40:60}$ prepared via inkjet printing.*

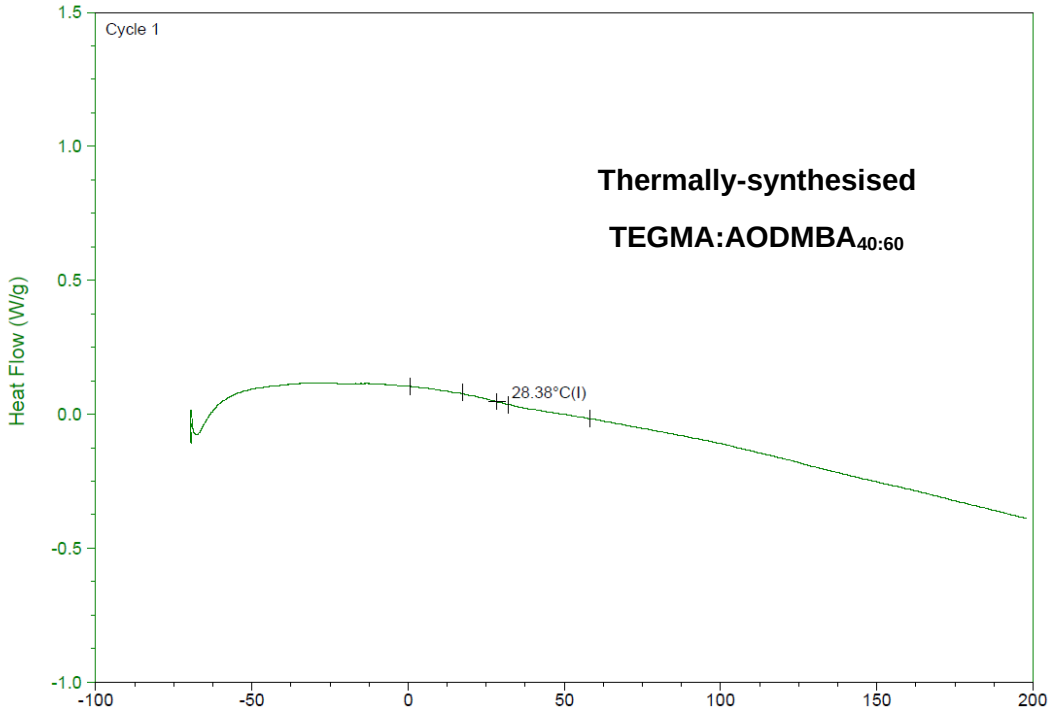


Figure 6.10: *DSC of TEGMA:AODMBA$_{40:60}$ prepared thermally via radical polymerisation.*

6.4 Processing TEGMA:AODMBA$_{40:60}$ with Inkjet Printing and Dip Coating

From the above extensive studies carried out in sections 6.2 and 6.3 TEGMA:AODMBA$_{40:60}$ was found to have continuous fungal anti-attachment within the target of < 25 %, and it also exhibited a T_g that fell into the target range for a flexible medical device. Therefore TEGMA:AODMBA$_{40:60}$ was selected as the final ratio for inkjet printing and dip coating. The thermally synthesised TEGMA:AODMBA$_{40:60}$ copolymer, as mentioned in section 6.3, was also used for the dip coating process. The dip coating process was straightforward and performed as per described in chapter 3, section 3.7, where surface texture and colour change were visually observed after silicone rubber was dip coated and dried (Figure 6.11).

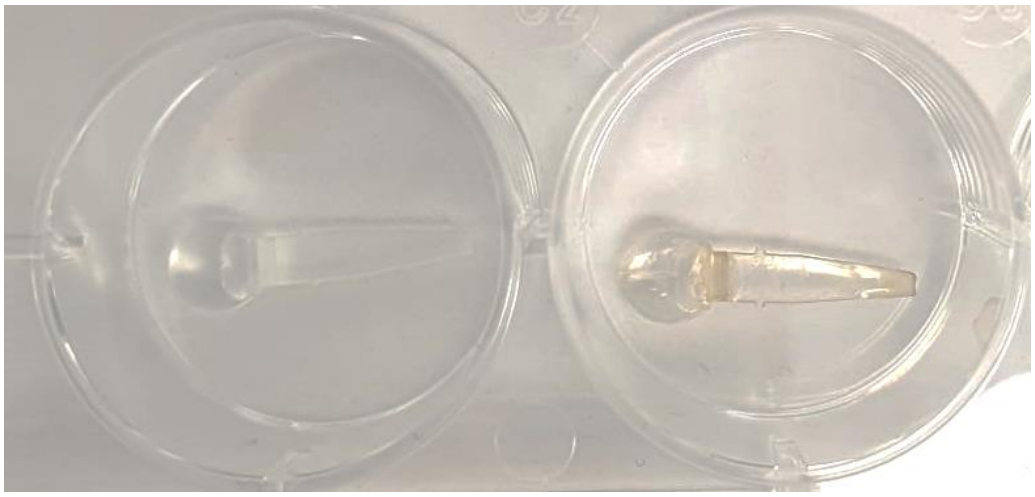


Figure 6.11: *(Left) Silicone rubber voice prosthesis flap, (Right) Dip coated voice prosthesis flap.*

The inkjet printing protocol applied in this experiment was as per the protocol described in earlier printing trials. TEGMA:AODMBA$_{40:60}$ was printable (as shown in Figure 6.12)

and had more details captured as compared to TEGMA:AODMBA$_{50:50}$ (section 6.2, Figure 6.3), a vague outline of the detail in the design of the flap can be visually observed.

Still, the printing resolution of the TEGMA:AODMBA$_{40:60}$ copolymer device was found to have less fidelity when compared to the AODMBA homopolymer. The details were not as defined and structured as seen in Figure 6.13. However, as previously stated the AODMBA homopolymer was unsuitable as it was very brittle and is not sufficiently flexible.

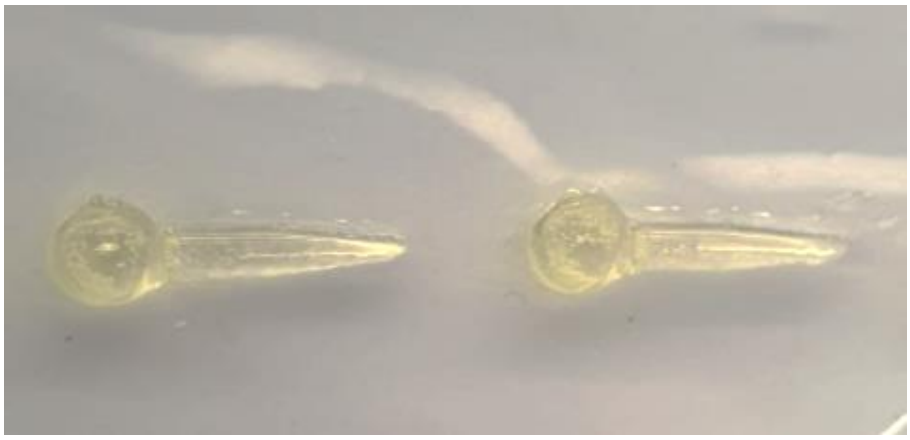


Figure 6.12: *Inkjet-printed TEGMA:AODMBA$_{40:60}$.*



Figure 6.13: *TEGMA:AODMBA$_{40:60}$ copolymer printed voice prosthesis (top sample), AODMBA homopolymer printed voice prosthesis (bottom sample).*

6.5 Fungal Anti-Attachment of Inkjet-Printed & Dip-Coated Samples

Printed TEGMA:AODMBA$_{40:60}$ was the final copolymer ratio selected for this study and therefore was subjected to another round of fungal anti-attachment. Evaluating the printed part allows us to determine if the inkjet printing process would induce additional toxicity to the final product. The printed 3 mm diameter TEGMA:AODMBA$_{40:60}$ discs were tested with *C. albicans* in a 96-well plate alongside PEGDA and AODMBA as known negative and positive controls, respectively. Both positive and negative controls were also printed layer by layer with an inkjet printing process to ensure the preparation methods were similar.

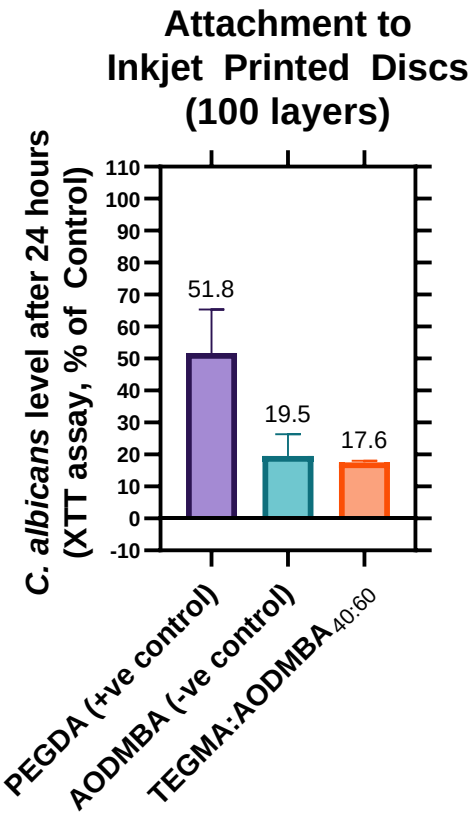


Figure 6.14: *Fungal assessment for inkjet-printed samples.*

As per Figure 6.14 above, PEGDA continues to have a high *C. albicans* attachment of 51.8 % when compared to AODMBA and TEGMA:AODMBA$_{40:60}$ which both have attachment below 25 %. The results of the *C. albicans* attachment for the printed parts are in agreement with polymers/ copolymers prepared via HTS methodology as per chapters 4 and 5.

As an attempt to evaluate the fungal attachment on the printed voice prosthesis (bigger printed part), the inkjet-printed and dip-coated voice prosthesis flap was placed in 12-well plates and crystal violet staining as per a written protocol[194] was carried out. Crystal violet is described to bind to negative charge surface molecules and polysaccharides of the cell's extracellular matrix. An advantage of this protocol is that it enables visual observation of areas with *C. albicans* attachment. Crystal violet is also lower in cost when compared to XTT. Samples included in this study were: 3D printed TEGMA:AODMBA$_{40:60}$; silicone rubber voice prosthesis flap (from Atos Chemical); silicone rubber coated voice prosthesis flap coated with TEGMA:AODMBA$_{40:60}$ copolymers and AODMBA as a negative control.

This evaluation did not generate the anticipated outcome, especially for both printed and dip-coated TEGMA:AODMBA$_{40:60}$ voice prosthesis flap. The samples with TEGMA:AODMBA$_{40:60}$ copolymer started to soften visibly, swell and deform which was likely to be due to the presence of TEGMA as TEGMA is both hydrophilic and has lower curability. From visual observation, the dye adhered all over the TEGMA:AODMBA$_{40:60}$ regardless of potential *C. albicans* attachment. Also mentioned in the actual protocol,[194] it was reported that the crystal violet evaluation was also found unsuitable for PEGDA polymer as the dye was stuck all over the PEGDA polymer even in control well that did

not contain *C. albicans* cells. Hence, this protocol may be generally unsuitable for ethylene oxide-containing polymers.

For evaluation under UV spectrophotometer for crystal violet, ethanol is required to dissolve the crystal violet attached to the tested parts which further impacts TEGMA:AODMBA$_{40:60}$ copolymer. Soaking of TEGMA:AODMBA$_{40:60}$ in ethanol to obtain colorimetric results of crystal violet further disintegrated the shape of the printed voice prosthesis leaving behind a shapeless gel after a few hours of soaking.

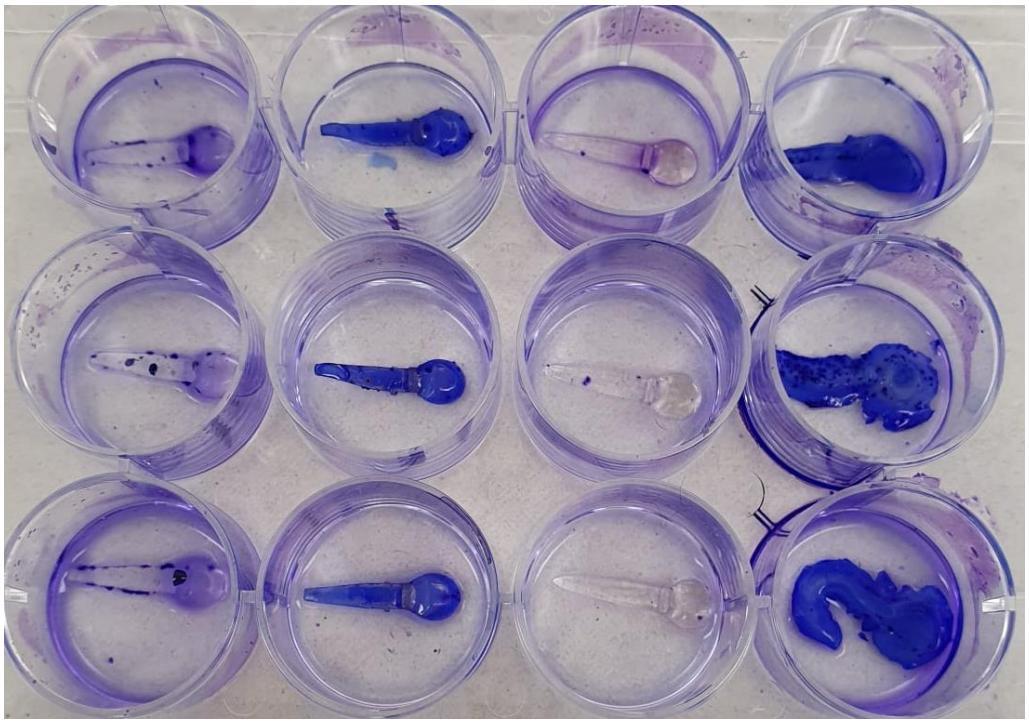


Figure 6.15: *From Left to Right – PDMS, dip-coated TEGMA:AODMBA$_{40:60}$, inkjet-printed AODMBA and inkjet-printed TEGMA:AODBMA$_{40:60}$ voice prosthesis flaps (three replicate of each material type were placed in each column).*

Table 6.2: *Raw data of fungal attachment with crystal violet tested by UV spectrophotometry at 600 nm. Values shown are OD_{600} for dissolved crystal violet. Triplicate data with mean value in the last row (highlighted in bold).*

Silicone Rubber Flap	TEGMA: AODMBA Dip-Coated Flap	AODMBA Inkjet-Printed Flap	TEGMA:AODMBA Inkjet-Printed Flap
0.51	0.42	0.40	0.83
0.54	0.53	0.33	0.77
0.70	0.49	0.30	0.96
0.59	**0.48**	**0.34**	**0.85**

The crystal violet fungal attachment studies conclude that this method was not suitable for evaluating hydrophilic type material or ethylene oxide containing polymers such as TEGMA:AODMBA$_{40:60}$. However, comparing silicone rubber flap and AODMBA printed flap, pockets of *C. albicans* were present especially at the edges of the silicone rubber voice prosthesis flaps whereas, in AODMBA, there was much lesser crystal violet attached to its surface (as per Figure 6.15). The values from the crystal violet ethanol solution to evaluate the intensity of the crystal violet shade also confirm that AODMBA has a lower value of 0.34 when compared to silicone rubber voice prosthesis flap which obtained a value of 0.59 (Table 6.2). As mentioned earlier, TEGMA:AODMBA$_{40:60}$ samples (both dip-coated and inkjet-printed) appeared to have crystal violet dye stuck and penetrating the soft swollen sample resulting in unusually high value. This is especially so for the inkjet-printed TEGMA:AODMBA$_{40:60}$ samples which were swollen and had deformed immensely.

6.6 Other Evaluations of Printed TEGMA:AODMBA$_{40:60}$

The printed TEGMA:AODMBA$_{40:60}$ was evaluated for several of its molecular/ material properties to understand if the printing process would yield material that differs from using HTS UV-cured method. As per DSC data curve shown in earlier section 6.3, the inkjet-

printed TEGMA:AODMBA has a T_g of 13.3 °C. The copolymer ratio was evaluated via both NMR and Raman analysis. Assessment of the ratio was tabulated based on methoxy group of TEGMA, which has a singlet peak and dimethyl group in AODMBA with a doublet peak as shown in Figure 6.16 (NMR of inkjet-printed TEGMA:AODMBA$_{40:60}$). The summary Table 6.3 showed that inkjet-printed copolymer ratio has the closest copolymer ratio to the feed ratio when compared to thermally synthesised and HTS UV-cured copolymers.

Table 6.3: *Comparing NMR data of TEGMA:AODMBA ratio prepared by thermally synthesised, inkjet printing and HTS UV apparatus cured.*

TEGMA:AODMBA$_{40:60}$ Copolymer	**TEGMA Ratio**	**AODMBA Ratio**
Thermally synthesised	39.85	60.15
Inkjet-Printed	41.04	58.96
HTS UV-Cured	41.45	58.55

Raman spectroscopy was also utilised to study the degree of conversion (DOC) and to determine the copolymer ratio based on surface analysis, as this is the area that will be in contact with the fungi. The CLS score was used to evaluate the copolymer ratio on the surface by comparing its intensity and the DOC of the copolymer was conducted by investigating the peak areas. The DOC valuation compares the C=C peak area which represents the presence of C=C bonds in monomers against C=O bonds found in the polymer. When compared to the HTS moulded UV-cured TEGMA:AODMBA$_{40:60}$ sample, the inkjet-printed sample generally achieves a slightly lower DOC than HTS moulded samples, as summarised in Table 6.4 below.

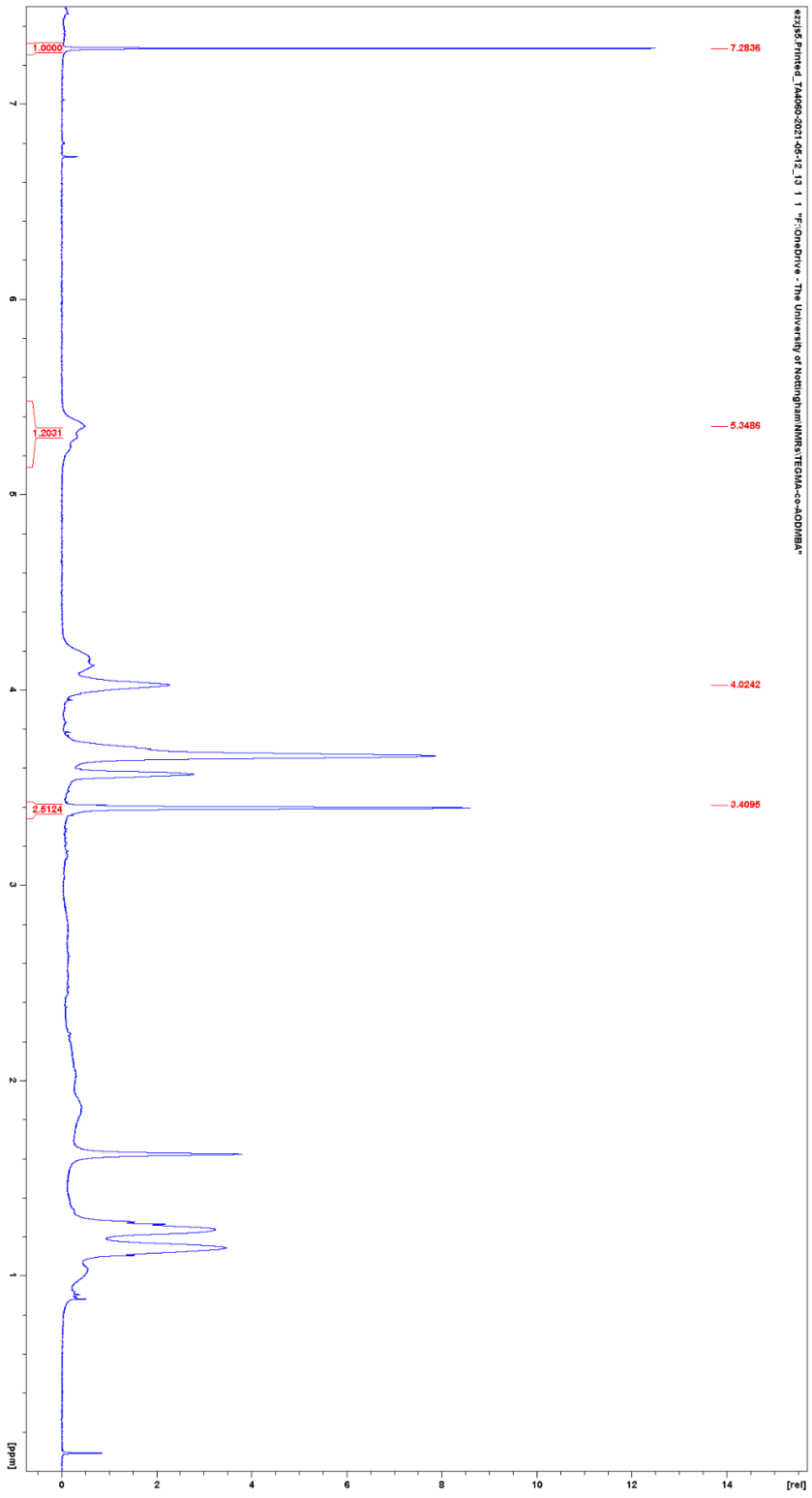


Figure 6.16: *^{1}H NMR spectrum of inkjet-printed TEGMA:AODMBA$_{40:60}$. AODMBA 1H peak visible at 5.35 ppm and TEGMA 3H peak at 3.39 ppm.*

Table 6.4: *Comparing Raman data of TEGMA:AODMBA$_{40:60}$ prepared by HTS and inkjet printing.*

TEGMA:AODMBA$_{40:60}$ Copolymer	Measured CLS Score/ %	No.	C=C Peak Area	C=O Peak Area	DOC (%)
HTS UV-Cured	38.1±0.6/ 61.9±0.6	1	0.0	28561.0	100.0
		2	0.0	38585.8	100.0
		3	0.0	41300.9	100.0
Inkjet-Printed	35.7±0.7/ 64.3±0.7	1	3427.0	30327.4	97.7
		2	5971.4	35475.1	96.6
		3	4862.3	35017.7	97.2

In the inkjet-printed samples, the C=C peak area was still visible but it was not in the HTS UV-cured samples. The average DOC of inkjet-printed sample has a DOC of 97.2 % while HTS moulded samples have 100 % DOC. The copolymer ratio of the inkjet-printed samples also was shown to have a much lower ratio of TEGMA when compared to the added feed ratio. The copolymer ratio assessed from Raman spectroscopy (ratio: 38.1:61.9) as per Table 6.4) and NMR (ratio: 41.04:58.96, as per Table 6.3) differs by a few per cent, but both results found more TEGMA incorporation in the HTS UV-cured samples than the inkjet-printed samples.

Lastly, M_n and M_w of inkjet-printed TEGMA:AODMBA$_{40:60}$ was assessed with GPC and were found to be 5218 and 33010 respectively (as per chromatogram and results shown in Figure 6.17 below). While DOC of inkjet-printed TEGMA:AODMBA$_{40:60}$ was only slightly lower (97.7 % as mentioned in Table 6.4) in Raman analysis when compared to 100 % of HTS UV-Cured TEGMA:AODMBA$_{40:60}$. Inkjet-printed sample has a much lower M_n and M_w as compared to the same copolymer prepared with thermal synthesis and HTS UV curing discussed in Table 6.1. The low molecular weight on top of the hydrophilic nature

of TEGMA would likely be the reason for the swelling and deformation seen in section 6.5 when evaluating the copolymers with crystal violet staining.

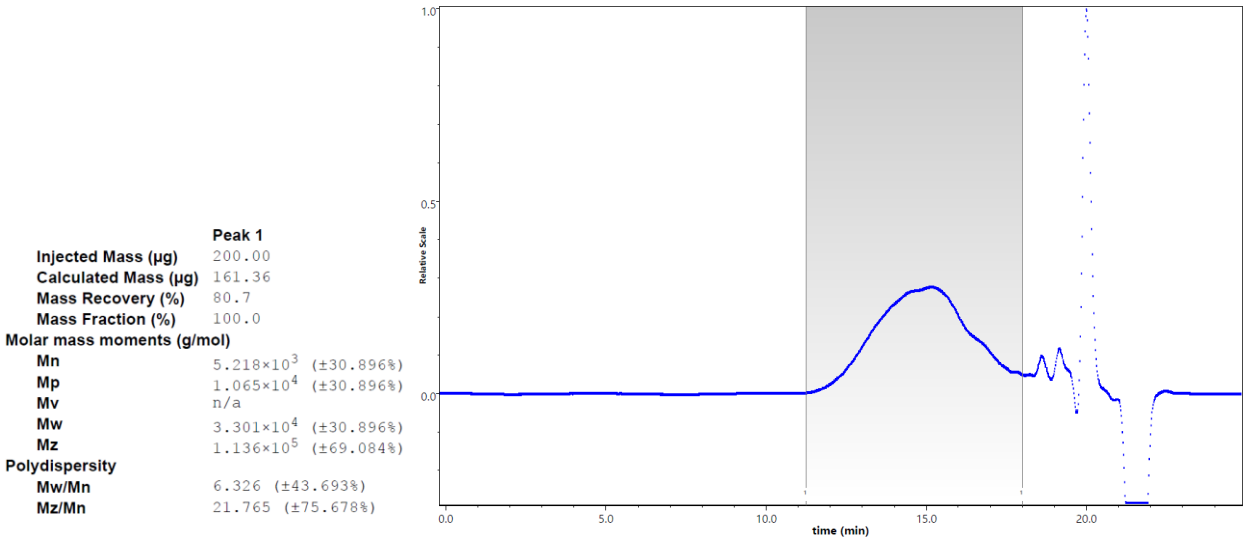


Figure 6.17: *Chromatogram and peak analysis from GPC.*

6.7 Ways to Improve Printing Resolution of TEGMA:AODMBA$_{50:50}$

The last section of this chapter investigates other potential methods to improve inkjet printing curability of TEGMA:AODMBA$_{50:50}$. As demonstrated in section 6.2, TEGMA:AODMBA$_{50:50}$ was able to be inkjet-printed but had poor resolution. The fine details present in the prepared CAD file (as per Figure 6.2 in section 6.2) show the detail of a protruding vertical line and “22.5” (The “22.5” detail mimics an actual voice prosthesis flap which refers to the diameter size of the medical device) was not visible as the TEGMA:AODMBA$_{50:50}$ ink exhibited low reactivity. “22.5” detail was used as a gauge for resolution as Dimatix printer requires slicing of CAD file into a Bitmap (BMP) for every printed layer. Hence, it would be relatively tedious to prepare various geometrical prints to evaluate the resolution. The printed TEGMA:AODMBA$_{50:50}$ copolymer was also

observed to creep after a few days of storage (Figure 6.18), which was also due to the low curing and molecular weight

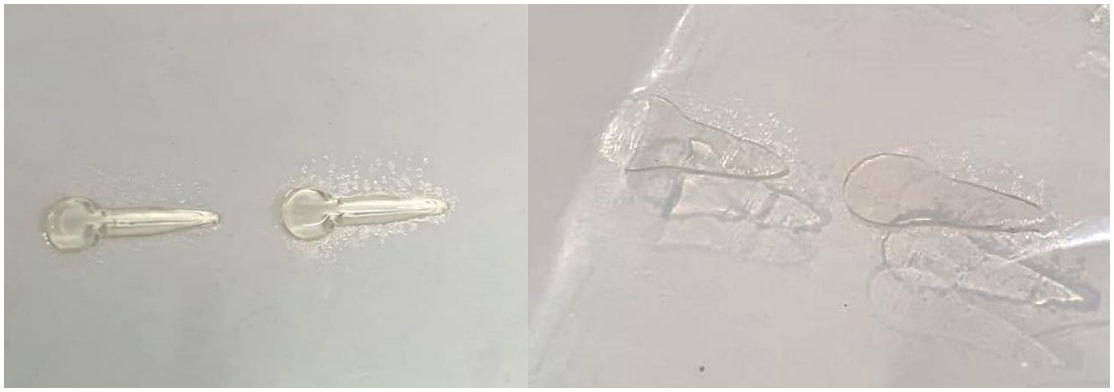


Figure 6.18: *TEGMA:AODMBA$_{50:50}$, (Left) after removing the printed sample from the printer. (Right) after samples were stored for a few days.*

In comparison, AODMBA ink had good printing resolution on its own and was able to capture the details incorporated into the voice prosthesis flap design file as shown in Figure 6.19 (Left). The improvement made on ratio adjustment of TEGMA:AODMBA in section 6.3 and section 6.4 resulted in TEGMA:AODMBA$_{40:60}$. TEGMA:AODMBA$_{40:60}$ remains flexible and managed to capture some vague detail as seen in Figure 6.19 (Right image).

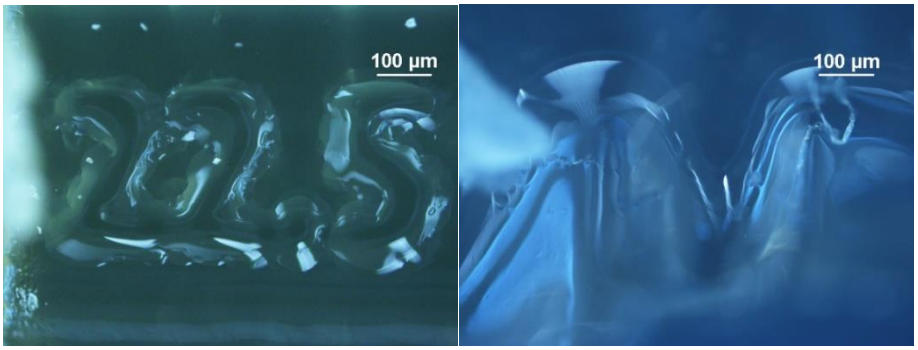


Figure 6.19: *(Left) "22.5" detail on the AODMBA printed voice prosthesis flap, (Right) Vague "22.5" detail on the TEGMA:AODMBA$_{40:60}$ printed voice prosthesis flap.*

In this section three other possible ways to adjust TEGMA:AODMBA$_{50:50}$ co-monomer formulation to achieve improvement in inkjet printing resolution were explored. The key methods (as summarised in Figure 6.20) that could improve curability include – increasing initiator per cent, using TEGMA oligomers in replacement of TEGMA monomers, and consideration of methacrylate-based TEGMA with acrylate equivalent alternatives and inclusion of additives such as hyperbranched polymer to improve reactivity and introduce crosslinking.

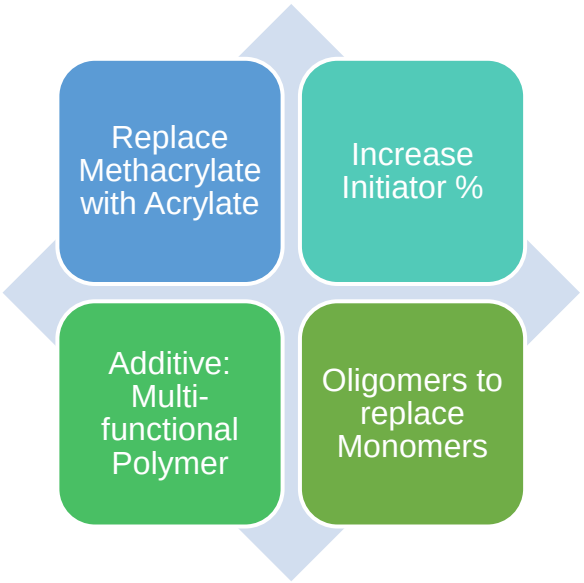


Figure 6.20: *Potential ways to improve the reactivity of TEGMA:AODMBA$_{50:50}$.*

Since the initiator percentage had already been increased from 1 % to 4 % in prior chapters 4 and 5. It was decided that this would not be considered in this chapter. Further increase in initiator concentration could result in the formation of shorter polymeric chains, adversely affecting its mechanical properties.[2]

6.7.1 Usage of TEGMA Oligomers

As TEGMA monomer was believed to be the key reason for these ink formulations' slow and low curability, the use of oligomers was investigated. Oligomers are very small polymers which have only a few repeating units of TEGMA making up their backbone chains. Thus, as they are already polymerised, it was postulated that they could help to mitigate this concern by reducing the amount of polymerisation that has to be done to cure the resin and overcoming oxygen inhibition. However, it was necessary to ensure a balance between incorporating sufficient TEGMA oligomers to ensure improved curing and also achieving a viscosity that the inkjet printing process can process.

TEGMA oligomer was prepared via radical polymerisation using CCTP agent to control the degree of polymerisation. The TEGMA oligomers produced were subjected to GPC analysis to evaluate their molecular weight and polydispersity index (PDI), and the results obtained were that it exhibited an M_n of 1234, M_w of 3242 and PDI of 2.63 (GPC results and chromatogram in Appendix 5.8 and 6.8). The oligomer was then used as a direct replacement of TEGMA monomers in the formulation and the ink was prepared as per the method mentioned in chapter 3, subsection 3.5.1.

Using the protruding vertical part and “22.5” on the voice prosthesis flap design as a benchmark again (discussed earlier in section 2.7 when comparing AODMBA and TEGMA:AODMBA inks). It was found that the resolution of the printed structure using the formulated $TEGMA_{(oligomer)}$:$AODMBA_{50:50}$ ink showed very minimal improvement compared to the direct use of TEGMA monomer. Visual observation using an optical microscope with five times magnification (Figure 6.21), did highlight some details that were loosely formed with the utilisation of oligomers unlike TEGMA:$AODMBA_{50:50}$ which

had presented a flat surface (see Figure 6.18) with no details. More trials with different TEGMA oligomer chain lengths can be considered in future work to make further improvements in the printing resolution.

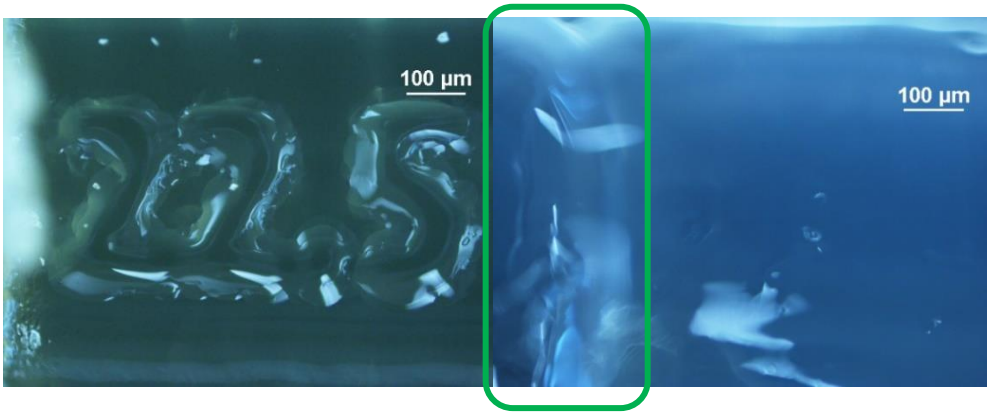


Figure 6.21: *(Left) AODMBA with good printing resolution as a comparison. (Right) $TEGMA_{(oligomer)}$:$AODMBA_{50:50}$ showed little improvement, a vertical protruding design was captured unlike $TEGMA_{(monomer)}$:$AODMBA_{50:50}$.*

6.7.2 Hyperbranched Polymer as Additives

The addition of polymers with multi-functional groups would also potentially improve curability. Hyperbranched polymers (HBP) are highly branched polymers with three-dimensional structures (as shown in Figure 6.22 below), the structures of which differ greatly from the typical linear polymeric chain. One of the key benefits of HBP is their ability to introduce a large number of functional groups while maintaining low viscosity in the final ink. The viscosity can be kept low due to its globular structure which does not result in a higher degree of entanglement of the polymeric chains that were usually found in linear polymers of similar molecular weight.

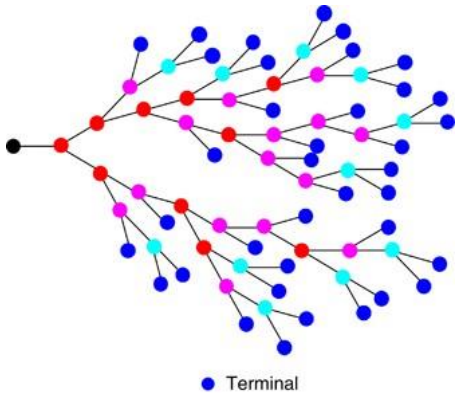


Figure 6.22: *Schematic of hyperbranched polymer.*[209]

For this work, tripropylene glycol diacrylate (TPGDA) was synthesised in one pot synthesis under inert argon conditions as described in chapter 3, subsection 3.6.3 (NMR showing synthesis kinetic in Appendix 8.3). TPGDA was chosen as the monomer because two functional (polymerisable) groups would further enhance its curability. The synthesised HBP TPGDA exhibited GPC data of M_n of 70000, M_w 203000 and PDI 2.87.

TEGMA:AODMBA$_{50:50}$ co-monomer ink was prepared as per protocol mentioned in chapter 3, section 3.5.1 and 10 % w/v of TPGDA was added to the ink before purging the ink under N_2 gas for five minutes. The voice prosthesis flap design was again printed to assess its resolution. Figure 6.23 shows the product of the printed part and Figure 6.24, focuses on visually inspecting the “22.5” details similar to what was discussed in section 2.7 and evaluated in section 2.7.1.



Figure 6.23: *Voice prosthesis flap of TEGMA:AODMBA$_{50:50}$ with 10 % HBP TPGDA.*

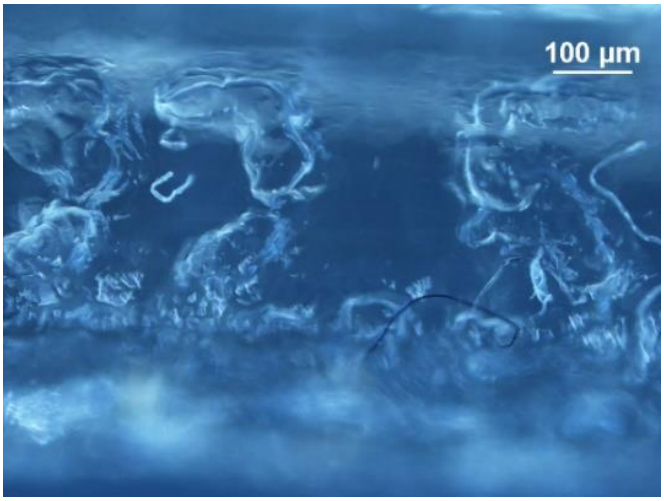


Figure 6.24: *Printing resolution of detail "22.5" in formulation with HPB-TPGDA as additive.*

The printed part exhibited better resolution with the addition of 10 % HBP-TPGDA. However, as the exact printing parameters used to print TEGMA:AODMBA$_{50:50}$ formulation was used to print this new formulation, the inconsistent rough finishing suggests that there were some challenges in jetting after the inclusion of the HPB-TPGDA. This is likely to be related to an increase in viscosity. Thus, further adjustment of the printing parameter will be required to allow for the change in formulation created by adding

the HBP-TPGDA. For example, parameters such as increasing cartridge temperature may be able to help with allowing a smoother ink jetting process for future work. It also showed that the addition of a cross-linker aids in improving the resolution of the final printed structures.

6.7.3 Use of Acrylate Monomers

Lastly, methacrylate is known to exhibit a slower curing process as discussed in the earlier chapters. Another method that could improve the printing resolution was to replace the TEGMA monomer with an acrylate of a similar structure. As no acrylate of TEGMA was directly available, the nearest alternative available was the acrylate version similar to the structure of DEGMA. This was because DEGMA:AODMBA$_{50:50}$ was also found to be one of the fungal-resistant copolymers in chapter 5, section 5.3, Table 5.3. Di(ethylene glycol) ethyl ether acrylate (DEGEEA) as shown in Figure 6.25 below has a similar chemical structure to DEGMA.

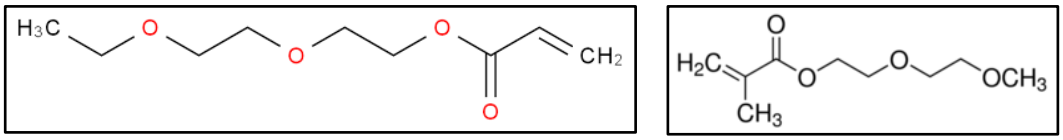


Figure 6.25: *(Left) DEGEEA chemical structure, (Right) DEGMA chemical structure.*

A prepared ink of DEGEEA:AODMBA$_{50:50}$ was assessed for inkjet printing of 3 mm disc shape used for insertion into a 96-well plate. AODMBA homopolymer (Left in Figure 6.26) printed disc structure was defined in its circular shape and had clear fine line resolution created from the printing direction of the inkjet-printed. In TEGMA:AODMBA$_{50:50}$ (Middle image in 6.26), the printed parts were soft and were slightly distorted due to their low T_g and poor curing leading to a creep-like effect. Lastly, in DEGEEA:AODMBA$_{50:50}$ (as per

the right picture in Figure 6.26), the printed part regains its disc shape definition and did not have creep and distortion seen in TEGMA:AODMBA$_{50:50}$.

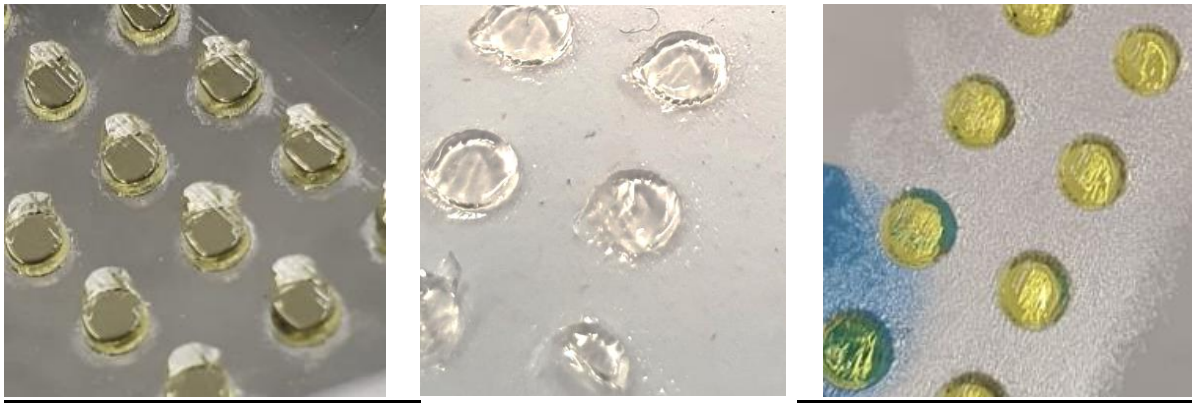


Figure 6.26: *(Left) AODMBA homopolymer printed, (Middle)TEGMA:AODMBA$_{50:50}$ and (Right) DEGEEA:AODMBA$_{50:50}$ inkjet-printed.*

However, due to time limitations, there was insufficient time to fully evaluate this potential formula further for its actual T_g, its fungal anti-attachment ability, and printability in a voice prosthesis flap as per the other formulations demonstrated above. The copolymer would also have to undergo a thorough evaluation with NMR, FTIR and GPC for a full understanding of its molecular and mechanical properties.

6.8 Summary

Chapter 6 focuses on the printing and development of the formulation for a fungal-resistant copolymer to be demonstrated for printing and application of flexible voice prosthesis flap. The initial chosen TEGMA:AODMBA$_{50:50}$ and TEGMA:TBCHA$_{50:50}$ selected from chapter 5 were put into trial prints. Between the two co-monomers, TEGMA:AODMBA$_{50:50}$ was shown to have better curability when processed using the inkjet printer. As a result, the most significant level of printing was conducted using

TEGMA:AODMBA$_{50:50}$ co-monomer and had its formulation modified to improve curability in the remaining sections of chapter 6.

TEGMA:AODMBA$_{40:60}$ was adjusted from TEGMA:AODMBA$_{50:50}$ as it improves the printing resolution and did not have creep issue found in TEGMA:AODMBA$_{50:50}$. Copolymer in the same ratio was also prepared via thermal polymerisation and applied as a coating on silicone rubber voice prosthesis flap. Fungal assessment with XTT assay found consistent results to demonstrate that printed TEGMA:AODMBA$_{40:60}$ have fungal attachment below 25 %. However, crystal violet staining assessment to evaluate both printed and dip coated TEGMA:AODMBA$_{40:60}$ voice prosthesis flap did not work out well for the polymers as the copolymer deform in the presence of ethanol used for the evaluation and also adhere to more dye than expected with polymer swelling and deformation.

Lastly, a demonstration of different methods to improve inkjet curability for TEGMA:AODMBA$_{50:50}$ was shown, and good resolution improvement was achieved with the 10 % addition of HBP-TPGDA as an additive and replacing of methacrylate with similarly structured acrylate. However, due to time limitations, further testing of these formulations was not possible for this thesis chapter and these formulations require more studies and trials to find their optimal performance. Chapter 6 summarises the key methods and challenges in balancing a 3D printing formulation to achieve both its printability while retaining its fungal resistance. The work in this chapter will lay the groundwork for future studies when developing fungal-resistant 3D printing formulations for flexible medical devices.

Chapter 7: Conclusion & Future Work

7.1 Conclusion

The thesis began with several aims and objectives. The key aim was to “develop novel bio-functional materials that exhibit *C. albicans* anti-attachment behaviour. These materials can potentially be used in AM formulation, or they can also be applied directly as an antifouling coating on biomedical devices using dip coating process”. The work done had met the targets and has also achieved several milestones as documented in the different chapters.

HTS methodology developed for fungal anti-attachment polymers was able to evaluate several monomers/ polymers in a shorter amount of time in comparison to testing the monomers/ polymers individually. The evaluation aims to find out a few crucial properties that are important for the key objective of this thesis including fungal anti-attachment, polymer toxicity, degree of conversion (DOC), curability, viscosity, surface tension and printability (Z parameter) for inkjet printing.

Through the work described in chapter 4, I was able to correlate a preliminary regression model with an R^2 value of 82 % on the DOC of the HTS curing method when compared to the DOC of the inkjet-printed materials. This demonstrates that the fast UV curing setup (that allows the curing of 96 polymers in 5 minutes) could replicate the DOC achieved by inkjet printing. However, to achieve a more accurate prediction on curability in the inkjet printer, more samples should be evaluated, and future considerations should also study

T_g, type/ number of functional groups in monomers. Otherwise, the HTS methodology could also quickly evaluate and prepare monomers/ polymers to identify their fungal resistance. Using the HTS, TBCHA and TBCHMA on top of AODMBA were identified as printable, curable and fungal-resistant potential homopolymers to work with.

The following chapter 5 of the work look at applying this HTS methodology to a large library of copolymers consisting of fungal anti-attachment monomers/ polymers that met the target in earlier chapter 4. A total of 30 co-monomer/ copolymer types were rapidly mixed and prepared with this HTS methodology. While the initial hypothesis was that since many of these homopolymers themselves had fungal resistance ability, therefore the same should be the case for copolymers prepared with them.

However, this hypothesis was found to be untrue, the combination of monomers led to changes in the fungal resistance ability. New phenomena were observed with the co-monomers/ copolymers prepared, most of the copolymers only have better fungal resistance when they consist of at least 50 % of TEGMA/ DEGMA incorporated into the copolymer. Out of the 30 copolymers tested for fungal resistance, 19 of them were found to have fungal anti-attachment performance within the targeted range of < 25 %. The T_g of the individual homopolymers were tested and for copolymers, they were predicted with Flory-Fox Equation as another quick high throughput way of estimating T_g for 30 copolymers.

On top of polymer toxicity, in chapter 5, residue toxicity on fungi was also considered. In a nutshell, secondary polymer types were found to have a significant impact on the overall toxicity of the copolymer. This suggests that the copolymers have a slight killing effect on

the fungi on top of its anti-attachment ability. To achieve the minimal killing effect of fungi, the removal of the residue process has to be studied more in-depth for future work.

The work in the last result chapter, chapter 6 was to apply the materials found in earlier chapters and to prepare a fungal anti-attachment flexible medical device with T_g of -10 to 15 °C. The two selected copolymers from chapter 5 were TEGMA:AODMBA$_{50:50}$ and TEGMA:TBCHA$_{50:50}$. While both copolymers showed relatively poor curability, TEGMA:AODMBA$_{50:50}$ could still be printed with inkjet printing while TEGMA:TBCHA was unable to form stable layers. Therefore, TEGMA:AODMBA$_{50:50}$ was selected for further evaluation and had its formulation finetuned.

Formulation improvements were made via adjusting the ratio of copolymer to reach an optimal ratio of TEGMA:AODMBA$_{40:60}$ which was able to meet targeted T_g and also targeted fungal resistance to *C. albicans*. TEGMA:AODMBA$_{40:60}$ was inkjet-printed and also thermally synthesised to assess if a different process was also considered and if it may have any impact on its fungal resistance performance. The fungal assessment for inkjet-printed TEGMA:AODMBA$_{40:60}$ continue to show it has fungal resistance ability. However, in the fungal attachment study for voice prosthesis flap prepared with both dip-coated thermally-polymerised TEGMA:AODMBA$_{40:60}$ and inkjet-printed TEGMA:AODMBA$_{40:60}$, the crystal violet staining assessment did not work out well for the copolymer. TEGMA:AODMBA$_{40:60}$ swell and turned soft upon contact with crystal violet solution and ethanol. Future work would have to consider other ways of evaluating fungal attachment, especially for such hydrophilic and ethylene oxide-containing polymers.

Lastly, the chapter also discussed the different possible ways that may be effective in improving printing resolution and curability of TEGMA:AODMBA$_{50:50}$ apart from adjusting its ratio. The key methods considered included hyperbranched polymer as an additive, finding better curing acrylate with a similar structure of TEGMA/ DEGMA and also utilisation of TEGMA oligomers instead of monomers. The addition of hyperbranched polymer and alternative acrylate for DEGMA proves to show significant improvement in the printing solution. However, more work will have to be performed to evaluate again the T_g and fungal resistance of these new formulations.

7.2 Recommendation for Future Work

There are several rooms for improvement to this work and also many possibilities of future work to further derive a copolymer that can be printed and meet all the targets of a flexible fungal-resistant copolymer.

The following suggestions below are steps that can further improve this research work:

- A more thorough residue removal step is to be considered to minimise the impact of the residual monomers and oligomers on fungal toxicity.
- A regression model developed to evaluate DOC of HTS UV prepared polymer over inkjet-printed polymer would be even more useful, should it be able to incorporate prediction of the impact of T_g, initiator concentration and functional groups on inkjet printing.
- The use of a micro/ ultrasensitive DSC system could allow for a more prominent and accurate T_g measurement for the polymers/ copolymers.

- A more suitable method for fungal attachment studies for a larger part (voice prosthesis flap) should be considered, i.e., scale up XTT assay instead of switching to crystal violet studies.
- A complementary technique to XTT assay would be beneficial for confirming the XTT results, leveraging the tagged fluorescence (CAF2-yCherry) of *C. albicans* used in this work, microscopy can visually confirm the presence of *C. albicans*.
- Post-processing steps for inkjet-printed parts to improve the curability and stability of the copolymer can be studied. Processes such as further exposure of part to UV curing would be required to improve the long-term stability of the printed medical voice prosthesis flap.
- New formulations developed to improve the curability of TEGMA:AODMBA$_{50:50}$ in chapter 6 should undergo again fungal anti-attachment evaluation, toxicity test and T_g evaluation to assess if it is still suitable for fungal anti-attachment medical device application.

In the longer term, the following areas can be investigated for future work:

- Clinical *C. albicans* strain can also be used to confirm if the anti-attachment properties of polymers would be similar to the actual clinical strain.
- Formulations were only tested on fungal toxicity, derived formulations should be evaluated for mammal toxicity in vitro and in vivo.
- As many medical devices would be susceptible to both fungal and bacteria attachment. Other species of common microorganisms that could attach to the

medical device together with *C. albicans* should also be evaluated, such as bacteria *P. aeruginosa* and *S. aureus*.

- With the above consideration of different microorganism species, often biofilm will have multispecies organism biofilm which is difficult to remove. The antimicrobial formulation should then be designed and evaluated to work on such multispecies biofilms.
- The key mechanism on why some polymers have reduced fungal attachments compared to others was not fully understood in this work. Further evaluation such as studying the behaviour of *C. albicans* on these polymers could help us to reverse engineer the reason why *C. albicans* prefer attachment to certain polymers and not others.
- The inkjet printer used in this work is small scale and has only one print head, further work leading to commercialising this fungal anti-attachment formulation could consider a larger and more sophisticated inkjet printing system.
- The development of a robust UV ink formulation for flexible medical devices that can work on both material jetting and SLA processes would be attractive to the biomedical industry.

References

1. Tofail, S. A. M. *et al.* Additive manufacturing: scientific and technological challenges, market uptake and opportunities. *Mater. Today* **21**, 22–37 (2018).
2. Singh, S. & Ramakrishna, S. Biomedical applications of additive manufacturing: Present and future. *Curr. Opin. Biomed. Eng.* **2**, 105–115 (2017).
3. Beg, S. *et al.* 3D printing for drug delivery and biomedical applications. *Drug Discov. Today* **25**, 1668–1681 (2020).
4. Kumar, R., Kumar, M. & Chohan, J. S. The role of additive manufacturing for biomedical applications: A critical review. *J. Manuf. Process.* **64**, 828–850 (2021).
5. Javaid, M. & Haleem, A. Additive manufacturing applications in medical cases: A literature based review. *Alexandria J. Med.* **54**, 411–422 (2018).
6. Bongomin, F., Gago, S., Oladele, R. O. & Denning, D. W. Global and multi-national prevalence of fungal diseases—estimate precision. *J. Fungi* **3**, (2017).
7. Shoham, S. Invasive candidiasis in patients with implants. *Curr. Fungal Infect. Rep.* **5**, 12–17 (2011).
8. Nobile, C. J. & Johnson, A. D. Candida albicans Biofilm and Human Disease. *Annu. Rev. Microbiol.* **69**, 71–92 (2016).
9. Kojic, E. M. & Darouiche, R. O. Candida Infections of Medical Devices. *Clin. Microbiol. Rev.* **17**, 255–267 (2004).
10. González-Henríquez, C. M., Sarabia-Vallejos, M. A. & Hernandez, J. R. Antimicrobial polymers for additive manufacturing. *Int. J. Mol. Sci.* **20**, (2019).
11. Geneva: World Health Organization. *WHO global model regulatory framework for medical devices including in vitro diagnostic medical devices. WHO Medical device technical series. Licence: CC BY-NC-SA 3.0 IGO.* (2017).
12. Stethoscope. https://www.littmann.com/3M/en_US/littmann-stethoscopes/products/~/3M-Littmann-Master-Classic-II-Stethoscope/?N=5932256+8711017+3293188501+3294857497&preselect=8727096+3293786499&rt=rud.
13. Surgical Gloves. https://www.fishersci.com/shop/products/cardinal-health-protexis-micro-latex-surgical-gloves-classic-size-8/19163114.
14. Neonatal Incubator. https://www.phoenixmedicalsystems.com/infant-care/incubators/neonatal-intensive-care-incubator-inc-200/.
15. Cardiac Pacemaker. https://www.dicardiology.com/article/new-pacemaker-technologies.
16. Population, D. of E. and S. A. *Social and family characteristics associated with elder abuse in Pasto, Colombia 2016*. *World Population Ageing 2015* vol. 12 (2019).
17. Stirling, C., Kapadia, A., Heuvel, R. van de & Zhou, J. Medical devices in 2030 – being part of the solution. *KPMG Int.* 1–25 (2018).
18. Darouiche, R. O. Device-Associated Infections: A Macroproblem that Starts with Microadherence. *Clin. Infect. Dis.* **33**, 1567–1572 (2001).

19. Deorukhkar, S. C. & Saini, S. Medical Device-Associated Candida Infections in a Rural Tertiary Care Teaching Hospital of India. *Interdiscip. Perspect. Infect. Dis.* **2016**, (2016).

20. *Stop neglecting fungi*. *Nature Microbiology* vol. 2 https://doi.org/10.1038/nmicrobiol.2017.120 (2017).

21. Rodrigues, M. L. & Nosanchuk, J. D. Fungal diseases as neglected pathogens: A wake-up call to public health officials. *PLoS Negl. Trop. Dis.* **14**, 1–9 (2020).

22. Fausto, A., Rodrigues, M. L. & Coelho, C. The still underestimated problem of fungal diseases worldwide. *Front. Microbiol.* **10**, 1–5 (2019).

23. Chu, V. H. *et al.* Staphylococcus aureus bacteremia in patients with prosthetic devices: Costs and outcomes. *Am. J. Med.* **118**, 1416.e19-1416.e24 (2005).

24. Darouiche, R. O. Treatment of infections associated with surgical implants. *N. Engl. J. Med.* **350**, 1422–1429 (2004).

25. Davis C. P. *Medical Microbiology*.

26. Vinh, D. C. & Embil, J. M. Device-Related Infections : A Review. **15**, 467–488 (2005).

27. Rimondini, L., Fini, M. & Giardino, R. The microbial infection of biomaterials: A challenge for clinicians and researchers. A short review. *J. Appl. Biomater. Biomech.* **3**, 1–10 (2005).

28. Bardell, D. The roles of the sense of taste and clean teeth in the discovery of bacteria by Antoni van Leeuwenhoek. *Microbiol. Rev.* **47**, 121–126 (1983).

29. Percival, S. L., Thomas, J. G. & Williams, D. W. *Microbiology of Wounds*. (2010).

30. Laverty, G., Gorman, S. P. & Gilmore, B. F. *Biofilms and implant-associated infections*. *Biomaterials and Medical Device - Associated Infections* (Woodhead Publishing Limited, 2015). doi:10.1533/9780857097224.1.19.

31. Elek, S. D. & Conen, P. E. The virulence of staphylococcus pyogenes for man. *Br. J. Exp. Pathol.* **38**, 573–586 (1957).

32. Totu, E. E., Nechifor, A. C., Nechifor, G., Aboul-Enein, H. Y. & Cristache, C. M. Poly(methyl methacrylate) with TiO2 nanoparticles inclusion for stereolitographic complete denture manufacturing − the fututre in dental care for elderly edentulous patients? *J. Dent.* **59**, 68–77 (2017).

33. Nagrath, M. *et al.* Functionalized prosthetic interfaces using 3D printing: Generating infection-neutralizing prosthesis in dentistry. *Mater. Today Commun.* **15**, 114–119 (2018).

34. Vallieres, C. *et al.* Discovery of (meth)acrylate polymers that resist colonization by fungi associated with pathogenesis and biodeterioration. *Sci. Adv.* **6**, 1–13 (2020).

35. González-Henríquez, C. M., Sarabia-Vallejos, M. A. & Hernandez, J. R. Antimicrobial polymers for additive manufacturing. *Int. J. Mol. Sci.* **20**, (2019).

36. Roemer, T. & Krysan, D. J. Antifungal Drug Development: Challenges, Unmet Clinical Needs, and New Approaches. *Cold Spring Harb Perspect Med* **4**, a019703 (2014).

37. Carris, L. M., Little, C. R. & Stiles, C. M. Introduction to Fungi. *Plant Heal. Instr.* (2012) doi:10. 1094/PHI-I-2012-0426-01.

38. Meyer, V. *et al.* Current challenges of research on filamentous fungi in relation to human welfare and a sustainable bio-economy: a white paper. *Fungal Biol. Biotechnol.* **3**, 1–17 (2016).

39. O'Brien, H. E., Parrent, J. L., Jackson, J. A., Moncalvo, J. M. & Vilgalys, R. Fungal community

analysis by large-scale sequencing of environmental samples. *Appl. Environ. Microbiol.* **71**, 5544–5550 (2005).

40. Fisher, M. C., Hawkins, N. J., Sanglard, D. & Gurr, S. J. Worldwide emergence of resistance to antifungal drugs challenges human health and food security. *Science (80-.).* **742**, 739–742 (2018).

41. Kainz, K., Bauer, M. A., Madeo, F. & Carmona-Gutierrez, D. Fungal infections in humans: The silent crisis. *Microb. Cell* **7**, 143–145 (2020).

42. Seneviratne, C. J., Jin, L. & Samaranayake, L. P. Biofilm lifestyle of Candida: A mini review. *Oral Dis.* **14**, 582–590 (2008).

43. Pereira, R., dos Santos Fontenelle, R. O., de Brito, E. H. S. & de Morais, S. M. Biofilm of Candida albicans: formation, regulation and resistance. *J. Appl. Microbiol.* **131**, 11–22 (2021).

44. Koehler, P. *et al.* Morbidity and mortality of candidaemia in Europe: an epidemiologic meta-analysis. *Clin. Microbiol. Infect.* **25**, 1200–1212 (2019).

45. Brown, G. D. *et al.* Hidden killers: Human fungal infections. *Sci. Transl. Med.* **4**, (2012).

46. Hartman, T. C. olde & Rijswik, E. van. Fungal nail infection. *BMJ* **337**, (2008).

47. Centre for Disease Control and Prevention. *Drug-Resistant Candida Auris*. t www.cdc.gov/DrugResistance/Biggest-Threats.html doi:t www.cdc.gov/DrugResistance/Biggest-Threats.html.

48. Allaw, F. *et al.* First candida auris outbreak during a covid-19 pandemic in a tertiary-care center in Lebanon. *Pathogens* **10**, 1–10 (2021).

49. Villanueva-Lozano, H. *et al.* Outbreak of Candida auris infection in a COVID-19 hospital in Mexico. *Clin. Microbiol. Infect.* **27**, 813–816 (2021).

50. Cauda, R. Candidaemia in patients with an inserted medical device. *Drugs* **69 Suppl 1**, 33–38 (2009).

51. Guinea, J. Global trends in the distribution of Candida species causing candidemia. *Clin. Microbiol. Infect.* **20**, 5–10 (2014).

52. Cavalheiro, M. & Teixeira, M. C. Candida Biofilms: Threats, challenges, and promising strategies. *Front. Med.* **5**, 1–15 (2018).

53. Nobile Cl & Johnson AD. *Candida albicans* biofilm and human disease. *Annu. Rev. Microbiol.* **69**, 71–92 (2015).

54. Ramage, G., Martínez, J. P. & López-Ribot, J. L. Candida biofilms on implanted biomaterials: A clinically significant problem. *FEMS Yeast Res.* **6**, 979–986 (2006).

55. Martinez, L. R. & Fries, B. C. Fungal biofilms: Relevance in the setting of human disease. *Curr. Fungal Infect. Rep.* **4**, 266–275 (2010).

56. Hawser, S. P. & Douglas, L. J. Resistance of Candida albicans biofilms to antifungal agents in vitro. *Antimicrob. Agents Chemother.* **39**, 2128–2131 (1995).

57. Xiao, Z., Wang, Q., Zhu, F. & An, Y. Epidemiology, species distribution, antifungal susceptibility and mortality risk factors of candidemia among critically ill patients: A retrospective study from 2011 to 2017 in a teaching hospital in China. *Antimicrob. Resist. Infect. Control* **8**, 1–7 (2019).

58. Ricotta, E. E. *et al.* Invasive Candidiasis Species Distribution and Trends, United States, 2009-2017. *J. Infect. Dis.* **223**, 1295–1302 (2021).

59. Tsui, C., Kong, E. F. & Jabra-Rizk, M. A. Pathogenesis of Candida albicans biofilm. *Pathog. Dis.*

74, ftw018 (2016).

60. Lim, S. J. *et al.* Opportunistic yeast pathogen Candida spp.: Secreted and membrane-bound virulence factors . *Med. Mycol.* **59**, 1127–1144 (2021).

61. Douglas, L. J. Candida biofilms and their role in infection. *Trends Microbiol.* **11**, 30–36 (2003).

62. Finkel, J. S. & Mitchell, A. P. GENETIC CONTROL OF CANDIDA ALBICANS BIOFILM DEVELOPMENT. *Nat. Rev. Microbiol.* **9**, 109–118 (2011).

63. Arastehfar, A. *et al.* Drug-resistant fungi: An emerging challenge threatening our limited antifungal armamentarium. *Antibiotics* **9**, 1–29 (2020).

64. Somogyi-ganss, E., Chambers, M. S., Lewin, J. S., Tarrand, J. J. & Hutcheson, K. A. Considerations for Oral Decontamination. **274**, 405–413 (2018).

65. Ponde, N. O., Lortal, L., Ramage, G., Naglik, J. R. & Richardson, J. P. Candida albicans biofilms and polymicrobial interactions. *Crit. Rev. Microbiol.* **47**, 91–111 (2021).

66. Swidergall, M., Ernst, A. M. & Ernst, J. F. Candida albicans mucin Msb2 is a broad-range protectant against antimicrobial peptides. *Antimicrob. Agents Chemother.* **57**, 3917–3922 (2013).

67. Firacative, C. Invasive fungal disease in humans: Are we aware of the real impact? *Mem. Inst. Oswaldo Cruz* **115**, 1–9 (2020).

68. Talpaert, M. J. *et al.* Candida biofilm formation on voice prostheses. *J. Med. Microbiol.* **64**, 199–208 (2015).

69. Natarajan, B., Richardson, M. D., Irvine, B. W. H. & Thomas, M. The Provox® voice prosthesis and Candida albicans growth: A preliminary report of clinical, mycological and scanning electron microscopic assessment. *J. Laryngol. Otol.* **108**, 666–668 (1994).

70. Van Der Mei, H. C. *et al.* Voice prosthetic biofilm formation and Candida morphogenic conversions in absence and presence of different bacterial strains and species on silicone-rubber. *PLoS One* **9**, 1–6 (2014).

71. Coenye, T., Prijck, K. D., Nailis, H. & Nelis, H. J. Prevention of Candida albicans Biofilm Formation. *Open Mycol. J.* **5**, 9–20 (2011).

72. Neu, T. R. *et al.* Microflora on explanted silicone rubber voice prostheses: taxonomy, hydrophobicity and electrophoretic mobility. *J. Appl. Bacteriol.* **76**, 521–528 (1994).

73. Tsikopoulos, A. *et al.* In vitro Inhibition of Biofilm Formation on Silicon Rubber Voice Prosthesis: A Systematic Review and Meta-Analysis. *Orl* (2021) doi:10.1159/000516345.

74. Pentland, D. R. & Mühlschlegel, F. A. CO2 enhances the ability of Candida albicans to form biofilms, overcome 2 nutritional immunity and resist antifungal treatment. (2020).

75. Lefebvre, J. L. Laryngeal preservation in head and neck cancer: multidisciplinary approach. *Lancet Oncol.* **7**, 747–755 (2006).

76. Miyazaki, T., Haji, T., Satou, S., Ichimaru, K. & Chiyoda, T. A review of the complications and candida colonization associated with voice rehabilitation using a voice prosthesis. *Nihon Jibiinkoka Gakkai Kaiho* 34–40 (2014) doi:10.3950/jibiinkoka.117.34.

77. Spałek, J. *et al.* Biofilm growth causes damage to silicone voice prostheses in patients after surgical treatment of locally advanced laryngeal cancer. *Pathogens* **9**, 1–17 (2020).

78. Atos Medical. *Provox ® Voice Prostheses Literature Review*. (2015).

79. Messing, B. P. *et al.* Evaluation of prophylaxis treatment of Candida in alaryngeal patients with

tracheoesophageal voice prostheses. *Laryngoscope* **125**, 1118–1123 (2015).

80. Pentland, D. R. *et al.* Precision Antifungal Treatment Significantly Extends Voice Prosthesis Lifespan in Patients Following Total Laryngectomy. *Front. Microbiol.* **11**, 1–17 (2020).

81. Brook, I. & Goodman, J. F. Tracheoesophageal Voice Prosthesis Use and Maintenance in Laryngectomees. *Int. Arch. Otorhinolaryngol.* **24**, E535–E538 (2020).

82. Rodrigues, L., Banat, I. M., Teixeira, J. & Oliveira, R. Strategies for the prevention of microbial biofilm formation on silicone rubber voice prostheses. *J. Biomed. Mater. Res. - Part B Appl. Biomater.* **81**, 358–370 (2007).

83. Sionov, R. V. *et al.* Voice prosthesis coated with sustained release varnish containing clotrimazole shows long-term protection against Candida albicans: An in vitro study. *Molecules* **26**, (2021).

84. Arweiler-Harbeck, D. *et al.* Does metal coating improve the durability of silicone voice prostheses? *Acta Otolaryngol.* **121**, 643–646 (2001).

85. Kress, P., Schäfer, P. & Schwerdtfeger, F. P. Clinical use of a voice prosthesis with a flap valve containing silver oxide (Blom-Singer Advantage), biofilm formation, in-situ lifetime and indication. *Laryngorhinootologie.* **85**, 893–896 (2006).

86. de Prijck, K., de Smet, N., Coenye, T., Schacht, E. & Nelis, H. J. Prevention of Candida albicans Biofilm Formation by Covalently Bound Dimethylaminoethylmethacrylate and Polyethylenimine. *Mycopathologia* **170**, 213–221 (2010).

87. Rishpana, M. S. & Kabbin, J. S. Candiduria in catheter associated urinary tract infection with special reference to biofilm production. *J. Clin. Diagnostic Res.* **9**, DC11–DC13 (2015).

88. Hu, B. *et al.* Catheter-related Candida bloodstream infection in intensive care unit patients: A subgroup analysis of the China-SCAN study. *BMC Infect. Dis.* **14**, 1–9 (2014).

89. Dias, V. Candida species in the urinary tract: Is it a fungal infection or not? *Future Microbiol.* **15**, 81–83 (2020).

90. Selek, M. B. *et al.* First report of macroscopic biofilm formation caused by Candida albicans on silver hydrogel–coated urinary catheters. *Am. J. Infect. Control* **44**, 1174–1175 (2016).

91. Fesharaki, S. H., Aghili, S. R., Shokohi, T. & Boroumand, M. A. Catheter-related candidemia and identification of causative Candida species in patients with cardiovascular disorder. *Curr. Med. Mycol.* **4**, 7–13 (2018).

92. Zhang, L. *et al.* Risk factors and clinical analysis of peripherally inserted central catheter-related fungal colonization in premature infants. *Sci. Rep.* **11**, 1–7 (2021).

93. Escolà-Vergé, L. *et al.* Candida periprosthetic joint infection: A rare and difficult-to-treat infection. *J. Infect.* **77**, 151–157 (2018).

94. Baradkar, V. P., Mathur, M., Sonavane, A. & Kumar, S. Candidal infections of ventriculoperitoneal shunts. *J. Pediatr. Neurosci.* **4**, 73–75 (2009).

95. Bottagisio, M., Bidossi, A., Logoluso, N., Pellegrini, A. & De Vecchi, E. A spacer infection by Candida albicans secondary to a Staphylococcus capitis prosthetic joint infection: a case report. *BMC Infect. Dis.* **21**, 1–5 (2021).

96. Saconi, E. S., de Carvalho, V. C., de Oliveira, P. R. D. & Lima, A. L. L. M. Prosthetic joint infection due to Candida species: Case series and review of literature. *Medicine (Baltimore).* **99**, e19735 (2020).

97. Puryer, J. Prosthodontics " Denture Stomatitis – A Clinical Update ". *Univ. Bristol* **43**, 1–19 (2016).

98. Gleiznys, A., Zdanavičienė, E. & Žilinskas, J. Candida albicans importance to denture wearers. A literature review. *Stomatologija* **17**, 54–66 (2015).

99. Ribeiro, A. B. *et al.* Hygiene protocols for the treatment of denture-related stomatitis: Local and systemic parameters analysis - A randomized, double-blind trial protocol. *Trials* **20**, 1–10 (2019).

100. Dorocka-Bobkowska, B. *et al.* Candida-associated denture stomatitis in type 2 diabetes mellitus. *Diabetes Res. Clin. Pract.* **90**, 81–86 (2010).

101. Al-Kebsi, A. M. *et al.* Multiple Risk Factors of Candida Albicans Associated Denture Stomatitis. *Online J. Dent. Oral Heal.* **1**, 5–9 (2018).

102. Li, Z., Sun, J., Lan, J. & Qi, Q. Effect of a denture base acrylic resin containing silver nanoparticles on Candida albicans adhesion and biofilm formation. *Gerodontology* **33**, 209–216 (2016).

103. Tammer, I., Reuner, J., Hartig, R. & Geginat, G. Induction of Candida albicans biofilm formation on silver-coated vascular grafts. *J. Antimicrob. Chemother.* **69**, 1282–1285 (2014).

104. Hachem, R. *et al.* Novel antiseptic urinary catheters for prevention of urinary tract infections: Correlation of in vivo and in vitro test results. *Antimicrob. Agents Chemother.* **53**, 5145–5149 (2009).

105. Mahmoud, Y. A. G. & Aly, M. M. Anti-Candida and mode of action of two newly synthesized polymers: A modified poly (methylmethacrylate-co-vinylbenzoylchloride) and a modified linear poly (chloroethylvinylether-co-vinylbenzoylchloride) with special reference to Candida albicans and Candi. *Mycopathologia* **157**, 145–153 (2004).

106. Zhang, Y. *et al.* The antifungal effects and mechanical properties of silver bromide/cationic polymer nano-composite-modified Poly-methyl methacrylate-based dental resin. *Sci. Rep.* **7**, 1–13 (2017).

107. Everaert, E. P. J. M. *et al.* In vitro and in vivo microbial adhesion and growth on argon plasma-treated silicone rubber voice prostheses. *J. Mater. Sci. Mater. Med.* **9**, 147–157 (1998).

108. Michl, T. D., Giles, C., Cross, A. T., Griesser, H. J. & Coad, B. R. Facile single-step bioconjugation of the antifungal agent caspofungin onto material surfaces: Via an epoxide plasma polymer interlayer. *RSC Adv.* **7**, 27678–27681 (2017).

109. Naderi, J., Giles, C., Saboohi, S., Griesser, H. J. & Coad, B. R. Surface coatings with covalently attached anidulafungin and micafungin prevent Candida albicans biofilm formation. 360–364 (2019) doi:10.1093/jac/dky437.

110. Giles, C., Lamont-Friedrich, S. J., Michl, T. D., Griesser, H. J. & Coad, B. R. The importance of fungal pathogens and antifungal coatings in medical device infections. *Biotechnology Advances* vol. 36 264–280 (2018).

111. Segura, T. *et al.* Materials with fungi-bioinspired surface for efficient binding and fungi-sensitive release of antifungal agents. *Biomacromolecules* **15**, 1860–1870 (2014).

112. Fazly, A. *et al.* Chemical screening identifies filastatin, a small molecule inhibitor of Candida albicans adhesion, morphogenesis, and pathogenesis. *Proc. Natl. Acad. Sci. U. S. A.* **110**, 13594–13599 (2013).

113. Vargas-Blanco, D. *et al.* A pre-therapeutic coating for medical devices that prevents the attachment of Candida albicans. *Ann. Clin. Microbiol. Antimicrob.* **16**, 1–12 (2017).

114. Santos, T. B. *et al.* Flexible camphor diamond-like carbon coating on polyurethane to prevent Candida albicans biofilm growth. *J. Mech. Behav. Biomed. Mater.* **68**, 239–246 (2017).

115. Freitas, F. *et al.* Beneficial Effects of Ethyl- Cyanoacrylate Coating Against Candida Albicans

Biofilm Formation. **30**, 266–271 (2019).

116. Schneller, T., Waser, R., Kosec, M. & Payne, D. Chemical solution deposition of functional oxide thin films. *Chem. Solut. Depos. Funct. Oxide Thin Film.* **9783211993**, 1–796 (2013).

117. Glocker, David Ranade, S. *Medical Coatings and Deposition Technologies*. *Medical Coatings and Deposition Technologies* (Scrivener Publishing LLC, 2016). doi:10.1002/9781119308713.

118. Soufiani, M. J. Investigation And Modeling of Dip-Coating Process for Dispersions. (2016).

119. Obregón, S. & Rodríguez-González, V. Photocatalytic TiO2 thin films and coatings prepared by sol–gel processing: a brief review. *J. Sol-Gel Sci. Technol.* (2021) doi:10.1007/s10971-021-05628-5.

120. Ossila. Dip Coating Theory. https://www.ossila.com/pages/dip-coating-theory-film-thickness#Overview.

121. Rheology, C. for I. Dip Coating Viscosity, Yield Stress and Surface Tension. https://www.rheologylab.com/articles/coatings-paints-inks/dip-coating/.

122. Sheardown, H. Subbaraman, L. *Ophthalmic coatings*. (2012). doi:10.1533/9780857093677.2.336.

123. Driver, M. & Specialties, V. Coatings for cardiovascular devices: coronary stents. (2012) doi:10.1533/9780857093677.2.223.

124. Ghosh, S. & Haldar, J. *Cationic polymer À based antibacterial smart coatings*. *Advances In Smart Coatings And Thin Films For Future Industrial and Biomedical Engineering Applications* (Elsevier Inc., 2020). doi:10.1016/B978-0-12-849870-5.00011-2.

125. MarketsandMarkets. Antimicrobial Coatings Market. https://www.marketsandmarkets.com/PressReleases/antimicrobial-coatings.asp.

126. Tan, Y., Ma, S., Leonhard, M., Moser, D. & Ludwig, R. Materials Science & Engineering C Co-immobilization of cellobiose dehydrogenase and deoxyribonuclease I on chitosan nanoparticles against fungal / bacterial polymicrobial biofilms targeting both biofilm matrix and microorganisms. **108**, (2020).

127. Huang, K. S. *et al.* Recent advances in antimicrobial polymers: A mini-review. *Int. J. Mol. Sci.* **17**, (2016).

128. Li, B. & Fintan, T. *Racing for the Surface*. *Racing for the Surface* (2020). doi:10.1007/978-3-030-34475-7.

129. Vasilev, K. Nanoengineered Antibacterial Coatings. *Coatings* **9**, 654 (2019).

130. Singh, A., Tiwari, A., Bajpai, J. & Bajpai, A. K. *Polymer-based antimicrobial coatings as potential biomaterials: From action to application*. *Handbook of Antimicrobial Coatings* (Elsevier Inc., 2017). doi:10.1016/B978-0-12-811982-2.00003-2.

131. Yang, C. *et al.* Brush-like polycarbonates containing dopamine, cations, and PEG providing a broad-spectrum, antibacterial, and antifouling surface via one-step coating. *Adv. Mater.* **26**, 7346–7351 (2014).

132. Xu, G., Neoh, K. G., Kang, E. T. & Teo, S. L. M. Switchable Antimicrobial and Antifouling Coatings from Tannic Acid-Scaffolded Binary Polymer Brushes. *ACS Sustain. Chem. Eng.* **8**, 2586–2595 (2020).

133. Hadjesfandiari, N., Yu, K., Mei, Y. & Kizhakkedathu, J. N. Polymer brush-based approaches for the development of infection-resistant surfaces. *J. Mater. Chem. B* **2**, 4968–4978 (2014).

134. Garle, A. L. & Budhlall, B. M. PEG Bottle Brush Copolymers as Antimicrobial Mimics: Role of

Entropic Templating in Membrane Lysis. *Langmuir* **35**, 3372–3382 (2019).

135. Zhang, Z. & Wagner, V. E. *Antimicrobial coatings and modifications on medical devices*. *Antimicrobial Coatings and Modifications on Medical Devices* (2017). doi:10.1007/978-3-319-57494-3.

136. Laschewsky, A. Structures and synthesis of zwitterionic polymers. *Polymers (Basel).* **6**, 1544–1601 (2014).

137. Peng, W. *et al.* Multi-functional zwitterionic coating for silicone-based biomedical devices. *Chem. Eng. J.* **398**, (2020).

138. Choi, W. *et al.* Quantitative Interpretation of Hydration Dynamics Enabled the Fabrication of a Zwitterionic Antifouling Surface. *ACS Appl. Mater. Interfaces* **12**, 7951–7965 (2020).

139. Liu, Y. *et al.* Molecular simulations and understanding of antifouling zwitterionic polymer brushes. *J. Mater. Chem. B* **8**, 3814–3828 (2020).

140. Zhou, L. *et al.* Parylene coating hinders Candida albicans adhesion to silicone elastomers and denture bases resin. *Arch. Oral Biol.* **55**, 401–409 (2010).

141. Golda-Cepa, M., Engvall, K., Hakkarainen, M. & Kotarba, A. Recent progress on parylene C polymer for biomedical applications: A review. *Prog. Org. Coatings* **140**, (2020).

142. El-Chami, M. F. *et al.* Reduced bacterial adhesion with parylene coating: Potential implications for Micra transcatheter pacemakers. *J. Cardiovasc. Electrophysiol.* **31**, 712–717 (2020).

143. Infection, G. L. The 1999 Garrod Lecture Infection in the twenty- rst century: predictions and postulates. *J. Antimicrob. Chemother.* 873–877 (2000).

144. Gottenbos, B., Van Der Mei, H. C., Klatter, F., Nieuwenhuis, P. & Busscher, H. J. In vitro and in vivo antimicrobial activity of covalently coupled quaternary ammonium silane coatings on silicone rubber. *Biomaterials* **23**, 1417–1423 (2002).

145. AST Products. Inc. RepelaCOAT. (2008).

146. Cliff, N. N. Jaynes, B. S. Song, Z. Q. Guinta, A. Feese, E. Gande, M. E. US20140170238A1. (2014).

147. Hydromer. Hydromer® Hydrophilic Medical Device Coatings. https://www.hydromer.com/medical-device-coatings/hydrophilic-medical-device-coatings/.

148. Writer, M. S. Hydromer, N8 Medical in new antimicrobial coatings development agreement. https://www.nsmedicaldevices.com/news/hydromer-n8-medical-in-new-antimicrobial-coatings-development-agreement-290612/.

149. Hydromer, Inc. Enters Into a Strategic Development Agreement With N8 Medical Inc. for a New Class of Antimicrobial Coatings. https://www.biospace.com/article/releases/hydromer-inc-enters-into-a-strategic-development-agreement-with-n8-medical-inc-for-a-new-class-of-antimicrobial-coatings-/.

150. Onis, S. Burrows, F. Kapoor, K. Rhodes, A. Luthra, A. K. WO2014174237A1. (2014).

151. Jiménez, M., Romero, L., Domínguez, I. A., Espinosa, M. D. M. & Domínguez, M. Additive Manufacturing Technologies: An Overview about 3D Printing Methods and Future Prospects. *Complexity* **2019**, (2019).

152. Gornet, T. History of Additive Manufacturing. 1–24 (2017) doi:10.4018/978-1-5225-2289-8.ch001.

153. Berman, B. 3-D printing: The new industrial revolution. *Bus. Horiz.* **55**, 155–162 (2012).

154. Sedacca, B. Hand built by lasers. *Eng. Technol.* **6**, 58–59 (2011).

155. Rafiee, M., Farahani, R. D. & Therriault, D. Multi-Material 3D and 4D Printing: A Survey. *Adv. Sci.* **7**, 1–26 (2020).

156. Gibson, I., Rosen, D. & Stucker, B. *Additive manufacturing technologies: 3D printing, rapid prototyping, and direct digital manufacturing, second edition*. *Additive Manufacturing Technologies: 3D Printing, Rapid Prototyping, and Direct Digital Manufacturing, Second Edition* (2015). doi:10.1007/978-1-4939-2113-3.

157. Perrot, A. & Amziane, S. 3D printing in concrete: General considerations and technologies. *3D Print. Concr. State Art Challenges Digit. Constr. Revolut.* 1–40 (2019) doi:10.1002/9781119610755.ch1.

158. Al Rashid, A., Ahmed, W., Khalid, M. Y. & Koç, M. Vat photopolymerisation of polymers and polymer composites: Processes and applications. *Addit. Manuf.* **47**, 102279 (2021).

159. Materials, B. *et al.* E ff ects of Post-Curing Time on the Mechanical and Color Properties of Three-Dimensional Printed.

160. Tumbleston, J. R. *et al.* Continuous liquid interface production of 3D objects. *Science (80-.).* **347**, 1349–1352 (2015).

161. Stampfl, J., Liska, R. & Ovsianikov, A. *Multiphoton Lithography: Techniques, Materials, and Applications*. (Wiley-VCH, 2016).

162. Miller, J. S. & Burdick, J. A. Editorial: Special Issue on 3D Printing of Biomaterials. *ACS Biomater. Sci. Eng.* **2**, 1658–1661 (2016).

163. Maleki, H. & Bertola, V. Recent advances and prospects of inkjet printing in heterogeneous catalysis. *Catal. Sci. Technol.* **10**, 3140–3159 (2020).

164. Zhou, Z. *et al.* High-throughput characterization of fluid properties to predict droplet ejection for three-dimensional inkjet printing formulations. *Addit. Manuf.* **29**, 100792 (2019).

165. Quan, H. *et al.* Photo-curing 3D printing technique and its challenges. *Bioact. Mater.* **5**, 110–115 (2020).

166. Malik, M. S., Schlögl, S., Wolfahrt, M. & Sangermano, M. Review on UV-induced cationic frontal polymerisation of epoxy monomers. *Polymers (Basel).* **12**, (2020).

167. Bagheri, A. & Jin, J. Photopolymerisation in 3D Printing. *ACS Appl. Polym. Mater.* **1**, 593–611 (2019).

168. Tajau, R. *et al.* Development of palm oil-based UV-curable epoxy acrylate and urethane acrylate resins for wood coating application. *AIP Conf. Proc.* **1584**, 164–169 (2014).

169. Shamsi, M., Huynh, C., Gordon, J. & Patloori, S. 3D opportunity for health care, Demystifying FDA regulations for medical devices. https://www2.deloitte.com/us/en/insights/focus/3d-opportunity/additive-manufacturing-fda-regulations-medical-devices.html.

170. Salmi, M. Additive manufacturing processes in medical applications. *Materials (Basel).* **14**, 1–16 (2021).

171. Ballard, D. H. *et al.* Antibiotics in 3D-printed implants, instruments and materials: benefits, challenges and future directions. *J. 3D Print. Med.* **3**, 83–93 (2019).

172. Process of 3D Printing Medical Devices. https://www.fda.gov/medical-devices/3d-printing-medical-devices/process-3d-printing-medical-devices.

173. Tabaković, S., Zeljković, M., Milojević, Z. & Živković, A. Design of custom made prosthesis of the

hip. *Teh. Vjesn.* **26**, 323–330 (2019).

174. Jin, Y. A., Plott, J., Chen, R., Wensman, J. & Shih, A. Additive manufacturing of custom orthoses and prostheses - A review. *Procedia CIRP* **36**, 199–204 (2015).

175. Cox, S. C. *et al.* Adding functionality with additive manufacturing: Fabrication of titanium-based antibiotic eluting implants. *Mater. Sci. Eng. C* **64**, 407–415 (2016).

176. He, Y. *et al.* Inkjet based 3D Printing of bespoke medical devices that resist bacterial biofilm formation. (2020) doi:10.1101/2020.06.30.180596.

177. Negi, S., Dhiman, S. & Sharma, R. K. Basics and applications of rapid prototyping medical models. *Rapid Prototyp. J.* **20**, 256–267 (2014).

178. O'Sullivan, K. J. *et al.* Use of 3D printing to create a bespoke repair of a Percutaneous Endoscopic Gastrostomy (PEG) tube in patient unfit for surgical replacement. *BMJ Innov.* **4**, 29–31 (2018).

179. Dunne, C. P., O'Sullivan, K. J., O'Sullivan, L., Linnane, B. & O'Connell, N. H. Foreseeing the microbiology of bespoke 3D-printed medical devices. *J. Hosp. Infect.* **99**, 237–238 (2018).

180. Yue, J. *et al.* 3D-Printable Antimicrobial Composite Resins. *Adv. Funct. Mater.* **25**, 6756–6767 (2015).

181. Wang, J. C., Zheng, H., Chang, M. W., Ahmad, Z. & Li, J. S. Preparation of active 3D film patches via aligned fiber electrohydrodynamic (EHD) printing. *Sci. Rep.* **7**, 1–13 (2017).

182. Al-Ahmad, A. *et al.* Bacterial and Candida albicans adhesion on rapid prototyping-produced 3D-scaffolds manufactured as bone replacement materials. *J. Biomed. Mater. Res. - Part A* **87**, 933–943 (2008).

183. Puppi, D., Piras, A. M., Pirosa, A., Sandreschi, S. & Chiellini, F. Levofloxacin-loaded star poly(ε-caprolactone) scaffolds by additive manufacturing. *J. Mater. Sci. Mater. Med.* **27**, 1–11 (2016).

184. Salerno, C. *et al.* Candida-associated denture stomatitis. *Med. Oral Patol. Oral Cir. Bucal* **16**, (2011).

185. Gutierrez, E. *et al.* 3D Printing of Antimicrobial Alginate/Bacterial-Cellulose Composite Hydrogels by Incorporating Copper Nanostructures. *ACS Biomater. Sci. Eng.* **5**, 6290–6299 (2019).

186. Abudula, T. *et al.* 3D Printing of Metal/Metal Oxide Incorporated Thermoplastic Nanocomposites With Antimicrobial Properties. *Front. Bioeng. Biotechnol.* **8**, 1–8 (2020).

187. Li, Z., Wang, C., Qiu, W. & Liu, R. Antimicrobial Thiol–ene–acrylate Photosensitive Resins for DLP 3D Printing. *Photochem. Photobiol.* **95**, 1219–1229 (2019).

188. Navaruckiene, A. *et al.* 1. Voet, V. S. D. et al. Biobased Acrylate Photocurable Resin Formulation for Stereolithography 3D Printing. ACS Omega 3, 1403–1408 (2018).Vanillin acrylate-based resins for optical 3D printing. *Polymers (Basel).* **12**, (2020).

189. Navaruckiene, A., Kasetaite, S. & Ostrauskaite, J. Vanillin-based thiol-ene systems as photoresins for optical 3D printing. *Rapid Prototyp. J.* **26**, 402–408 (2020).

190. Navaruckiene, A., Bridziuviene, D., Raudoniene, V., Rainosalo, E. & Ostrauskaite, J. Influence of vanillin acrylate-based resin composition on resin photocuring kinetics and antimicrobial properties of the resulting polymers. *Materials (Basel).* **14**, 1–20 (2021).

191. Stratasys. *Water-Based Antimicrobial Coating For 3D Printed Medical Devices Water-Based Antimicrobial Coating For 3D Printed Medical Devices devices produced via 3D printing . As reported in this*. (2019).

192. Hamilton. Microlab STAR Line. https://pdf.medicalexpo.com/pdf/hamilton-robotics/microlab-star-

line/94379-159297-_4.html.

193. Perkin Elmer. *DSC 8000 Installation and Hardware Guide*. https://www.s4science.at/wordpress/wp-content/uploads/2019/04/09931448A-DSC-8000-Installation-and-Hardware-Guide.pdf (2017).

194. He, Y., Vallières, C., Alexander, M. R., Wildman, R. D. & Avery, S. V. Inkjet 3dprinting of polymers resistant to fungal attachment. *Bio-protocol* **11**, 1–10 (2021).

195. FUJIFILM Dimatix, I. *Dimatix Materials Printer DMP-2800 Series User Manual*. (2006).

196. Ramírez-Jiménez, A., Montoya-Villegas, K. A., Licea-Claverie, A. & Gónzalez-Ayón, M. A. Tunable thermo-responsive copolymers from DEGMA and OEGMA synthesized by RAFT polymerisation and the effect of the concentration and saline phosphate buffer on its phase transition. *Polymers (Basel).* **11**, (2019).

197. Matsumoto, A., Mizuta, K. & Otsu, T. Radical Polymerisation of 4-tert-Butylcyclohexyl Methacrylate: Polymerisation Kinetics and Polymer Properties. *Macromolecules* **26**, 1659–1665 (1993).

198. Wen, M. *et al.* Kinetic Study of Free-Radical Polymerisation of Multifunctional Acrylates and Methacrylates. 564–569 (1997).

199. Reis, N. & Derby, B. Ink jet deposition of ceramic suspensions: Modelling and experiments of droplet formation. *Mater. Res. Soc. Symp. - Proc.* **624**, 65–70 (2000).

200. Dundas, A. A. *et al.* Validating a Predictive Structure–Property Relationship by Discovery of Novel Polymers which Reduce Bacterial Biofilm Formation. *Adv. Mater.* **31**, 1–6 (2019).

201. Adlington, K. *et al.* Application of Targeted Molecular and Material Property Optimization to Bacterial Attachment-Resistant (Meth)acrylate Polymers. *Biomacromolecules* **17**, 2830–2838 (2016).

202. Le, P. H. *et al.* Nanoscale Surface Roughness Influences Candida albicans Biofilm Formation. *ACS Appl. Bio Mater.* **3**, 8581–8591 (2020).

203. Leonhard, M. *et al.* Impact of surface roughness on long-term candida biofilm colonization of prosthetic silicone : A pilot study . *Hard Tissue* **3**, 1–6 (2014).

204. Chandra, J. *et al.* Modification of surface properties of biomaterials influences the ability of Candida albicans to form biofilms. *Appl. Environ. Microbiol.* **71**, 8795–8801 (2005).

205. Cabanillas, B., Mallma-Medina, A., Petkova-Gueorguieva, M., Alvitez-Temoche, D. & Mendoza, R. Influence of the Surface Energy of Different Brands of Polymethyl Methacrylate on the Adherence of Candida albicans: An In Vitro Study. *J. Int. Soc. Prev. Community Dent.* **11**, 6–12 (2021).

206. Yoshii, E. Cytotoxic effects of acrylates and methacrylates:Relationships of monomer structures and cytotoxicity. *J. Biomed. Mater. Res.* **37**, 517–524 (1997).

207. Yarusso, D. J. *Effect of rheology on PSA performance*. *Adhesion Science and Engineering* (Elsevier B.V., 2002). doi:10.1016/b978-0-444-51140-9.50040-8.

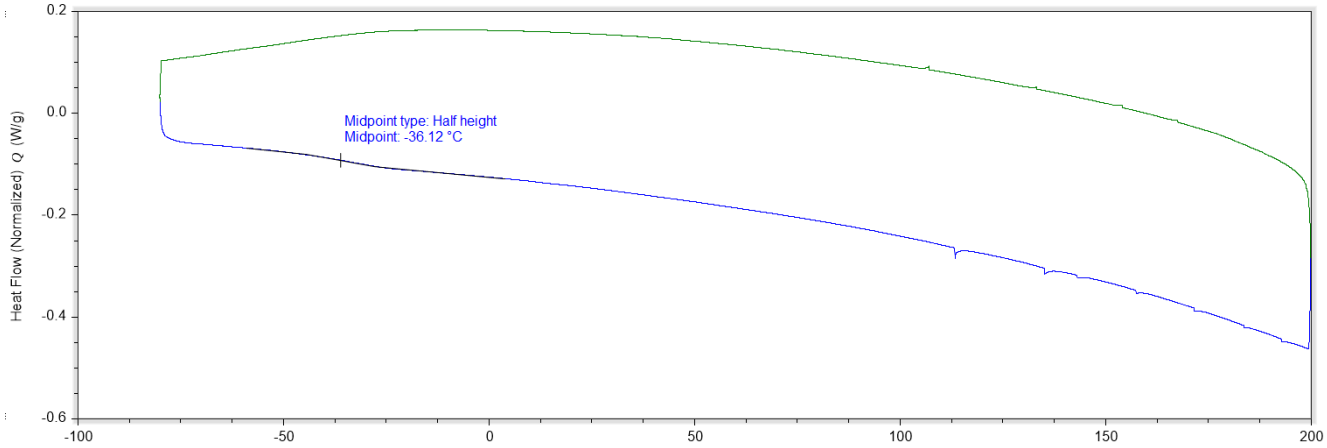
208. Schneider, H. A. & Di Marzio, E. A. The glass temperature of polymer blends: comparison of both the free volume and the entropy predictions with data. *Polymer (Guildf).* **33**, 3453–3461 (1992).

209. Kakimoto, M. A., Grunzinger, S. J. & Hayakawa, T. Hyperbranched poly(ether sulfone)s: Preparation and application to ion-exchange membranes. *Polym. J.* **42**, 697–705 (2010).

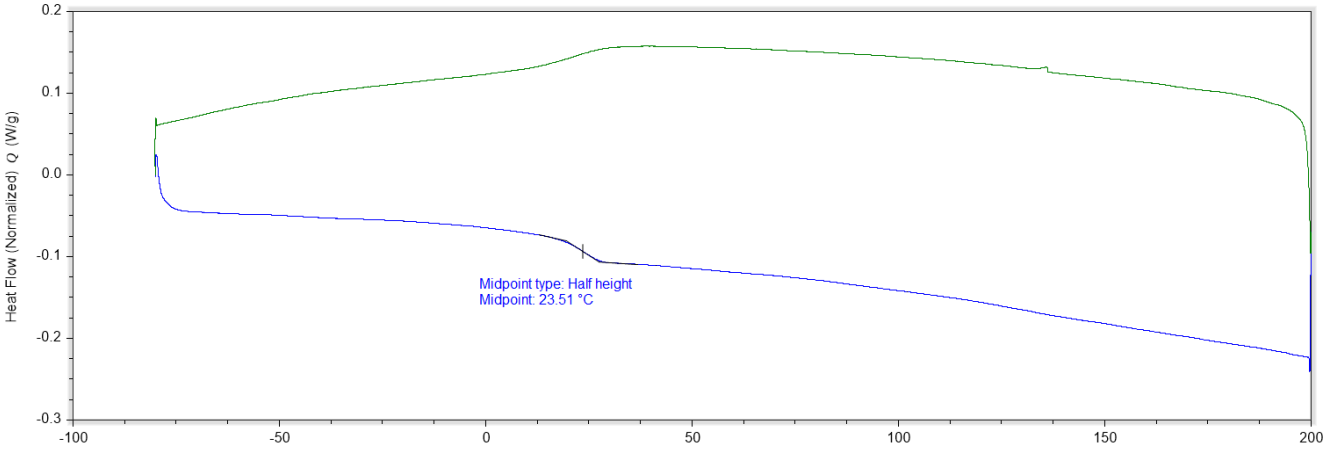
Appendix

Appendix 1. Differential Scanning Calorimetry (DSC) Thermogram

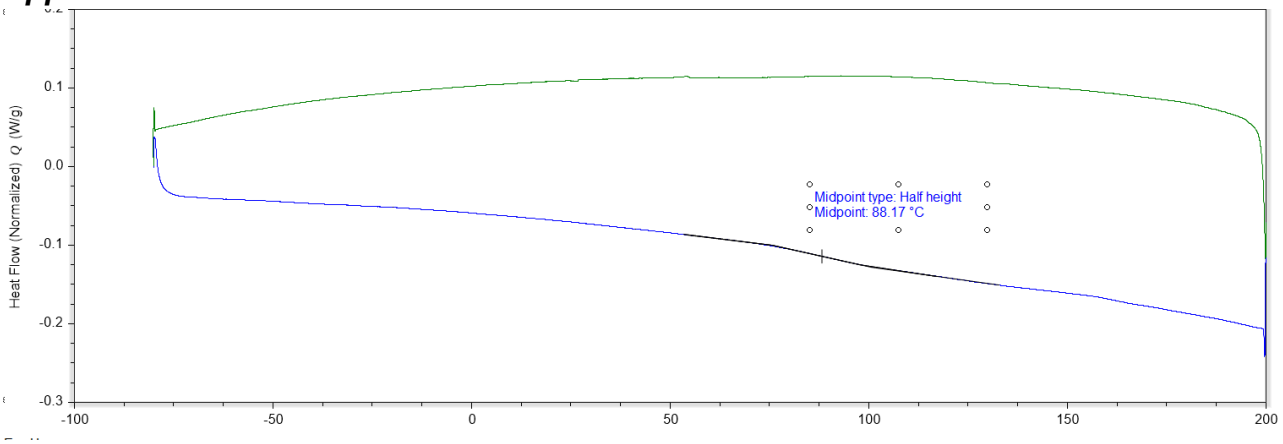
Appendix 1.1: DSC of DEGMA



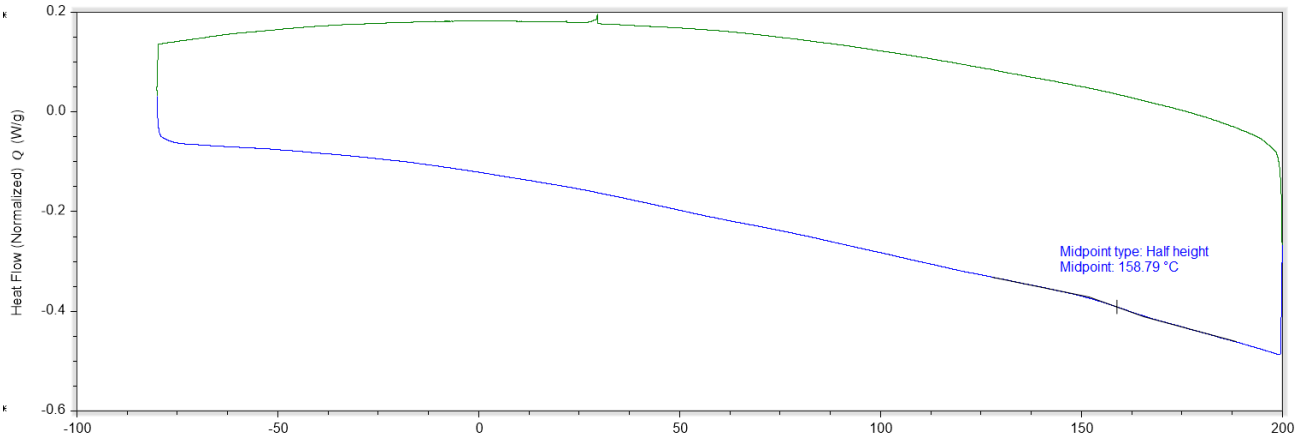
Appendix 1.2: DSC of EGDPEA



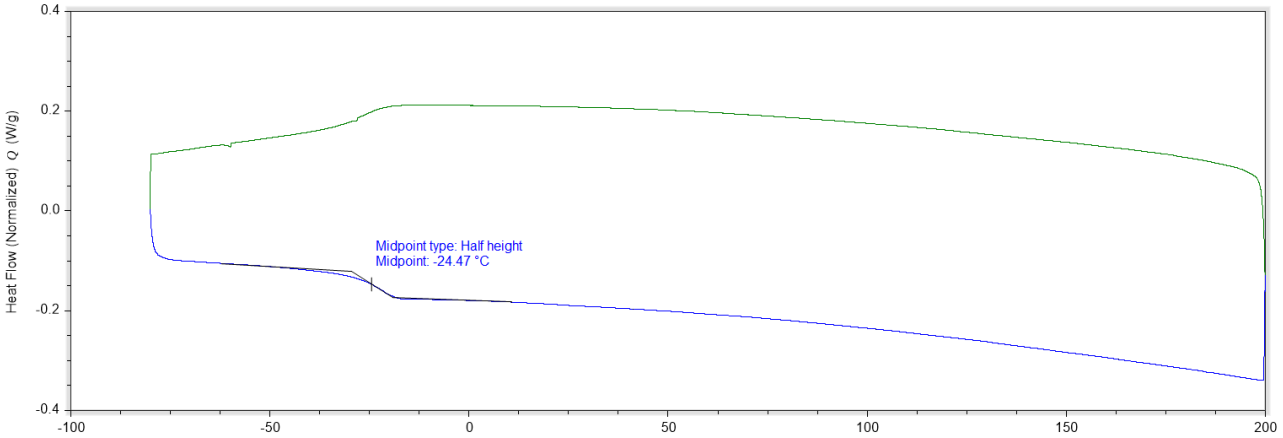
Appendix 1.3: DSC of IBMA



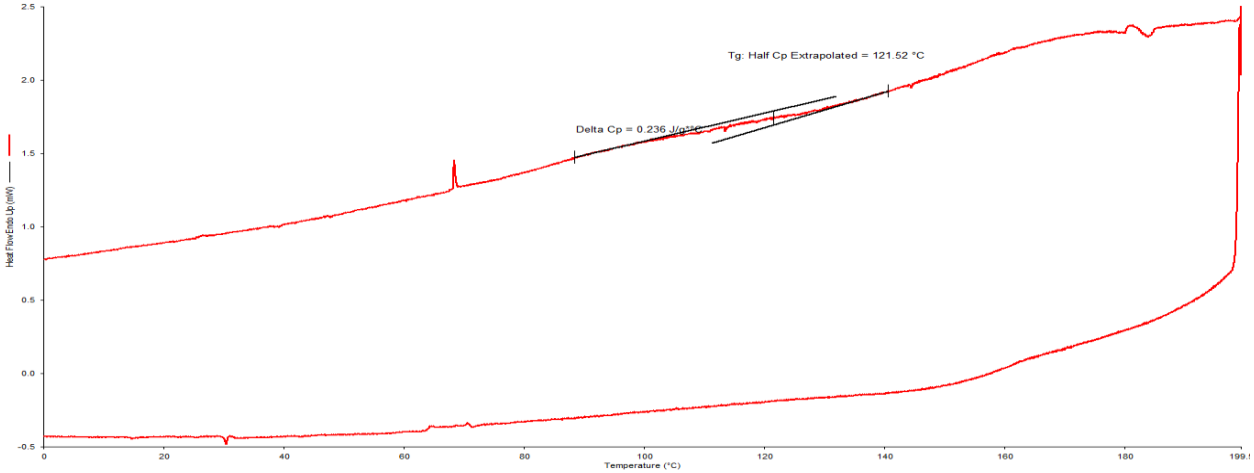
Appendix 1.4: DSC of TBCHMA



Appendix 1.5: DSC of TBCHMA



Appendix 1.6: DSC of TBCHA



Appendix 2. Fourier-Transform Infrared Spectroscopy (FTIR) Data

Appendix 2.1: DOC of HTS UV Cure Homopolymer with 1 % DMPA initiator.

Measurement, n = 3.

Polymer Abbreviation	Moulded Polymer – 1 % Initiator				
	DOC (%) 1	DOC (%) 2	DOC (%) 3	Mean	Std. Dev.
TEGMA	66.5	60.1	59.7	62.1	3.8
DEGMA	53.9	52.4	63.6	56.6	6.1
AODMBA	61.4	75.4	60.3	65.7	8.4
TBCHA	80.5	83.9	84.4	83.0	2.1
TBCHMA	68.7	79.8	82.4	76.9	7.3
IBMA	47.5	57.0	55.4	53.3	5.1
EGDPEA	71.4	81.7	75.5	76.2	5.2
PEGDA	48.1	61.6	71.7	60.5	11.8

Appendix 2.2: DOC of HTS UV Cure Homopolymer with 4 % DMPA initiator.

Measurement, n = 3.

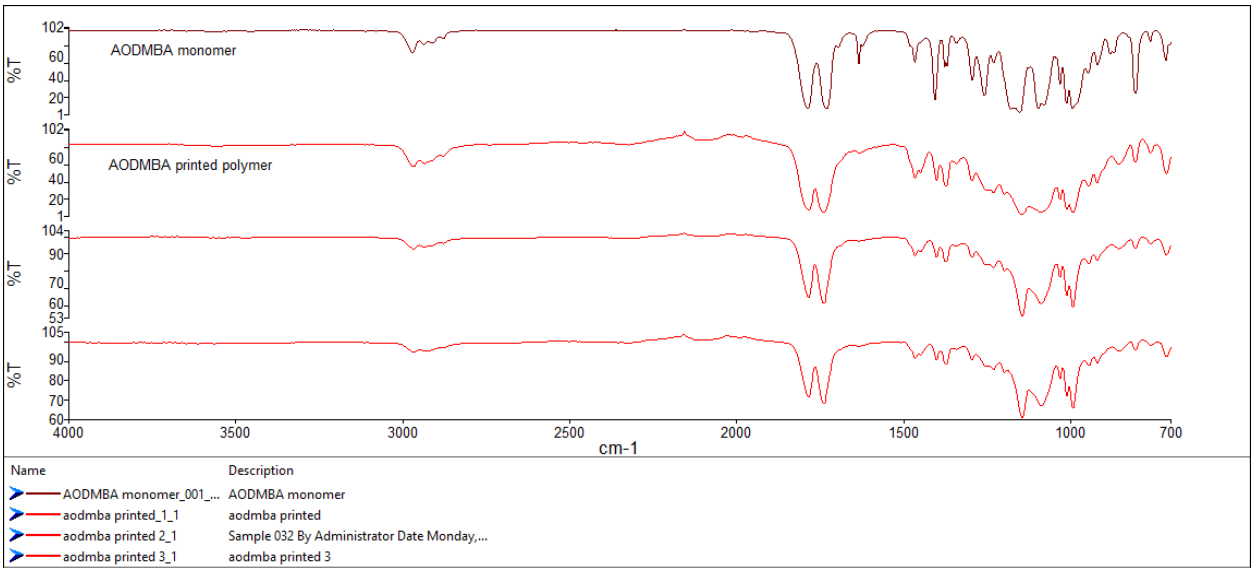
Polymer Abbreviation	Moulded Polymer – 4 % Initiator				
	DOC (%) 1	DOC (%) 2	DOC (%) 3	Mean	Std. Dev.
TEGMA	82.1	80.5	77.2	79.9	2.5
DEGMA	89.3	85.5	96.1	90.3	5.3
AODMBA	83.4	81.9	78.9	81.4	2.3
TBCHA	88.5	88.7	86.4	87.9	1.3
TBCHMA	95.7	92.9	96.9	95.2	2.1
IBMA	74.2	77.1	62.3	71.2	7.8
EGDPEA	87.5	89.4	93.3	90.1	3.0

PEGDA	82.0	64.9	81.2	76.0	9.7

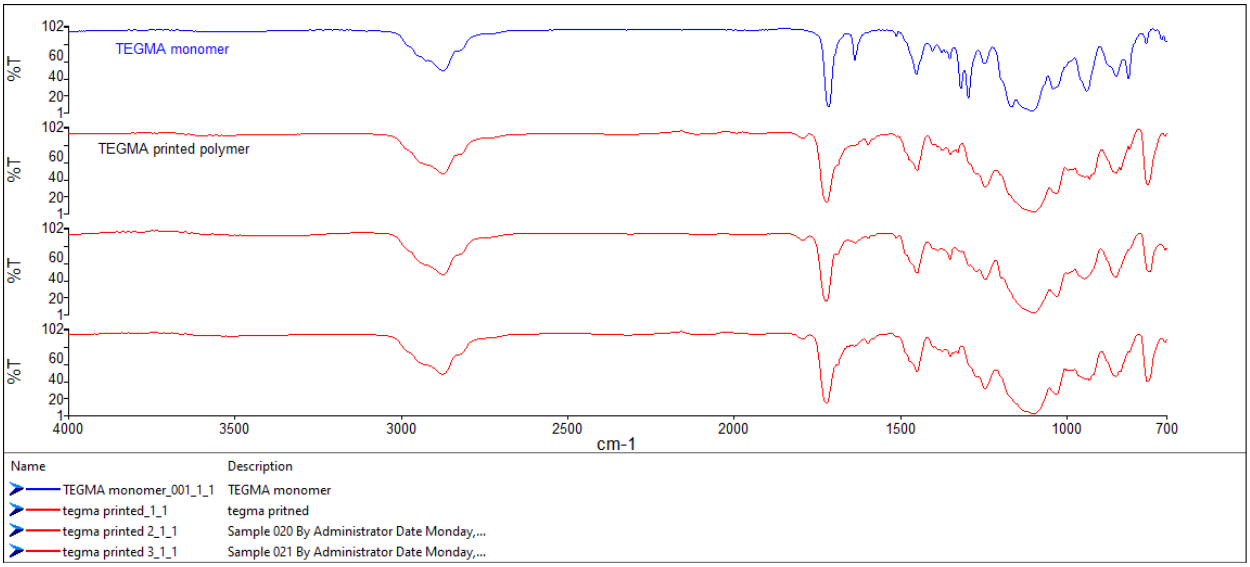
Appendix 2.3: DOC of 3D Printed Homopolymer with 4 % DMPA initiator.
Measurement, n = 3.

Polymer Abbreviation	Printed Polymer (2 Layers) - 4% Initiator				
	DOC (%) 1	DOC (%) 2	DOC (%) 3	Mean	Std. Dev.
TEGMA	96.2	79.7	92.0	89.3	8.6
DEGMA	85.3	82.7	86.5	84.8	1.9
AODMBA	87.9	97.7	97.0	94.2	5.5
TBCHA	85.6	83.4	67.8	78.9	9.7
TBCHMA	82.8	82.3	82.5	82.5	0.3
IBMA	63.7	66.3	60.0	63.3	3.2
EGDPEA	90.0	91.7	91.3	91.0	0.9
PEGDA	91.1	90.0	91.5	90.9	0.8

Appendix 2.4: Example FTIR spectrum, AODMBA
(Monomer vs printed, n=3)



Appendix 2.5: Example of FTIR spectrum, TEGMA
(monomer vs printed, n=3)



Appendix 3. Statistical Analysis (ANOVA)

Appendix 3.1: EGDPEA 1 % vs 4 % DMPA

Source	DF	Adj SS	Adj MS	F-Value	P-Value
Factor	1	288.70	288.70	16.26	0.016
Error	4	71.01	17.75		
Total	5	359.71			

Appendix 3.2: DEGMA 1 % vs 4 % DMPA

Source	DF	Adj SS	Adj MS	F-Value	P-Value
Factor	1	1701.2	1701.18	51.87	0.002
Error	4	131.2	32.80		
Total	5	1832.4			

Appendix 3.3: TBCHA 1 % vs 4 % DMPA

Source	DF	Adj SS	Adj MS	F-Value	P-Value
Factor	1	36.11	36.113	11.83	0.026
Error	4	12.21	3.054		
Total	5	48.33			

Appendix 3.4: IBMA 1 % vs 4 % DMPA

Source	DF	Adj SS	Adj MS	F-Value	P-Value
Factor	1	481.2	481.15	10.98	0.030
Error	4	175.3	43.82		
Total	5	656.4			

Appendix 3.5: TBCHMA 1 % vs 4 % DMPA

Source	DF	Adj SS	Adj MS	F-Value	P-Value
Factor	1	498.9	498.86	17.41	0.014
Error	4	114.6	28.65		
Total	5	613.5			

Appendix 3.6: PEGDA 1 % vs 4 % DMPA

Source	DF	Adj SS	Adj MS	F-Value	P-Value
Factor	1	363.3	363.3	3.11	0.152
Error	4	467.0	116.8		
Total	5	830.3			

Appendix 3.7: TEGMA 1 % vs 4 % DMPA

Source	DF	Adj SS	Adj MS	F-Value	P-Value
Factor	1	477.22	477.22	46.40	0.002
Error	4	41.14	10.28		
Total	5	518.36			

Appendix 3.8: AODMBA 1 % vs 4 % DMPA

Source	DF	Adj SS	Adj MS	F-Value	P-Value
Factor	1	368.5	368.48	9.68	0.036
Error	4	152.3	38.08		
Total	5	520.8			

Appendix 3.9: Effect of Polymer Ratio on Polymer Toxicity Results

Source	DF	Adj SS	Adj MS	F-Value	P-Value
Primary Polymer Ratio	1	1071	1071.1	1.11	0.297
Error	55	53177	966.8		
Total	56	54248			

Appendix 3.10: Effect of Primary Polymer Type on Polymer Toxicity Results

Source	DF	Adj SS	Adj MS	F-Value	P-Value
Primary Polymer	1	2952	2952.4	3.17	0.081
Error	55	51295	932.6		
Total	56	54248			

Appendix 3.11: Effect of Secondary Polymer Type on Polymer Toxicity Results

Source	DF	Adj SS	Adj MS	F-Value	P-Value
Secondary Polymer	4	12458	3114.5	3.88	0.008
Error	52	41790	803.7		
Total	56	54248			

Appendix 3.12: Effect of Secondary Polymer – Methacrylate/ Acrylate on Polymer Toxicity

Source	DF	Adj SS	Adj MS	F-Value	P-Value
Acrylate/ Methacrylate	1	3780	3780.1	4.12	0.047
Error	55	50468	917.6		
Total	56	54248			

Appendix 3.13: Effect of Polymer Ratio on Residue Toxicity

Source	DF	Adj SS	Adj MS	F-Value	P-Value
Primary Polymer Ratio	1	1387	1387	0.77	0.384
Error	55	98904	1798		
Total	56	100291			

Appendix 3.14: Effect of Polymer Type on Residue Toxicity

Source	DF	Adj SS	Adj MS	F-Value	P-Value
Primary Polymer	1	10955	10955	6.74	0.012
Error	55	89336	1624		
Total	56	100291			

Appendix 3.15: Effect of Secondary Polymer on Residue Toxicity

Source	DF	Adj SS	Adj MS	F-Value	P-Value
Secondary Polymer	4	38606	9651	8.14	0.000
Error	52	61685	1186		
Total	56	100291			

Appendix 3.16: Effect of Secondary Polymer – Methacrylate/ Acrylate on Residue Toxicity

Source	DF	Adj SS	Adj MS	F-Value	P-Value
Acrylate/ Methacrylate	1	26589	26589	19.84	0.000
Error	55	73702	1340		
Total	56	100291			

Appendix 3.17: Impact of Copolymer Ratio on Fungal Anti-Attachment

TEGMA:AODMBA$_{50:50}$ to TEGMA:AODMBA$_{40:60}$

Source	DF	Adj SS	Adj MS	F-Value	P-Value
TEGMA	1	22.81	22.815	4.61	0.098
Error	4	19.78	4.945		
Total	5	42.60			

Appendix 3.18: Impact of Copolymer Ratio on Fungal Anti-Attachment
From TEGMA:AODMBA$_{50:50}$ to TEGMA:AODMBA$_{35:65}$

Source	DF	Adj SS	Adj MS	F-Value	P-Value
TEGMA	1	4907.8	4907.76	83.92	0.001
Error	4	233.9	58.48		
Total	5	5141.7			

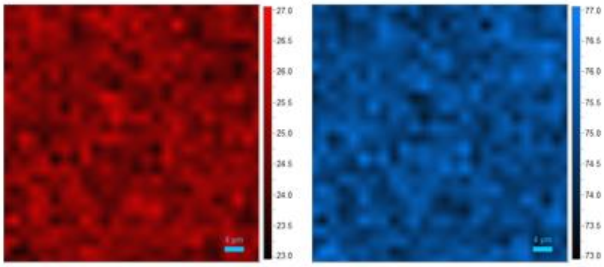
Appendix 3.19: Impact of Copolymer Ratio on Fungal Anti-Attachment
From TEGMA:AODMBA$_{50:50}$ to TEGMA:AODMBA$_{30:70}$

Source	DF	Adj SS	Adj MS	F-Value	P-Value
TEGMA	1	2633.4	2633.41	53.41	0.002
Error	4	197.2	49.31		
Total	5	2830.7			

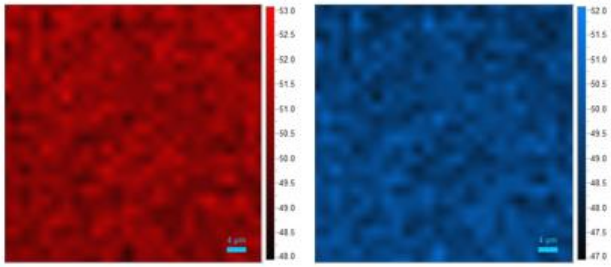
Appendix 4. Raman Spectroscopy Data (CLS Images)

TEGMA (Red), AODMBA (Blue), TBCHA (Green)

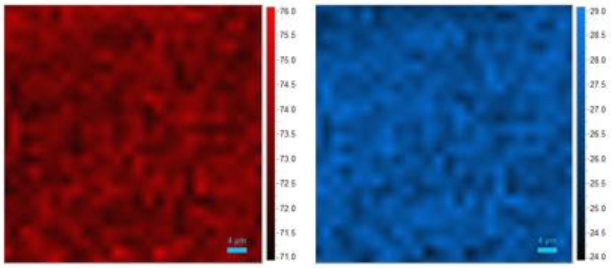
Appendix 4.1: TEGMA:AODMBA$_{25:75}$ (HTS UV-Cured)



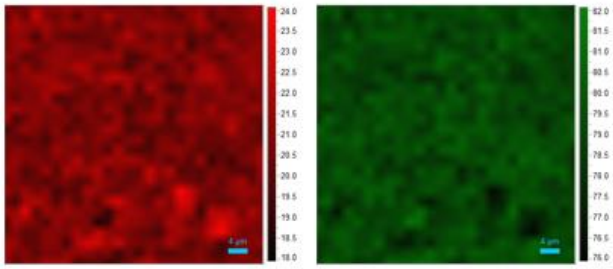
Appendix 4.2: TEGMA:AODMBA$_{50:50}$ (HTS UV-Cured)



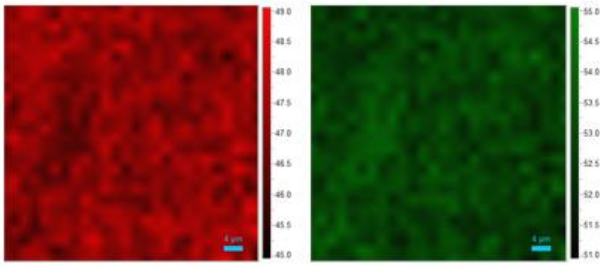
Appendix 4.3: TEGMA:AODMBA$_{75:25}$ (HTS UV-Cured)



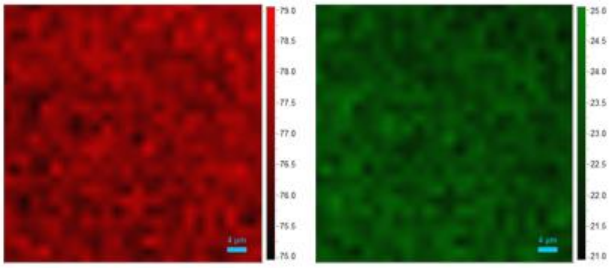
Appendix 4.4: TEGMA:TBCHA$_{25:75}$ (HTS UV-Cured)



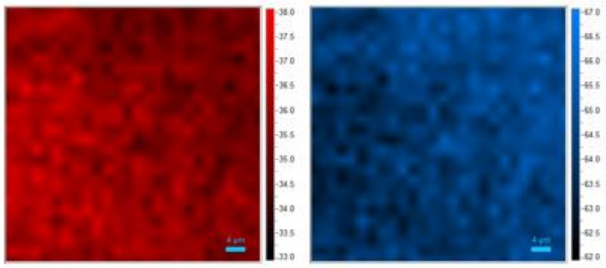
Appendix 4.5: TEGMA:TBCHA$_{50:50}$ (HTS UV-Cured)



Appendix 4.6: TEGMATBCHA:$_{75:25}$ (HTS UV-cured)



Appendix 4.7: TEGMA:AODMBA$_{40:60}$ (3D Printed)



Appendix 5. Gel Permeation Chromatography (GPC) Peak Analysis Results

Appendix 5.1: Thermally synthesised TEGMA:AODMBA$_{35:65}$

	Peak 1	Peak 2	Peak 3	Peak 4
Masses				
Injected Mass (µg)	100.00	100.00	100.00	100.00
Calculated Mass (µg)	116.76	-18.66	12.07	14.49
Mass Recovery (%)	116.8	-18.7	12.1	14.5
Mass Fraction (%)	93.7	-15.0	9.7	11.6
Molar mass moments (g/mol)				
Mn	4.145×10^{4} (±7.251%)	n/a	1.142×10^{3} (±7.251%)	4.651×10^{2} (±7.251%)
Mp	1.110×10^{5} (±7.251%)	0.000	1.135×10^{3} (±7.251%)	4.082×10^{2} (±7.251%)
Mv	n/a	n/a	n/a	n/a
Mw	1.139×10^{5} (±7.251%)	n/a	1.201×10^{3} (±7.251%)	4.916×10^{2} (±7.251%)
Mz	2.203×10^{5} (±16.213%)	n/a	1.263×10^{3} (±16.213%)	5.192×10^{2} (±16.213%)
Polydispersity				
Mw/Mn	2.748 (±10.254%)	n/a	1.052 (±10.254%)	1.057 (±10.254%)
Mz/Mn	5.316 (±17.760%)	n/a	1.106 (±17.760%)	1.116 (±17.760%)

Appendix 5.2: HTS UV-cured TEGMA:AODMBA$_{35:65}$

	Peak 1	Peak 5	Peak 6	Peak 7	Peak 8	Peak 9
Masses						
Injected Mass (µg)	100.00	100.00	100.00	100.00	100.00	100.00
Calculated Mass (µg)	-19.52	11.08	5.43	5.41	84.64	13.93
Mass Recovery (%)	-19.5	11.1	5.4	5.4	84.6	13.9
Mass Fraction (%)	-19.3	11.0	5.4	5.4	83.8	13.8
Molar mass moments (g/mol)						
Mn	n/a	2.485×10^{2} (±7.251%)	3.911×10^{2} (±7.251%)	5.925×10^{2} (±7.251%)	5.801×10^{4} (±7.251%)	1.535×10^{3} (±7.251%)
Mp	0.000	2.472×10^{2} (±7.251%)	3.854×10^{2} (±7.251%)	5.909×10^{2} (±7.251%)	1.141×10^{5} (±7.251%)	1.021×10^{3} (±7.251%)
Mv	n/a	n/a	n/a	n/a	n/a	n/a
Mw	n/a	2.516×10^{2} (±7.251%)	3.950×10^{2} (±7.251%)	6.001×10^{2} (±7.251%)	1.967×10^{5} (±7.251%)	1.977×10^{3} (±7.251%)
Mz	n/a	2.548×10^{2} (±16.213%)	3.989×10^{2} (±16.213%)	6.079×10^{2} (±16.213%)	4.397×10^{5} (±16.213%)	2.537×10^{3} (±16.213%)
Polydispersity						
Mw/Mn	n/a	1.012 (±10.254%)	1.010 (±10.254%)	1.013 (±10.254%)	3.390 (±10.254%)	1.288 (±10.254%)
Mz/Mn	n/a	1.025 (±17.760%)	1.020 (±17.760%)	1.026 (±17.760%)	7.580 (±17.760%)	1.653 (±17.760%)

Appendix 5.3: Thermally synthesised TEGMA:AODMBA$_{50:50}$

	Peak 1	Peak 2	Peak 3
Injected Mass (µg)	100.00	100.00	100.00
Calculated Mass (µg)	140.18	11.17	-17.45
Mass Recovery (%)	140.2	11.2	-17.5
Mass Fraction (%)	104.7	8.3	-13.0
Molar mass moments (g/mol)			
Mn	4.993×10^{4} (±7.251%)	4.681×10^{2} (±7.251%)	n/a
Mp	1.348×10^{5} (±7.251%)	5.564×10^{2} (±7.251%)	0.000
Mv	n/a	n/a	n/a
Mw	1.484×10^{5} (±7.251%)	4.927×10^{2} (±7.251%)	n/a
Mz	2.983×10^{5} (±16.213%)	5.177×10^{2} (±16.213%)	n/a
Polydispersity			
Mw/Mn	2.972 (±10.254%)	1.052 (±10.254%)	n/a
Mz/Mn	5.974 (±17.760%)	1.106 (±17.760%)	n/a

Appendix 5.4: HTS UV-cured TEGMA:AODMBA$_{50:50}$

	Peak 1	Peak 4	Peak 5	Peak 6	Peak 7	Peak 8
Masses						
Injected Mass (µg)	100.00	100.00	100.00	100.00	100.00	100.00
Calculated Mass (µg)	-16.99	11.76	3.46	7.76	16.02	93.69
Mass Recovery (%)	-17.0	11.8	3.5	7.8	16.0	93.7
Mass Fraction (%)	-14.7	10.2	3.0	6.7	13.8	81.0
Molar mass moments (g/mol)						
Mn	n/a	2.721×10^{2} (±7.251%)	4.261×10^{2} (±7.251%)	6.492×10^{2} (±7.251%)	1.817×10^{3} (±7.251%)	5.054×10^{4} (±7.251%)
Mp	0.000	2.699×10^{2} (±7.251%)	4.273×10^{2} (±7.251%)	6.428×10^{2} (±7.251%)	1.127×10^{3} (±7.251%)	8.340×10^{4} (±7.251%)
Mv	n/a	n/a	n/a	n/a	n/a	n/a
Mw	n/a	2.758×10^{2} (±7.251%)	4.288×10^{2} (±7.251%)	6.630×10^{2} (±7.251%)	2.350×10^{3} (±7.251%)	1.956×10^{5} (±7.251%)
Mz	n/a	2.798×10^{2} (±16.213%)	4.315×10^{2} (±16.213%)	6.772×10^{2} (±16.213%)	3.037×10^{3} (±16.213%)	5.536×10^{5} (±16.213%)
Polydispersity						
Mw/Mn	n/a	1.014 (±10.254%)	1.006 (±10.254%)	1.021 (±10.254%)	1.293 (±10.254%)	3.871 (±10.254%)
Mz/Mn	n/a	1.028 (±17.760%)	1.013 (±17.760%)	1.043 (±17.760%)	1.672 (±17.760%)	10.953 (±17.760%)

Appendix 5.5: Thermally synthesised TEGMA:AODMBA$_{40:60}$

	Peak 1	Peak 2	Peak 3
Injected Mass (µg)	100.00	100.00	100.00
Calculated Mass (µg)	160.85	101.22	3.61
Mass Recovery (%)	160.9	101.2	3.6
Mass Fraction (%)	60.5	38.1	1.4
Molar mass moments (g/mol)			
Mn	4.400×10^{4} (±7.251%)	3.023×10^{2} (±7.251%)	1.118×10^{1} (±7.251%)
Mp	1.165×10^{5} (±7.251%)	3.288×10^{2} (±7.251%)	1.102×10^{1} (±7.251%)
Mv	n/a	n/a	n/a
Mw	1.216×10^{5} (±7.251%)	3.133×10^{2} (±7.251%)	1.141×10^{1} (±7.251%)
Mz	2.348×10^{5} (±16.213%)	3.249×10^{2} (±16.213%)	1.165×10^{1} (±16.213%)
Polydispersity			
Mw/Mn	2.764 (±10.254%)	1.036 (±10.254%)	1.021 (±10.254%)
Mz/Mn	5.335 (±17.760%)	1.075 (±17.760%)	1.042 (±17.760%)

Appendix 5.6: HTS UV-cured TEGMA:AODMBA$_{40:60}$

	Peak 1	Peak 4	Peak 5	Peak 6	Peak 7	Peak 8
Masses						
Injected Mass (µg)	100.00	100.00	100.00	100.00	100.00	100.00
Calculated Mass (µg)	-17.24	9.66	4.55	6.70	14.66	55.21
Mass Recovery (%)	-17.2	9.7	4.5	6.7	14.7	55.2
Mass Fraction (%)	-23.4	13.1	6.2	9.1	19.9	75.1
Molar mass moments (g/mol)						
Mn	n/a	2.690×10^{2} (±7.251%)	4.189×10^{2} (±7.251%)	6.458×10^{2} (±7.251%)	1.724×10^{3} (±7.251%)	5.893×10^{4} (±7.251%)
Mp	0.000	2.660×10^{2} (±7.251%)	4.141×10^{2} (±7.251%)	6.339×10^{2} (±7.251%)	1.112×10^{3} (±7.251%)	1.180×10^{5} (±7.251%)
Mv	n/a	n/a	n/a	n/a	n/a	n/a
Mw	n/a	2.721×10^{2} (±7.251%)	4.227×10^{2} (±7.251%)	6.573×10^{2} (±7.251%)	2.244×10^{3} (±7.251%)	1.834×10^{5} (±7.251%)
Mz	n/a	2.754×10^{2} (±16.213%)	4.266×10^{2} (±16.213%)	6.692×10^{2} (±16.213%)	2.969×10^{3} (±16.213%)	4.228×10^{5} (±16.213%)
Polydispersity						
Mw/Mn	n/a	1.012 (±10.254%)	1.009 (±10.254%)	1.018 (±10.254%)	1.302 (±10.254%)	3.111 (±10.254%)
Mz/Mn	n/a	1.024 (±17.760%)	1.018 (±17.760%)	1.036 (±17.760%)	1.723 (±17.760%)	7.175 (±17.760%)

Appendix 5.7: 3D Printed TEGMA:AODMBA$_{40:60}$

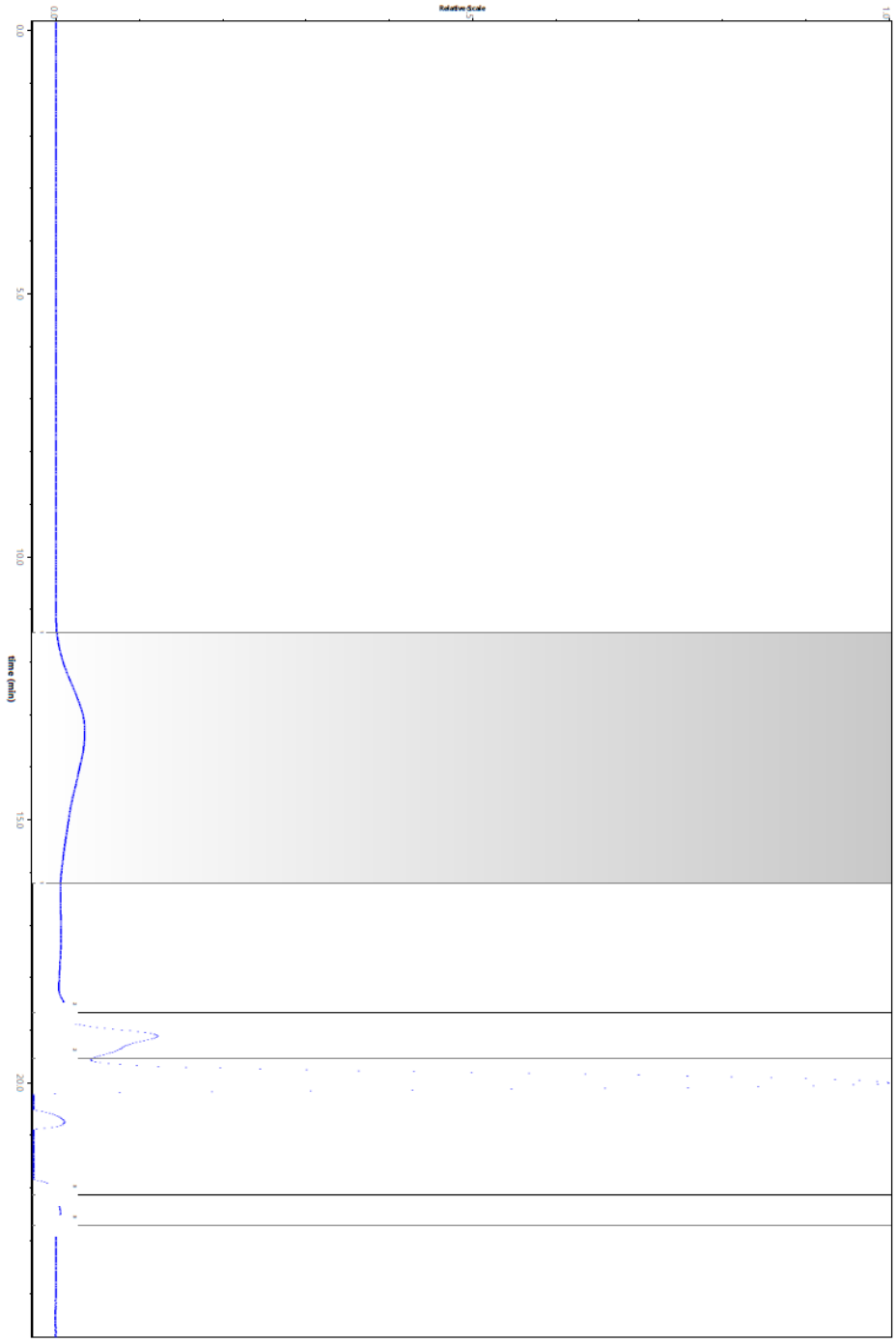
	Peak 1
Injected Mass (µg)	200.00
Calculated Mass (µg)	161.36
Mass Recovery (%)	80.7
Mass Fraction (%)	100.0
Molar mass moments (g/mol)	
Mn	5.218×10^{3} (±30.896%)
Mp	1.065×10^{4} (±30.896%)
Mv	n/a
Mw	3.301×10^{4} (±30.896%)
Mz	1.136×10^{5} (±69.084%)
Polydispersity	
Mw/Mn	6.326 (±43.693%)
Mz/Mn	21.765 (±75.678%)

Appendix 5.8: TEGMA Oligomer

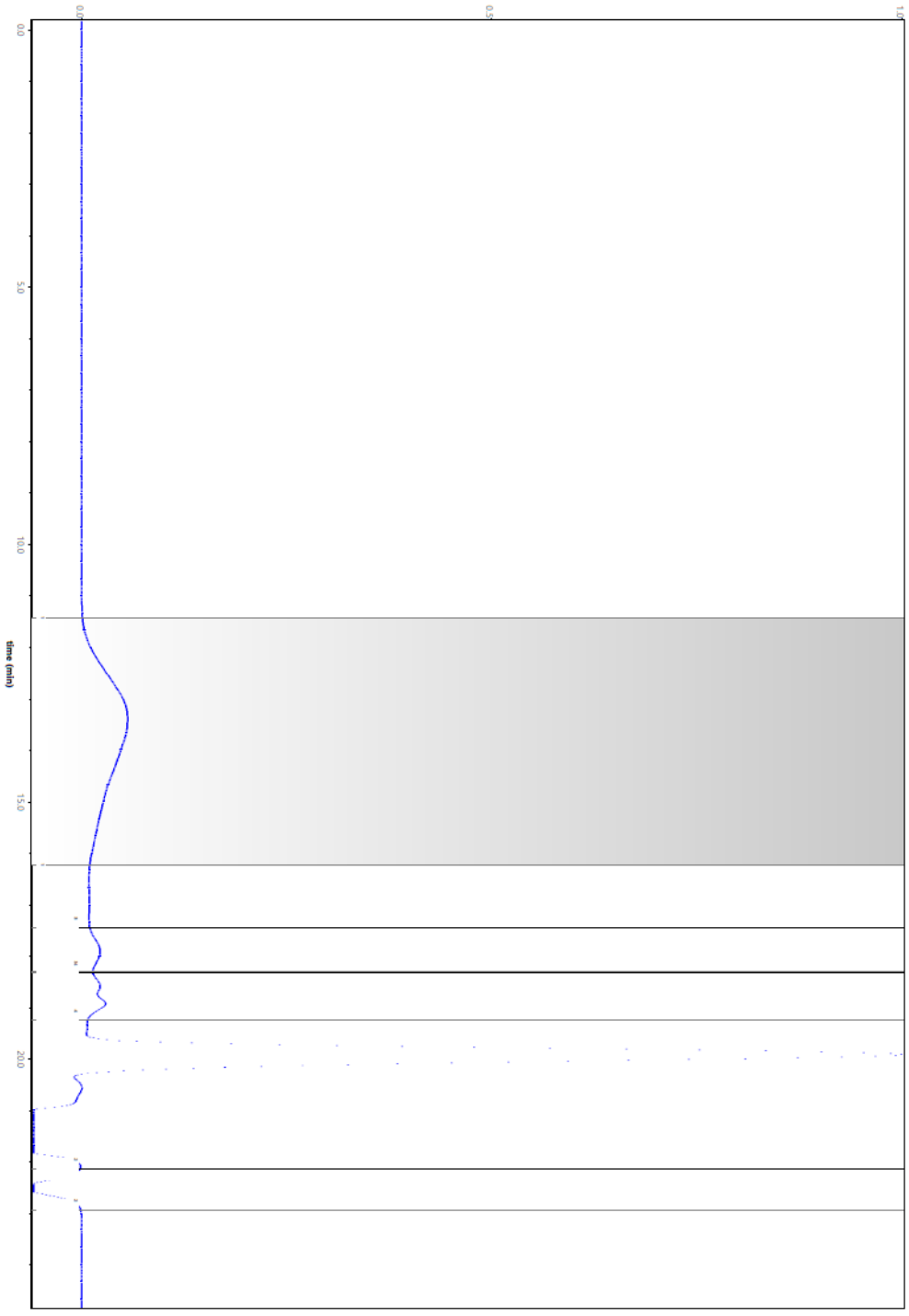
	Peak 1	Peak 2	Peak 3
Injected Mass (µg)	100.00	100.00	100.00
Calculated Mass (µg)	130.04	-16.88	5.75
Mass Recovery (%)	130.0	-16.9	5.7
Mass Fraction (%)	109.4	-14.2	4.8
Molar mass moments (g/mol)			
Mn	1.234×10^{3} (±30.896%)	n/a	1.203×10^{2} (±30.896%)
Mp	2.112×10^{3} (±30.896%)	0.000	1.414×10^{2} (±30.896%)
Mv	2.898×10^{3} (±2.416%)	NaN (±NaN%)	n/a
Mw	3.242×10^{3} (±30.896%)	n/a	1.265×10^{2} (±30.896%)
Mz	6.371×10^{3} (±69.084%)	n/a	1.327×10^{2} (±69.084%)
Polydispersity			
Mw/Mn	2.627 (±43.693%)	n/a	1.052 (±43.693%)
Mz/Mn	5.163 (±75.678%)	n/a	1.104 (±75.678%)

Appendix 6. Gel Permeation Chromatography (GPC) Chromatogram

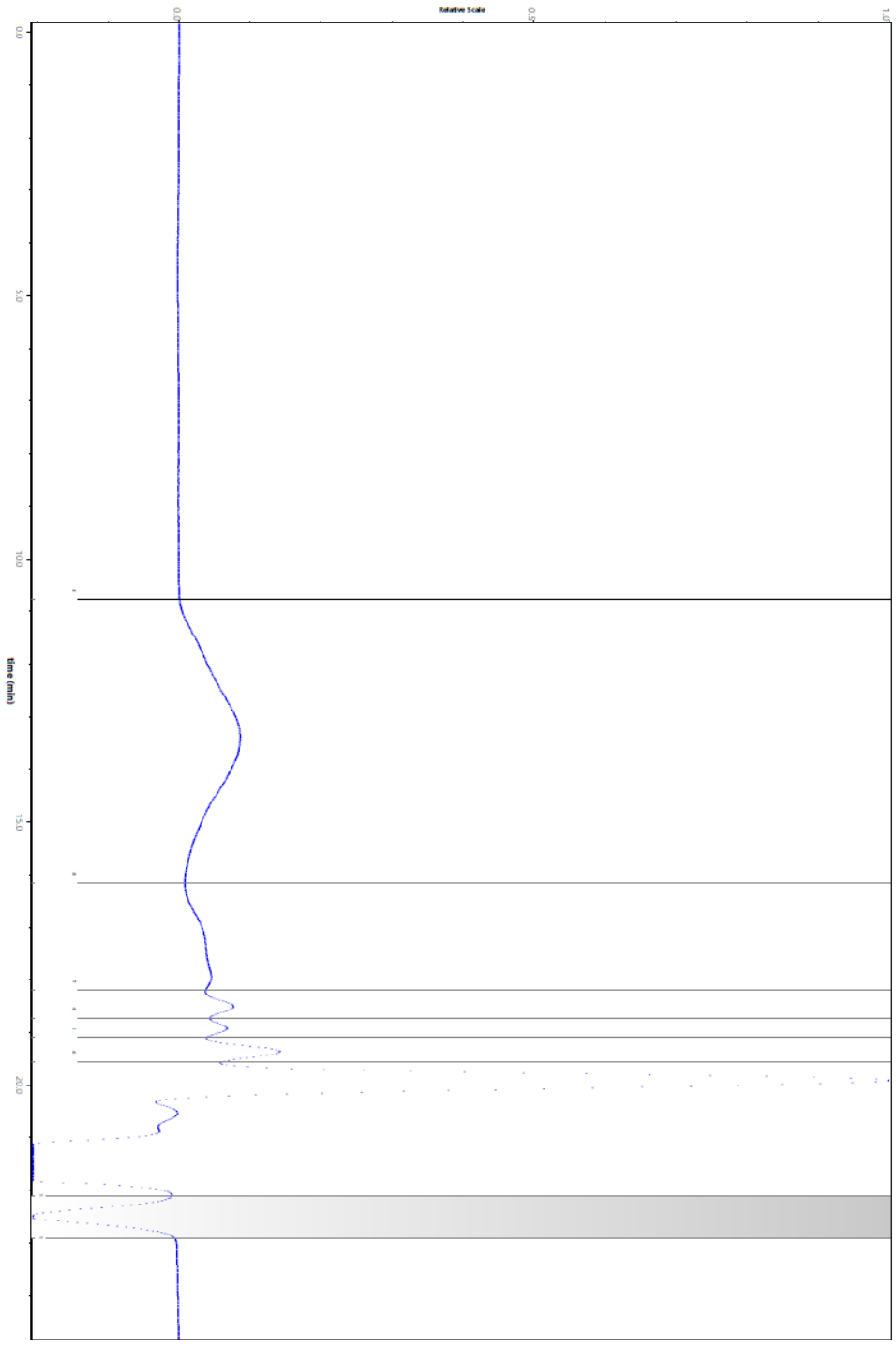
Appendix 6.1: Thermally synthesised TEGMA:AODMBA$_{40:60}$



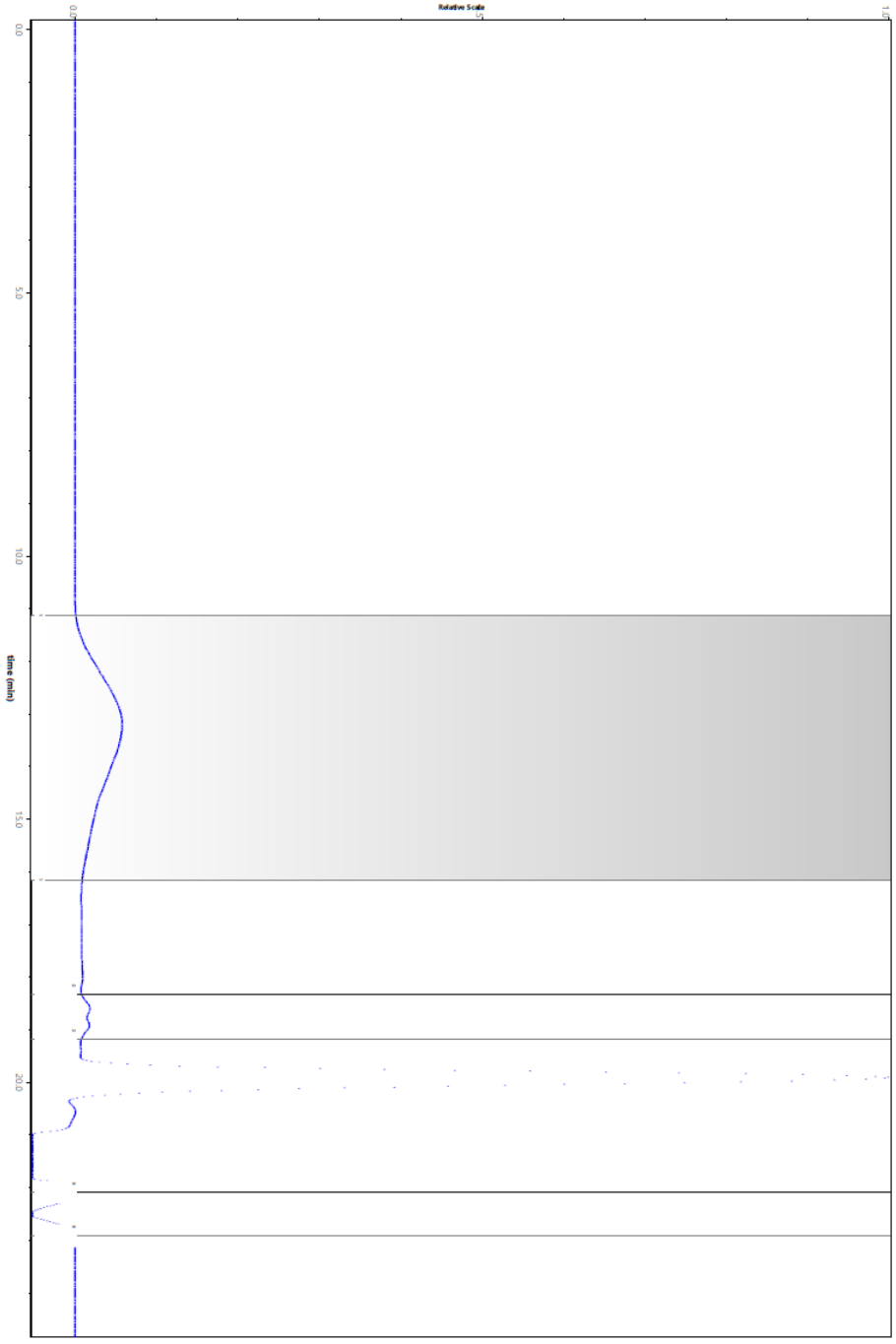
Appendix 6.2: HTS UV-cured TEGMA:AODMBA$_{40:60}$



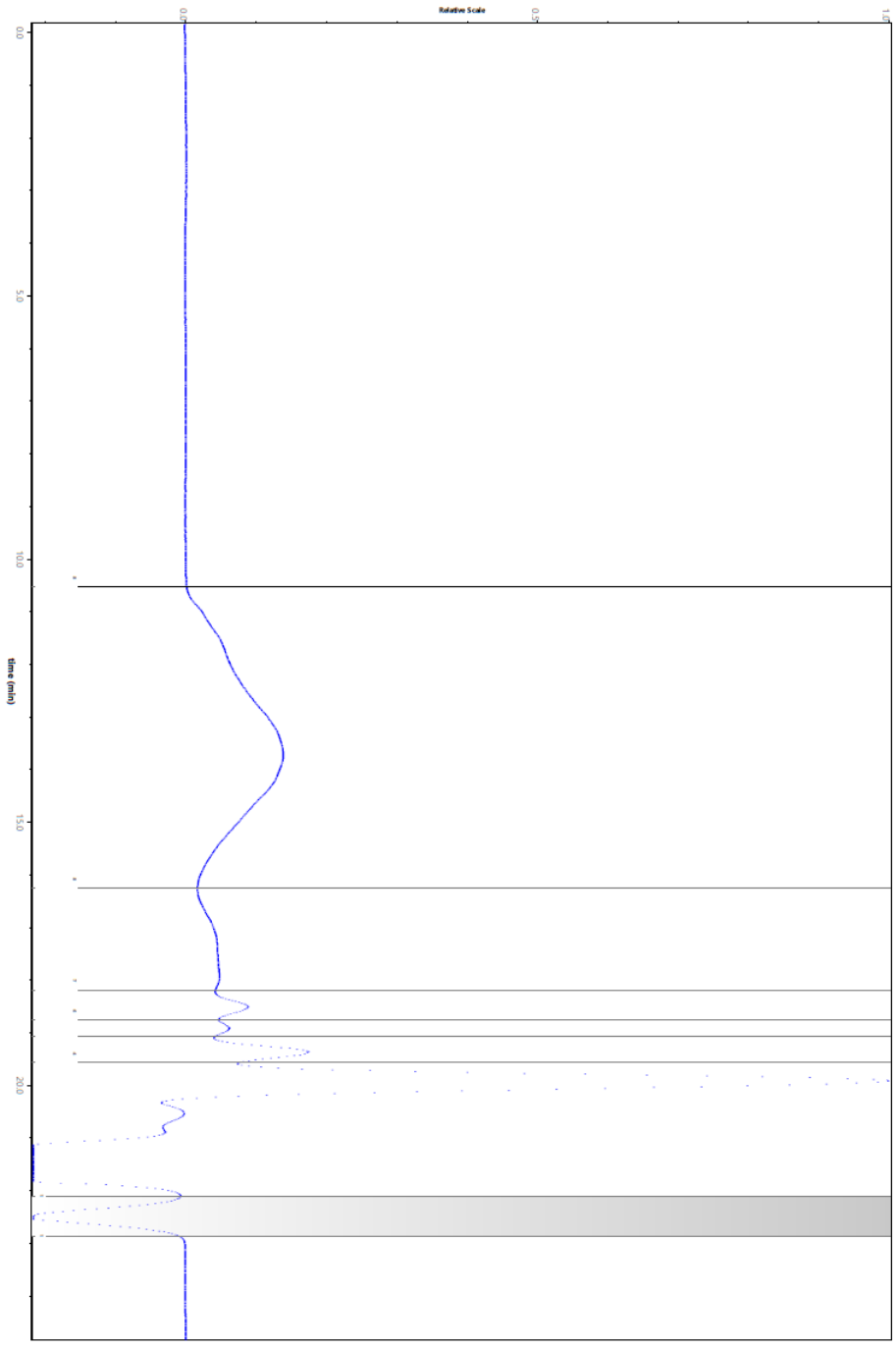
Appendix 6.3: 3D Printed TEGMA:AODMBA$_{40:60}$



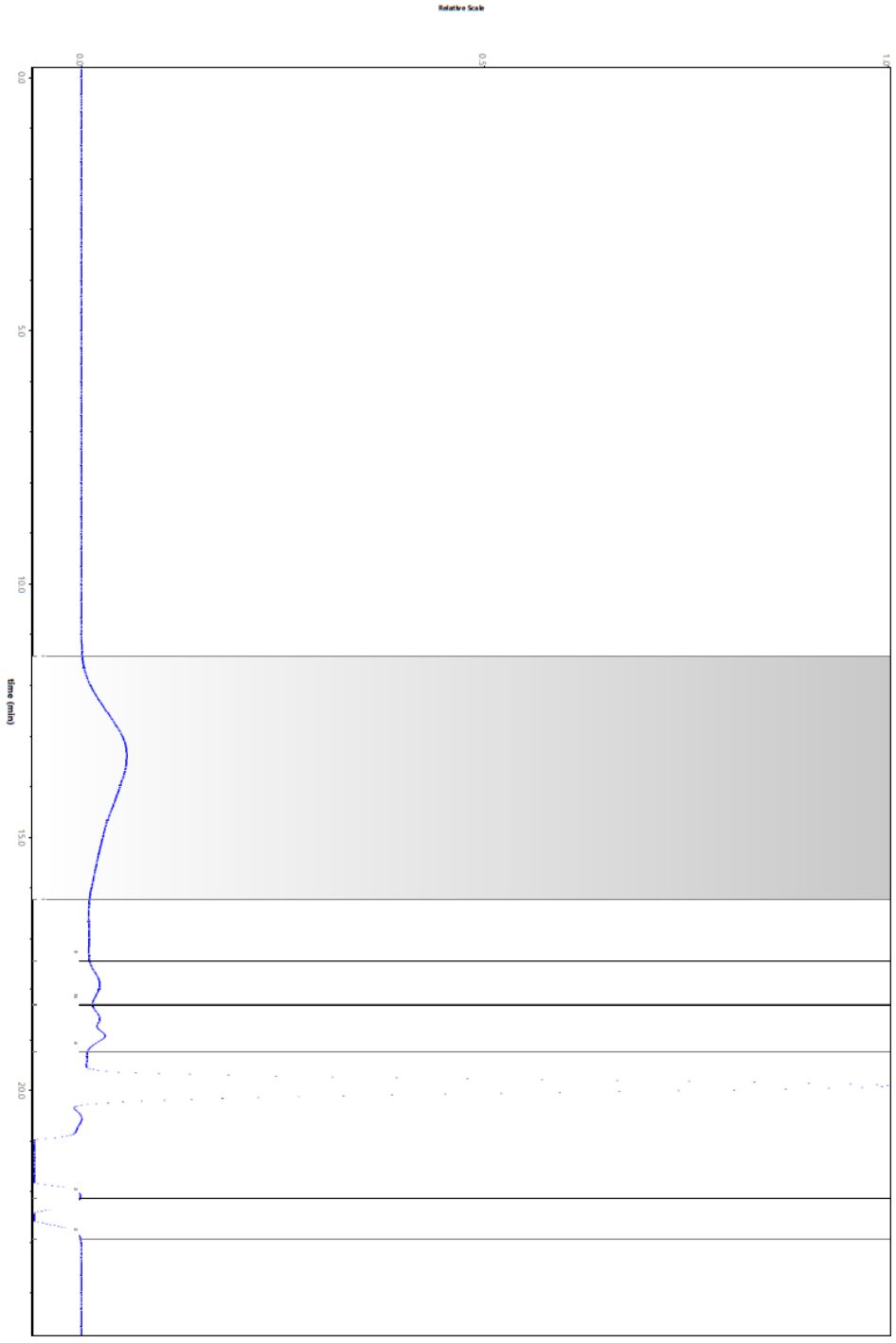
Appendix 6.4: Thermally synthesised TEGMA:ADOBMA$_{50:50}$



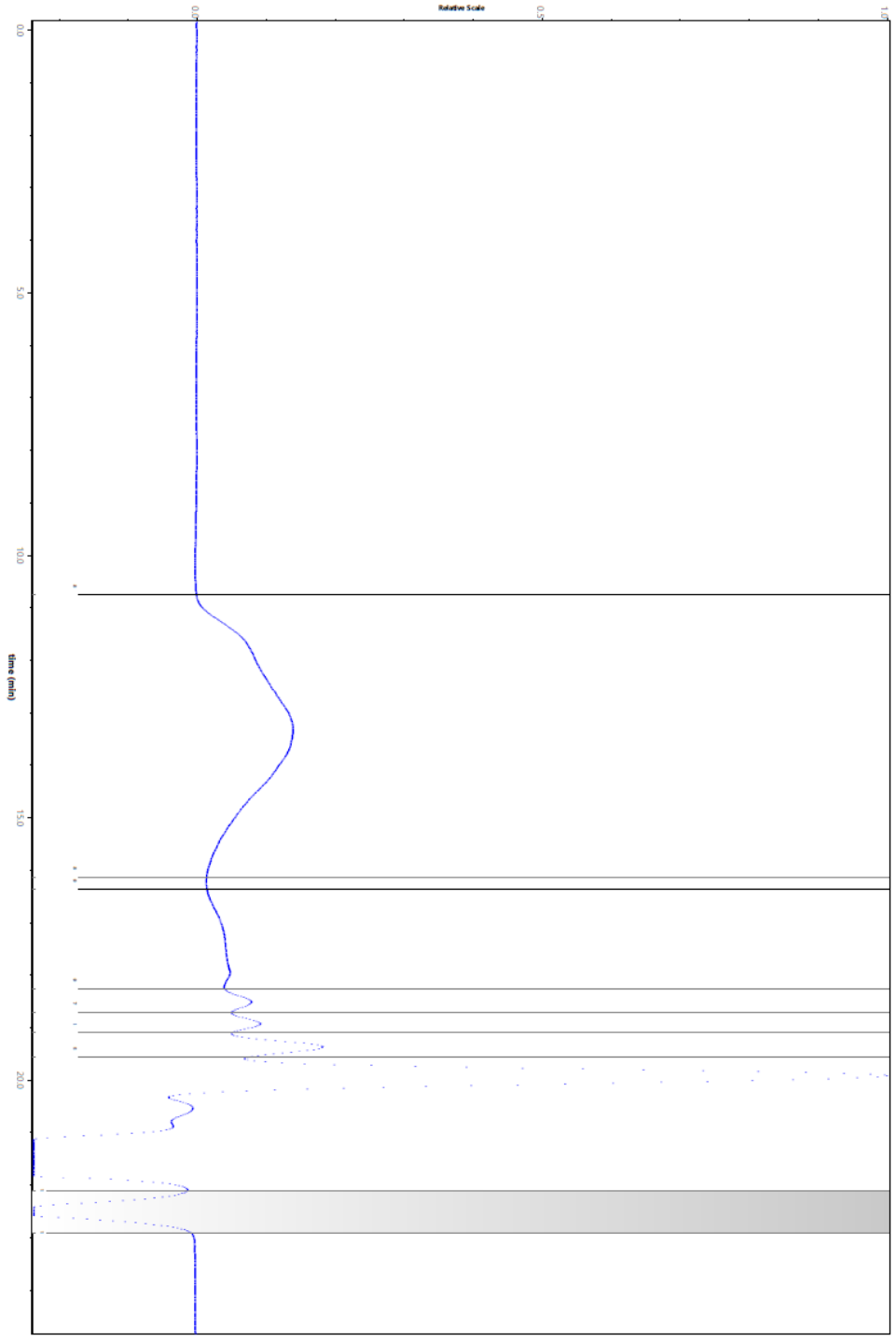
Appendix 6.5: HTS UV-cured TEGMA:AODMBA$_{50:50}$



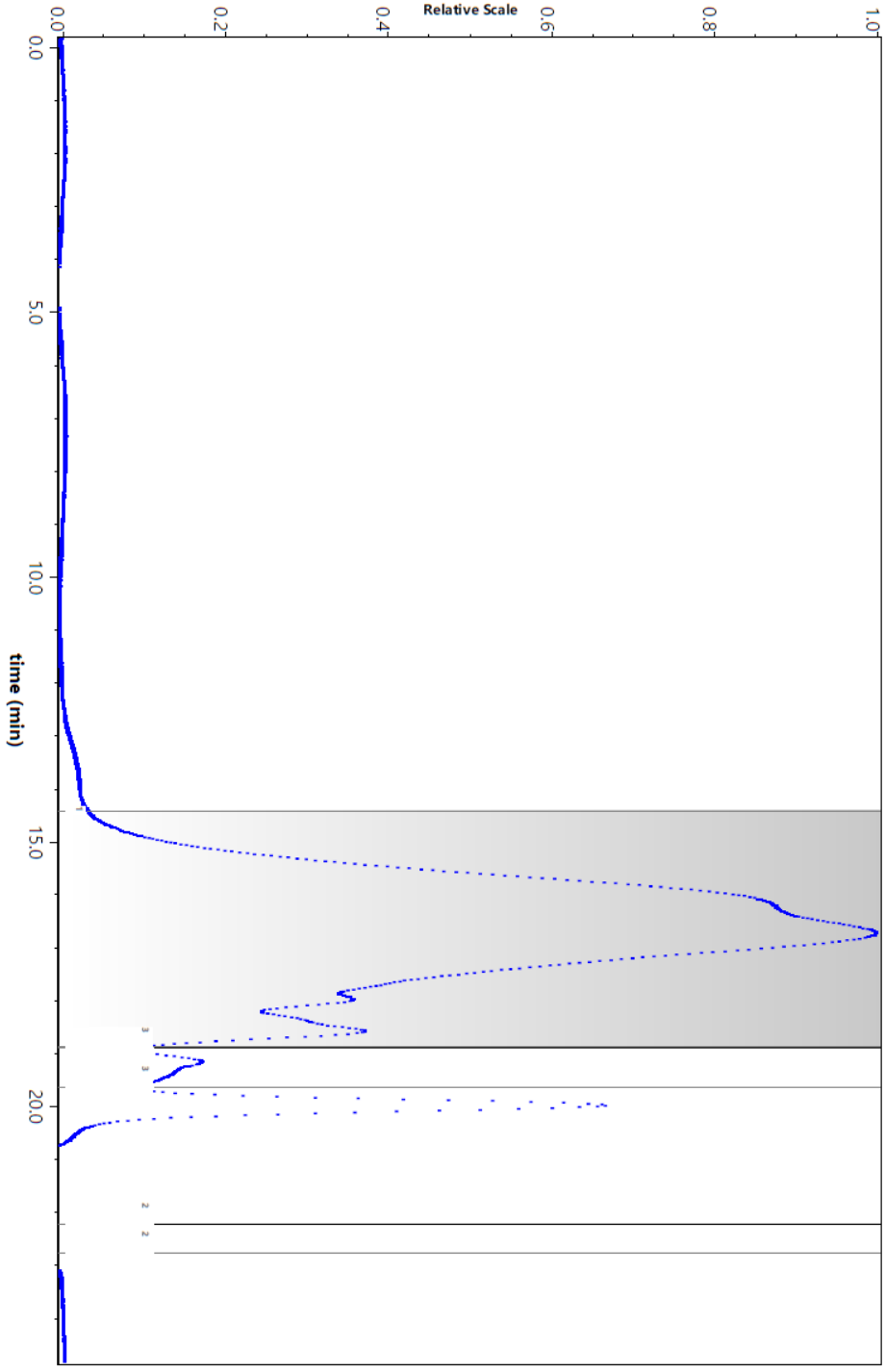
Appendix 6.6: Thermally synthesised TEGMA:AODMBA35:65



Appendix 6.7: HTS UV-cured TEGMA:AODMBA$_{35:65}$

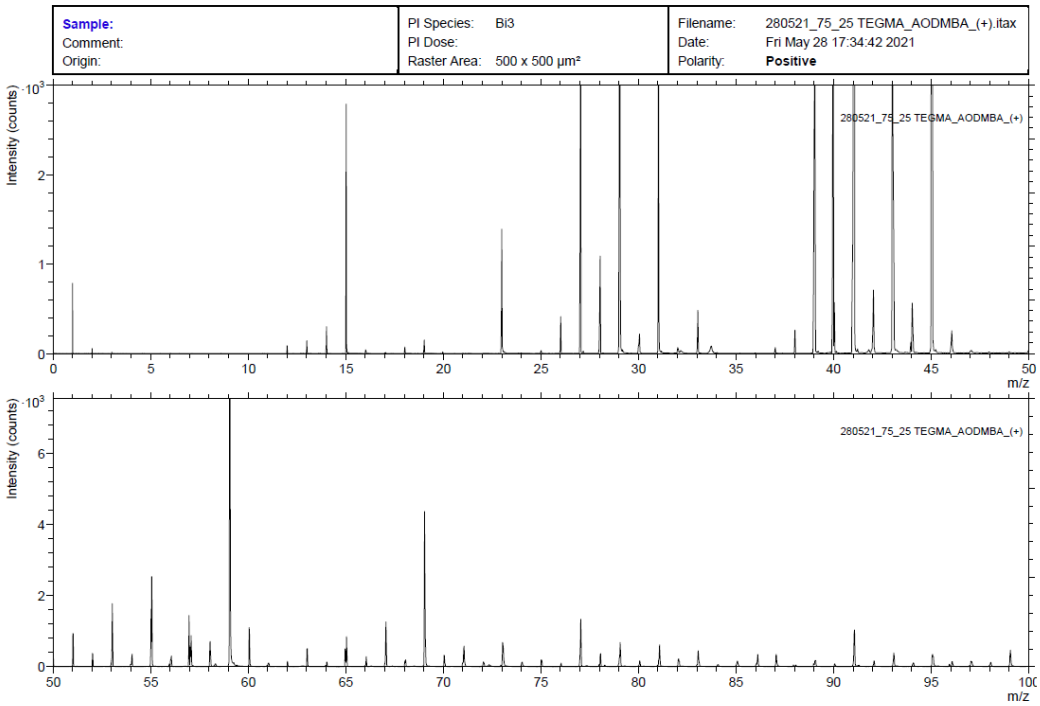


Appendix 6.8: Thermally synthesised TEGMA Oligomer

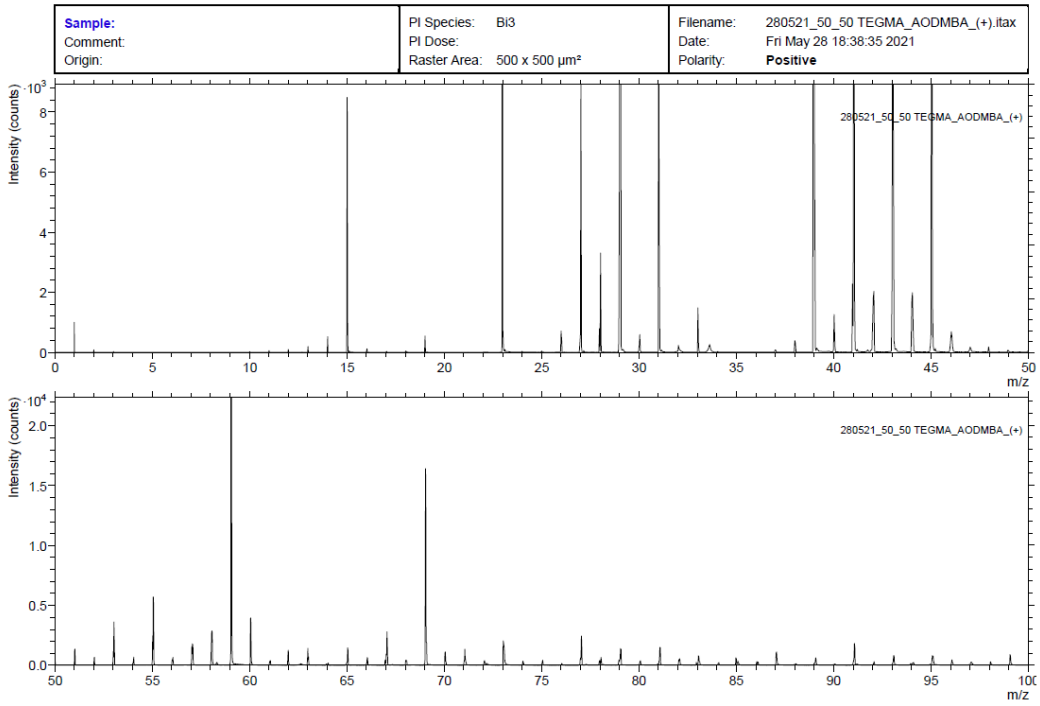


Appendix 7. Time-of-Flight Secondary Ion Mass Spectrometry (ToF-SIMS)

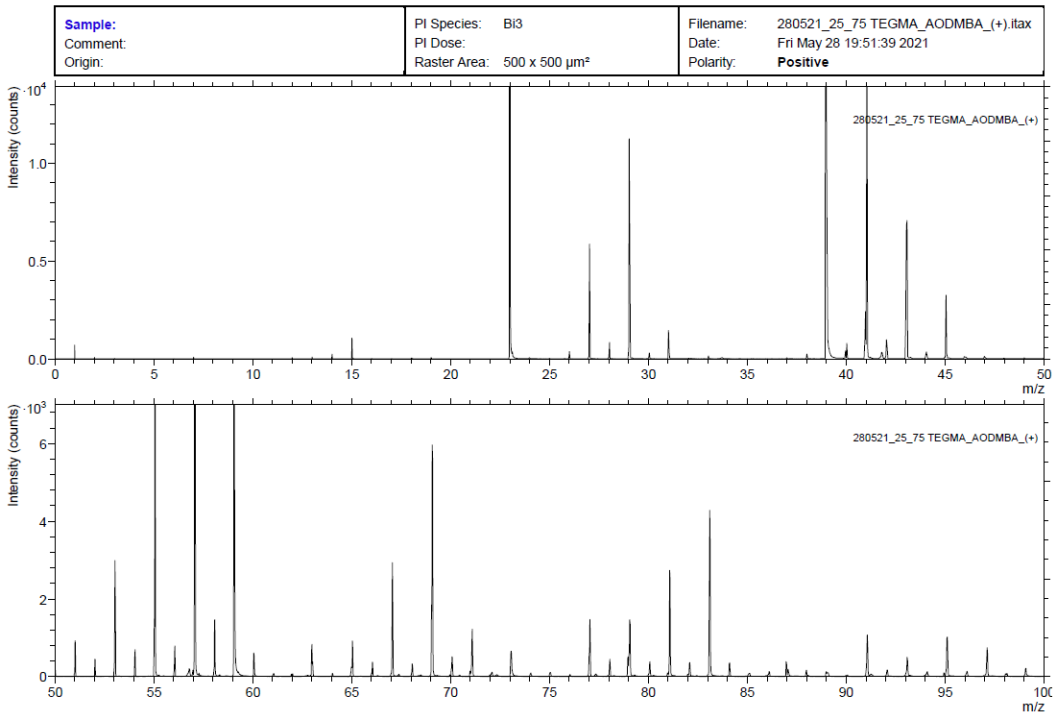
Appendix 7.1: TEGMA:AODMBA$_{75:25}$ (0 – 100 m/z)



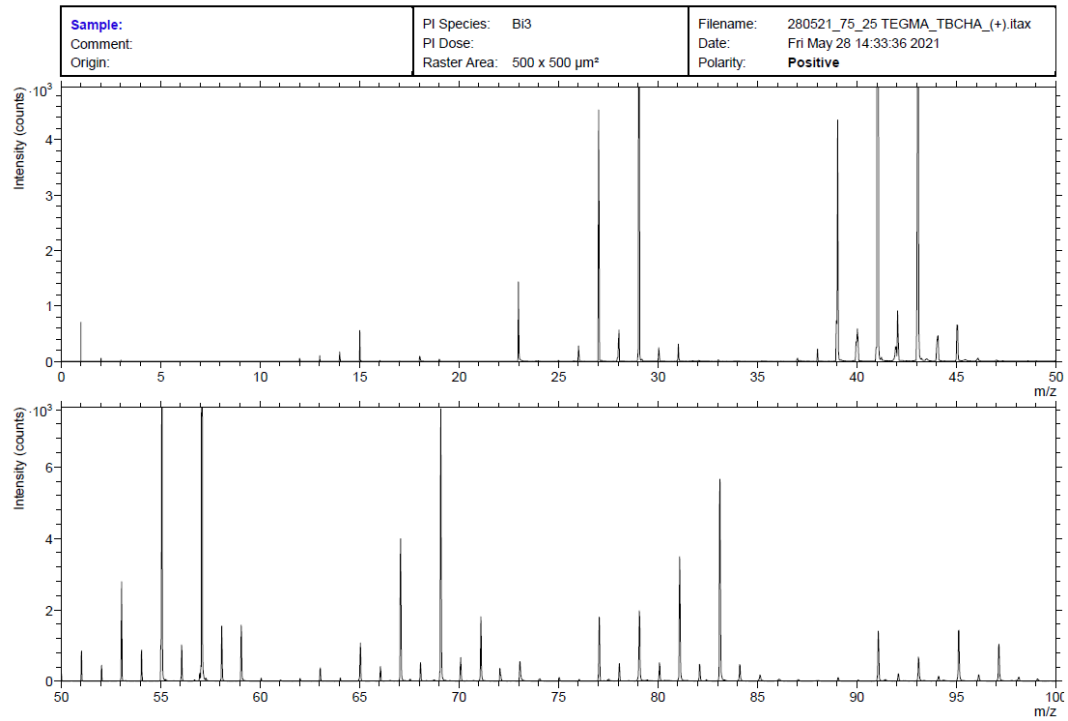
Appendix 7.2: TEGMA:AODMBA$_{50:50}$ (0 – 100 m/z)



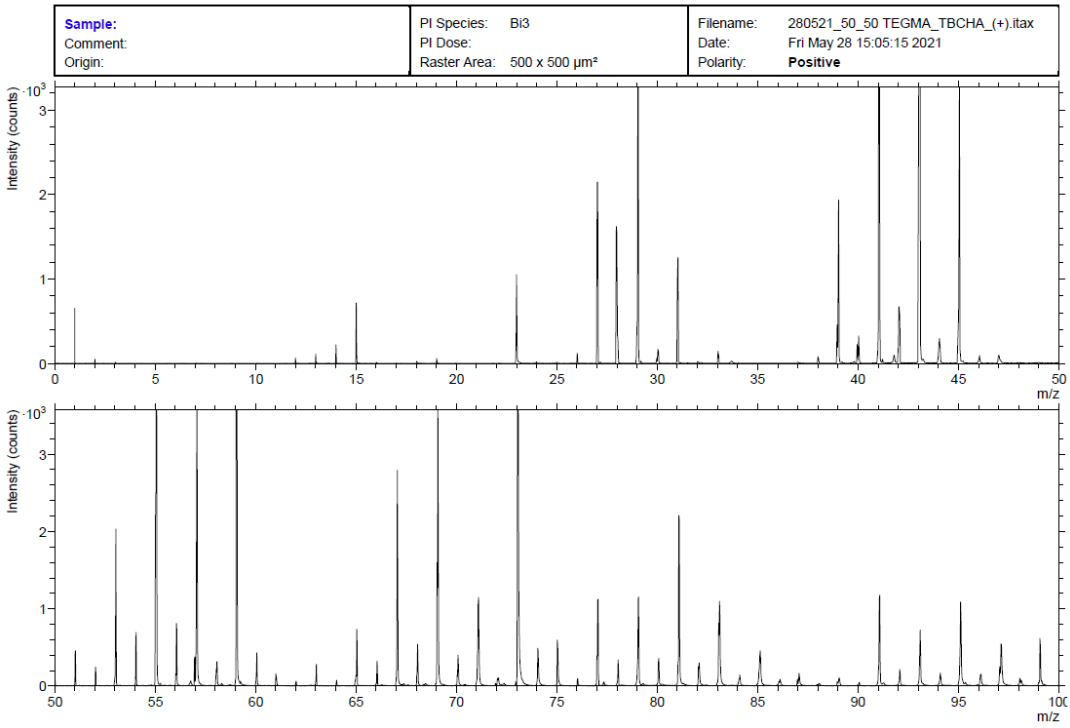
Appendix 7.3: TEGMA:AODMBA$_{25:75}$ (0 – 100 m/z)



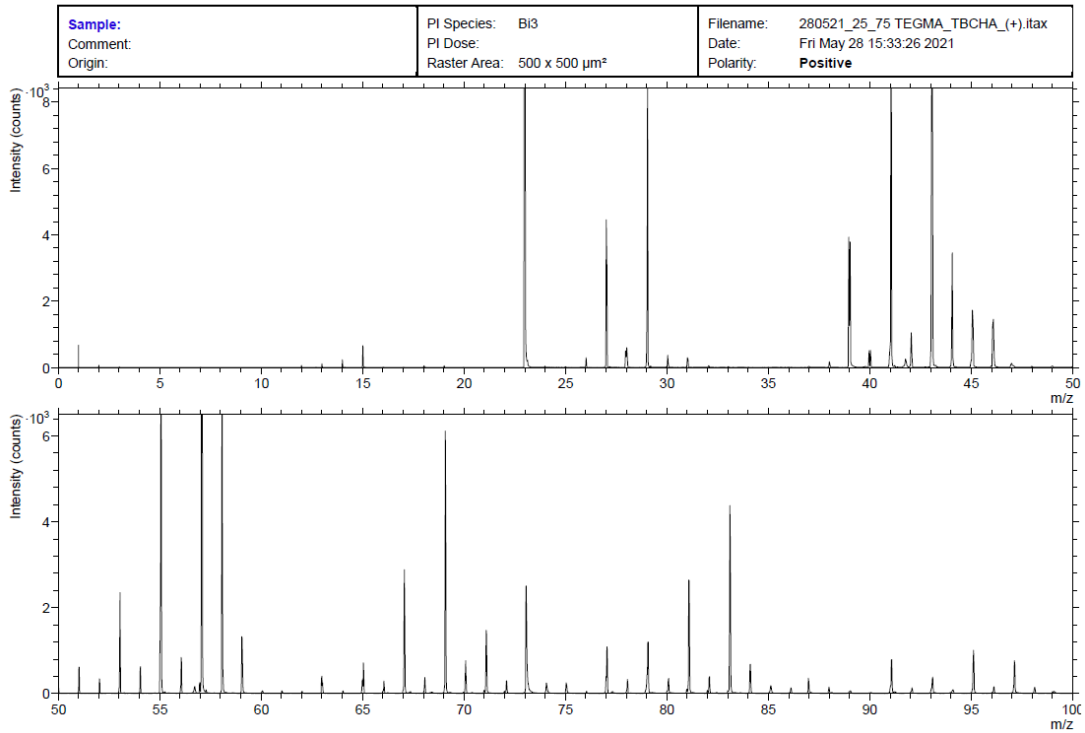
Appendix 7.4: TEGMA:TBCHA$_{75:25}$ (0 – 100 m/z)



Appendix 7.5: TEGMA:TBCHA$_{50:50}$ (0 – 100 m/z)

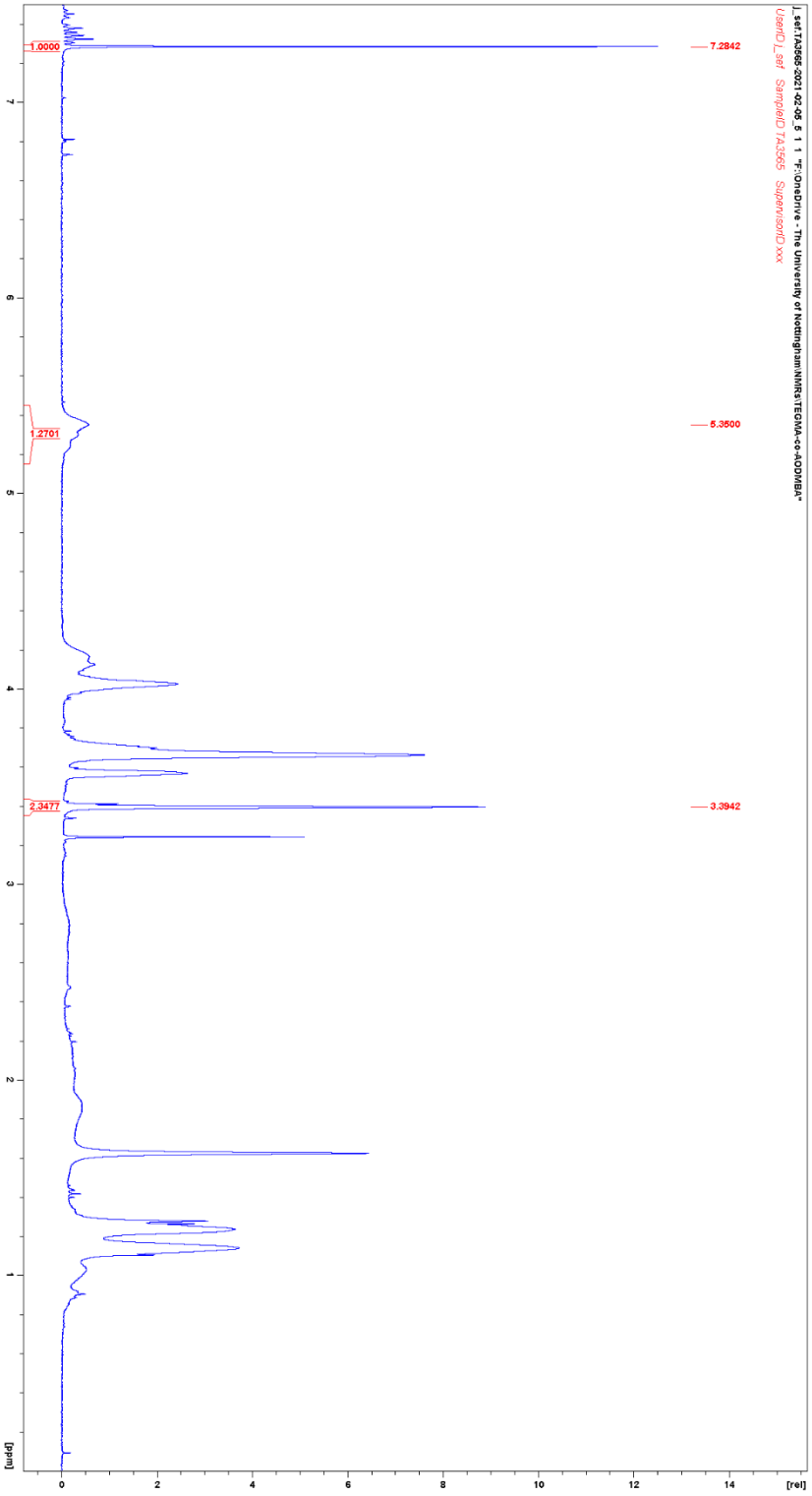


Appendix 7.6: TEGMA:TBCHA$_{25:75}$ (0 – 100 m/z)

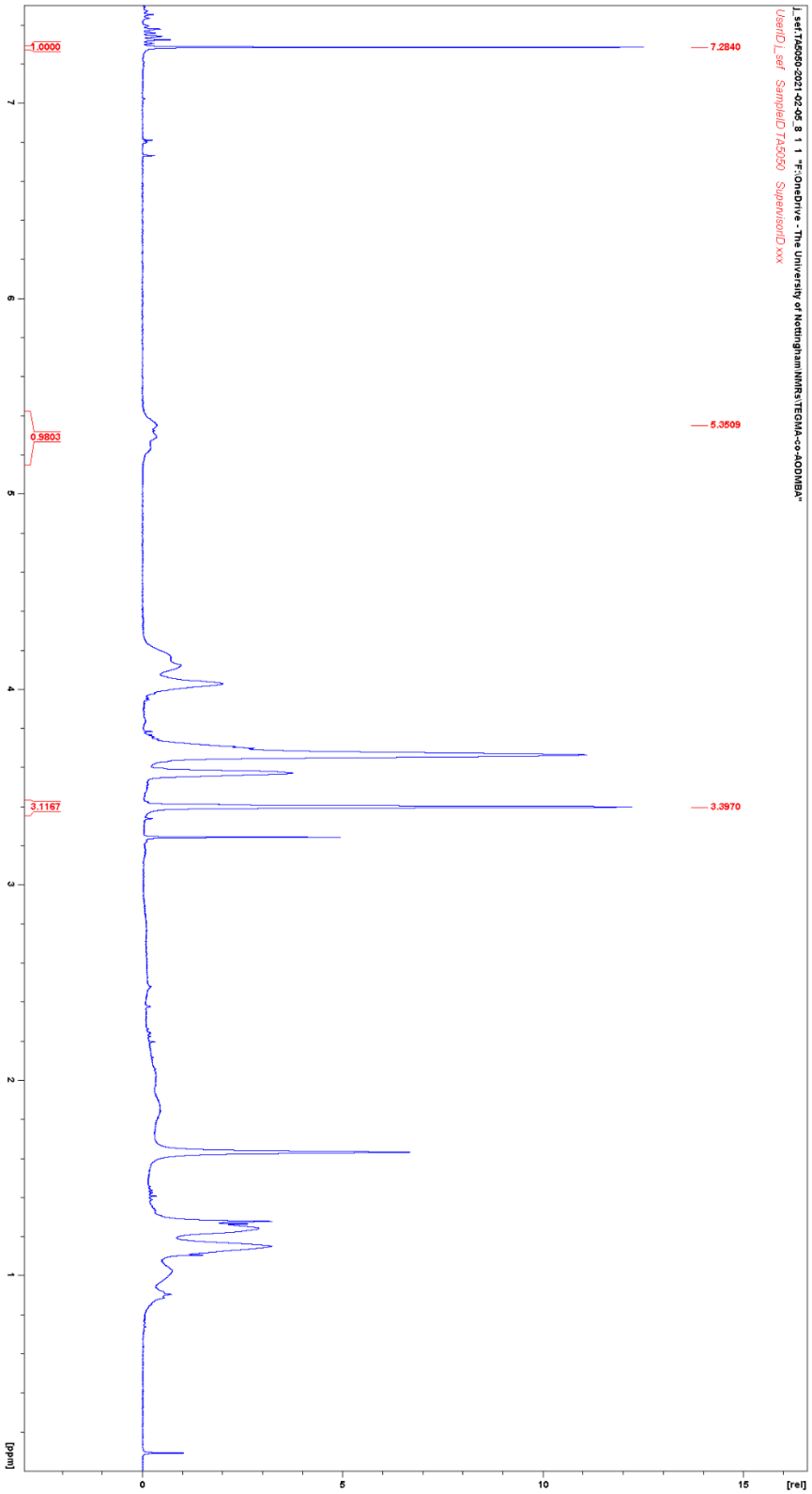


Appendix 8. Nuclear Magnetic Resonance (NMR)

Appendix 8.1: NMR of HTS UV-cured TEGMA:AODMBA$_{35:65}$

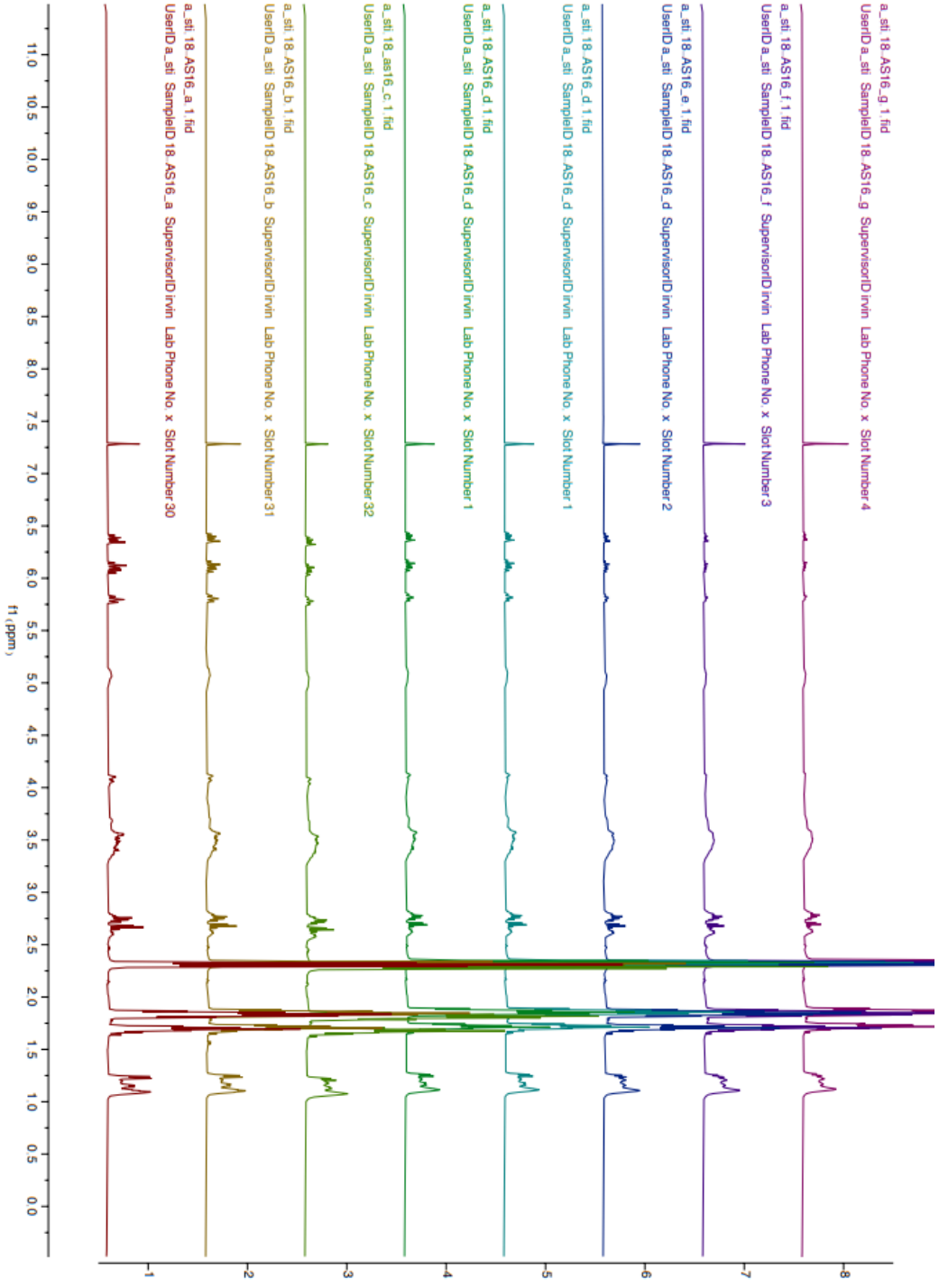


Appendix 8.2: NMR of HTS UV-cured TEGMA:AODMBA$_{50:50}$



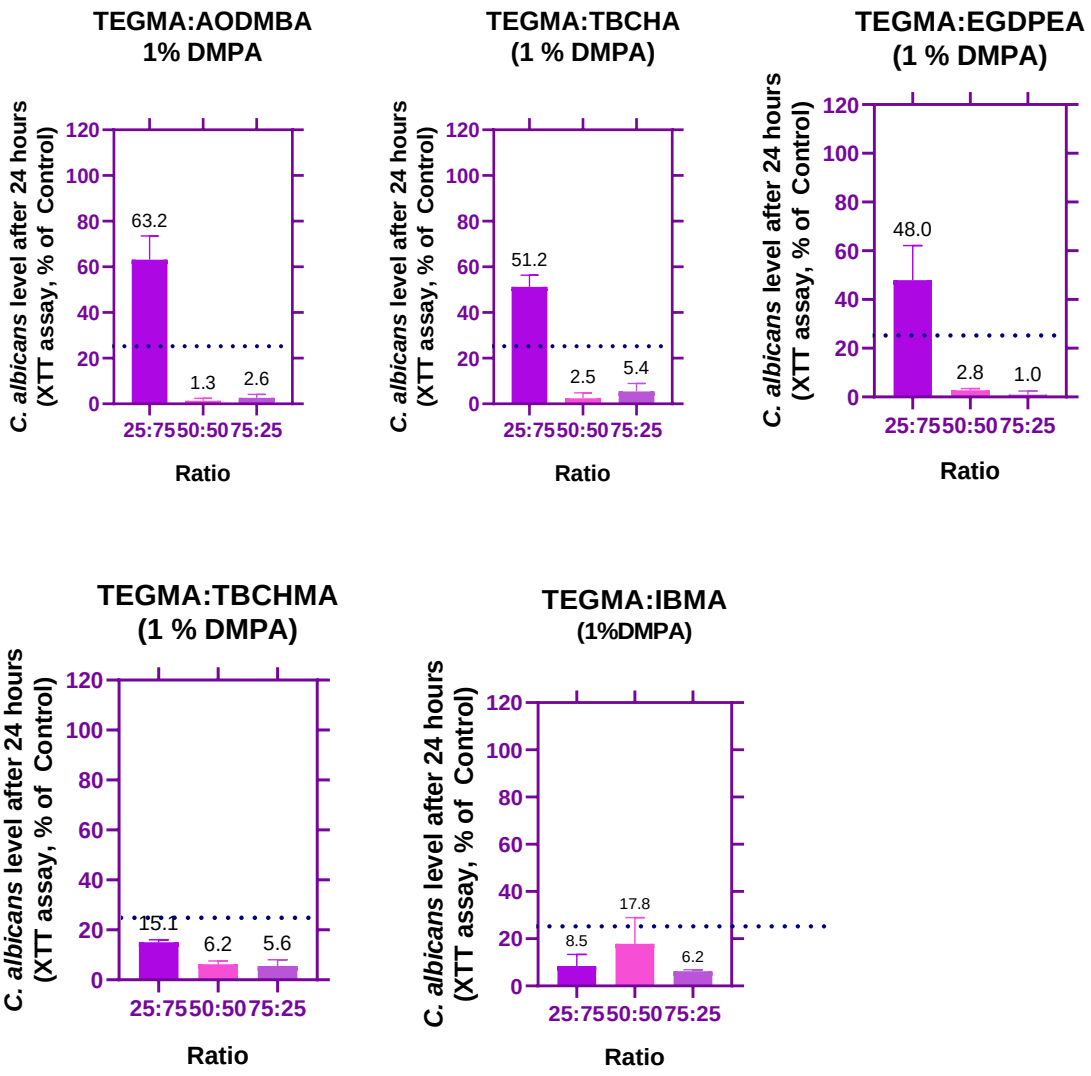
Appendix 8.3: NMR of showing HPB-TPGDA Polymerisation Process

Reduction in acrylate peak at 5.5-6.5 ppm from lowest NMR graph to highest NMR graph signifies depletion of monomers with polymerisation process.

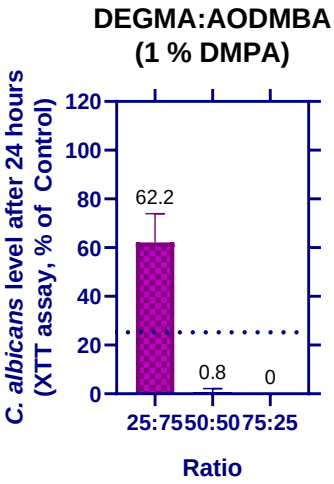


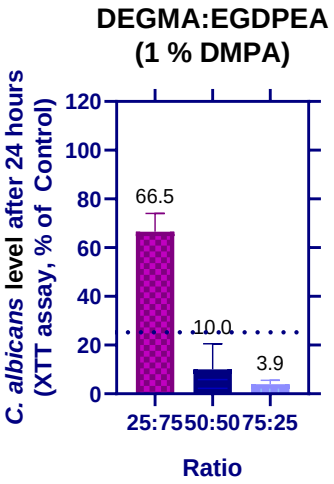
Appendix 9. Fungal Attachment Studies for Copolymer (XTT Assay)

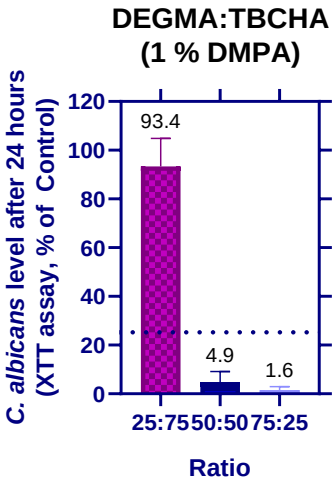
Appendix 9.1: TEGMA-based Copolymers with 1 % DMPA initiator

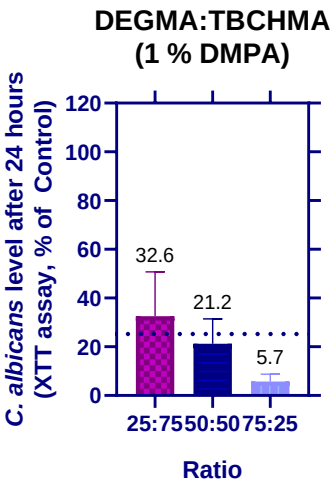


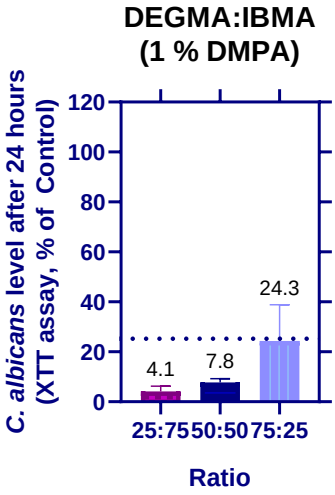
Appendix 9.2: DEGMA-based Copolymers with 1 % DMPA initiator



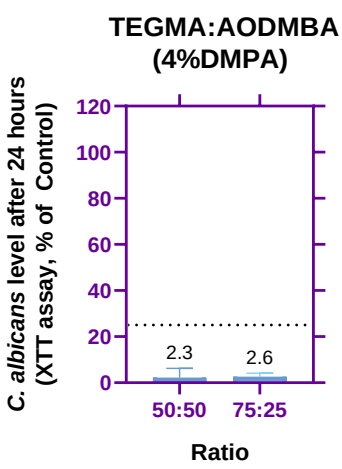


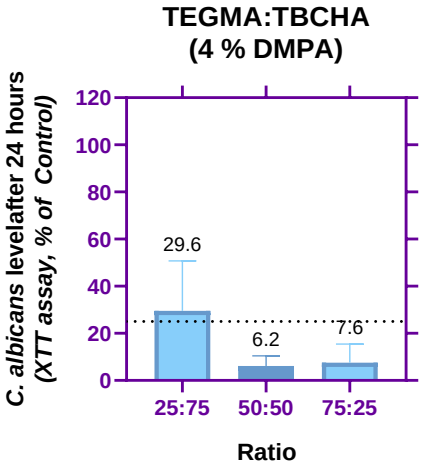


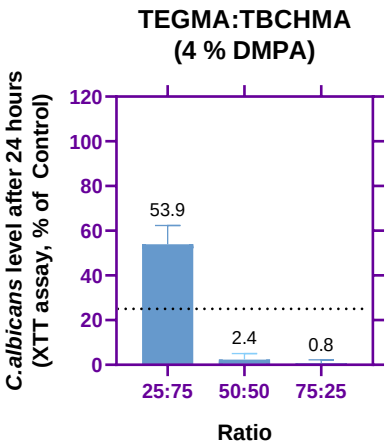


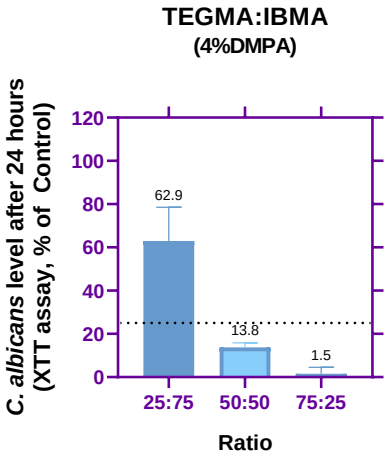


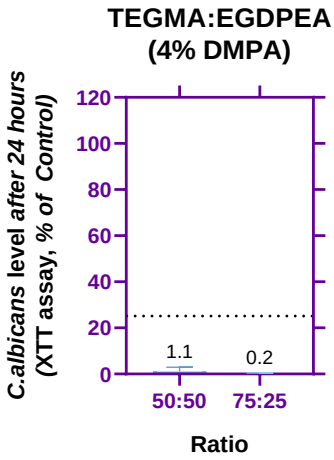
Appendix 9.3: TEGMA-based Copolymers with 4 % DMPA initiator



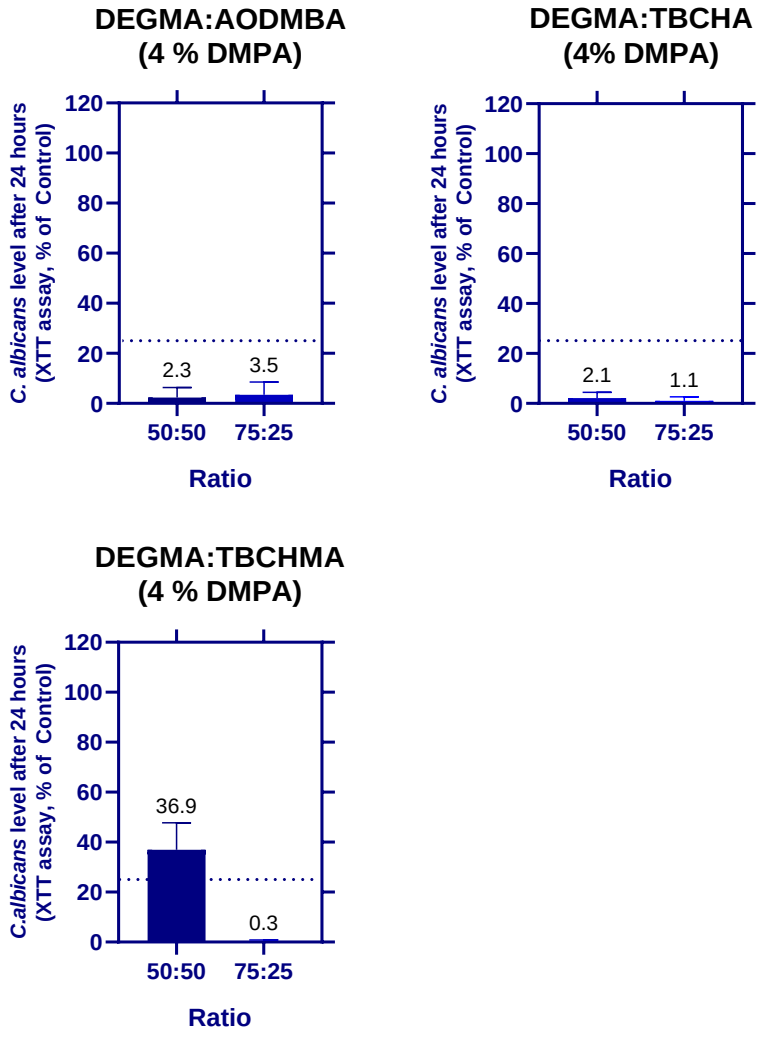


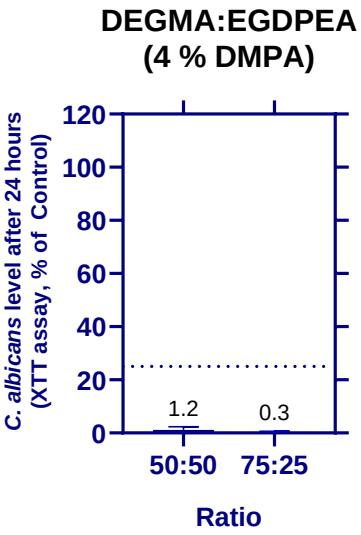


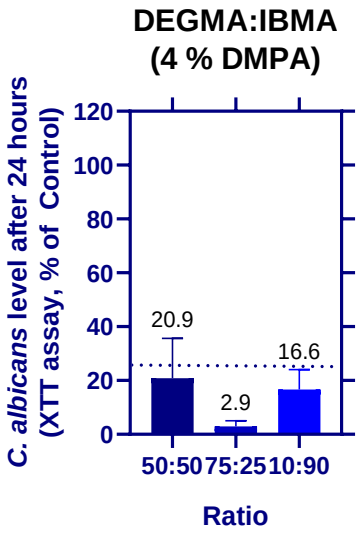




Appendix 9.4: DEGMA-based Copolymers with 4 % DMPA initiator




DEGMA:EGDPEA
(4 % DMPA)
C. albicans level after 24 hours
(XTT assay, % of Control)
120
100
80
60
40
20
0
1.2
0.3
50:50
75:25
Ratio


DEGMA:IBMA
(4 % DMPA)
C. albicans level after 24 hours
(XTT assay, % of Control)
120
100
80
60
40
20
0
20.9
2.9
16.6
50:50
75:25
10:90
Ratio